PROCESSING AND EVALUATION OF HYDROXYAPATITE-ETHYLENE VINYL ACETATE COPOLYMER COMPOSITES FOR CRANIOPLASTY

SHINY VELAYUDHAN

A THESIS SUBMITTED FOR THE DEGREE OF

DOCTOR OF PHILOSOPHY

SREE CHITRA TIRUNAL INSTITUTE FOR MEDICAL SCIENCES AND TECHNOLOGY THIRUVANATHAPURAM 695 012

DECEMBER 2004

DECLARATION

I, Shiny Velayudhan, hereby declare that I have personally carried out the work depicted in the thesis entitled **'Processing and evaluation of hydroxyapatite-ethylene vinyl acetate copolymer composites for cranioplasty'** under the direct supervision of Dr. P. Ramesh, Scientist, Polymer Processing Laboratory, Biomedical Technology wing, Sree Chitra Tirunal Institute for Medical Sciences and Technology, Thiruvananthapuram, Kerala.

Shiny Velayudhan

Tele: 0471-2340801
Fax : 0471-2341814

Grams : CHITRAMET
Telex : 0435 - 6290

श्री चित्रा तिरुनाल आयुर्विज्ञान तथा प्रौद्योगिकी संस्थान
बायो मेडिकल टैक्नोलॉजी विंग
पूजापुरा, तिरुवनन्तपुरम-695 012, इन्डिया

SREE CHITRA TIRUNAL INSTITUTE FOR MEDICAL SCIENCES AND TECHNOLOGY
BIO MEDICAL TECHNOLOGY WING
POOJAPPURA, THIRUVANANTHAPURAM-695 012, INDIA
(An Institute of National Importance under Govt. of India)

Ref: Dr. P. Ramesh, M. Tech, Ph. D.
Scientist-D
Polymer Processing Lab

Date: 31.12.2004

CERTIFICATE

This is to certify that the thesis entitled '**Processing and evaluation of hydroxyapatite-ethylene vinyl acetate copolymer composites for cranioplasty**' which is being submitted by Ms. Shiny Velayudhan, for the award of the degree of Doctor of Philosophy to the Sree Chitra Tirunal Institute for Medical Sciences and Technology, Thiruvananthapuram, is a record of bonafide work carried out by her under my direct supervision.

Ms. Shiny Velayudhan has worked on this research problem for about four years (2000-2004). The results embodied in this thesis have not been submitted for any other degree or diploma. This thesis has fulfilled the requirements according to the regulations. Seven research papers have been accepted/communicated for publication in international journals from this work.

P. Ramesh

PROCESSING AND EVALUATION OF HYDROXYAPATITE-ETHYLENE VINYL ACETATE COPOLYMER COMPOSITES FOR CRANIOPLASTY

SHINY VELAYUDHAN

A THESIS SUBMITTED FOR THE DEGREE OF

DOCTOR OF PHILOSOPHY

SREE CHITRA TIRUNAL INSTITUTE FOR MEDICAL SCIENCES AND TECHNOLOGY, THIRUVANATHAPURAM – 695 012

Supervisor

Thesis examiner

CONTENTS

ACKNOWLEDGEMENTS

It gives me great relief to sit back and write the acknowledgements after the long and hefty exercise of writing this thesis. I whole-heartedly thank the Almighty for blessing me with the patience, courage and inner strength that kept me going through all the ups and downs. I also thank DST (India) and DAAD (Germany) for the financial assistance that enabled me to carry out this investigation.

I am greatly indebted to my supervisor Dr. P. Ramesh for the support, informed guidance and advice he has extended to me throughout my work towards this thesis. I also extend my gratitude to him for being patient with me through all the times I have been frustrated. I acknowledge my Doctoral Advisory Committee members, Dr. G. S. Bhuvaneshwar, Dr. Mira Mohanty, Dr. K. Sreenivasan and Dr. H. K. Varma, for their ideas and guidance through the various aspects of the studies.

I am grateful to the Director SCTIMST for providing the necessary facilities throughout the doctoral programme.

Prof. K. Friedrich, Research Director, Institute for Composite Materials (IVW) Ltd, Kaiserslautern, Germany, has had a significantly positive influence on my development through his role as both my project leader and my advisor for the collaborative project that was carried out at IVW, Germany. His patience and willingness to discuss the minutiae of the different obstacles I encountered while working on this project are invaluable. I am also grateful to Prof. M. Neitzel, former Director, IVW, Kaiserslautern, Germany for giving me an opportunity to work with his wonderful and enthusiastic team at IVW, Germany.

I am thankful to Dr. Mira Mohanty, Dr. A. V. Lal, Dr. T. V. Kumary, Dr. P. V. Mohanan, Dr. A. C. Fernandez, Dr. P. R. Umasankar, Dr. T. V. Anilkumar and their entire team for helping me out with the biological evaluations of my samples. The discussions carried out with Dr. T. V. Anilkumar and Dr. Mira Mohanty for the preparation of the manuscripts on biological evaluation is also kindly acknowledged. Thanks are also due to Mr. R. Sreekumar (SEM), Mrs. Radhakumary (DSC & TGA), Mr. P. R. Hari (GPC), Mr. S. Sureshbabu (HAP synthesis), and Mr. S. Vijayan (XRD). I thank

Dr. Manoj Komath, Dr. Roy Joseph and Mr. Ramesh Babu for the encouragement and help they provided throughout my doctoral program. I am grateful to Dr. Kallyanakrishnan for the encouragement and care he has shown. I thank Dr. R. N. Bhattacharya and Dr. R. Girish Menon for their involvement and guidance during the cranioplasty experiments despite their busy and tight schedules.

I would place on accord the help extended by Dr. Ing. J. Hoffmann in helping me out with my experiments carried out at IVW, Germany. To Hr. Stefan Schmitt, I express my personal gratitude for making my stay in Germany a memorable one. The support extended by Hr. H. Giertzsch, Hr. R. Schimmele, Dipl.-Ing. W. Rolf, Dipl.-Ing. S. Geihl and Dr. C. Breidt, is also gratefully acknowledged. I also thank Dr. Ing. P. Klein, Dr. G. Xian and Dr. Ing. F. Henninger for their camaraderie and help. Thanks are also due to Fr. B. Geib for helping me with interlibrary loans.

It is difficult to find words to express my gratitude to my friends and collegues. I am grateful to Rajeev for the emotional support and care he provided which kept me going through my thicks and thins. Rajeev and my other friends Soney, Muraleekrishnan, Vikram, Vijay and Mohanraj never turned down any of my requests for the reprints. The constant help that I received from Anil for the formatting and setting this thesis is also gratefully acknowledged. I am also thankful to my wonderful colleague and friend Elizabeth who was always around with her kind gesture and help. My friend Mithra did a great job by helping me out in the processing of my samples for histopathological evaluation. I am thankful to Mr. M. C. Sunny for the encouragement and help he has given me throughout the course of my doctoral programme. I am also grateful to my friends Nissey, Asha, Divya, Siddharth, Krishnaprasad, Abiraman, Sugandhi, Biji, Nishi, Becky and Sailaja for their good companionship.

This thesis is dedicated to my beloved parents and my brother, who always supported me in my endeavors, always gave strength and encouragement to follow my dreams and never left me in doubt of their love for me.

Shiny Velayudhan

LIST OF FIGURES

LIST OF TABLES

ABBREVIATIONS

CNC	Computer numerically controlled
CSO	Cotton seed oil
CT	Computed tomography
DCPA	Dicalcium phosphate anhydrous
DCPD	Dicalcium phosphate dihydrate
DSC	Differential scanning caloriemetry
DTA	Differential thermal analysis
EDTA	Diaminoethanetetra-acetic acid
EVA	Ethylene vinyl acetate co polymer
FSHAC	Fast setting hydroxyapatite cement
FTIR	Fourier transform infra-red
GPC	Gel permeation chromatography
HAC	Hydroxyapatite cement
HAP	Hydroxyapatite
HDPE	High density polyethylene
HOS	Human osteosarcoma
IP	Indian pharmacopoeia
JCPDS	Joint committee for powder diffraction standards
MFI	Melt flow index
MRI	Magnetic resonance imaging
OCP	Octacalcium phosphate
PCL	Polycaprolactone
PE	Polyethylene
PEEK	Polyetheretherketone
PES	Polyethersulphone
PET	Polyethyleneterephthalate
PGA	Poly (glycolic acid)
PLA	Poly (lactic acid)
PLGA	Poly (lactic acid co-glycolic acid)

PLLA	Poly (l-lactic acid)
PMMA	Polymethylmethacrylate
PTFE	Polytetrafluroethylene
SBF	Simulated body fluid
SCA	Starch cellulose acetate
SCORIM	Shear controlled orientation injection moulding
SEVA-C	Starch ethylene vinyl alcohol copolymer
SL	Stereolithography
SPCL	Starch polycaprolactone
SPLA	Starch poly (lactic acid)
SR	Self-reinforced
TCP	Tricalcium phosphate
TCPM	Tetracalcium phosphate monoxide
TCPS	Tissue culture grade polystyrene
TGA	Thermogravimetric analysis
UHMWPE	Ultra high molecular weight polyethylene
XRD	X-ray diffraction

NOTATION

α_r	Radial expansion coefficient
α_l	Longitudinal expansion coefficient
E'	Storage modulus
E''	Loss modulus
E_c'	Storage modulus of composite
E_m'	Storage modulus of matrix
E_r'	Relative storage modulus
F_b	Bending force
F_c	Compressive force
F_r	Frictional force
F_t	Tensile force
ϕ	Volume fraction of filler
$\dot{\gamma}$	Shear rate
η_r	Relative viscosity
k	Self crowding factor
$\overline{M}_e$	Critical molecular weight
$\overline{M}_w$	Weight average molecular weight
T_g	Glass transition temperature
tan δ	Loss tangent
Γ	Torque

ABSTRACT

This investigation deals with the preparation and evaluation of a 'surgeon friendly' cranioplastic substitute fabricated from hydroxyapatite (HAP) and ethylene vinyl acetate co-polymer (EVA). Two grades of polymers (EVA) and two grades of HAP were selected for the study. The raw materials were characterized and the composites were prepared by making use of established polymer processing techniques. Composites containing up to 50vol.% of HAP were prepared and the mechanical and biological performance of the composites were evaluated.

For the mechanical property evaluation, the composites were subjected to both the static (tensile, flexural, impact) and dynamic testing conditions. In general, the composites fabricated from HAP with smaller particle size were found superior to the higher particle size counterpart. The composites also exhibited superior properties than the existing cranioplastic analogues of similar material chemistry. The composites were sufficiently pliable to be shaped by the surgeon's scalpels in the surgical theatre. Biological evaluations were performed on selected formulations of the composites. The evaluation was carried out as per the procedures detailed in the International Organization for Standardization (ISO)-10993. The biocompatibility and osteoconductivity of the composites were confirmed from the implantations in rabbit muscle and cranium. A simple method, namely stamp forming, was devised to contour the composites into clinically significant three-dimensional forms. Hemispherical forms, similar to the skull contours could be easily fabricated by this technique.

CHAPTER 1

INTRODUCTION

Globally millions of people receive head injuries from accidents or sporting activities. The impact created by the massive external force from these events on the cranium can often shatter the cranial bone and produce irregularly shaped defects, exposing the underlying brain. Mass bone loss from the skull following tumours, infection and although infrequent, decompressive craniectomies for the amelioration of high intracranial pressure, also result in undesirable exposure of the underlying brain causing serious biological concerns. These lead to malformed appearance of skull and correction of the defect become imperative for both protective and cosmetic reasons. The neurosurgical procedure that is employed for putting the skull back to its normal topography by means of operative repair of the skull defect is called cranioplasty.

The materials currently in use for cranioplasty include biological grafts such as autografts and heterografts, metals like titanium, polymers like polymethylmethacrylate (PMMA), and ceramics like hydroxyapatite (HAP) (Gosain, 2002). All these materials though efficacious for the repair of cranial defects, are less than ideal. The major limitations identified for the existing cranioplastic materials are (i) lack of bioactivity i.e., the inability of the material to integrate with the bone tissue in contact with it by forming ultra-structural chemical bonds (e.g., titanium and PMMA) and (ii) lack of malleability i.e., the difficulty in shaping the implants intra-operatively to fit the complex topography of the skull defect (e.g., PMMA, HAP, and biological grafts) (Gosain and Persing, 1999). The requirements of bioactivity and malleability for cranioplastic implants are necessary

to obtain a stable interface with the surrounding host tissue. It has been identified that a bioactive material facilitates early fixation of the prosthesis onto the bone and improves the prosthesis lifetime even if the biomechanical mismatch of the implant and the tissue remains (Bonfield, 2003). Several researchers attempted to combine HAP with biodegradable polymers to produce bioactive and malleable composites for cranioplasty (Pompili *et al.*, 1998; Lin *et al.*, 1998; Schliephake and Kage, 2001; Zanetti and Nassif, 2003). This approach was, however, not successful as the acidic degradation products from the polymers interfered with the new bone formation and thus the healing of the defect. Combination of HAP with titanium was also attempted to repair large cranial defects; but the alarmingly high rate of infection was reported for these constructs (Durham *et al.*, 2003).

In this scenario, it would be attractive to develop a non-biodegradable, bioactive, and pliable material for cranioplasty. This thesis discusses the development of a composite material that meets the above requirements by using HAP and ethylene vinyl acetate co-polymer (EVA). The thesis begins with a literature survey on the materials used for cranioplasty and their advantages as well as the limitations are discussed (Chapter 2). An overview on the structure and properties of the bone is also included in the literature survey.

The chapter 3 details the experimental methods and various methodologies employed in the development of the HAP-EVA composites. Two grades of EVA with different vinyl acetate contents were chosen for the study. The HAPs for the study were synthesized in the laboratory via., two different processing routes, namely, spray drying and freeze drying. The HAPs differed from each other with respect to the morphology and particle size. Composites were prepared by mixing HAP and EVA in a torque rheometer. The effect of size and morphology of HAP and vinyl acetate content of EVA on the compounding variables such as mixing torque, mixing time and temperature was studied. Some of the selected formulations were further characterized for the mechanical properties and the biological performance.

The results of the experiments and their discussions are given in the following chapters. The raw material characterization and the preparation of HAP-EVA composites are given in chapter 4. This is followed by chapter 5, which gives the results and the discussion of the mechanical properties of the HAP-EVA composites. The biological

evaluation of the composites was carried out as per the procedures detailed in the International Organization for Standardization (ISO)-10993. The results and discussion of the biological evaluation are detailed in chapter 6. A novel forming technique, namely stamp forming, was adopted to shape the HAP-EVA composites into clinically significant three-dimensional geometry. The stamp forming process optimization and characterization of the stamp formed geometries are discussed in chapter 7. The thesis concludes with chapter 8, which gives a brief summary of the investigation along with the conclusions of the study and directions for future research.

CHAPTER 2

LITERATURE SURVEY

2.1. INTRODUCTION

Medical procedures to address bone related injuries are prevalent worldwide. For example, in United States, around 900000 hospitalizations due to fractures and over 800000 grafting procedures are reported annually (Laurencin *et al.*, 1999), which showers light to the high magnitude of the need for bone substitutes. To meet the need for intervention in these cases, various materials are currently in use to repair or replace bone that has been damaged due to trauma or disease. The development of materials for any replacement application should be based on the understanding of the structure to be substituted. This is true in many fields, but particularly exigent in substitution medicine. Ideally, a replacement material should mimic the living tissue from the mechanical, chemical, biological and the functional point of view.

2.2. BONE

2.2.1. Elementary constituents

Bone is a natural composite material, which contains about 69wt.% mineral, 22wt.% organic matrix (of which 90-96wt.% is collagen), and water (9wt.%) (Vaughan, 1981). Sub-microscopic crystals of apatite of calcium and phosphate, resembling hydroxyapatite in its crystal structure [$Ca_{10}(PO_4)_6(OH)_2$], constitute the major sub-phase of the mineral content. Other mineral ions such as citrate ($C_6H_5O_6^{4-}$), carbonate (CO_3^{2-}), fluoride (F^-), and hydroxyl ions (OH^-), also contribute to the constitution of the mineral phase. The apatite crystals are embedded in the collagen fiber matrix as slender needles,

20-40 nm in length by 1.5-3 nm in thickness. These mineral-containing fibrils are arranged into lammellar sheets that run helically with respect to the long axis of the cylindrical osteons (or sometimes called Harvesian systems). The osteons, typically from 150-250 μm in diameter, are arranged in concentric rings around the harvesian canal (Park and Lakes, 1992). The interstitial systems between the osteons are sharply divided by the cementing line. The metabolic substances can be transported by the intercommunicating pore systems known as canaliculi, lacunae, and Volksmann'cannals, which are connected with the marrow cavity. The external and internal surfaces of the bone are called periosteum and endosteum, respectively, and both have osteogenic properties (Posner, 1978). Figure 2.1 shows the typical organization of the bone.

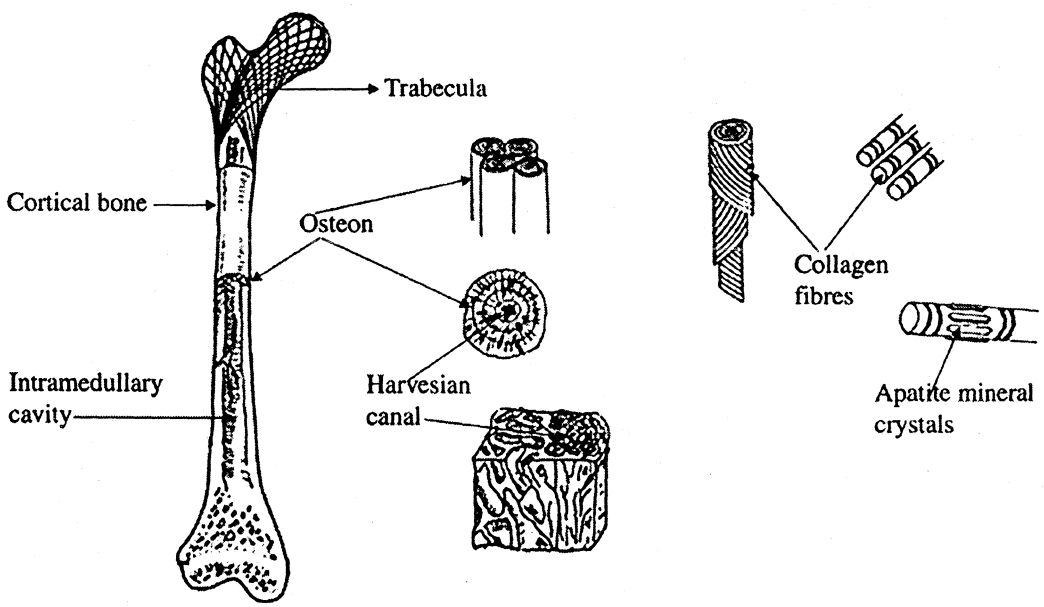

Figure 2.1. Organization of human bone (adapted from Park and Lakes, 1992)

2.3. MATERIALS FOR BONE SUBSTITUTE APPLICATIONS

A myriad of materials are in use for substituting defective or fractured bone. The most important considerations for a biomaterial are with respect to its mechanical and biological compatibility. The success of a biomaterial in the body also depends on other factors like the design, the surgical technique, health of the patient and quality of the natural tissue with which they are interfacing.

Biological grafts, such as autografts and allografts have been used for knitting together injured and damaged bones. However, these grafts suffer from many limitations.

Autografts are associated with additional trauma resulting from harvesting of bone tissue. They also undergo unpredictable resorption, are of limited quantity and may result in secondary donor site morbidity (Nickell *et al.*, 1972; Prolo *et al.*, 1979; Wolfe, 1982). The use of allografts is limited by possibility of an immunological response and the risk of disease transmission. In this light, manmade materials stand out as a potential solution being easily available, processed and modified to suit the needs of a given application. The materials that are currently in use for substituting defective bone can be divided into metals, polymers, ceramics and composites. Table 2.1 lists the examples of materials that have found use in various bone substitute applications.

Table 2.1. Biomaterials in various bone substitute applications

Devices	Function	Biomaterials
Artificial total hip, knee, shoulder, elbow, wrist	Reconstruct arthritic or fractured joints	316 stainless steel (SS), Cobalt (Co)-chromium (Cr) alloys, Ti and Ti-6Al-4V alloy, High-density alumina, Ultra-high molecular weight polyethylene (UHMWPE).
Bone plates, screws, wires	Repair fractures	316 SS, Co-Cr alloys, Ti and Ti-6Al-4V.
Intramedullary nails	Align fractures	316 SS, Co-Cr alloys, Ti and Ti-6Al-4V, polysulphone-carbon fibre composites.
Spinal fusion	Immobilize vertebrae to protect spinal cord	Bioglass, Hydroxyapatite (HAP), Tricalcium phosphate (TCP).
Alveolar bone replacements, mandibular bone reconstructions	Restore the alveolar ridge to improve denture fit	Polytetrafluroethylene (PTFE) - carbon composite, Porous Al_2O_3, Bioglass, dense HAP.
Cranioplasty	Repair the defective skull and restore the skull contour	Polyethylene (PE), PMMA, titanium, HAP, TCP, HAP cements.

2.3.1. Metals

Metals are crystalline materials that form from atoms that have high mobile electrons and are built up of repeating unit cells containing specific number of atoms in specific positions (Helsen and Breme, 1998). Metals, in general, have high Young's modulus, are tough and ductile. These properties confer the metals the ability to mimic the support and protective functions of bone. With the exception of pure titanium, metals are generally used in the form of alloys. Typical examples of metals used as bone substitutes are austenite stainless steel, cobalt (Co)-chromium (Cr) alloys, commercially

pure titanium and its alloys. Table 2.2 lists the mechanical properties of metals used in bone substitute applications.

Table 2.2. Mechanical properties of metals used as bone substitutes

Material	Young's Modulus, (GPa)	Ultimate tensile strength, (MPa)	Ultimate strain, (%)
Austenite stainless steel	200[£]	190-260[#]	12-40[#]
Co-Cr alloy	230[£]	720-890[Ψ]	5-17[Ψ]
Ti-6Al-4V	105[£]	825*	8*

[£] Tanner, (1998); [#] ASTM F138-97; [Ψ] ASTM F75-01; *ASTM F136-02.

2.3.2. Polymers

Polymers are long chain high molecular weight materials composed of repeated units termed monomers. Polymers generally have low modulus and strength, but higher strain to failure than metals. They can be fabricated easily, which enable them to be contoured to clinically significant forms. Two polymers that are widely used as bone substitutes are PE and PMMA. Recently, polyetheretherketone (PEEK) is also used for replacement of bones in the high load bearing regions (Abu Baker, 2003a, 2003b, 2003c).

The use of biodegradable polymers has attracted the interest of the surgeons because of their inherent property of breaking down into natural metabolites that are then excreted out of the body (Athanasiou *et al.*, 1998; Tormala *et al.*, 1998; Griffet *et al.*, 1999; Zhao *et al.*, 2002). The degradation helps in the elimination of a second surgical event for the removal of the prosthesis. The most currently studied degradable polymers are poly (α-hydroxy esters). The poly (α-hydroxy esters) belong to a class of polyesters whose repeating units, $[-O-CO-CHR-]_n$, are derived from α-hydroxy-acids, HO-CHR-COOH. The commonly used poly (α-hydroxy esters) in the medical applications are poly (lactic acid) (PLA), poly (glycolic acid) (PGA) and poly (lactic acid-co-glycolic acid) (PLGA). Table 2.3 lists the mechanical properties of the polymers used as bone substitutes.

Table 2.3. Mechanical properties of polymers used as bone substitutes (Wise *et al.*, 1995)

Material	Young's Modulus, (GPa)	Tensile strength, (MPa)	Strain at break, %
Polymethylmethacrylate	3	46	2-6
Ultra high molecular weight polyethylene	1	200	300-500
Poly(l-lactic acid)	2-4	55-80	3-10
Poly(glycolic acid)	6	60-70	15-20

2.3.3. Ceramics

Ceramics are refractory, polycrystalline compounds usually inorganic, including silicates, metallic oxides, carbides and various refractory hydrides, sulfides, and selenides (Park and Lakes, 1992). Ceramics are known for their high hardness and modulus. They are highly brittle and cannot be sheared like the metals or polymers. Recently, ceramic materials have been given a lot of attention as candidates for implants. Based on the response of the body to the ceramics, they are classified as bioinert and bioactive ceramics. Bioinert ceramics like alumina (Al_2O_3) and zirconia (ZrO_2) show no chemical activity under the physiological environment and forms no interfacial bonds with the living tissues. Bioacitve ceramics like TCP and HAP, on the other hand, promote growth of bone onto the surface of the implant and form a direct chemical bond with the hard tissue. Table 2.4 lists the mechanical properties of the ceramics used in bone substitute applications.

Table 2.4 Mechanical properties of bioceramics used as bone substitutes (Ravaglioli and Krajewski, 1992).

Material	**Young's Modulus, (GPa)**	**Compressive strength, (MPa)**	**Hardness, HV**
Alumina	380	4000	2000-3000
Zirconia	150-200	2000	1000-3000
Bioglass®	75	1000	-
Hydroxyapatite	73-117	600	500

2.3.3.1. Calcium phosphates

Calcium phosphates can be crystallized into vast range of salts, including HAP and TCP, depending upon the calcium to phosphorous (Ca/P) ratio, presence of water, impurities and temperature (Park and Lakes, 1992). A convenient way to classify calcium

phosphate compounds is by groups of definite Ca/P ratios. Table 2.5 lists some of the synthetic calcium phosphates that have biological use as surgical materials. Calcium phosphate ceramics with Ca/P > 1.5 are generally considered as bioactive.

Table 2.5 Synthetic calcium phosphate compounds that have biological use as surgical materials (Ravaglioli and Krajewski, 1992).

Name	Phase name	Chemical formula	Ca/P ratio
Dicalcium phosphate dihydrate (DCPD)	Brushite	$CaHPO_4.2H_2O$	1.00
Dicalcium phosphate anhydrous (DCPA)	Monetite	$CaHPO_4$	1.00
Octacalcium phosphate (OCP)	-	$Ca_8H_2(PO_4)_6.5H_2O$	1.33
Tricalcium phosphate (TCP)	β-whitlockite	$Ca_3(PO_4)_2$	1.50
Hydroxyapatite (HAP)	Hydroxyapatite	$Ca_{10}(PO_4)_6(OH)_2$	1.67
Tetracalcium phosphate monoxide (TCPM)	Hilgenstockite	$Ca_4O(PO_4)_2$	2.00

The most commonly used calcium phosphate is HAP, which has a similar composition to bone mineral. Hydroxyapatite is insoluble in body fluids unless the environment is acidic. However, the bone resorbing cells (osteoclasts) resorbs it slowly. Synthetic HAP can be easily manufactured and processed into various forms like powder, granules, and blocks to suit the various orthopaedic requirements.

2.3.4. Composites

Traditionally a composite is defined as a material with at least two phases, a continuous phase and a dispersed phase. The continuous phase is responsible for filling the volume and transfer loads to the dispersed phase. The dispersed phase is usually responsible for enhancing one or more properties of the composite. A composite is designed to have a combination of best characteristics of each of the component materials (Hull and Clyne, 1996). Most of the composites target enhancement of mechanical properties such as stiffness and strength, but other properties may be of interest such as transport properties (electrical or thermal) or density. For biomedical composites, even though excellent mechanical performance is desirable and often targeted for improvement, the biocompatibility of the material is of paramount concern (Wang, 2003).

Matrix materials for composites can be metal, ceramic, or polymer. Figure 2.2 shows the relation between stiffness and strength for a number of materials of interest for

biomedical applications. It can be observed that metals and ceramics are always stiffer and can have larger strength than biologic hard tissue. Polymers are mostly more compliant (lower modulus) than hard tissue and can have strengths of the same order of magnitude as that of soft tissue. Biological tissues show larger spectra of mechanical properties than the other materials. This picture clearly illustrates the great interest of compounding polymers and other materials to obtain polymer matrix composites that attain combinations of mechanical and biological properties similar to those of biological hard tissue.

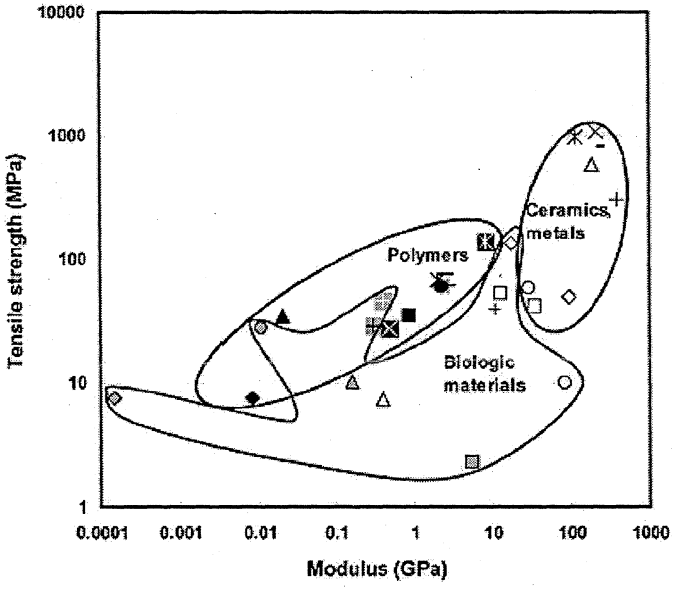

Figure 2.2. Tensile strength vs. modulus of materials with relevance for composite design when considering biomedical applications (adapted from Basso and Heersche, 2002)

Polymer matrix composites can be subdivided based on the type of reinforcement used. Fibre-reinforced composites use fibres that may be up to several millimeters in diameter and can even run the full length of the structure. Micrometer-sized particles of hard filler in a polymer matrix form a particulate reinforced composite. Particulate inclusions may be spherical, ellipsoidal, polyhedral, or irregular.

2.3.4.1. Fibre-reinforced composites

A variety of composites have been developed for orthopaedic applications. One among the earliest to be developed was based on carbon reinforced with carbon fibre (Bradley *et al.*, 1980). The material was highly anisotropic and had excellent biocompatibility. Bradley *et al.* (1980) produced carbon fibre reinforced epoxy resin

internal fixation plates, giving a material that was mechanically compatible with bone. These devices had excellent mechanical properties to match the properties of the cortical bone. Nevertheless, these devices were abandoned, as the polymer resin could not be shaped in the operation theatre, thus only permitting the internal fixation plates to be used on straight bones. Additionally, the interface between the fibre and the polymer was also weak.

Hench (1973) reported the Bioglass® filament reinforced high-density polyethylene (HDPE) systems, which were biocompatible and had comparable elastic modulus to bone. Sclippa and Piekarski (1973) attempted to modify UHMWPE used in total knee replacements by incorporating carbon fibre. In 1994 Rotem reported the development of a hip replacement prosthesis fabricated using graphite fibres embedded in polysulfone matrix. Lin *et al.,* (1997) reported the results of cell culture studies of a composite made from polyetherether ketone (PEEK) reinforced with 10% random chopped E-glass fibres. The composite supported proliferation of osteoblast like cells in *in vitro* cell culture studies. Marcolongo *et al.* (1997, 1998) reported their results of animal implantation studies of a fibre reinforced polymer composite system fabricated from bioactive glass fibres and polysulfone. These composites exhibited interfacial bond strength of 12.4 MPa after six weeks implantation in rabbit femora. Failure sites for the composite at six weeks occurred either at bone-tissue interface or in the composite. They found that the bioactive glass fibre/polysulfone composite achieved fixation to bone through a triple mechanism: a bond to the bioactive glass fibre, mechanical interlocking between the tissue and the glass fibres, and close apposition and possible chemical bonding between the portions of the polymer and bone tissue. The last mechanism resulted from an overspill of bioactivity reactions from the fibres onto the surface of the surrounding polymer, which the authors called the "halo" effect.

Degradable polymers represent an area of increasing interest in orthopaedics, mainly in orthopaedic fracture fixation (Bostman *et al.,* 1987; Yamamuro *et al.,* 1994). However, the poorer material properties of biodegradable polymers were a matter of concern. Alexander *et al.* (1981a, 1981b) proposed absorbable polymers of filamentous carbon tissue scaffold for tendon and ligament replacements using carbon fibres coated with poly (l-lactic acid). The results were convincing enough to allow the human implantation of this filamentous carbon composite for tendon and cruciate ligament

replacements. Lewis (1981) investigated properties of biodegradable PLLA plates combined with carbon or ceramic fibres. *In vitro* data indicated that satisfactory flexural properties could be maintained for about six weeks. However, concern for the fate of the non-resorbable carbon fibres led others to explore different methods for increasing the strength of the implants fabricated from these materials. Several groups developed biodegradable implants with increased strength, compared to the basic polymer. Tormala *et al.*, (1987) and Vainionpaa *et al.*, (1987) studied the effects of fibre reinforcement on the flexural and tensile strength of PGLA copolymer materials *in vitro* and suggested that self-reinforced PGA/PLA composites may be used for the treatment of fractures in cancellous bone. The self- reinforcement approach utilizes a composite material in which the reinforcing fibres are of the same base material as the matrix but have a higher molecular weight. Thomson *et al.* (1998) developed a process to manufacture biodegradable composite foams of poly (dl-lactic-co-glycolic acid) and hydroxyapatite short fiber for use in bone regeneration.

2.3.4.2. Particulate reinforced composites

Polymer-ceramic composite materials for bone substitute applications were first implemented in an effort for upgrading the traditional PMMA based bone cements. The PMMA based bone cements that are frequently used in fixation of metallic implants, serve only as a filler or grouting agent to distribute the load and have many disadvantages (Gough and Downes, 2001). In 1979 Henning *et al.*, reported on the use of "bone cement" consisting of PMMA in combination with surface-active glass-ceramic granules. The bioactive bone cement reduced the temperature rise during the *in situ* polymerization and apparently reduced the free monomer transport in the circulatory system as well. Beruto *et al.*, (2000) produced a new class of bioactive composite from PMMA and TCP. The PMMA formed a solid cellular matrix with open cells about 100 mm in size and incorporating the TCP clusters. Recently, Dalby *et al.*, (2002) prepared PMMA cements containing 0, 4.6, and 8.8vol.% of HAP. The biological evaluation of this material carried out on human osteosarcoma cells (HOS) showed that HOS anchored preferentially to HAP rather than PMMA indicating that increasing the HAP incorporation into the PMMA cement makes it more bioactive.

Bonfield *et al.*, (1981) proposed the use of composites HDPE with HAP, introducing the so-called bone-analogue concept. At 40vol.% of HAP loading, the

composite was sufficiently bioactive and had a modulus approaching the lower band of the range of values associated with the natural bone (Huang *et al.,* 1997; di Silvio *et al.,* 2002). Although not yet used in high load bearing applications, the composites of HDPE/HAP are already used to produce middle ear implants, under the trade name HAPEX^{TM} (Bonfield, 1997). Alternative bioactive reinforcements have been also investigated for HDPE, namely bioactive glasses (Wang *et al.,* 1995; Huang *et al.,* 1995, 1996) and glass-ceramic (Huang *et al.,* 1996; Bonfield, 1996; Wang *et al.,* 1996).

Attempts by Bonfield and co-workers (Ladizesky *et al.,* 1997a; 1997b; Ward *et al.,* 1997; Wang *et al.,* 2000) to develop bone matching mechanical performance have relied on the inducement of a strong anisotropic character by means of hydrostatic extrusion. The application of this solid state processing technique has enabled for the attainment of significant improvements in the composite stiffness. Values of modulus up to 13 GPa were reported (Ladizesky *et al.,* 1997b). A complementary approach has relied on the reinforcement of the HDPE/HAP composites with high modulus polyethylene fibres (Ladizesky *et al.,* 1998). In this case, the use of very stiff and chemically compatible fibres allowed for further improvements of mechanical performance. An alternative approach to the mechanical performance enhancement of HDPE/HAP composites was followed by Reis and co-workers (Reis *et al.,* 2001; Sousa *et al.,* 2002a) with the use of shear controlled orientation injection moulding (SCORIM).

Recently, Abu Bakar *et al.* (2003a, 2003b, 2003c) proposed the use of hydroxyapatite-polyetheretherketone (HAP-PEEK) composites for bone substitution. It was found that at 40% volume fraction of HAP loading, the range of stiffness of the composite was 2.8-6.0 GPa and tensile strength was 45.5-69.0 MPa, which crosses the lower bound of the properties of human bone. The biological responses of HAP-PEEK composites carried out *in vivo* suggested the favourable bioactivity and biocompatibility, promising the use of this composite for high load bearing applications such as medical implants, devices and structural scaffolds.

The most currently studied bioactive degradable composites are obtained by combination of poly (α-hydroxy esters) and HAP; combinations with polycaprolactone (PCL) were also proposed (Ural *et al.,* 2000). The poly (α hydroxy esters)-HAP composites are mainly prepared by incorporating the ceramic into the polymeric solution (Higashi *et al.,* 1986). An interesting list of references assigned to the different ways of

preparing such composites may be found in a work of Durucan and Brown (2000). Nevertheless, non melt based routes led to the development of systems with lower mechanical performance and many times require the use of toxic solvents and intensive hand labour. One of the PLA-HAP composites showing highest mechanical properties was developed by Shikinami and Okuno (1999). These composites exhibited an initial bending strength of 280 MPa that exceeds the bending strength of the cortical bone (120 – 210 MPa); this strength could be maintained above 200 MPa up to 25 weeks in phosphate-buffered saline solution. *In vivo* studies on these composites carried out on rabbits were investigated (Furukawa *et al.*, 2000a). The non-inflammatory response of the tissues pointed out the bioactive behaviour of the implants (Yasunaga *et al.*, 1999; Furukawa *et al.*, 2000b).

Porous bioabsorbable materials have gained increasing interest, especially in the area of tissue engineering (Langer and Vacanti, 1993; Ishaug *et al.*, 1997). However, there is a need for enhancing the mechanical properties of such systems. Therefore, porous composite materials of polylactide/HAP have been proposed to overcome this problem, and also increasing the osteoconductivity of the scaffolds (Marra *et al.*, 1999; Ma *et al.*, 2001; Wang *et al.*, 2001). These scaffolds could improve, for example, the bulk penetration of osteoblasts into the inner pores, whereas in pure PLLA scaffolds the osteoblast attached primarily on the outer surface of the foam (Ishaug *et al.*, 1997).

Reis *et al.*, (1996) proposed the blends of starch with (1) ethylene vinyl alcohol copolymer (designated as SEVA-C), (2) cellulose acetate (designated as SCA), (3) polycaprolactone (designated as SPCL) and (4) poly (lactic acid) (designated as SPLA) as potential alternative biodegradable materials for a wide range of biomedical applications (Reis *et al.*, 1997a, 1997b, 1997c, 1998; Reis and Cunha, 2000; Sousa *et al.*, 2000, 2002b; Leonor *et al.*, 2000; Gomes *et al.*, 2001a; Mendes *et al.*, 2001; Vaz *et al.*, 2002). *In vitro* and *in vivo* biocompatibility studies carried out on these composites showed them to be promising bone substitutes (Gomes *et al.*, 2001b; Marques *et al.*, 2002).

Polymer-ceramic systems have been widely used as injectable cements; prepared mainly by the addition of viscous polymer gels to calcium phosphate ceramics. TenHuisen and Brown (1994) reported the preparation of gelatin-HAP cements at room temperature for filling bone defects. Sodium alginate was also proposed as the polymer component for the preparation of injectable cements (Ishikawa *et al.*, 1995; Miyamoto *et*

al., 1996). Later the interest moved to chitosan, because of its superior pharmacological benefits for bone formation than the alginate (Takechi *et al.*, 1996; Wan *et al.*, 1997; Yamaguchi *et al.*, 2001).

Biomimetic calcium phosphate coating on polymers improves their bioactivity. Bone like apatite coatings and biomimetic composites have been produced in aqueous solutions at physiological temperatures by various investigators (Takeuchi *et al.*, 2003; Tampieri *et al.*, 2003; Eglin *et al.*, 2004; Kawai *et al.*, 2004; Zhang and Ma, 2004). Kokubo and co-workers prepared apatite-polymer composites by biomimetic process using different polymers, namely polyethyleneterephthalate (PET), PMMA, polyamide 6, polyethersulphone (PES), polyethylene (PE) and polytetraflouroethylene (PTFE) (Kokubo *et al.*, 2003). Varma *et al.*, (1999a; 1999b; 2003) reported formation of calcium phosphate over phophorylated chitosan films, functionalised cotton fibers and surface modified PMMA film. It is generally found that the biomimetic processes potentially enhanced osteoconductivity of the polymer by providing a favourable environment for osteoblasts or osteoprogenitor cell attachment and proliferation.

2.4. BIOMATERIALS FOR CRANIOPLASTY

2.4.1. Cranioplasty

Cranioplasty is one of the oldest neurosurgical procedures that involve operative repair of a defect of the skull. Generally, a cranioplastic procedure is implemented either to treat the congenital diseases that result in abnormal or undesirable bone growth or to repair the acquired defects such as loss of skull bone due to infection following surgery, skull bone loss due to degradation and/or resorption, skull bone loss due to a pathological process.

2.4.2. Material requirements

Any material to be used in the body should meet the requirements of biological as well as mechanical compatibility. Biological compatibility is required to prevent the material rejection and mechanical compatibility is essential for proper load transfer. However, the mechanical properties of the tissue vary with the function as well as the anatomical site of the tissue (Currey, 1999). For e.g., while the long bones are designed for high stiffness, and resistance to fatigue failure; the mechanical role of the skull vault is impact resistance (Currey, 1984). In the literature, biomechanical analyses of neurocranial

osteosyntheses are very rare, and they are generally considered "non-loaded". It has, however, been demonstrated that a growing cranium, experiences diverse biomechanical stresses such as pulsating intracranial pressure, expansive forces caused by the growing brain and cranium, distractive forces caused by scalp closing tensions and wound contraction, and compressive extracranial forces, e.g., the pressure of the child's head against the contact area. Thus, to be mechanically safe, cranioplastic implants should have 1) high initial strength to carry physiological loads during healing, 2) appropriate initial modulus; not too stiff or too flexible for the special purpose where it is used (Tormala and Pohjonen, 1995). The additional qualities that an ideal cranioplastic material must possess include lack of adverse reactions (i.e., non-toxic, non-allergenic, non-immunogenic, non-mutagenic, or non-teratogenic), lack of interference with bone healing, lack of intracranial migration, lack of visibility and palpability, and avoidance of an implant removal operation (Constantino *et al.* 1993). Osteoconductivity is yet another important requirement of a cranial implant. Surgeons appreciate good handling property; such as malleability of plates in room temperature so that the implant could be sculpt according to the defect created in the cranium. Synthetic implants are preferred to biological grafts as they eliminate secondary donor site morbidity and rule out the possibility of disease transmission (Ross *et al.*, 1995). The implants should also be radiopaque so that they can be visualized on imaging tests.

2.4.2.1. Biological grafts

The biological grafts for cranioplasty include autografts (bones taken from individual's own body) and heterografts (bones taken from different individual belonging to the same species or different species). The autogenous bone graft is preferred to allograft because of the risk of adverse immunological response and disease transmission. Literature gives the evidence of split skull (Kiyokawa *et al.*, 1998) and split rib cranioplasty (Viterbo *et al.*, 1995), performed for correcting skull defects as large as 100sq. cm. The split rib cranioplasty has an added advantage that it could be performed in children too, who lack the skull thickness needed to undergo a split skull cranioplasty.

The biological grafts, however, suffer from certain limitations. Autogenous bone grafting requires a second surgical site for extracting blocks of bones, which could result in several complications like donor site morbidity and sufficient loss of blood. The grafts also present application difficulties because of its rigid nature, which makes it difficult to

be shaped into the precise contour required by complicated and large defects (Kulah and Kayaalp, 1991). The aesthetic results are often unacceptable, because the graft tends to undergo resorption. Rib cranioplasty suffers from the "washboard effect" in which the contour of the rib can be seen through the skin.

2.4.2.2. Metals

In the context of cranioplasty, metallic implants are primarily used for two purposes - as permanent devices (skull plates) to replace permanently a portion of the skull and as fixation devices to join two pieces of cranial bones together while they heal. Titanium is the preferred metal for cranioplasty because of its strength and biocompatibility and has been widely used in cranial repair and augmentation (O'Broin *et al.*, 1997; Joffe *et al.*, 1999; Miyake *et al.*, 2000; Kamyszek *et al.*, 2001). The use of micro/macro titanium plates (Jackson and Adham, 1986; Onishi *et al.*, 1995; Koppel *et al*, 1999), meshes (Malis, 1989; Ducic, 1997; Lara *et al.*, 1998; Kuttenberger and Hardt, 2001) and clamps (Ebel *et al.*, 2000; Estin *et al.*, 2000; Ducic, 2002) in cranio-maxillo facial surgery are reported in literature. The advantages of rigid metallic fixation include greater bony stability of osteotomized bone flaps and grafts, greater accuracy in bone reshaping, simplification of osteotomy design, and enhancement of primary bone healing with decreased resorption and infection rates (Jackson *et al.*, 1986; Muehlbauer *et al.*, 1987; Sadove and Eppley, 1991). Hence the new methods, especially microfixation techniques, were rapidly adopted in paediatric use. However, many problems associated with metallic plates and fixations are still an apprehension.

Local restriction of growth is one of the major concerns that have been documented with both rigid metallic and non-rigid wire fixation (Lin *et al.*, 1991; Yaremchuk *et al.*, 1994; Polley *et al.*, 1995; Polley *et al.*, 1998). The degree of growth restriction increases with the amount of fixation hardware used, but the growth restriction can be limited when the fixation devices are appropriately sized and located in non-growth centre regions (Lin *et al.*, 1991; Wong *et al.*, 1991; Mooney *et al.*, 1992; Wong *et al.*, 1993; Yaremchuk *et al.*, 1994; Polley *et al.*, 1995; Polley *et al.*, 1998).

Another major concern is the passive translocation of metallic implants. The initial reports on passive intracranial translocation of metallic hardware were published in 1995 (Fearon *et al.*, 1995; Goldberg *et al.*, 1995; Papay *et al.*, 1995), causing great concern and discussion (Posnick and Yaremchuk 1995; Yaremchuk and Posnick 1995;

Persing *et al.*, 1996). The device transposition is more likely to occur in infants (Goldberg *et al.*, 1995), especially with syndromic forms of craniosynostoses, and when (long) plates are placed in temporal and lateral areas (Goldberg *et al.*, 1995; Yaremchuk and Posnick, 1995). Metallic materials can be incorporated into the dura and pose a difficulty in surgical reoperations and possibly a risk in magnetic resonance imaging (Fearon *et al.*, 1995).

Metallic fixation devices may cause a distinct cosmetic deformity, palpability or wound dehiscence especially if placed under a scarred, tight scalp (Fearon *et al.*, 1995). Plate exposure has been reported to be associated especially with preoperative radiotherapy (McCann *et al.*, 1994). Common reasons for hardware removal have been reported to include palpable or prominent hardware (34.5%) of the patients needing implant removal, loosening of plates and screws (25.5%), pain (25.5%), infection (23.6%), wound dehiscence/exposure of hardware (20%), and removal at the time of secondary procedures (9.1%) (Orringer *et al.*,1998). Metallic devices also interfere with radiological investigations.

2.4.2.3. Polymers

Polymethyl methacrylate is the polymer that is widely used in cranioplasty. Occasionally, silicone rubber, PE and PTFE are also employed.

2.4.2.3.1 ***Polymethyl methacrylate***

Polymethyl methacrylate has long been used for the reconstruction of traumatic skull defects (Alesch and Bauer, 1985; Lara *et al.*, 1998; Moreira-Gonzalez *et al.*, 2003; Chiarini *et al.*, 2004). The polymer became popular among neurosurgeons as it permits simple and expeditious closure of calvarial defects (Wong and Manson, 1994; Sherburn and Silbergeld, 1997; Luparello *et al.*, 1998). Additional advantages of PMMA are its low cost and ready availability. Routine method of acrylic cranioplasty involves estimation of size and contour of the cranial defect; back table hardening of the plate, and subsequent fixation to the calvarial margin with wires, sutures or miniplates (Malis 1989; Sherburn and Silbergeld, 1996).

The method of back table hardening of PMMA, however, is cosmetically unappealing especially in the case of defects in the forehead region. The deleterious

thermal and chemical effects of curing PMMA were also a concern. However, with the advent of technology, stereolithography and rapid prototyping techniques are used for pre-fabrication of custom acrylic resin cranial implants with greater clinical predictability (Cheng and Wee, 1999; Hieu *et al.*, 2002; Dean *et al.*, 2003). These techniques remove the risks of heat or chemical damage to tissues and produce prostheses that significantly improve the capabilities for enhancing cosmetic appearance and, by virtue of accurate fit to the defect site, a reduction in operative time and complications associated with such surgeries (Agner *et al.*, 1997).

Polymethylmethacrylate has been reported to be unsuitable to pediatric population (Blum *et al.*, 1997) and also for rectifying bifrontal cranial defects involving both orbital rims and frontal sinus (Benzel *et al.*, 1990). Surgeons report infection rates of 22% for the acrylic cranioplasty involving the frontal sinus (Gosain, 2002). It is generally considered that PMMA is the material of choice in adults with good soft tissue quality who have not had previous infection (Manson *et. al.*, 1986). An additional criticism of PMMA is that it is an inert and a fixed substance that will not adapt to the changing cranial skeleton. This is particularly important if one is considering skeletal reconstruction in a growing child. Polymethylmethacrylate does not encourage bone incorporation or ingrowth, which makes it susceptible to infection (Gosain, 2002).

2.4.2.3.2 ***Silicone rubber***

Silicone rubbers are characterized by the presence of -Si-O-Si- bonds in the polymer backbone. It is a highly inert and flexible material and has found widespread use as joint prosthesis. Countemanche and Thompson (1968) reported the use of silicone rubbers (Silastics) for cranioplasty. Later on Chicarilli and Ariyan (1986) used silicone prosthesis in combination with split rib grafts for cranial repair. However, many serious complications were reported which made the silicone rubber unpopular among the neurosurgeons (Wright and Wilgis, 1986; Wang *et al.*, 2002).

2.4.2.3.3 ***Polyethylene***

Porous PE (Medpore; Porex Surgical) (Wellisz *et al.*, 1992; Wellisz, 1993; Couldwell *et al.*, 1994) is used in cranioplasty for repairing small to medium-sized cranial defects and correction of contour deformities. In clinical applications, it was found that the implant could be easily moulded and maintained. Thus Medpore offers a safe,

cosmetically equivalent alternative to standard acrylic cranioplasty while ease of implantation shortens operation time. The porous nature of the implant encourages osseointegration (Wellisz *et al.*, 1992, Odum *et al.*, 1998). This advantage is also a potential disadvantage if additional surgical access is needed over time. Another point of concern with regard to this material is its strength; as reported, this material cannot sustain blows and is easily broken. The limitation of this material to sustain weight or withstand trauma of even small proportions restricts the use of this material in many situations.

2.4.2.3.4 ***Polytetrafluoroethylene***

Polytetrafluoroethylene has been widely used in the facial plastic augmentation and reconstructive surgery. Expanded form of PTFE has been successfully used in duroplasty (Nagata *et al.*, 1999). However, only scanty reports on its use for cranial repair have been published in the literature (Zaborski and Szot, 1987). Recently, Grondahl *et al.*, (2003) attempted to induce calcium phosphate nucleation on the surface modified PTFE membranes so that it could be made bioactive. Studies carried out using simulated body fluid (SBF) for a period of four weeks showed that the modified PTFE could be a promising bioactive biomaterial for use in cranio-facial applications.

2.4.2.3.5 ***Biodegradable polymers***

Biodegradable polymers such as PLA, PGA and copolymers of PLA and PGA have been used in the reconstruction of craniofacial deformities (Eppley *et al.* 1997; Peltoniemi *et al.*, 1997; Wiltfang *et al.*, 1999; Imola *et al.*, 2001; Serlo *et al.*, 2001). These polymers are used mainly among very young or old population, where it was feared that the sharp metallic cranial plate edge might erode through the scalp. Table 2.6 lists some of the examples of the commercially available degradable cranioplastic implants.

Non-reinforced PLGA and PLLA implants are mechanically weak and brittle. Gosain *et al.*, (1998) studied the distractive and compressive forces (parallel to the plate) to failure in plate osteosyntheses in sheep cadaveric cranial bones. A distractive force of 270 N and a compressive force of 200 N broke the non-reinforced, stiff PLGA plate-screw fixation. In depth studies of the structure of these materials, led to the merging of self-reinforced (SR) technology to meet more demanding biomechanical conditions, e.g.,

in orthognatic surgery (Suuronen *et al.*, 1994; Fuente del Campo *et al.*, 1996; Haers and Sailer 1998; Haers *et al.*, 1998; Kallela *et al.*, 1998). Self-reinforced technique is based on reinforcing elements within the same material, which could lead to the manufacture of ultra-high strength implants. Self-reinforced PLGA implants have been used in paediatric craniofacial surgery (Peltoniemi, 2000).

Table 2.6 Commercially available cranioplastic implants (www.medcompare.com)

Trade name	Material	Description
Craniosorb	Primacryl	Absorbable Fixation System
Delta System	Tripolymer composed of poly l-lactide/d-lactide/glycolide in the ratio of 85/5/10.	Resorbable bone plates and screws fabricated from a unique tripolymer
Lactosorb®	Copolymer of 82 l-lactic acid and 18 glycolic acid.	Completely resorbable craniomaxillofacial fixation.
MacroPore ™	70:30 Poly(l-lactide-co-dl-lactide	Bioresorbable cranio-maxillofacial implant that retains 50% of its strength after 12 months and resorbs within 18-36 months.
Polymax	-	Resorbable cranial fixation system.

Biodegradability is quoted as the primary advantage of degradable devices as this saves the patient from undergoing a second surgical intervention for the removal of these devices. However, this advantage of biodegradable devices is of little value if the biocompatibility of the materials is questionable. Adverse tissue responses to fixation implants made of PGA and PLA have been reported in more than 15 clinical cases, the incidence varying from 2.0-46.7% (Bostman, 1993; Bostman and Pihlajamaki, 2000). The rapid release of acidic degradation products, leads to the accumulation of large quantities of glycolic acid/lactic acid monomers, which locally lower the pH and thus affect the tissue responses (Bostman, 1993). It has been reported that Lactosorb, a commercially available cranioplastic plate, when used in large configurations, could elicit osteolytic lesions due to the accumulation of acidic degradable products. Some investigators suggest that the implants made of degradable polymers are not safe for large complex or comminuted fractures (Tams *et al.*, 1995). Attempts were made to diminish the adverse effects caused due to the decrease in pH in the tissues adjacent to degrading biodegradable polymeric implants by the incorporation of alkaline salts within the polymer (Agrawal and Athanasiou, 1997). While the *in vitro* studies showed some

promising results (Agrawal and Athanasiou, 1997) complications were reported in *in vivo* studies (Schliephake and Kage, 2001).

2.4.2.4. Calcium phosphates

Studies demonstrating the safe use of HAP over the dura (Zide, 1987) popularized HAP among the neurosurgeons. Hydroxyapatite ceramic in the form of granules, buttons, plates, and blocks are used for rectifying skull defects (Yamashima, 1993; Dujovny *et al.,* 1997). In recent years, use of hydroxyapatite cement (HAC) has gained grounds (Kurashina *et al.*, 1998; Turk and Parhiscar, 2000; Johnson *et al.,* 2000; Magee *et al.,* 2004). The cement is prepared by mixing HAP with water so as to form a dense paste that sets in 15-30 minutes and isothermally converts *in vivo* to a microporous HAP implant. Hydroxyapatite cement facilitates contouring and is able to fit curves of the defect thus eliminating any spaces between the bone and the implant. The material is also highly osseo-conductive and readily osseo-integrated with the surrounding bone and hence finds use in a wide range of craniofacial applications.

While HAC provided handling and contouring comfort to the surgeons, it suffered from limitations too. It has been reported that when exposed to cerebrospinal fluid or blood, inadequate setting of cement occurs, resulting in the loss of its structural integrity (Constantino *et al.,* 2000). The development of fast setting hydroxyapatite cement (FSHAC) could circumvent the problems of standard HAC. Some application problems were, however, experienced with this material. It was found that in clinical setting the pulsations of the underlying brain and dura interfered with the crystallization of these cements, there by rendering their use in cranioplasty problematic (Losee *et al.,* 2003). Many clinicians have suggested interposing a synthetic resorbable plate or mesh between the dura and the cement. At the present time, however, little is known about the influence of such materials or their breakdown products on the fate of calcium phosphate cements. Hydroxyapatite cement also seems to induce what appears to be an immunoguided delayed inflammatory reaction that leads to thinning of the skin and exposure of the material, making secondary repair difficult (Moreira-Gonzalez *et al.,* 2003).

2.4.2.5. Composites

The use of composites in bone substitute applications has already been detailed in section 2.3.4. The concept of using composite material for rectifying cranial defects was

implemented in an effort for upgrading the traditionally used PMMA resins. The brittleness of PMMA was well known, and complications resulting from fractures were numerous (Pochon and Kloti, 1991; Gupta *et al.*, 1997; Meel, 2004). The use of a stainless steel wire mesh scaffold within the PMMA plate was introduced by Galicich and Hovind (1967) in an effort to reduce the fracture potential of acrylics. Later, titanium plates and meshes replaced the stainless steel in acrylic cranioplasty (Malis, 1989; Wong and Manson, 1994; Lara *et al.*, 1998). However, with these materials, it must be noted that the PMMA must be moulded above the titanium mesh at the surgical site, which because of the heat produced, toxic fumes and time spent during surgery, could increase the rate of complications (Agner *et al.*, 1997).

Titanium found use in supporting pre-formed HAP cranial prosthesis also (Ducic, 2002). Recently, Durham *et al.* (2003) reported the correction of large cranial defects (> 25 sq. cm) with tantalum mesh, and titanium mini plates in combination with HAC. This combination of materials provided internal structural support and increased stability of the construct.

Composites based on calcium phosphate ceramics (e.g. HAP and TCP) and polymer are of interest because, on one hand, they could improve the osteoconductive properties of the polymer component of such an implant and, on the other, they could provide better malleability for carving of the brittle ceramic part that otherwise is difficult to handle during adjustment to the individual shape of a defect.

Pompili *et al.*, (1998) described cranioplasty performed with a new osteoconductive osteoinducing HAP derived material. The material was termed Osprogel and consisted of calcium hydroxyapatite combined with synthetic, human bone-derived gelatin, glycerol, and water. The authors reported that Osprogel could be modeled onto the cranial defect intra-operatively and could induce osteogenesis when placed in contact with healthy cancellous bone, thus permitting the re-growth of nearly normal bone. The evaluation of the results, six months after surgery showed that Osprogel was washed out from the site of implantation and resorbed. It was concluded that the technique has to be refined in order to get good or excellent results.

Lin *et al.*, (1998) developed a malleable, biodegradable osteoconductive composite composed of TCP particles bound by gelatin, which is set by glutaraldehyde

mediated cross-linking. The composite was implanted into calvarial defect in rabbits. The authors reported the composite to be biocompatible, osteoconductive, and biodegradable, with progressive replacement of the composite by new bone, acellular matrix and bone-like material. Replacement of this composite by new bone is postulated to occur by a combination of osteoconduction and biodegradation. These results indicate that further experimental research to combine this malleable, biodegradable, osteoconductive composite with an osteoinductive agent such as bone morphogenetic protein, may generate new biomaterial for the full-thickness calvarial defect reconstruction.

Schliephake and Kage (2001) prepared solid composite implants of glass-ceramic/polylactic acid and implanted press-fit into parietal, full-thickness defects of the calvaria of adult rats. Histologic evaluation after 6, 13, 26 and 52 weeks of implantation indicated that the bone formed during initial stages had undergone resorption later on, so that bone repair after 52 weeks was not significantly enhanced. The study indicated that the balance between degradation and bone formation is delicate and that chemical events and cellular reaction during degradation may counteract complementary bone ingrowth.

Zanetti and Nassif (2003) reported the use of flexible composite sheets from PCL and HAP for the reconstruction of limited lateral skull base defects. Studies were carried out in seven patients. The defect was repaired with the new material and a connective tissue graft. None of the patients suffered from immediate side effects related to the implant or operation. The authors claim the preliminary results to be encouraging as the new material allows a minimally invasive approach to selected skull base defects.

2.5. SCOPE AND OBJECTIVES OF THE PRESENT STUDY

Although several attempts have been made to develop a material that could form an ideal seal for the defective skull, an ideal material has yet to be developed. Many of the currently used cranioplastic materials suffer either from application/handling difficulties or are not bioactive to facilitate bone bonding. The biodegradable implant materials have proved to be a bane in the long run because of their unpredictable degradation characteristics, for many of the bone substitute applications, especially cranioplasty. In this scenario, it would be attractive to develop a non-biodegradable, bioactive, and pliable material for cranioplasty. This thesis discusses the development of a composite material, fabricated by the incorporation of an osteoconductive bioceramic

HAP in a thermoplastic elastomer, ethylene vinyl acetate co-polymer (EVA). It has been already mentioned that HAP mimics the human bone with respect to its chemical composition and crystallographic structure. In the body, HAP performs as a bioactive material and promotes bone apposition to the surface rather than encouraging bone resorption (Jarcho, 1981). Hence, HAP was the natural choice when it came to the development of a bioactive and osteoconductive material for cranioplasty. Ethylene vinyl acetate co-polymer was combined with HAP to overcome the inherent limitations of HAP. Ethylene vinyl acetate co-polymer is a biocompatible polymer (Siegel and Langer, 1984; Shvarts *et al.,* 2002) that has been used in various applications like drug delivery, coatings of the Kirschner-wire used as intramedullary nails for fixing fractures in the bone (Wong *et al.,* 2003), coatings of intravascular stents (Pinchuk *et al.,* 2000) and pressure-sensitive adhesive tape for the damaged skin (Ohmori *et al.,* 2001). The thermoplastic-elastomeric and amorphous nature of EVA allows for the incorporation of high quantities of HAP without substantial loss of its ductility. Thus the combination of bioactive ceramic HAP and thermoplastic elastomer EVA could impart two distinctive advantages- (1) the presence of HAP improves the mechanical properties of the composite and also makes the composite bioactive, (2) presence of EVA would render the composite malleable and facilitate precise sculpting of the composite according to the defect formed/created in the skull. Thus fabrication of HAP-EVA composite by making use of suitable polymer processing techniques was the first objective of this study.

Characterizing the mechanical properties of implant materials has been and will continue to be an important step in implant design. Mechanical property evaluation forms the foundation for understanding the applicability of a specific material for use as an implant. Mechanical tests can be used to predict not only the failure thresholds for the implant but also the expected remodeling response of the bone once the implant has been placed *in situ* (Meaney, 1995). The evaluation of mechanical properties of HAP-EVA composites is the second objective of this study.

Critical biocompatibility evaluation is an essential step in the development of any material intended for biomedical applications. In essence, the biocompatibility tests should ensure, in so far as possible, the safety of the material. The material, when used in patients should not evoke any adverse or toxic stress to the patient. The overall aim is to provide the patient maximum benefit with minimum risk. Two selected formulations of

HAP-EVA composites were subjected to a battery of tests recognized internationally, based on the guidelines/protocols prepared by ISO-10993 to ensure the biocompatibility of the material. The composites were also implanted in the rabbit cranium for a period of 48 weeks to confirm the bone bonding ability. Thus the systematic biological evaluation of the HAP-EVA composites was yet another major objective of this study.

The final objective of this study was to device a cost-effective technique so that clinically significant three-dimensional silhouettes of HAP-EVA composites could be fabricated. A novel thermoforming technique, stamp forming, was employed to achieve this. Stamp forming is a very cost effective method that improves the performance/cost balance of reinforced polymeric composites via., high-speed manufacturing and shaping process (Breuer and Neitzel, 1996). The process was initially optimized with respect to a simple two-dimensional geometry. Three-dimensional stamp forming of the composites was carried out at the optimized conditions. The formed parts were analysed for uniformity in the wall thickness and also for the surface finish. The mechanism of deformation of the flat composite sheet into the hemispherical form was also elucidated.

CHAPTER 3

MATERIALS AND METHODS

3.1. RAW MATERIAL CHARACTERIZATION

Two grades of ethylene vinyl acetate co-polymers (EVA) and two grades of hydroxyapatite powders (HAP) were used. The polymers used were different with respect to the amount of vinyl acetate content and also with respect to the melt flow index (MFI). The hydroxyapatite powders used were different with respect to both the particle size and the surface morphology.

3.1.1. Ethylene vinyl acetate co-polymer

The polymer was procured from Shriswasan Chemicals (M) Ltd., Mumbai, India. The polymer was obtained in the form of cryogenically ground powder with particle size less than 300 μm. Two grades of EVA with different vinyl acetate content i.e., 18 and 28wt.% were chosen (Table 3.1.). The polymers were characterized by differential scanning caloriemetry (DSC), gel permeation chromatography (GPC), and thermogravimetric analysis (TGA).

Table 3.1. Properties of ethylene vinyl acetate co-polymers (EVA)

Polymer Grade	E18	E28
Vinyl acetate content, (wt.%)[#]	18	28
Melt flow index, {/g (10 min^{-1})}[#]	2	25
Density, g/cc[#]	0.93	0.95
Melting point, °C[#]	88	68
Molecular weight, $\overline{M}_w$ [Ψ]	Not determined	1, 16, 561

[#] Data taken from manufacturer's product data sheet; [Ψ]Data from GPC

3.1.1.1. Differential Scanning Caloriemetry

A DSC was used to measure the transitions in the polymers. The measurement was performed on DSC-2920 (TA instruments, USA), based on ASTM standards (ASTM E-1356, 1998). The test method involves continuously monitoring the differnce in heat flow into, or temperature between a reference material and a test material when they are heated and cooled at a controlled rate through the glass transition region of the test material and analyzing the resultant thermal curve to provide the glass transition temperature. A heating rate of 10°C/ min was employed and the material was scanned in the temperature range of -100°C to150°C.

3.1.1.2. Gel Permeation Chromatography

Gel Permeation Chromatography (GPC) is a macromolecular separation technique used to determine molecular weight and molecular weight distribution of polymers. The molecular mass of polymer matrix before and after processing was measured using GPC. The measurements were made using Waters 510 instrument (Milfore, USA) with tetrahydrofuran as the eluting solvent and polystyrene as the standard.

3.1.1.3. Thermogravimetric analysis

The degradation behaviour of the polymers was studied using a thermogravimetric analyzer. The analysis was conducted on SDT 2960 simultaneous DTA-TGA analyzer (TA instruments, USA). Here the weight percentage of the sample was measured continuously by heating the sample from room temperature to 800°C at a constant heating rate of 10°C/min.

3.1.2. Ultra high molecular weight polyethylene

Ultra high molecular weight polyethylene, procured from Solidur Plastics India Ltd, was used as the control material for the biocompatibility evaluation. The specifications of the polymer are given in Table 3.2.

Table 3.2. Properties of ultra high molecular weight polyethylene (UHMWPE)[#]

Parameter	
Density, g/cc	0.934
Tensile strength at break, (MPa)	48
Elongation at break, (%)	350
Young's Modulus, (MPa)	690

[#] Data taken from manufacturer's product data sheet

3.1.3. Polymethylmethacrylate

Cranioplastic grade PMMA was used as the control material for skull implantation studies in rabbits. The material was obtained from Codman Cranioplastic, De Puy International Ltd., England (Specifications given as addendum, section 9.1, in Page 163).

3.1.4. Hydroxyapatite

3.1.4.1. Synthesis of hydroxyapatite

Two grades of HAP (spray dried, H_s and freeze-dried, H_f) were used to prepare the composites. Both the grades were synthesized in the laboratory by a precipitation route involving ammoniated calcium nitrate and ammonium hydrogen phosphate solutions, following the procedure established by Varma *et al*, (1996). Initially, ammoniated hydrogen phosphate solution was added drop wise to ammoniated calcium nitrate solution, which was stirred constantly. The reaction was carried out at 80°C and at pH >10. After completion of addition, the reaction mixture was stirred for one hour at 80°C, and thereafter left unstirred for over 24 h. The gelatinous white precipitate was separated from the solution and washed to remove soluble by products. The washed precipitate was then converted into powder form. Two techniques of powder preparation were adopted - (1) freezing and drying technique and (2) spray drying technique. In the freezing and drying technique, the precipitated HAP was first froze to 0°C and subsequently dried in an air oven at 100°C for 24 h. The oven-dried HAP was ground to 125 μm or less in radius of secondary particles. In the spray drying technique, the

precipitated HAP was converted into slurry and spray dried in a laboratory size spray drier (Buchi Mini Spray Drier, B-181, Switzerland), with a maximum through put of dry air 35 m^3/h and at 90-92°C. The synthesis is schematically given in Figure 3.1.

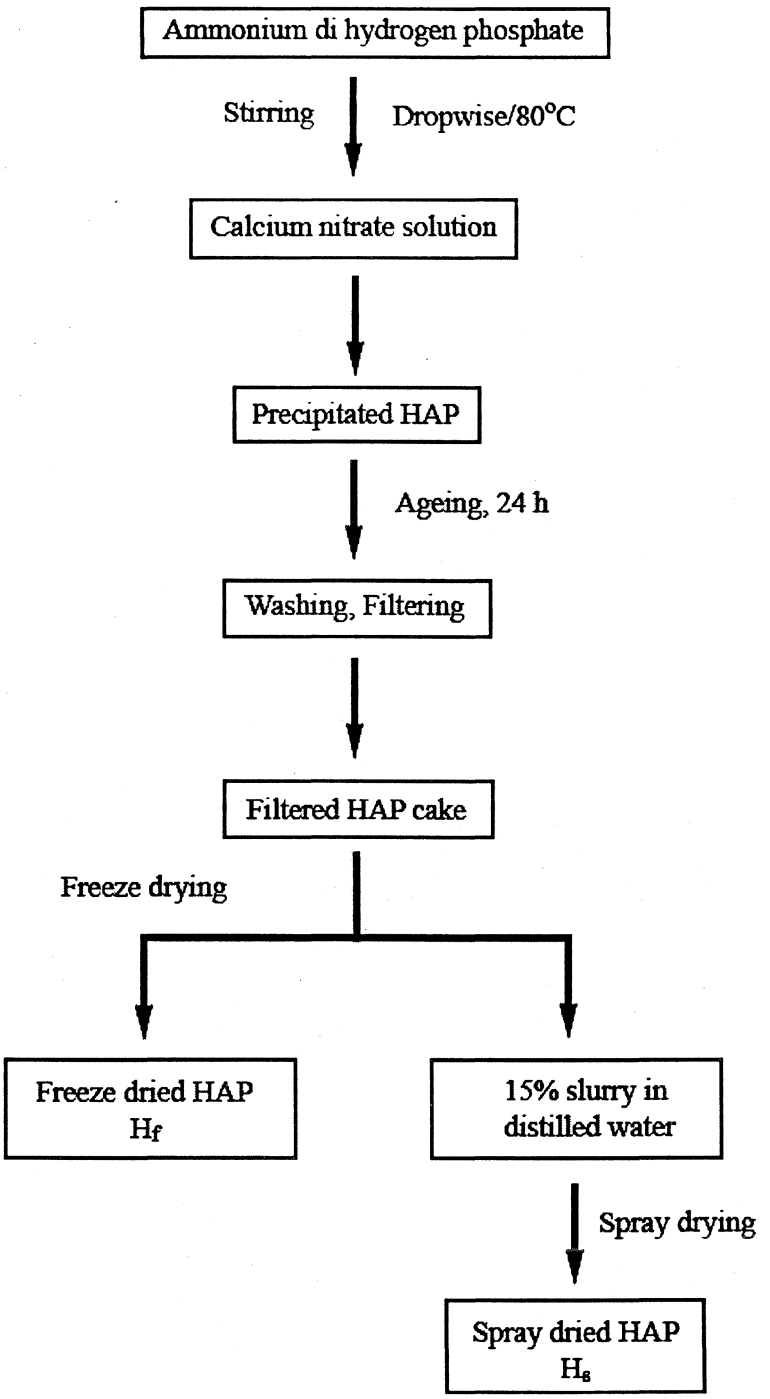

Figure 3.1. Schematic diagram showing synthesis of hydroxyapatite

The synthesized HAP powders were characterized for particle size distribution, surface morphology, phase consistency, chemical composition and biocompatibility.

3.1.4.2. Particle size distribution

The particle size analysis of HAP was carried out using a Malvern Mastersizer 2000 particle size analyzer (Malvern instruments, UK). A small amount of HAP powder was taken in a petridish and a suspension of HAP was prepared by adding few drops of dilute soap solution. The suspension thus prepared was added drop wise into the dispersant (water) where in the laser beam was passing through.

3.1.4.3. Surface morphology

The morphology of HAP powders was observed using a scanning electron microscope (JOEL JSM-5400, Japan). A small amount of powder was sprinkled on an adhesive tape pasted onto a stub. This was then sputter coated with gold and the images were taken.

3.1.4.4. Fourier Transform Infra-red spectroscopy

The Fourier Transform Infra-red (FTIR) spectroscopy data of HAP powders, calcined at 300°C for 3 h in a muffle furnace, were collected using a Nicolet Inc. (Madison, USA) model Impact 410 FTIR spectrophotometer.

3.1.4.5. Phase consistency

The phase consistency and crystallinity of the HAP powder was analyzed by X-ray diffraction technique. The measurement was performed on an X-ray powder diffractometer (Siemens D5005, Germany) with computer data acquisition facility. The powder was scanned in the angle range 20 to 50° at a speed of 0.1°. The diffraction data was compared with Joint Committee for Powder Diffraction Standards (JCPDS) Data Sheet for HAP (9-432).

3.1.4.6. Chemical analysis

The calcium to phosphorous (Ca/P) mole ratio was determined by chemical techniques. The calcium content was estimated by substitution titration method using 1,2-diaminoethanetetra-acetic acid (EDTA) solution. Phosphovanadomolybdate method was used to determine the phosphorous content. The bright yellow phosphovandomolybdate

complex formed between the phosphate, ammonium vanadate and ammonium molybdate was estimated spectrophotometrically in the absorbance range 460-480 nm (Mendham *et al.*, 2002).

3.2. PREPARATION OF THE COMPOSITES

The cryogenically ground EVA powder was blended with pre-dried HAP powder (dried at 100°C for 2 h) in a domestic blender for about 15 min. The HAP-EVA composites containing 10, 20, 30, 40, and 50vol.% of HAP were prepared using E28 polymer matrix. Composites with 40vol.% of HAP were prepared from E18 polymer matrix. The blended powder was then melt mixed in a torque rheometer (Polylab Rheomix 600, Haake, Germany) attached with a 120 c.c. mixing chamber. Counter rotating cam rotors with rotor speed of 40rpm was employed through out the compounding process. The density of E18, and E28 were 0.93, and 0.95 g/cc respectively. Theoretical density of 3.16 g/cc was assumed for HAP. These densities were used to calculate the weight required to produce the series of composites.

3.2.1. Torque rheometer

The torque rheometer consists of horizontally mounted, heavy-duty motor drive together with a torque sensor. The basic components of the rheometer are a motor, a torque sensor and a mixing head. Within the mixing head are the rotors that rotate at different speeds within adjoining circular cavities. The mixing head consists of a steel cell in which the sample fills a 'bowl' consisting of two adjoining cylindrical chambers. This cell may be heated either by circulating thermal fluid or by electrical heating elements. Once mixing is begun considerable dissipative heat can be generated, and it becomes necessary to remove the heat. Thermocouples are mounted in the mixing head to measure the temperature of the melt. While carrying out a processability test, the torque required to stir a molten polymer in the mixing chamber is measured as a function of time. The Rheomix 600 is the standard internal, intensive mixer used for a wide range of applications, particularly for testing thermoplastics. The three section mixing chamber is electrically heated and air cooled, thus enabling simple and rapid testing and cleaning.

The different compositions of the material produced along with their designations are given in Table 3.3.

Table 3.3. Summary of test materials of HAP/EVA composites

Material code	Polymer matrix (vol.%)		HAP (vol.%) *	
	E18	E28	H_f	H_s
E18	100	-	-	-
E28	-	100	-	-
E18H_f40	60	-	40	-
E18H_s40	60	-	-	40
E28H_f10	-	90	10	-
E28H_f20	-	80	20	-
E28H_f30	-	70	30	-
E28H_f40	-	60	40	-
E28H_f50	-	50	50	-
E28H_s10	-	90	-	10
E28H_s20	-	80	-	20
E28H_s30	-	70	-	30
E28H_s40	-	60	-	40
E28H_s50	-	50	-	50

The composites fabricated from E18 were processed at 140°C while those fabricated from E28 were processed at 120°C. The rotor speed used was 40rpm and the mixing time was 6 min. At the end of 6 min, the HAP-EVA composites were dumped out of the internal mixer and compression moulded in a laboratory model hydraulic press (Santhosh Industries, Mumbai). The temperature and pressure used for the compression moulding varied from 120-150°C and 20-100 kg/sq. cm, respectively, depending upon the volume percentage of HAP loaded in the composite material.

3.3. CHARACTERIZATION OF HAP-EVA COMPOSITES

3.3.1. Filler distribution studies

The dispersion and distribution of HAP particles in the EVA matrix were investigated for E28H_s40 and E28H_f40 composites. The compression-moulded E28H_s40 was microtomed and observed under transmission light microscope (Leitz, Germany). The composite E28H_f40 was fractured after immersing in liquid nitrogen for sufficient time. The fractured surface was sputter coated with gold and SEM examination was performed.

3.3.2. Determination of HAP content

The ash content of the various compression-moulded composites was measured to quantify the amount of HAP in the composites. Ashing was carried out for all the HAP-

EVA volume fractions for the two different particle sizes. The ashing process was undertaken at 700°C in a muffle furnace for 24 h. The specimen in flake forms were cut from random partes of moulded composite plates and kept in dried and preweighed alumina crucibles. After ashing, the specimens were cooled in a desiccator. All weight measruments were carried out at room temperature in an electronic balance (LA 230S, Sartorius, Germany) having accuracy of ± 0.1 mg. Ash contents were calculated as the percentage of the original specimen weight. The amount of HAP content in the composites was also confirmed from the density values of the composites (Refer Addendum; Section 9.2, Page 163)

3.3.3. Mechanical property evaluation of HAP-EVA composites

3.3.3.1. Tensile properties

The tensile mechanical properties were measured using universal testing machine (Zwick 1485, Germany) at 22 ± 2°C. The test was conducted according to the ISO 527-1: 1993. The specimen dimensions were in accordance with ISO 527 (type A2). The strain rate employed for testing was 1 min^{-1}. Mean values were derived from tests performed on six dumbbell specimens.

3.3.3.2. Flexural properties

The flexural property analysis of the composite was carried out on a universal testing machine (Zwick 1485, Germany). The three point bending method was employed for this purpose. The distance between supports (span length) was 32 mm maintaining ASTM D790-97 requirement. Rectangular specimens of dimensions (44 mm x 12.7 mm) were punched from compression moulded composite plaques of 2 mm thickness. The specimens were lightly polished using 1000-grade silicon paper, followed by 4000 grade paper to improve the surface finish. A crosshead speed of 1 mm/min was employed for the testing. Mean values were derived from tests performed on six rectangular bars.

3.3.3.3. Impact properties

Charpy impact tests on un-notched specimens were conducted on Impact Tester (Ceast 6545, Italy) using a 158 J pendulum as per ISO 179-1, 2000. The specimen type and specimen dimensions are given in Table 3.4. The span length employed was 60 ± 0.5 mm. At least six polished specimens were used for testing each composition of the composite material.

Table 3.4. Specimen type and specimen dimensions used for Charpy impact test.

Specimen type	Blow direction	Dimensions in mm		
1	Edgewise	l = 80 ± 2	b = 10 ± 2	h = 4 ± 2

3.3.3.4. Dynamic mechanical thermal analysis

The composites E28H$_s$40, E28H$_f$40, and unfilled E28 were sectioned into rectangular bars of dimensions (6 mm x 2 mm x 1 mm). The specimens were polished as mentioned in section 3.3.3.2. Analyses were carried out using 150N Gabo Qualimeter, Dynamic Mechanical Thermal Analyzer (Ahlden, Germany). The specimens were subjected to oscillating tensile loading using temperature scan mode as per the conditions given in Table 3.5.

Table 3.5. Conditions applied in dynamic mechanical thermal analysis

Parameters	Conditions
Temperature range	-80 to 80°C
Heating rate	1°C/min
Static Force	2 N
Dynamic Force	1N
Frequency	10 Hz

3.3.4. Fractography

The tensile fracture surfaces of the composite samples were examined in a JOEL JSM-5400 scanning electron microscope at various magnifications.

3.3.5. Biological Evaluation

3.3.5.1. *In vitro* cell culture cytotoxicity studies

In vitro cell culture cytotoxicity of E28H$_s$50 and E28H$_s$40 was assessed as per ISO 10993-5 (1999), using L929 (mouse fibroblast subcutaneous connective tissue) cell line procured from National Centre for Cell Sciences, Pune, India. The cells were maintained in Rosewell Park Memorial Institute (RPMI) 1640 (Himedia, Pune, India) medium supplemented with 10% foetal bovine serum (Sigma, USA) and 100 IU / ml pencillium and 100 µg / ml streptomycine (medical grade). The culture was incubated at 37 ± 2°C in a humidified atmosphere containing 5% carbondioxide with a medium change at an interval of 3 days.

3.3.5.1.1 ***Cytotoxicity – Direct contact test.***

Cytotoxicity of E28H$_s$50 and E28H$_s$40 by direct contact method was evaluated as per ISO 10993-5 (1999). High-density polyethylene was taken as the negative control and organotin stabilized polyvinyl chloride was used as the positive control and the results were compared. The test is briefly summarized below. A confluent monolayer of L929 mammalian fibroblast cell lines was prepared in a cell culture plate. The culture was incubated as per the conditions mentioned in 3.3.5.1 and examined under a light microscope (Leica DMIL, Germany). The culture medium was removed and replaced with fresh culture medium. Specimens of negative or positive controls and the test article are carefully placed in individually prepared cultures and incubated under the same conditions as in 3.3.5.1. It has to be ensured that the specimen covers approximately one-tenth of the cell layer surface. The culture medium and the specimen were removed and the cell cytotoxicity is evaluated qualitatively. The qualitative evaluation of cytotoxicity involves examining the cells microscopically to assess for changes in general morphology, vacuolization, detachment, cell lysis and membrane. The change from normal cell morphology is recorded as none, slight, moderate and severe, depending upon the extent of cell damage.

3.3.5.1.2 ***Cytotoxicity – Test on extract***

Cytotoxicity of E28H$_s$50 and E28H$_s$40 was also evaluated by test on extract as per ISO 10993-5 (1999). Extracts were prepared from the material to simulate the clinical use conditions so as to define the potential toxicological hazard without causing significant changes such as fusion or melting of the material pieces, or alter the chemical structure. The material extracts were prepared by incubating the samples in the culture medium at 37 ± 2°C for 24 h. Phenol and tissue culture grade polystyrene (TCPS) were used as the positive and negative controls, respectively. Culture medium from confluent cells was replaced with material extracts and cytotoxicity was assessed qualitatively after 24 h.

3.3.5.2. Intracutaneous irritation

Intracutaneous irritation study was carried out, to evaluate the local responses to the extracts of the composite material under test following intracutaneous injection into rabbit. The test was carried out in accordance with the procedure described in United States Pharmacopoeia (USP XXIII, 1995) and has been described below briefly.

Adult albino rabbits of either sex, with body weight not less than 2 kg, were used for the study. The animals for the study were prepared by clipping the fur on the dorsal side, close to the skin. Extracts of the material were prepared both in normal saline and cotton-seed oil as per USP. A 0.2 ml each of saline extract of the composite was injected at five anterior sites on the left side of each rabbit (Figure 3.2). Similarly, 0.2 ml each of saline control was injected at five posterior sites on the same side of each rabbit. The above procedure was repeated for cotton-seed oil (CSO) extracts of the composites and control solutions on the right side of each rabbit. The sites were then evaluated for skin reactions immediately and at 24, 48, and 72 h following the injection. Toxicity associated symptoms such as erythema, and oedema at 24, 48, and 72 h were recorded and the average irritation score was calculated.

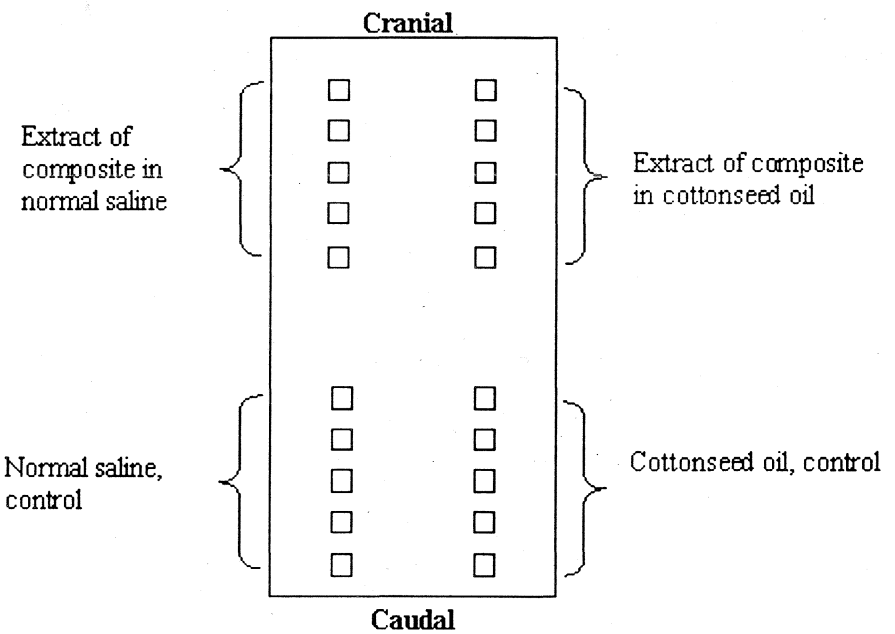

Figure 3.2 Arrangement of injection sites for the intracutaneous irritation studies

3.3.5.3. Systemic toxicity

Systemic toxicity of the material was assessed by evaluation of the systemic response of mice following an intravenous injection of normal saline extract of the composite material. This test was carried out according to the ISO 10993-11 (1993). A brief description of the test is given below.

Initially, extracts were prepared from sheets of the E28H$_s$40 composite material. Replicates of 60 sq. cm of the composite sample were extracted using 20 ml of normal saline at 37 ± 2°C, for an extraction period of 72 h. At the end of the extraction period the

test sample was removed from the extraction media. Aliquot of both extracts (test sample and control) was taken to check the pH. Twenty healthy Swiss albino mice of either sex, with body weight in the range 17.3-23.5 g were randomly assigned into two groups of five rabbits each. Each animal in accordance with its grouping was injected intravenously with, either the test sample extract or control extract, at a dose of 50 ml/kg body weight and observed for any adverse effects, immediately after injection and at 4, 24, 48, and 72 h after injection. The change in animal body weight was noted daily.

3.3.5.4. Closed patch sensitization

Closed patch sensitization test was carried out in guinea pigs to determine the potential of the composite material to produce skin sensitization. The test was done in accordance with ISO 10993-10 (1995) and is described briefly.

Composite sheets of E28H_s40 having dimensions 25 mm x 25 mm x 1 mm were used for testing the sensitivity of the material to the guinea pig skin. Four-ply gauze was used as the control material. A total of fifteen Hartley strain Guinea pigs, weighing between 300-500 g of either sex were selected for the experiment. Prior to each application period, the fur at the dorsal area on either sides of the vertebral column of each animal was clipped. The test was carried out in two phases – an induction phase followed by the challenge phase. In the induction phase the skin was lightly swabbed using 70% alcohol and air-dried. The composite sheet was moistened with physiological saline and applied topically on the clipped upper back region of 10 animals (test animals). Similarly moistened four-ply gauze was topically applied as control to other 5 animals. This was then covered with occlusive dressings. The occlusive dressings, from the test as well as the control, were removed after 6 h. The reaction at the site of application was observed after 24, 48, and 72 h for the evidence of any erythema or oedema. The procedure was repeated at weekly intervals for three weeks.

Fourteen days after the last application (induction period) all the test and control material were challenged with the test material. For this, the hair on the animal's flank area (untested area) was clipped and lightly swabbed with 70% alcohol and the moistened test material was topically applied. The challenge area was observed at 24 and 48 h for the evidence of any skin reaction such as erythema or oedema.

3.3.5.5. Implantation

3.3.5.5.1 Implantation in muscle

Twelve healthy New Zealand white rabbits, with body weight in the range 2.5-3kg were assigned into 6 groups of two rabbits each. The rabbits were anesthetized with xylazine (2 mg/kg) and ketamine hydrochloride injection IP (50 mg/kg) intramuscularly. The site of implantation was paravertebral muscle. The fur at the surgical site was clipped closely to the skin and swabbed with a surgical disinfectant. Three strips of the test sample E28H_s40, and one strip of the control sample, UHMWPE, each with dimensions 10 mm x 1 mm x 1 mm, were implanted along one side (left) of the spine, approximately 50 mm from the midline and parallel to the spinal column, and about 25 mm from each other. Similarly, three strips of test sample E28H_s50 and one strip of control sample, were implanted in the contra lateral muscle of each animal (Figure 3.3). Implantations were done using a sterile stylet with needle. Animals were housed in individual cages. Food and water were provided *ad libitum*. Animals were sacrificed at the end of 4, 12 and 24 weeks following implantation. The composite samples as well as the control samples were retrieved with their surrounding skeletal muscle.

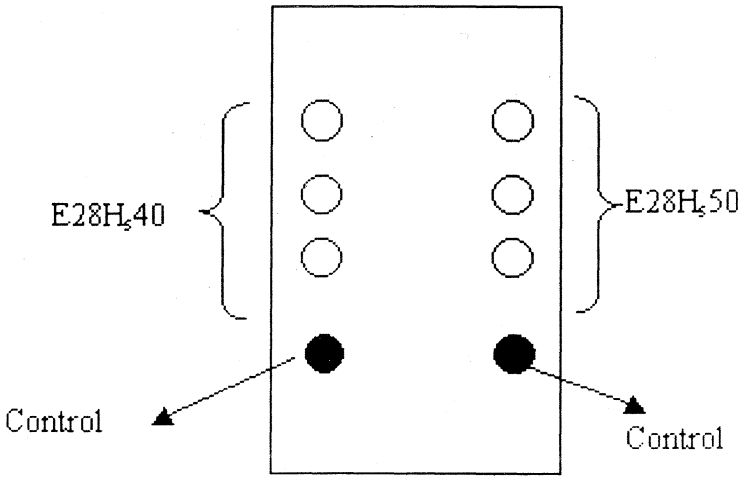

Figure 3.3. Arrangement of the test and control samples for the intramuscular implantation studies

The retrieved implanted samples with the surrounding muscle tissue were fixed immediately in 10% buffered formalin for 24 h. Following fixation, the samples along with the surrounding tissues were dehydrated in graded alcohol from 50 to 100%, cleared in chloroform, impregnated and embedded in paraffin wax. Multiple 5 μm thick sections were cut on an automatic rotary microtome (Leitz, Germany), stained with Harry's

heamotoxylin and eosin and examined under light microscope (Nikon Optiphot model XF-21, Japan). A semi-quantitative histological analysis of the processed samples was carried out and the photomicrographs of the most representative areas depicting the material-related changes were taken.

3.3.5.5.2 ***Implantation studies in rabbit cranium (cranioplasty)***

The surgical experiments were performed on eight adult New Zealand white rabbits (average weight 2.5-3 kg). The animals were divided into three groups – the experimental design of implantation is given in Table 3.6.

Table 3.6. Experimental design for cranioplasty

Group	Period of implantation, weeks	Animal number
I	Twelve	Two
II	Twenty four	Two
III	Forty eight	Four

For the implant placement, the animals were first premedicated with atropine sulphate-diazepam and anesthesia induced by xylazine-ketamine. All the injections were given intramuscularly. The bilateral linear fronto-parietal skin incision was made, skin retracted and two trephine-drilled holes of 10 mm diameter were prepared (Figure 3.4).

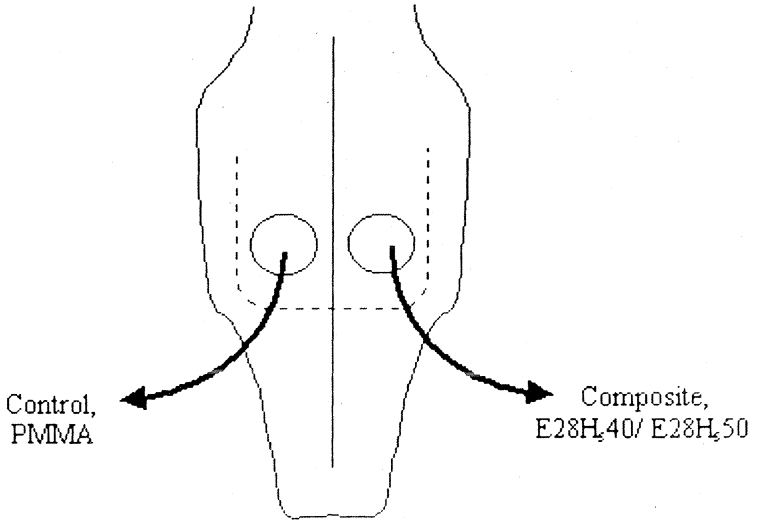

Figure 3.4. Arrangement of the test and control samples in the rabbit cranium

The composite material was placed in the left hole and the control material in the right. The samples were placed press fit in the defect created and the wound closed in layers using 3/0 silk (Figure 3.5 a–e). Then a sterile dressing was applied over the wound.

The animals were observed for any adverse clinical neurological symptoms during the study. At the end of the observation periods (12, 24, and 48 weeks post implantation), the animals were euthanized with excess dose of thiopentone sodium. The composite materials as well as the control samples were retrieved with their surrounding bone and adjacent soft tissues. The retrieved samples with their surrounding bone and soft tissues were immediately fixed in 10% buffered formalin, dehydrated, and embedded in PMMA. Un-decalcified sections (thickness 300 μm) of embedded specimen were cut with a diamond edge blade in a rotating saw (Buehler Isomet 2000, Germany). The sections were stained with stevenel's blue/toulidene blue and observed under transmitted light microscope (Nikon Optiphot model XF-21, Japan).

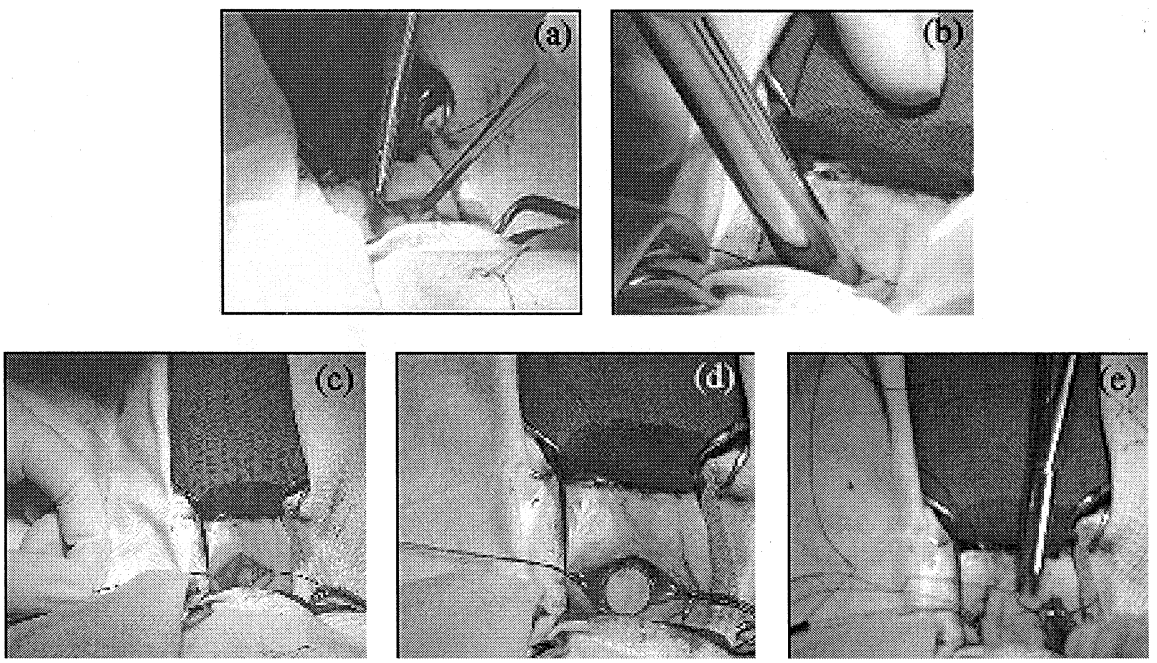

Figure 3.5. Cranioplasty in rabbits. (a) Skin incision; (b) Triphening; (c) Defect created with dura intact; (d) Material press fit in the defect; (e) Skin suturing after implantation.

3.4. STAMP FORMING OF HAP-EVA COMPOSITES INTO CLINICALLY SIGNIFICANT SHAPES

3.4.1. Stamp forming equipment

3.4.1.1. Forming press

Figure 3.6 shows the photograph of the stamp forming hydraulic press (HY-Power OP 2MI-TR8-115/30, Italy) used for the study. The press has two working strokes, i.e. an opening/closing and a compression stroke, and it can build up to a maximum load of 1 kN in the opening/closing stoke and 80 kN in the compression stroke through a hydraulic

cylinder. Further, it allows opening and closing velocities of 70-250 mm/s. The characteristic of the press is that the mould closes rapidly after the preheated laminate is inserted, and then it moves together slowly in the compression stroke to build up a higher pressure and to promote consolidation of the material in the mould.

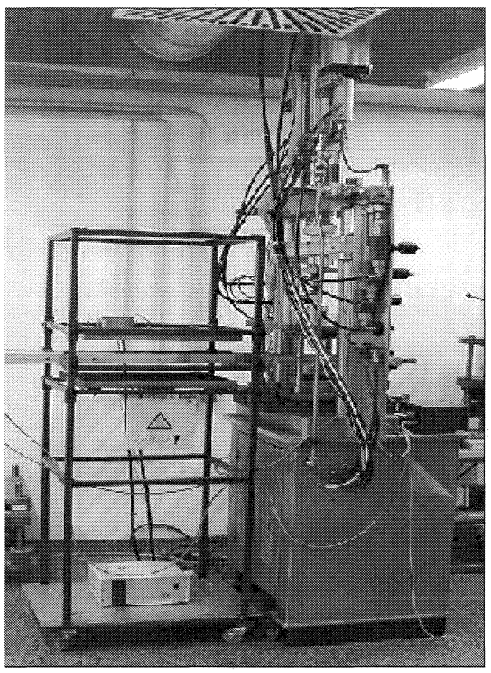

Figure 3.6. Photograph of the stamp forming hydraulic press

3.4.1.2. Forming moulds

The photograph of the right angle tool V-mould used for the two dimensional forming is given in Figure 3.7.

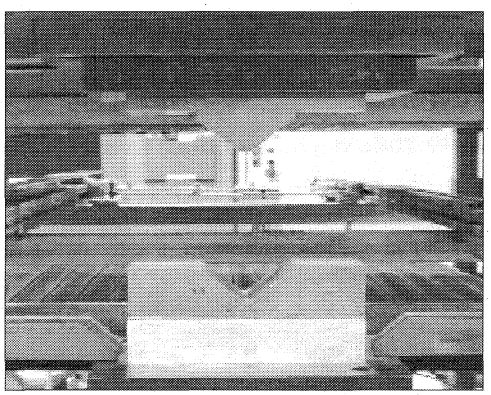

Figure 3.7. Photograph of the right angle V-tool used for two-dimensional forming.

The tool had fixed radius of 5 mm and was so designed that there was a uniform gap of 2.3 mm between the male and the female part, which is equivalent to the thickness of the compression moulded composite sheet. However, no measures were taken to prevent the mould from closing beyond this point.

The geometry of the three-dimensional hemisphere mould is given in Figure 3.8. The male half consists of a central forming stamper. The female half is a single piece containing a hemisphere or a segment of a half-sphere. The hemisphere stamper has a radius of 27.7 mm and the female mould has a radius of 30 mm, so that there exists a gap of 2.3 mm between the male and female part.

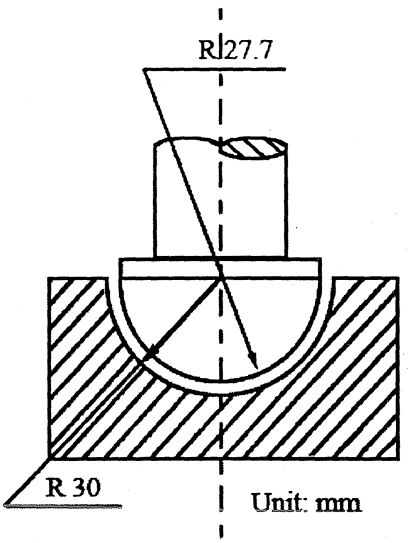

Figure 3.8. Geometrical details of the three-dimensional hemispherical mould.

3.4.2. Stamp forming procedure

3.4.2.1. V-bending

Due to the complexity of 3-D deformation of a flat composite sheet, it is very difficult to evaluate a suitable stamping temperature in relation to the formed part quality. Therefore, a 2-D stamp forming process, e.g., forming a right angle V-bend sample was used at first to study the influence of stamping temperature on part quality. The composite sheets of designations E28H_s40, E28H_f40, E18H_s40, and E18H_f40 were used as the feed materials. The thickness of all the composite sheets used for the study was 2.3 mm. Rectangular composite strips of dimensions 130 mm x 30 mm were cut from the compression moulded plaques and used for the forming operation. In order to measure the temperature profile of the sheets during forming, a thermocouple attached to a digital temperature display was embedded. This assembly was then placed in a convection oven and the specimen was heated to temperature 20-30°C above the melting point of the EVA matrix, after which it was removed from the air oven and positioned upon the female die

of the right angle V-mould. The sheet was then stamped by the male punch into the female die to conform to the geometry of the V-mould. During stamping, the sheet was pressed for about 40 s and cooled by the cold mould under pressure down to a temperature below the melting temperature of the polymer matrix. Once the material had completely cooled, the punch was withdrawn. Upon removal from the forming system, the parts had a surface temperature of about 30-40°C.

3.4.2.2. Hemisphere forming

The composite material was formed into a dome using a hemisphere mould. Composite plates of dimensions 130 mm x 130 mm and thickness 2.3 mm were used for the forming purpose. A thermocouple was embedded in the specimen and the whole assembly was placed in a convection oven to pre-heat the specimen. The assembly was removed from the oven and placed on the female mould, once the desired temperature was reached, where it was formed into a dome by the male hemisphere mould into the female mould. The male mould was withdrawn after the forming was completed and the formed composite specimen was removed. The three dimensional forming was carried out at the optimised conditions obtained from the two-dimensional forming technique.

3.4.3. Evaluation of stamp forming performance

The stamp forming performance is measured by the degree to which a material may be successfully formed. In the two-dimensional forming, the stamp forming performance was accessed in terms of (1) part thickness distribution along the formed bend, and (2) shape conformance ($\Delta\theta$).

3.4.3.1. Two dimensional contour (V-bending)

3.4.3.1.1 Part thickness

The uniformity in part thickness of the stamped bend was evaluated by measuring the thickness at various positions of the formed bend using a micrometer. All the measurements were made along the centerline illustrated in Figure 3.9 (a & b).

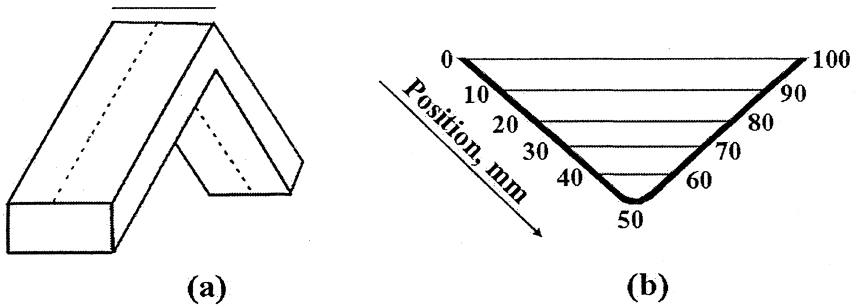

Figure 3.9. (a) Schematic diagram of the bend with the axis marked (b) the various positions on the bend at which the thickness was measured.

3.4.3.1.2 ***Shape conformance***

For single-curvature V-bending, the part quality is assessed in terms of shape conformance, which is the deviation angle ($\Delta\theta$), i.e., the angle of deviation of the formed bend from that of the mould. The final part angle of the formed bends was measured and the deviation in angle was calculated. The nature of angle of deviation depends on whether the specimen springs back or forward.

3.4.3.2. Three-dimensional contour (hemisphere forming)

3.4.3.2.1 ***Part thickness***

The formed prototypes from representative samples were cut into small pieces and their thickness was measured with a micrometer. The actual thickness variation along the formed area was thus measured.

3.4.3.2.2 ***Surface topography***

The representative samples were cut from the (1) apex and (2) sidewalls of the formed hemispheres (Figure 3.10), sputter coated with gold and the surface topography was examined using SEM.

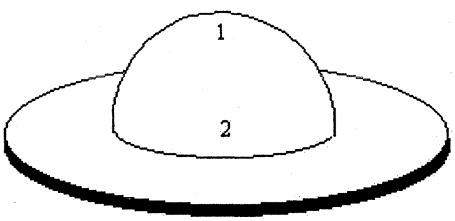

Figure 3.10. Schematic representation of formed hemisphere. The samples for surface topographic studies were cut from (1) the apex and (2) the sidewalls of the formed hemisphere.

3.4.3.2.3 ***Surface roughness measurements***

Surface roughness measurements were carried out using non-contact laser profilometry. A laser profilometer uses an infrared light from a semiconductor laser focused on the surface by an objective lens. The reflected light by the object surface is directed to a beam splitter and is imaged as a pair of spots onto an arrangement of photodiodes. When the objective lens is exactly at its focal distance from the surface, both diodes are illuminated equally. The changing illumination of the photodiode is translated into amplitude parameters, which measure the surface roughness, such as R_a, (the arithmetic average of the absolute values of all points of the profile), R_q (the root-mean-square of the values of all points) and R_z, (the average value of the absolute heights of the five highest peaks and the five depths of the deepest valleys). The working principle of the laser profilometer is illustrated in Figure 3.11.

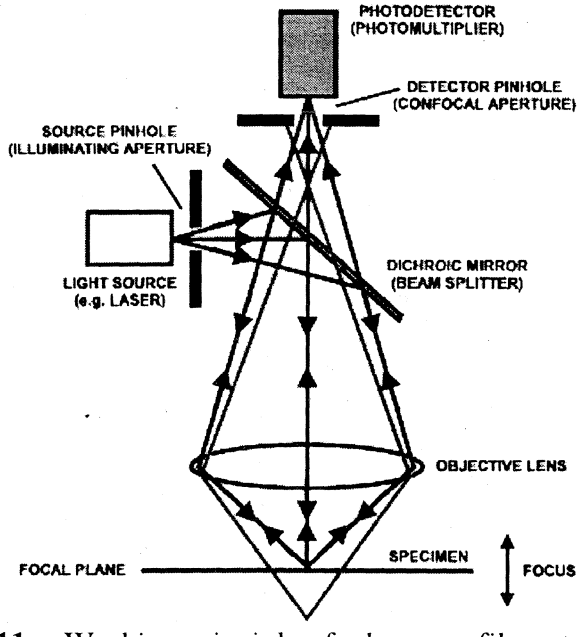

Figure 3.11. Working principle of a laser profilometer

The laser profilometer (UBM Messtechnik GmbH, Etllingen, Germany) used for the study had a light spot diameter of 1 μm. Area scans of outer surface of the representative samples of the composites (15 mm x 10 mm), cut from (1) the apex and (2) the side-wall nearer to the rim (Figure 3.10) of the formed hemisphere, were performed. The traverse lengths were 4 mm in the X-direction and 4 mm in the Y-direction, with a resolution of 200 points/mm in the X and Y directions. The roughness parameters such as R_s, R_q and R_z were calculated.

CHAPTER 4

PREPARATION OF HAP-EVA COMPOSITES

4.1. RAW MATERIALS CHARACTERIZATION

4.1.1. Ethylene vinyl acetate co-polymers

The results of DSC and GPC analysis of unfilled EVA along with some of the manufacturer's data are already given in Table 3.1

4.1.1.1. *In vitro* cell culture cytotoxity

Figure 4.1 (a) shows the optical micrograph of the L929 cells in direct contact with E28. The material did not show any cytotoxic response while in direct contact with the L929 cells for 24 h. The cells showed normal morphology when compared to the negative control (Figure 4.1 b & c). The results indicated that E28 is non-cytotoxic to mouse fibroblast cell lines and hence can be considered suitable for applications in living system.

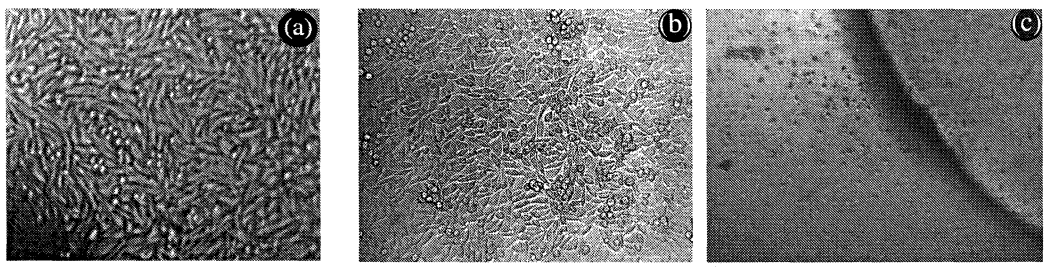

Figure 4.1. L929 cells incubated with (a) E28; (b) L929 cells incubated with negative control and (c) L929 cells incubated with positive control over 24 h.

4.1.2. Ultra high molecular weight polyethylene

The polymer was used as received. The specifications of the polymer as per manufacturer's data are given in Table 3.2.

4.1.3. Hydroxyapatite

4.1.3.1. Particle size analysis

Table 4.1. gives the results of the particle size analysis of the hydroxyapatites synthesized.

Table 4.1. Physical properties of synthesized hydroxyapatite powders

Material code	Specific surface area, $m^2 g^{-1}$	Particle size, μm		
		$d_{0.1}$	$d_{0.5}$	$d_{0.9}$
H_s	1.392	2.2	5.8	14.0
H_f	0.418	7.2	49.2	121.1

The particle size distributions of the two grades of HAP are given in Figure 4.2 (a & b). Figure 4.2 (a) gives the particle size distribution of the spray-dried HAP powder (H_s). The figure shows that the particulate H_s exhibited monomodal size distribution, with an average particle size of 5.8 μm. The freeze-dried HAP (H_f) also depicted monomodal size distribution (Figure 4.2 b). The average particle size was found to be 49.2 μm.

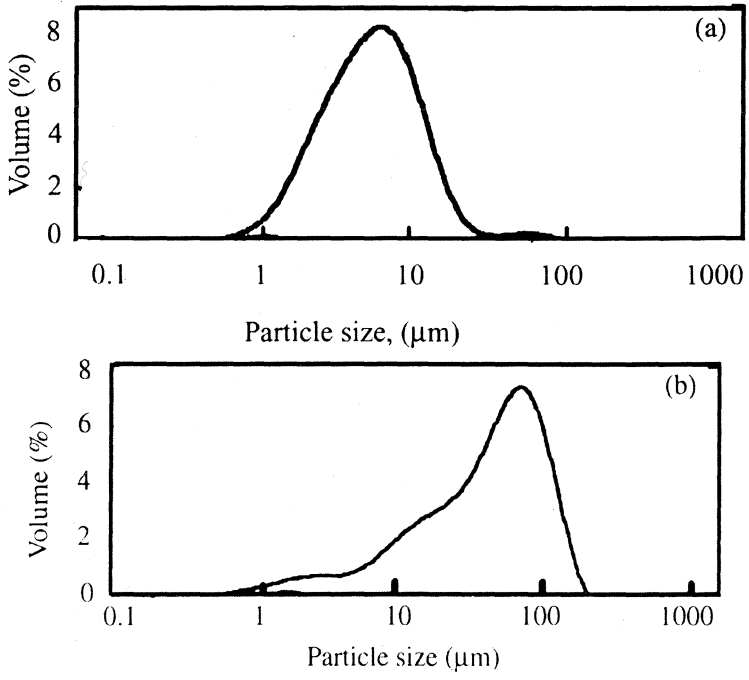

Figure 4.2. Particle size distribution curve of (a) spray dried and (b) freeze dried hydroxyapatite powder

4.1.3.2. Surface morphology

Figure 4.3. (a & b) gives the scanning electron micrographs of the spray dried and freeze-dried HAP powders. The spray dried powder had spherical shape. The freeze-dried powder on the other hand was irregular in shape and was found as agglomerates of sub micron HAP crystallites.

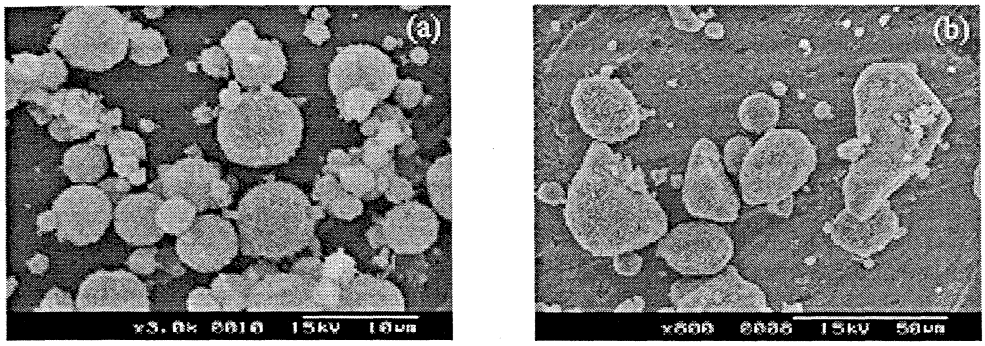

Figure 4.3. Scanning electron micrograph of (a) spray dried and (b) freeze dried hydroxyapatite powder

4.1.3.3. Phase consistency

Figure 4.4 (a & b) shows the XRD patterns of the spray dried and freeze dried HAP powders.

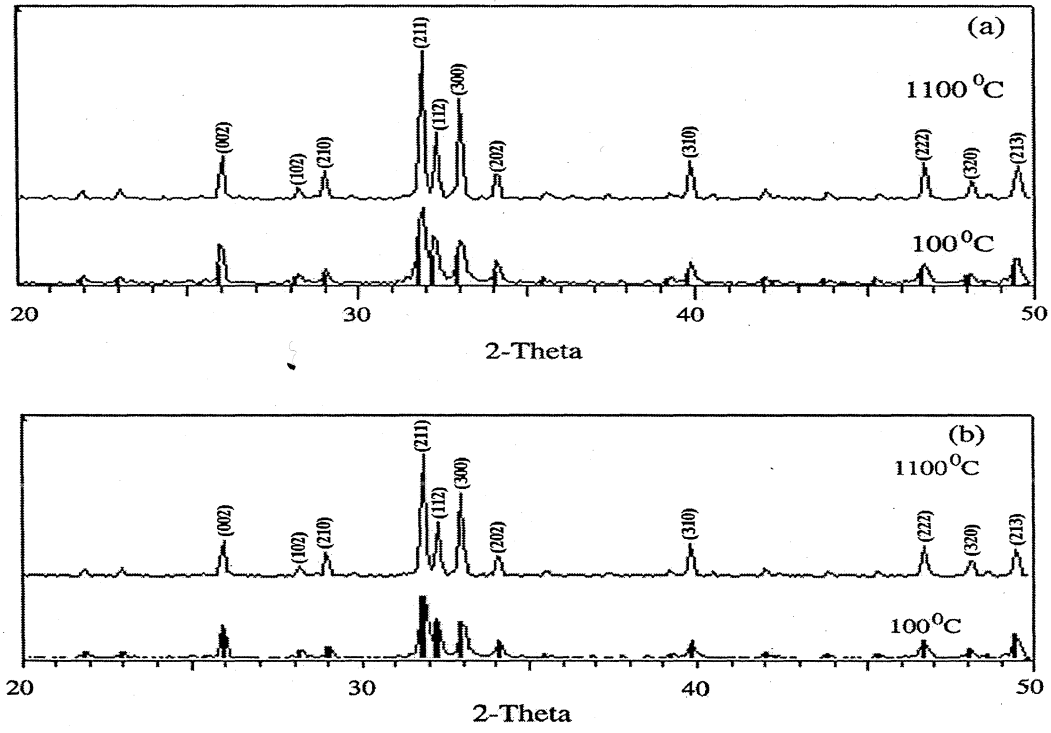

Figure 4.4. XRD patterns of the (a) spray dried and (b) freeze dried hydroxyapatite powders dried at 100 °C and sintered at 1100 °C.

The diffraction data of both spray dried and freeze dried HAP powders matched with the standard hydroxyapatite phase. It is important to note that almost all the peaks of the synthesized HAP closely match with the diffraction data obtained from Joint Committee for Powder Diffraction standards (JCPDS) data sheet for HAP (9-432) {marked as thick black lines in Figure 4.4 (a & b)}. The narrow half-width of the diffraction peaks indicate that the powder is well crystallized.

4.1.3.4. Chemical analysis

The calcium to phosphorous (Ca/P) mole ratios of H_f and H_s are given in Table 4.2. Both the HAP powders synthesized had the Ca/P molar ratio close to the theoretical stoichiometric ratio (1.67).

Table 4.2. Compositions of the synthesized hydroxyapatite

Material code	Calcium (mol%)	Phosphate (mol%)	Ca/P
H_s	58.2	36	1.67 ± 0.02
H_f	61.5	37.5	1.66 ± 0.02

4.1.3.5. Infra-red analysis

Figure 4.5 shows the FTIR spectra of both forms of HAP powders.

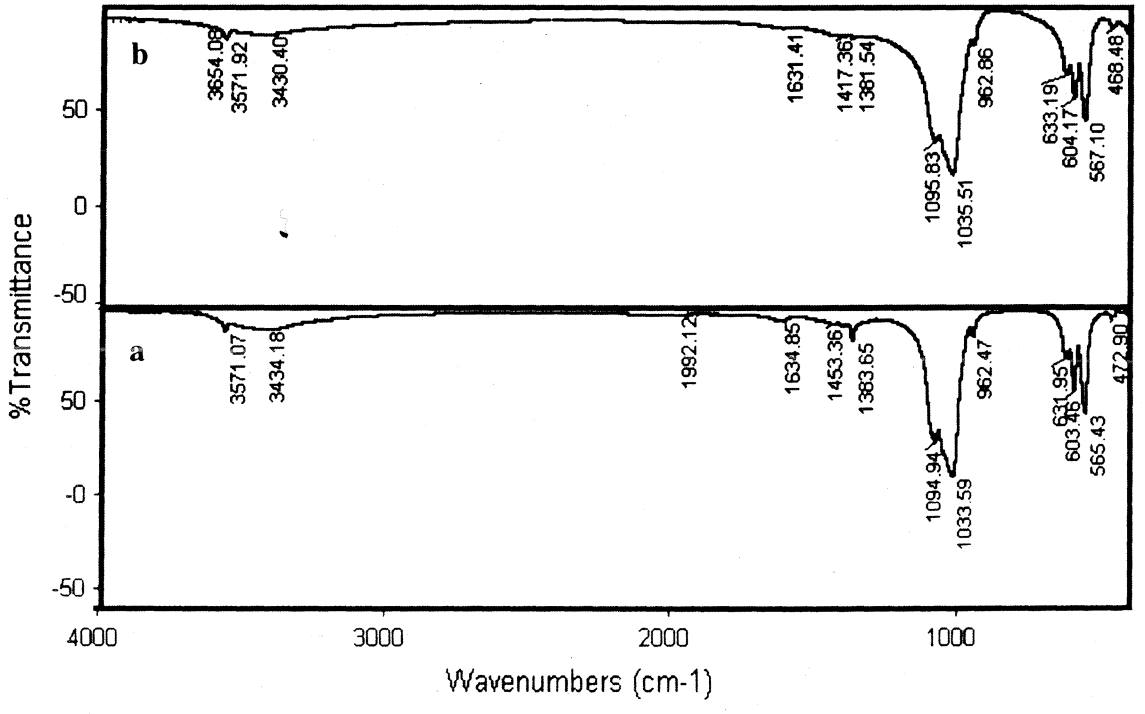

Figure 4.5. The FTIR spectra of (a) spray dried (b) freeze dried hydroxyapatite powders

The spectral data indicates the presence of carbonate ions (CO_3^{2-}) in trace quantities. This is expected considering that the synthesis of HAP was carried out in open air, which could lead to the incorporation of CO_3^{2-} into the HAP during precipitation.

Table 4.3. FTIR vibration positions of HAP powders

Material code	γ_{OH} (cm^{-1})	Adsorbed H-O-H, (cm^{-1})	CO_3^{2-} asymmetric stretch, (cm^{-1})	PO_4^{3-} asymmetric stretch, (cm^{-1})	PO_4^{3-} symmetric stretch, (cm^{-1})
H_s	3571.07 631.95	3434.18	1453.36	1094 603.46 565.43 472.9	1033.59 962.47
H_f	3571.92 633.19	3430.4	1417.36	1095.83 604.17 567.10 468.48	1035.51 962.86

4.2. PROCESSING OF HAP-EVA COMPOSITES

Polymers are usually filled with inert particles to enhance the mechanical properties and reduce cost (ASM, 1987). In the context of biomaterials, fillers are added to polymeric matrix mainly to induce bioactivity. The inclusion of filler, however, makes the processing of polymers more difficult. The flow behaviour of filled polymers has been well documented over the years (Utracki and Fisa, 1982; Saini *et al.*, 1985; Bhagawan *et al.*, 1988; Ghosh *et al.*, 1995). In filled systems or suspensions, particles often agglomerate and form a cluster structure, which changes during shear (Lakdawala and Salovey, 1985; 1987; Agarwal and Salovey, 1995). Particle clusters increase the viscosity of the filled systems (Lakdawala and Salovey, 1985; Park *et al.*, 1990). The processability of filled polymeric systems is controlled by many factors, including particle volume fraction, particle size and the state of aggregation of particles (Kosinski and Caruthers, 1986; Agarwal and Salovey, 1995; Bomal and Godard, 1996; Zhou *et al.*, 2001).

This section considers mainly the changes in flow properties and mixing temperature of HAP-EVA composites when processed in a torque rheometer. The torque rheometer has been used to evaluate the flow properties of the highly charged suspensions (Ayora *et al.*, 1997). It must be mentioned, however, that this equipment presents some disadvantages, for example, the surrounding gases (air or nitrogen) can be continuously entrained into the mix, since it operates partially full; and the three-dimensional nature of

the flow field in the mixer renders the flow not viscometric, so that the rheological parameters of the suspension can only be measured approximately (Goodrich and Porter, 1967; Blyler and Daane, 1967; Lee and Purdon, 1969; Marquez *et al.*, 1996). This section discusses the variation in mixing torque and mixing temperature of HAP-EVA composites with respect to the HAP content, HAP particle size and the nature of the polymer matrix.

4.3. VARIATION OF MIXING TORQUE OF HAP-EVA COMPOSITES

Typical torque vs. time curve for a polymer processed in a torque rheometer is given in Figure 4.6.

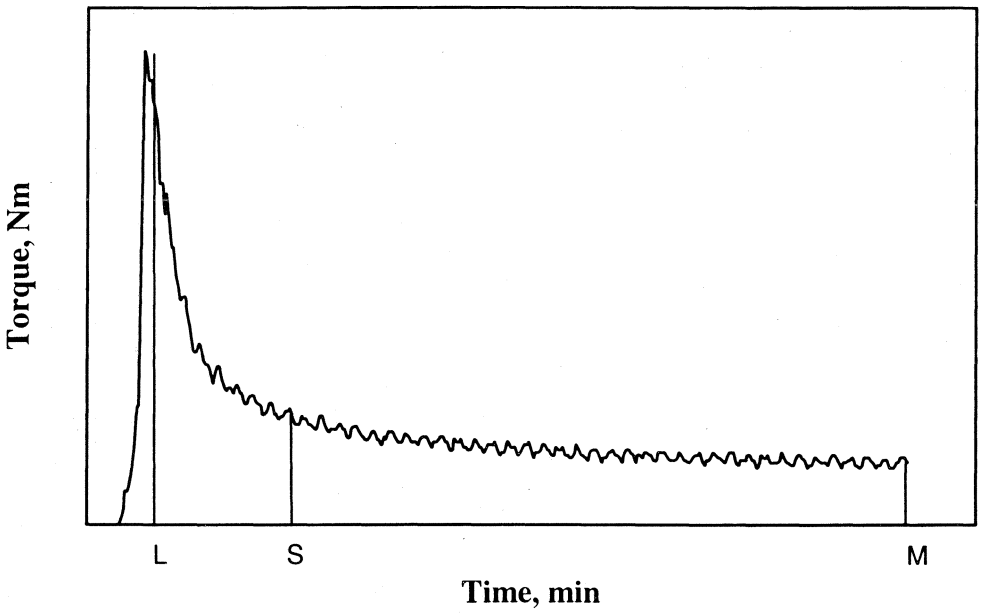

Figure 4.6. A typical mixing torque vs. mixing time curve obtained from the torque rheometer.

The curves display an initial increase, subsequent decrease and finally stabilization of the mixing torque. Three distinct regions could be identified from this curve. The point L is the loading peak, which shows when the mixer is completely filled and closed. At this point, the polymer chains are entangled which, makes the system highly viscous. This results in a high value of torque at this point. However, as the mixing progresses, the polymer chains are subjected to high mechanical shear from the counter rotating rotors, which leads to the scission/orientation of the polymer chains. Furthermore, the shear heat generated increases the temperature of the melt. Both these events lead to a decrease in the viscosity of the melt resulting in lowering of the torque. Point S is the

table torque point, which shows when torque reaches stable value. At point M, the melt has he lowest viscosity. The time between S and M is the stable torque time and gives the nformation about the processing time and stablity of the compound. The stabilization of he mixing torque signifies that complete mixing is achieved.

Figure 4.7. (a & b) shows the variation of the torque versus the time of mixing obtained vith HAP-EVA composites.

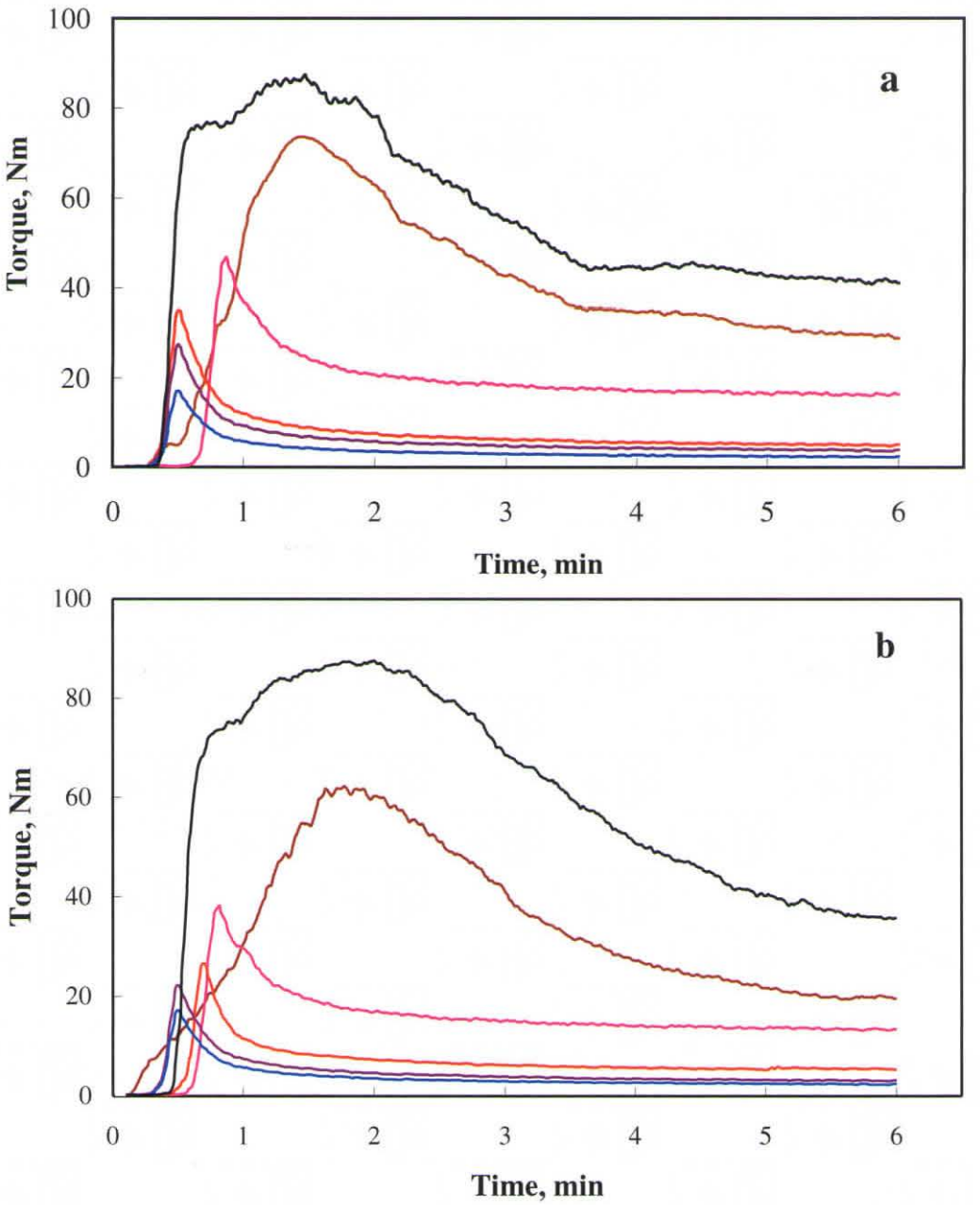

igure 4.7. Variation of mixing torque with mixing time for the composites fabricated rom various volume fractions of (a) spray dried and (b) freeze dried hydroxyapatite owders. (—) 0; (—) 0.1; (—) 0.2; (—) 0.3; (—) 0.4; and (—) 0.5 volume fraction of ydroxyapatite.

stable torque point, which shows when torque reaches stable value. At point M, the melt has the lowest viscosity. The time between S and M is the stable torque time and gives the information about the processing time and stablity of the compound. The stabilization of the mixing torque signifies that complete mixing is achieved.

Figure 4.7. (a & b) shows the variation of the torque versus the time of mixing obtained with HAP-EVA composites.

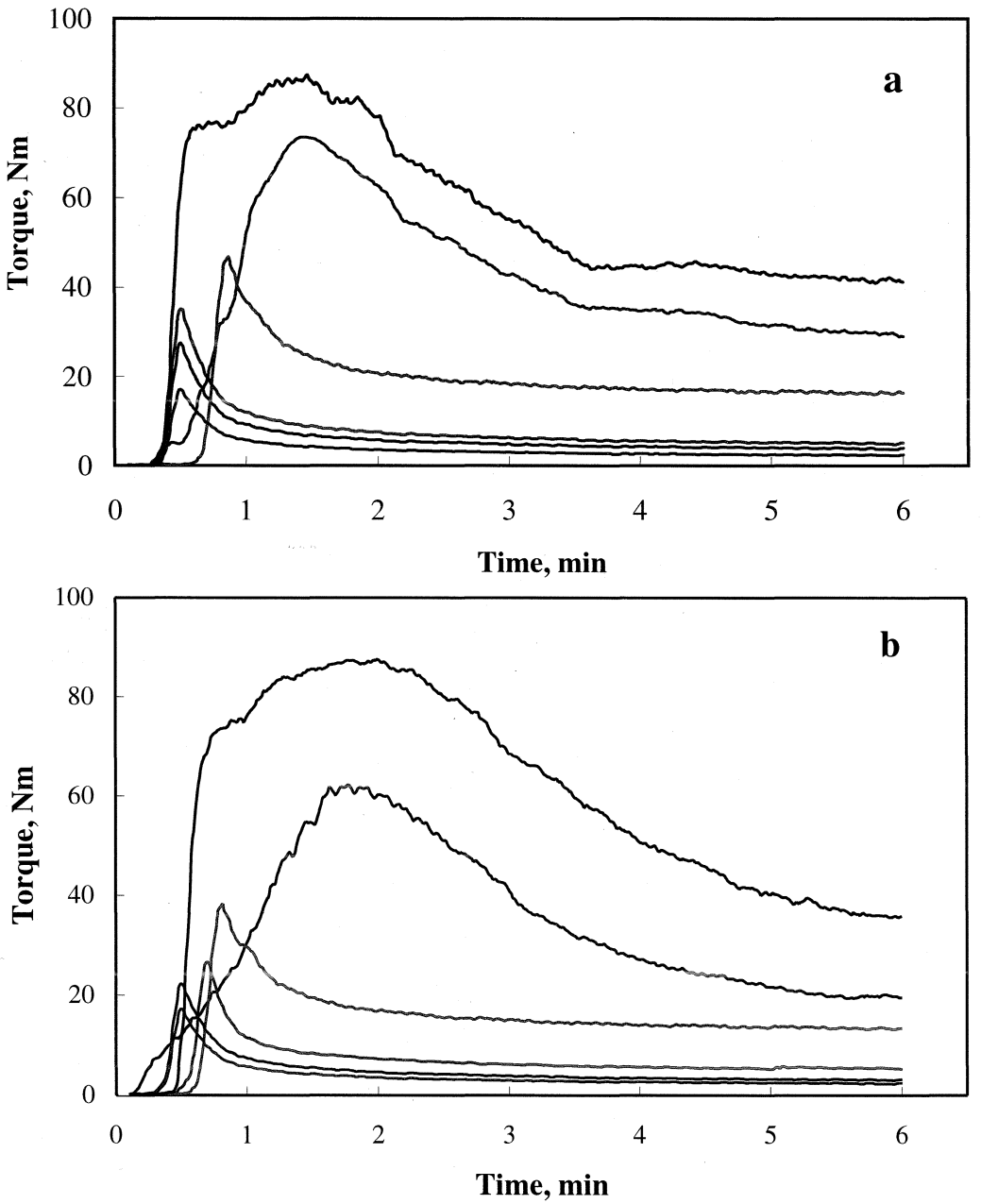

Figure 4.7. Variation of mixing torque with mixing time for the composites fabricated from various volume fractions of (a) spray dried and (b) freeze dried hydroxyapatite powders. (—) 0; (—) 0.1; (—) 0.2; (—) 0.3; (—) 0.4; and (—) 0.5 volume fraction of hydroxyapatite.

It is apparent that the value of mixing torque increased with the addition of HAP, the increase being proportional to the amount of HAP incorporated. This is expected because the fillers restrict the mobility of the polymer chains, which in turn leads to an increase in melt viscosity with a corresponding reduction in the melt elasticity (Bomal and Godard, 1996). However, for the same volume fraction of HAP incorporated, the torque values for the composites fabricated from H_s were found to be higher than the H_f counterparts. This is better understood by considering the relative shear viscosity (η_r) of the composites fabricated.

The composites were prepared in a Haake mixer that allowed measuring the effects of shear and deformation on the mixing. The data recorded during the mixing process consisted of torque measurements experienced by the rotors as they sheared the molten material. The apparent viscosity was calculated from the torque data generated from the mixer by the use of the following equation (Bousmina *et al.*, 1999):

$$\eta = \left(\frac{2\Gamma}{\pi L (R_e + R_i)^2 (1 + g^{n+1}) \dot{\gamma}} \right) \quad \text{.....4.1}$$

In this equation, Γ is the torque on the rotors, L is the length of the rotor, R_e is the effective radius (i.e. distance from the center of the rotor to the wall of the mixer), R_i is the radius of the rotor, g is the rotor ratio and $\dot{\gamma}$ is the shear rate. Since the rotors used in this study have the same rate, g = 1 and the $(1+g^{n+1})$ term in the above equation equals two and cancels the two in the numerator, leaving an expression based only on the geometry and physical parameters of the mixer. For a given rotor and mixer configuration, L, R_e, and R_i are constants. Hence the equation 4.1 could be simplified to

$$\eta = \frac{\Gamma}{\dot{\gamma}} \quad \text{.....4.2}$$

$\dot{\gamma}$ is equivalent to the rotor speed in rad s^{-1}. For non-Newtonian fluids, to correlate the relative viscosity η_r, with the volume fraction of the filler, Katoaka *et al.*, (1978; 1979) suggested taking the viscosities of the filled and unfilled polymer at the same shear stress. According to this definition, an asymptotic η_r could be determined in the range of low shear stresses. This method has an advantage as it avoids shear rate dependence of viscosity.

The relative viscosity η_r was calculated from equation 4.2 and plotted as a function of the volume fraction of HAP (ϕ) for the composites fabricated from both the forms of HAP under study (Figure 4.8).

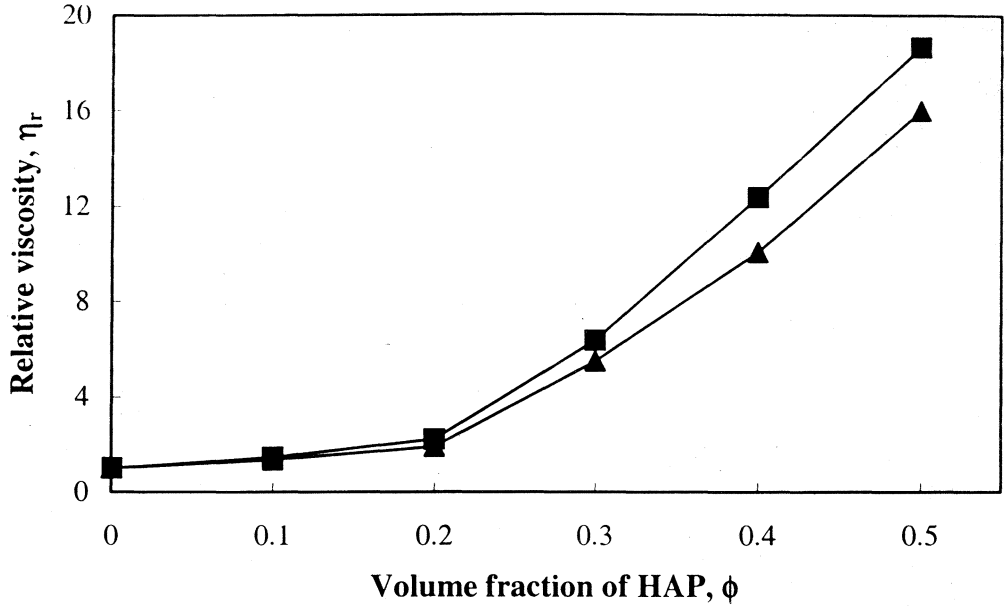

Figure 4.8. Variation of relative viscosity of the HAP-EVA composites with the volume fraction of hydroxyapatite fabricated from (■) spray dried and (▲) freeze dried hydroxyapatite powders.

The general increase in viscosity, as more HAP is added to the polymer, could be observed. The viscosity values of the composites fabricated from H_s were found to be higher than H_f at all the volume fractions of HAP loaded. Filler size effects on the flow properties of polymers originate from the cluster structure in the composites (Li and Salovey, 2004). When the loading of particles or total particle volume fraction is high, clusters form a network. At the same loading of particles, the smaller the particles, the larger the surface area, which generates more clusters. Consequently, stronger rejection by the matrix results in more matrix trapped by the cluster formation of small HAP particles, making less polymer matrix available for shear flow. Moreover, as HAP surface area is maximized the particle clusters may be bigger. Higher particle-particle interaction of small particles also favours cluster formation. Similar behaviour has been reported for a number of plastic and rubber composites (Mooney, 1951; Lee, 1969; Katoaka *et al.*, 1978; 1979).

The experimental curves generated from equation 4.2 were compared with theoretical curves obtained from equation 4.3 and equation 4.4 in order to examine the

extent of agreement of the experimental data with that of the theoretical models. Many mathematical correlations have been proposed to describe the viscosity of the suspensions as a function of particle concentration. Typical models are by Mooney (1951), and Maron and Pierce (1956), which satisfactorily predict the relationship between relative viscosity, η_r, and volume fraction of the filler ϕ. However, the Maron-Pierce model has wider acceptance than the models put forth by Mooney. The experimental curves obtained from equation 4.2 were compared with these two equations to verify the effect of HAP addition on the EVA matrix. The Mooney (equation 4.3) and Maron-Pierce (equation 4.4) relationship has been expressed in the following simplified form (Dealy and Wissburn, 1990).

$$\eta_r = \left(1 - \frac{\phi}{\phi_o}\right)^{-2} \quad \text{.....4.3}$$

$$\eta_r = \exp\left(\frac{2.5\phi}{1 - k\phi}\right) \quad \text{.....4.4}$$

ϕ_0 and k are constants relating to packing geometry. The values of ϕ_0 and k are assumed as 0.68 and 1.25 respectively, for random close packing of the spheres (Katoaka *et al.*, 1978). Figure 4.9 represents the comparison of experimental relative viscosity with that of the theoretical curves obtained from equations 4.3 and 4.4. The theoretical curves show good agreement with the experimental curves at lower volume fractions of HAP (<0.3). The theoretical values are significantly lower than the experimental values at higher volume fractions of HAP (>0.3). This is because the constants ϕ_0 and k varies with particle shape and state of agglomeration. At high volume fraction of HAP (>0.3), the chances of finding agglomerations and consequent network formation are higher, especially in the case of H_s. Additionally, the other form of HAP, H_f, has irregular morphology. Except in a few cases, it is difficult to predict the value of ϕ_0 and k from theory (Nielsen, 1974). Agglomerates and non-spherical particles generally have smaller values of ϕ_0 and k than spherical particle (Lewis and Nielsen, 1968).

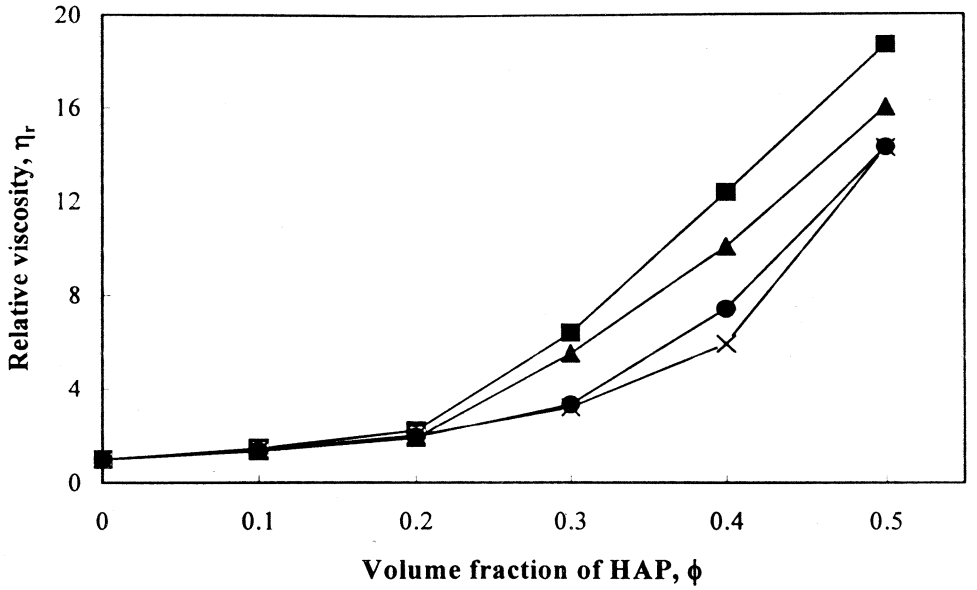

Figure 4.9. Comparison of experimental relative viscosity of the HAP-EVA composites with theoretical models (■) experimental (spray dried HAP); (▲) experimental (freeze dried HAP); (●) theoretical (Maron-Pierce model) and (x) theoretical (Mooney model)

The nature of the polymeric matrix employed for the preparation of the composites also influenced the flow properties of the HAP-EVA composites. Among the structural factors determining the flow properties of polymer, the molecular weight is the most important (Agarwal and Salovey, 1995). Below a critical molecular weight $\overline{M}_e$, the viscosity of a molten polymer is roughly proportional to the weight average molecular weight $\overline{M}_w$. i.e.,

$$\eta = K \overline{M}_w \quad \ldots\ldots\ldots\ldots \quad \overline{M}_e \leq \overline{M}_w \quad \ldots\ldots\ldots\ldots \quad 4.5$$

For most of the polymers, $\overline{M}_e$ is between 10, 000 and 40, 000. The $\overline{M}_w$ on the other hand is related to the melt flow index (MFI) by the following relationship

$$\overline{M}_w \alpha \frac{1}{MFI} \quad \ldots\ldots\ldots\ldots \quad 4.6$$

i.e., a polymer with a higher MFI has a lower molecular weight.

Figure 4.10 gives the variation of mixing torque with the time of mixing. It could be noted that E18 experiences a higher torque when compared with the E28 counterpart.

This is expected considering the lower MFI (hence higher $\overline{M}_w$) associated with E18. When the molecular weight is higher, the chains are long enough to become entangled, flow becomes much more difficult because the forces applied to one polymer chain become transmitted to and distributed among many other chains (Nielsen, 1977). Thus more energy is required to make E18 flow when compared to the low molecular weight E28, which results in a higher mixing torque for E18.

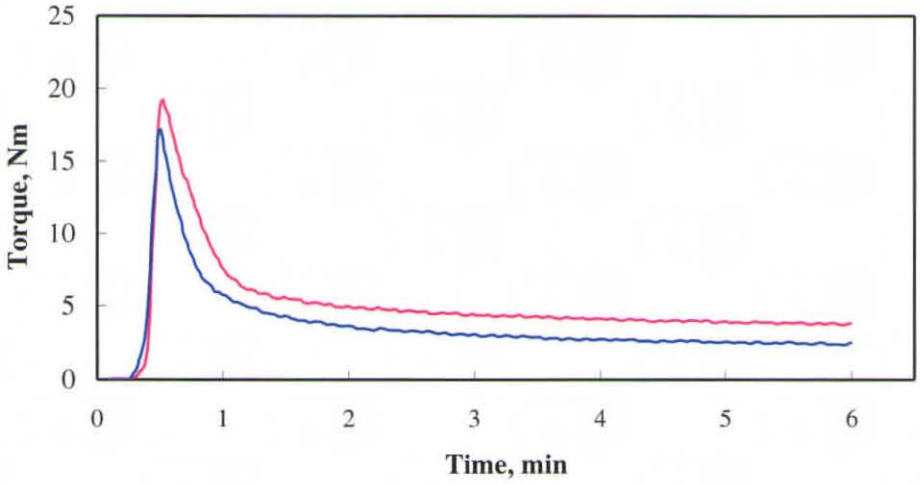

Figure 4.10. Variation of mixing torque with mixing time for the virgin polymers; (—) E28 and (—) E18.

The molecular weight effect is reflected on the viscosities of the composites E18H_s40 and E18H_f40. The viscosities of E18, E18H_s40 and E18H_f40 were calculated using equation 4.2 and compared with E28, E28H_s40 and E28H_f40 (Figure 4.11).

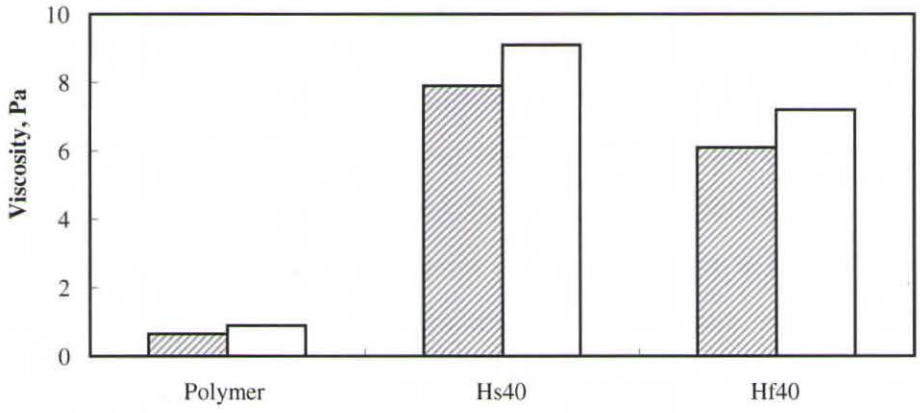

Figure 4.11. A comparison of viscosities of the virgin polymers and the composites fabricated from them. ▨ E28 and □ E18

This is expected considering the lower MFI (hence higher $\overline{M}_w$) associated with E18. When the molecular weight is higher, the chains are long enough to become entangled, flow becomes much more difficult because the forces applied to one polymer chain become transmitted to and distributed among many other chains (Nielsen, 1977). Thus more energy is required to make E18 flow when compared to the low molecular weight E28, which results in a higher mixing torque for E18.

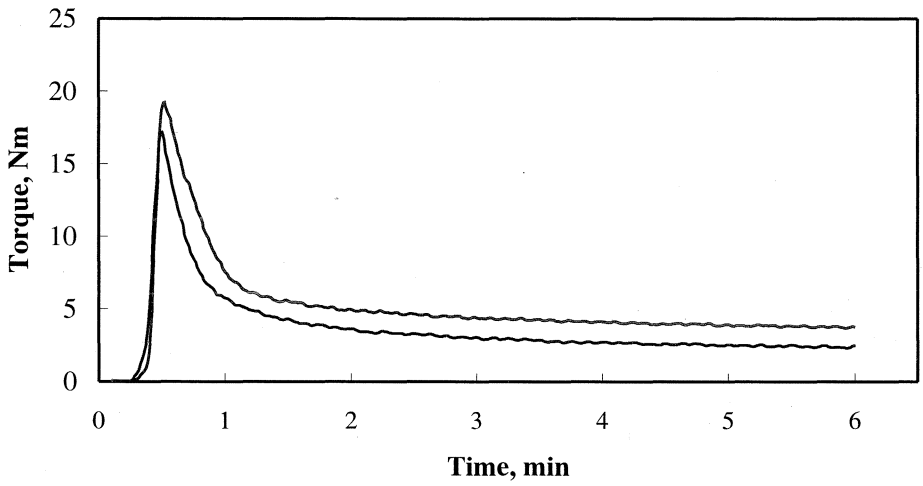

Figure 4.10. Variation of mixing torque with mixing time for the virgin polymers; (—) E28 and (—) E18.

The molecular weight effect is reflected on the viscosities of the composites E18H_s40 and E18H_f40. The viscosities of E18, E18H_s40 and E18H_f40 were calculated using equation 4.2 and compared with E28, E28H_s40 and E28H_f40 (Figure 4.11).

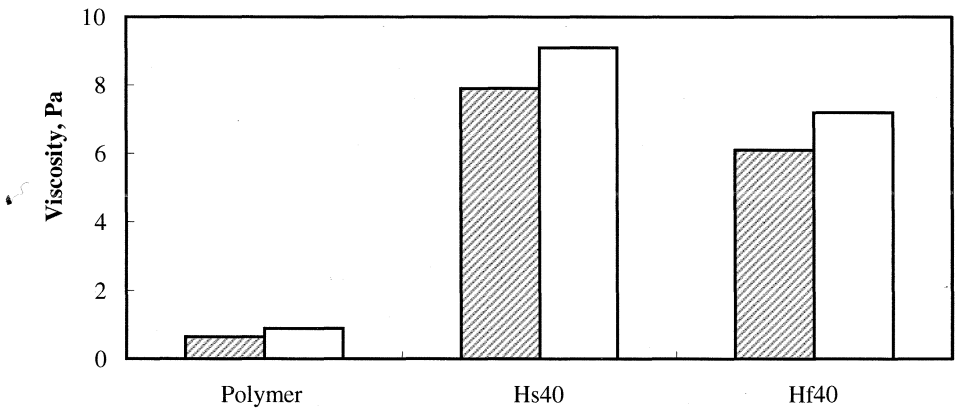

Figure 4.11. A comparison of viscosities of the virgin polymers and the composites fabricated from them. ▨ E28 and □ E18

As expected, the viscosities, associated with E18 and the composites fabricated from it were found to be higher.

4.4. VARIATION IN MELT TEMPERATURE DURING PROCESSING OF HAP-EVA COMPOSITES

The variation of the melt temperature of the HAP-EVA composites as a function of volume fraction of HAP is given in Figure 4.12.

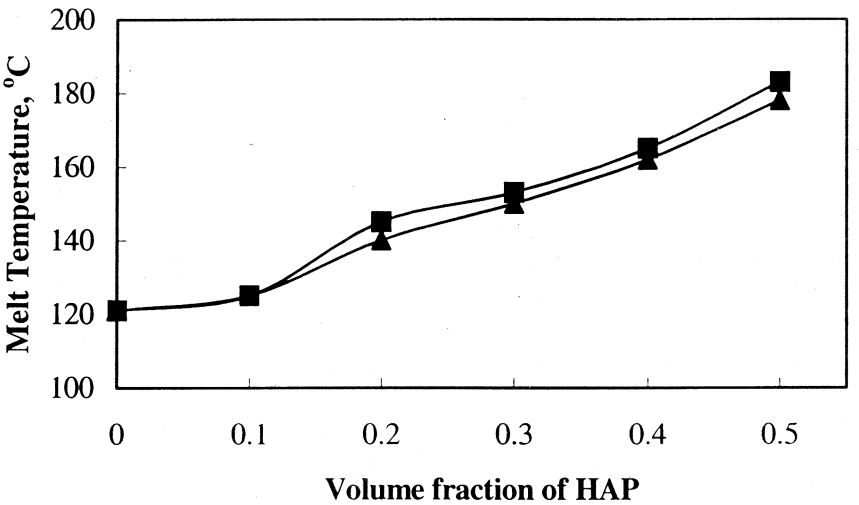

Figure 4.12. Variation of melt temperature of the HAP-EVA composites with different volume fraction of hydroxyapatite fabricated from (■) spray dried and (▲) freeze dried hydroxyapatite powders.

The increase in melt temperature with the increase in HAP loading is evident from the figure. Since the initial set temperature and the shear rate (rotor speed) for mixing are similar for all the composites under study, the difference in rise in the melt temperature at various volume fractions of HAP could be due to the shear heat generated during the mixing cycle. As the volume fraction of HAP increases in the composite, the possibility of agglomerate formation also increases. High shear forces thus come into play in order to break the agglomerated HAP and disperse it homogeneously in the polymer matrix. Heat is thus liberated resulting in overall increase in temperature with the increase in HAP loading. It could be noted that for the same loading of HAP, the melt temperature for the composites fabricated from H_s was significantly higher than that of H_f. This is expected because the smaller particle sized H_s has higher surface area and requires more polymer matrix for wetting. As a result, the viscosity of the system increases and higher shear forces are required to make the system flow which ultimately results in increase in the

melt temperature. This also explains the higher value of the melt temperature observed for E18 when compared to E28 (Figure 4.13).

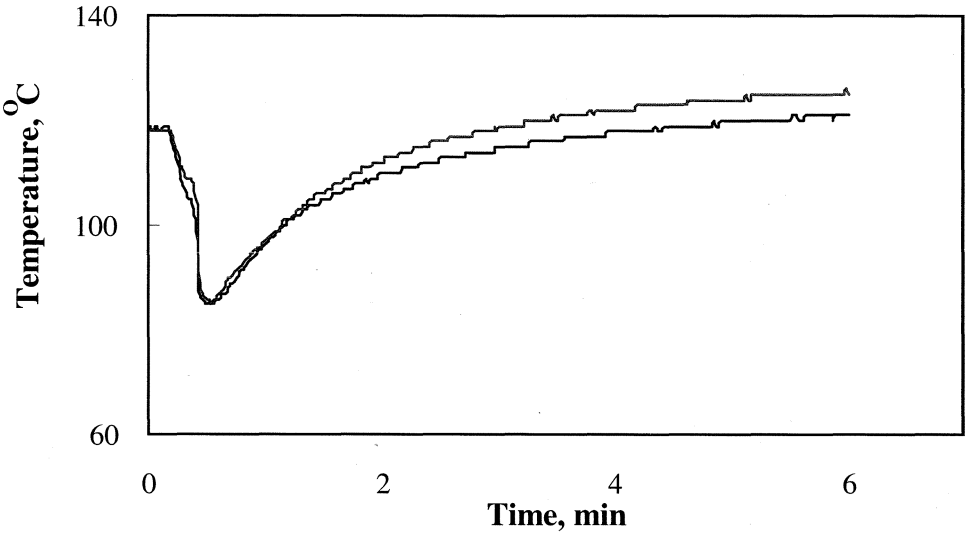

Figure 4.13. Variation of melt temperature with mixing time for the virgin polymers; (—) E28 and (—) E18.

At this point, it is worth mentioning that the temperature of the melt for all the other compositions under study could be kept well below the degradation temperature of the polymer matrix. The thermal degradation profile of E28H$_s$40 and E18H$_s$40 is given in Figure 4.14.

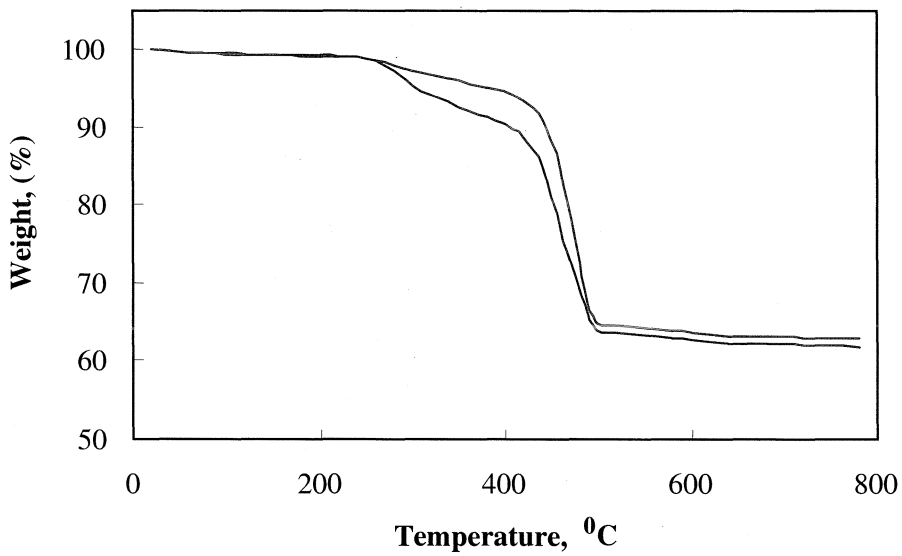

Figure 4.14. Thermal degradation profile of HAP-EVA composites; (—) E28H$_s$40 and (—) E18H$_s$40.

It could be inferred from the figure 4.14 that the thermal degradation of EVA takes place at two distinct stages. The weight losses over the two distinctive temperature ranges indicate the selective volatilization of the functional groups. The first decomposition step involves loss of acetic acid and takes place around 240-260°C. The second decomposition step involves the cleavage of C-H bonds and takes place at a much higher temperature (>400°C).

4.5. EFFECTS OF PROCESSING VARIABLES USED FOR THE PREPARATION OF HAP-EVA COMPOSITES

Best mixing conditions are ascertained by (a) minimal degradation of the matrix polymer, (b) good composite homogeneity, and (c) minimal loss of filler particles during the entire process of mixing and moulding. During processing, the polymer is subjected to both thermal as well as mechanical stresses. Hence some amount of degradation in the molecular weight of the polymeric matrix is expected in any processing operations. Table 4.4. gives the molecular weight of the neat polymer E28 and that of the matrix in the composites with 40vol.% of HAP as determined by GPC.

Table 4.4. Weight average molecular weight ($\overline{M}_w$) of E28 in HAP-EVA composites

Material code	Weight average molecular weight ($\overline{M}_w$)	Polydispersity index
E28	1, 16, 561	2.6
$E28H_s40$	95, 820	2.26
$E28H_f40$	98, 328	2.16

It is apparent that the addition of HAP particles reduced the $\overline{M}_w$ value due to the breakdown of polymer chains both by thermal and mechanical stresses. However, the polymer chain breakdown during the thermal processing is not severe and a molecular weight of greater than 90, 000 could be obtained for the HAP-EVA composites. The observed trend of decreasing molecular weight with incorporation of filler is consistent with that of other bioactive composites (Wang *et al*, 1998a).

An essential requirement for the processing of particulate-filled polymer composite is the homogeneity of mixture. Composite with good dispersion and distribution of the particulate would eventually produce a consistent composite morphology having isotropic properties (Abu Bakar *et al.*, 2003a). Microscopic examination of fractured surfaces of $E28H_s40$ and $E28H_f40$ revealed that HAP particles

were well dispersed in the composites and that a reasonably homogeneous distribution of HAP particles in the polymer matrix had been achieved after the mixing process (Figure 4.15).

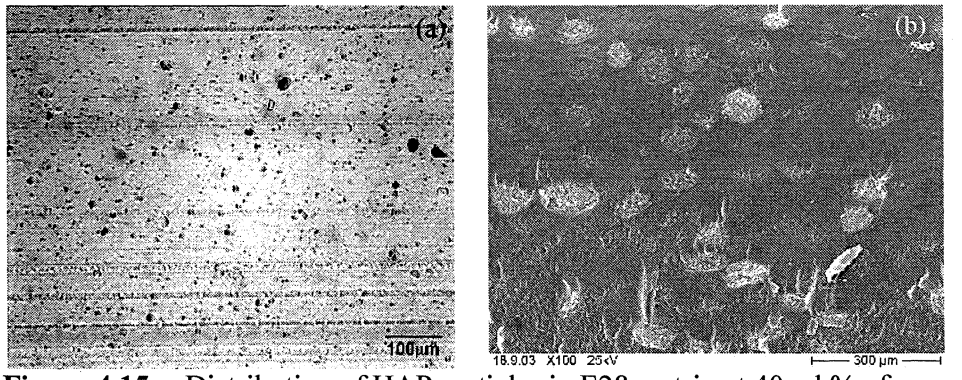

Figure 4.15. Distribution of HAP particles in E28 matrix at 40vol.% of HAP loading. (a) $E28H_s40$ and (b) $E28H_f40$

It could hence be inferred that the counter-rotating rotors generated high shear forces to disperse hard particles of HAP in the polymeric matrix. Therefore, a good dispersion and a homogeneous distribution of HAP particles in the EVA matrix were achieved. Such a distribution of HAP particles is important because when a biological apatite layer develops between the HAP and the surrounding tissue, these particles provide uniformly distributed anchors for the prosthesis. It could be seen from the Figure 4.15 that fracturing exposed the HAP particles. Bearing in mind the envisaged biomedical applications, the homogeneous distribution of HAP particles in the polymer matrix and the exposed HAP particles on the composite surface together suggest considerable potential for the HAP-EVA composite as a hard tissue bonding biomaterial.

The results of ashing analysis obtained from the moulded specimens of the composites are given in the Table 4.5.

Table 4.5. Ashing analysis data showing the extent of HAP incorporated in the HAP-EVA composites

HAP (vol.%)	HAP (wt.%)	HAP incorporated			
		$E28H_s$	$E28H_f$	$E18H_s$	$E18H_f$
10	26.9	24.7	25.1	-	-
20	45.4	42.8	43.3	-	-
30	58.7	56.0	56.5	-	-
40	68.9	66.2	66.9	66.0	66.5
50	76.9	74.3	75.2	-	-

It is encouraging to note that the majority of the HAP particles have been incorporated in the resulting composite. A loss of HAP particles of less than 3 wt.% was observed in the whole processing route.

4.6. CONCLUSIONS

The polymers (E28 and E18) used for the study were characterized. Hydroxyaptite was prepared by precipitation reaction involving ammoniated calcium nitrate and ammonium hydrogen phosphate solutions. Freeze-drying and spray drying of the precipitated HAP gave rise to two grades of HAP powders – namely freeze-dried HAP (H_f) and spray dried HAP (H_s). Particle size analysis of the synthesized HAP powders showed that both H_f and H_s had monomodal distribution of particle size. The SEM micrographs of powders showed the irregular and spherical shapes of H_f and H_s, respectively. Both H_f and H_s were highly crystalline, and monophasic as revealed from the XRD studies. The XRD patterns of H_f and H_s matched closely to that of the diffraction data obtained from Joint Committee for Powder Diffraction Standards (JCPDS) Data Sheet for HAP (9-432). The Ca/P molar ratio of the synthesized HAP was found to be matching with the theoretical stoichiometric ratio of 1.67. The infrared data of the synthesized HAP powders showed the typical peaks OH^- and PO_4^{3-}, of HAP. Trace amounts of carbonates were also present.

The flow behaviour of HAP-EVA composites was found to be dependent on both the nature of the HAP particles and also the nature of the polymer used. In general, HAP having smaller particle size increased the viscosity of the composite for the same volume fraction of HAP loaded. Also the polymer with lower value of melt flow index increased the viscosity of the HAP-EVA composites. The relative viscosity of the melts could be predicted using Maron-Pierce as well as Mooney equation at lower volume fractions of HAP (<30vol.%). However, at higher volume fractions, the experimental values were considerably higher than the theoretical values. For the processing conditions employed the composites fabricated from E28 gave easier processing. The processing conditions employed were found to be optimum as evident from the good dispersion of HAP particles in the polymer matrix, the minimum loss of HAP and also the minimum degree of degradation of the polymer matrix.

CHAPTER 5

MECHANICAL PROPERTY EVALUATION

5.1. BACKGROUND

The determination of mechanical properties of implant materials has been and will continue to be an essential step in implant design and development. This is because the mechanical compatibility of an implant is as important as its biocompatibility to be safe for clinical applications. Physically, the implant must stabilize the fracture or osteotomy until it has consolidated. The implants must also have sufficient strength to resist mechanical stresses occurring during surgical procedure. Mechanical property evaluation studies provide an understanding of the applicability of a specific material for use as an implant, and can be used to predict not only the failure thresholds for the implant but also the expected remodeling response of the bone once the implant has been placed *in situ* (Meaney, 1995).

Mechanical properties of particulate composite systems are influenced by a number of factors like the nature of the polymer matrix, nature of filler, filler to matrix ratio, extent of wetting and adhesion between filler and matrix (Han *et al.*, 1978; Malik *et al.*, 1992; Sidess *et al.*, 1993; Cook and Harper, 1998). It is known that the shape, size and size distribution of filler particles significantly affect the mechanical properties of particulate composite materials (Ahmed and Jones, 1990). This chapter focuses on the behaviour of the HAP-EVA composites when subjected to various mechanical solicitations including linear elastic, plastic, and viscoelastic behavior. The composite

behaviour with respect to HAP particle size and loading under tensile, bending, impact and dynamic mechanical loading is discussed.

5.2. TENSILE PROPERTIES

5.2.1. Effect of HAP loading and particle size

5.2.1.1. Stress-strain curves

The incorporation of rigid ceramic particulate into the polymer matrix affects the mechanical properties of the composite to a great extent. This is clear from the tensile stress-strain curves of HAP-EVA composites, fabricated from E28, containing different volume fractions of HAP (Figure 5.1. a & b). The HAP-EVA composite materials exhibited both ductile and brittle behaviour, depending upon the amount of HAP incorporated into the EVA polymer. Unfilled EVA exhibits typical stress-strain curve of a soft and tough polymer material, characterized by low modulus and low yield stress, but very high elongation at break. The stress-stain curves for the composites with 10, 20 and 30vol.% HAP were also similar to that seen for E28. The strain at failure was however found to be decreasing with the increase in HAP loading. Necking was also noted for the composites with less than 30vol.% of HAP during tensile testing. For composite with 40vol.% HAP, the stress-strain curve showed linear elastic behaviour followed by a plastic behaviour without a sharp yield point, typical to highly filled elastomeric materials with rigid filler (Kauly *et al.,* 1996). It is worth mentioning that even at such high loading of HAP the material failed beyond the linear elastic region, indicating that the ductility of the composite was maintained. At 50vol.% HAP, the ductile behaviour was no longer a dominant feature. The stress-strain curve for $E28H_s50$ shows that the fracture of the composite occurred at a lower stress value within the linear region of the stress-strain curve with little yielding. As the filler content increased, the recorded stress-strain curves became steeper and the elongation at break lower. The nature of the stress-strain curves at various loadings of HAP obtained for $E28H_f40$ was also similar to the ones recorded for $E28H_s40$, but at lower values of stress, strain and modulus.

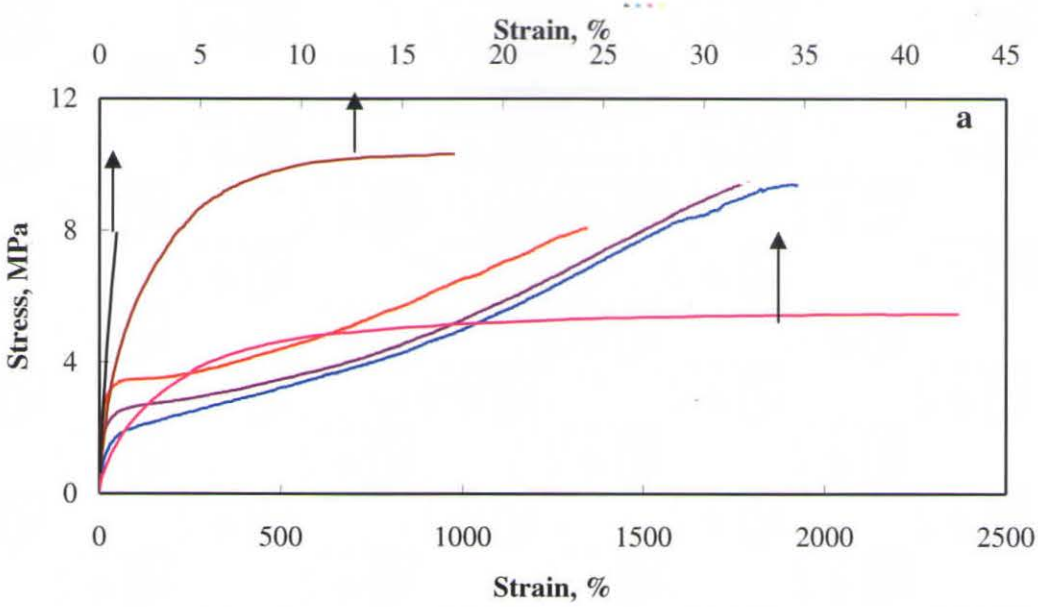

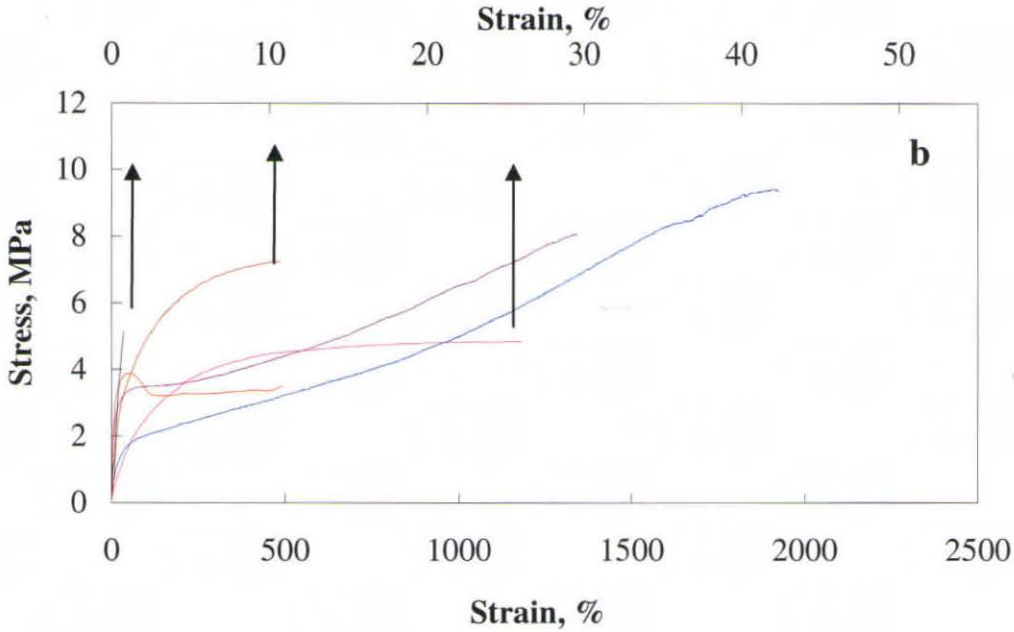

Figure 5.1. Tensile stress-strain curves for the composites fabricated from various volume fractions of (a) spray dried and (b) freeze dried hydroxyapatite powders. (—) 0; (—) 0.1; (—) 0.2; (—) 0.3; (—) 0.4; and (—) 0.5 volume fraction of hydroxyapatite.

5.2.1.2. Tensile strength

Figure 5.2 shows the variation of tensile strength with respect to HAP loading. At 10, 20 and 30vol.% of HAP loading, the tensile strength decreased when compared to the unfilled polymer. The decrease in the value of tensile strength for E28H$_s$30 was found to be 14%, while a catastrophic drop of nearly 50% was noted for E28H$_f$30.

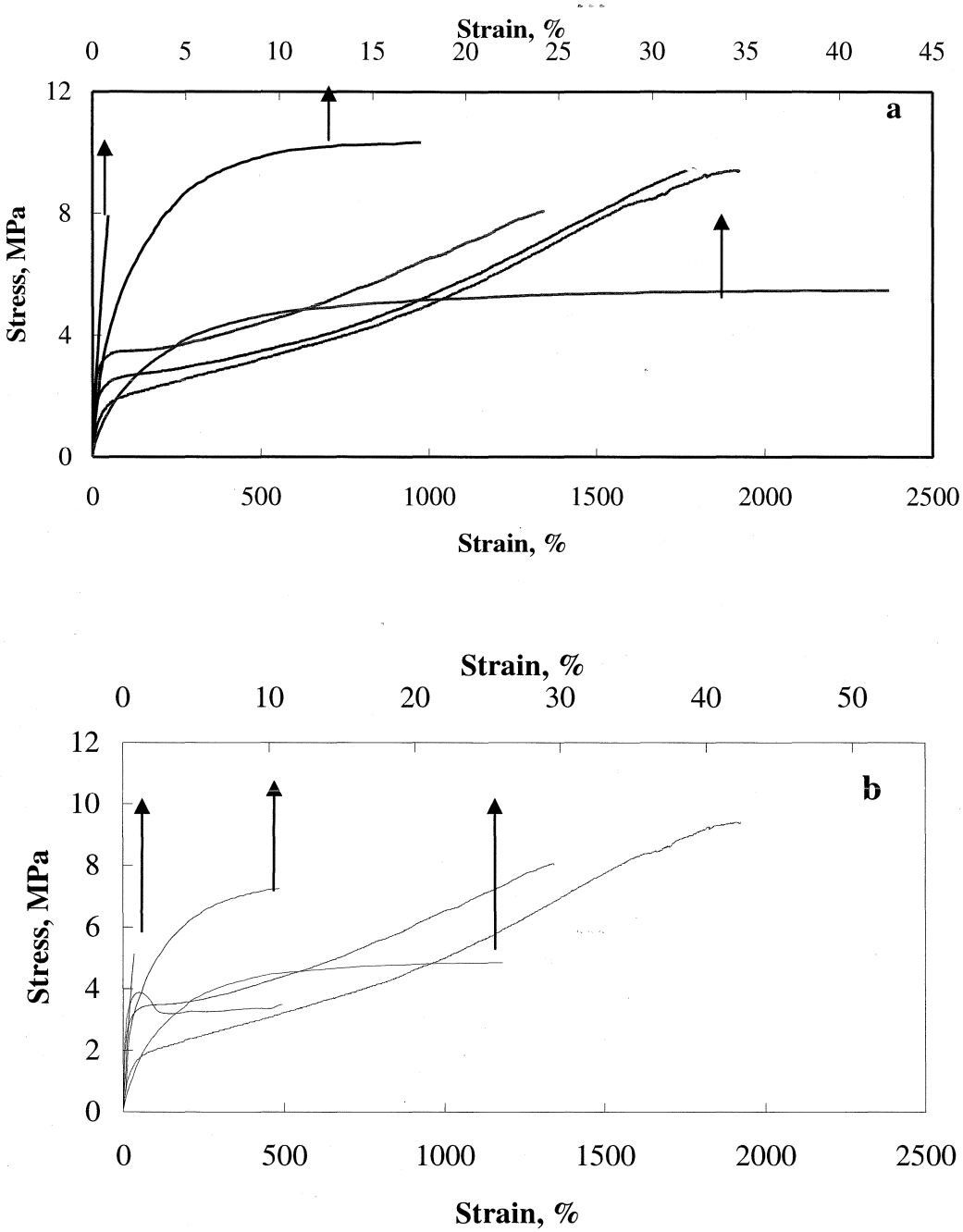

Figure 5.1. Tensile stress-strain curves for the composites fabricated from various volume fractions of (a) spray dried and (b) freeze dried hydroxyapatite powders. (—) 0; (—) 0.1; (—) 0.2; (—) 0.3; (—) 0.4; and (—) 0.5 volume fraction of hydroxyapatite.

5.2.1.2. Tensile strength

Figure 5.2 shows the variation of tensile strength with respect to HAP loading. At 10, 20 and 30vol.% of HAP loading, the tensile strength decreased when compared to the unfilled polymer. The decrease in the value of tensile strength for E28H$_s$30 was found to be 14%, while a catastrophic drop of nearly 50% was noted for E28H$_f$30.

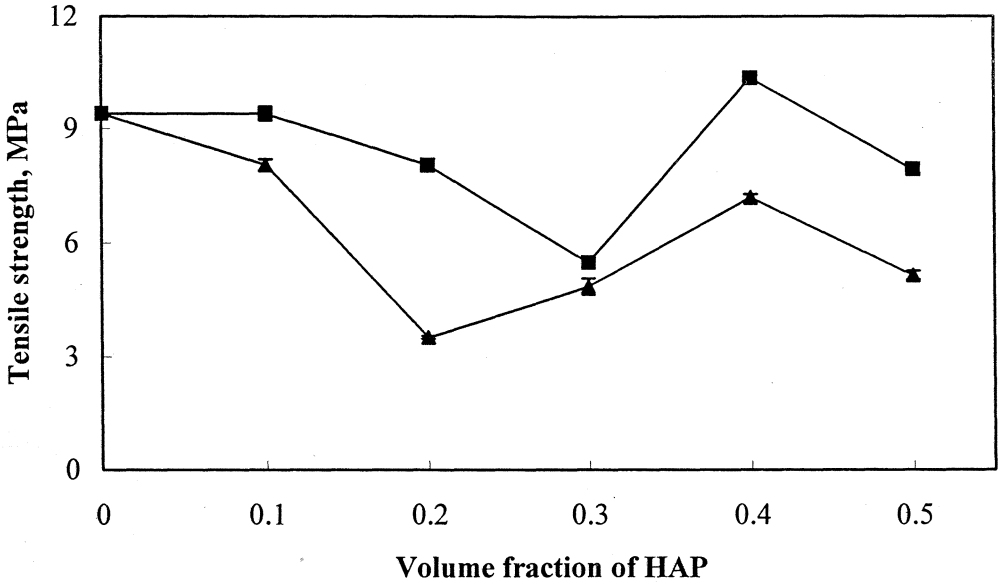

Figure 5.2. Variation of tensile strength of HAP-EVA composites, fabricated from E28 as a function of HAP volume fraction for the composites fabricated from (■) spray dried and (▲) freeze dried hydroxyapatite.

Rigid fillers often decrease the tensile strength of polymeric materials (Wang *et al.,* 1998a; Cheang and Khor, 2003, Abu Bakar *et al.,* 2003a), excluding some exceptions (Cai and Salovey, 1999; Gan *et al.,* 2001; Verbeek, 2002a). Rigid inclusions act as stress concentration points and create stress fields in the vicinity of the particles. This weakens the composites leading to decrease in the tensile strength of the composite, as encountered in the present situation. The stress fields near a particle are independent of the particle size (Nielsen and Landrel, 1994). The volume of polymer that experiences a given value of stress concentration increases with particle size, so that the probability of finding a large flaw within this volume also increases (Berlin *et al.,* 1990). The probability of finding a large flaw within the area of stress concentration of H_f is higher than that of H_s. Also, large voids are more detrimental than small ones to strength; hence after dewetting, larger filler particle produces larger void. This explains the lower tensile strength value of composites fabricated from H_f when compared to their H_s counterparts for the same loading of HAP. At 40vol.% of HAP loading, however, an increase in the value of tensile strength was noted for both E28H_s40 and E28H_f40. It has been reported that in filled elastomeric systems, at certain concentrations, the filler particles or particle aggregates can act as physical crosslinks (Cai and Salovey, 1999). As a result, strong linkages may exist between the polymer chains and the filler particles, making the chains extending

between adjacent particles stressed. Highly stressed chains extended between adjacent filler particles support a much larger than average stress, which subsequently increase the tensile strength of the composite. Since the number of attached chains is proportional to the available surface area of the fillers, small particle size fillers are found to be more effectively reinforcing, a possible reason for the higher tensile strength obtained for $E28H_s40$ than $E28H_f40$. Some authors report that the physical cross-links formed between the filler particles and the polymer can lead to deviation of tear path caused by the anisotropy of stress around the crack tip, which also causes an increase in the strength of the composites (Gent, 1978; Xavier *et al.,* 1990). Further addition of HAP, however, resulted in lowering of tensile strength in either case. This could be due to the 'dilution effect'. At very high filler loading the polymer matrix available is insufficient to hold all the filler particles together (Verbeek, 2002b). Using too little polymer regardless of the particle size, the polymer will not effectively wet the surface to get good stress transfer between the polymer and the filler. Similar variation in tensile strength was reported by Wang *et al.,* (1998b) in their studies on HAP filled HDPE composite system. Comparing the results of the two groups of composites, it was demonstrated that the increase in tensile strength for the composites fabricated from H_s with 10 to 40vol.% of HAP was over 44% greater than that seen in the case of the composites fabricated from H_f.

5.2.1.3. Young's modulus

The variation of Young's modulus of composites fabricated from H_s and H_f with HAP content is given in Figure 5.3. Generally, the modulus was seen to increase exponentially with HAP content for both types of composites (see also addendum, section 9.2, page 163). This increase in modulus is expected because HAP is a ceramic material, which is much stiffer than EVA (E_{HAP} = 80 GPa (Wang *et al.,* 1998a); E_{E28} = 9 MPa [Figure 5.1]). Incorporating particles of HAP into the EVA matrix thus stiffens EVA by an amount depending on the HAP content. The reinforcing effect of the HAP particulate is evident even with the slightest inclusion of HAP. At higher HAP contents of 20% and above, a significant increase in the modulus of 2-5 fold as observed.

Theory indicates that the elastic moduli of a composite material should be independent of the size of the filler particles (Manson and Sperling, 1976.). However, experiments generally show an increase in modulus as the particle size decreases (Figure 5.3). This is because as size decreases surface area of the particles increases. If the

polymer is changed in some manner at the interface, as by adsorption, then the properties should change with particle size because of the change in surface area.

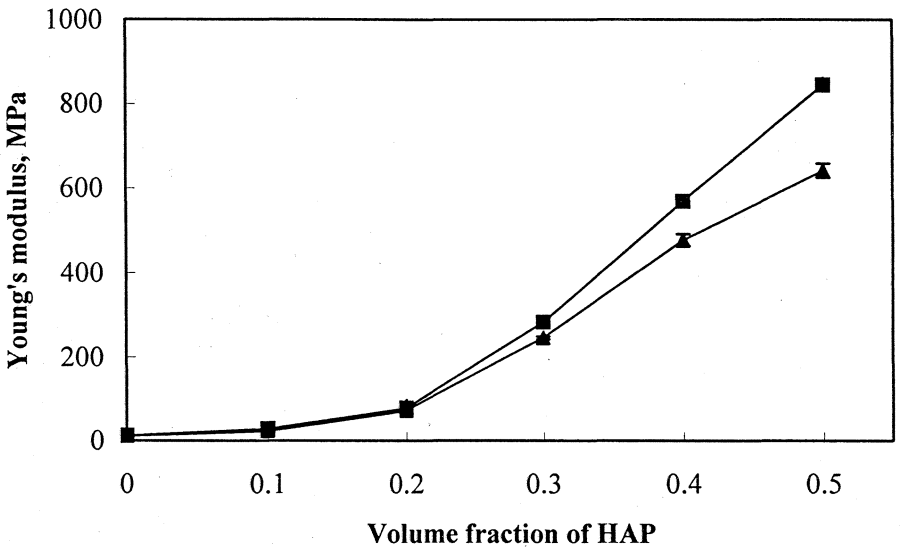

Figure 5.3. Variation in Young's modulus of HAP-EVA composites, fabricated from E28 as a function of HAP volume fraction for the composites fabricated from (■) spray dried and (▲) freeze dried hydroxyapatite.

For composites E28H_s50 and E28H_f50, the fracture occurred at lower stress and elongation than that at 40vol.% HAP. Although addition of rigid filler particles increases the modulus, the composite with 50vol.% filler behaved like a more brittle material showing high modulus, but a low fracture strength and elongation at break. Here, excessive particle attachment and aggregation restrict deformation of the polymer chain. Moreover, the over "crowding" of filler particles causes poor wetting and weak adhesion between the particles and the matrix. It hence follows that there exists an optimum filler concentration for reinforcement in an elastomeric matrix. Various other authors also drew similar conclusions in their theoretical and experimental investigations (Ogunniyi, 1988; Furukawa and Yamada, 1994).

5.2.1.4. Strain to fracture

The variation of the strain to fracture with volume percentage of HAP is given in Figure 5.4. The general trend observed was that the strain to failure decreased with increase in HAP content. The decrease in the value of strain to fracture was not disastrous at 10vol.% of HAP. However, at HAP loading >10vol.%, the strain to fracture decreased catastrophically, suggesting loss of ductility due to reduction in volume fraction of

polymer matrix. At 50vol.% of HAP the composite showed brittle mode of fracture. There was also a shift from the ductile to brittle fracture behaviour when progressive amounts of HAP were added to the EVA matrix.

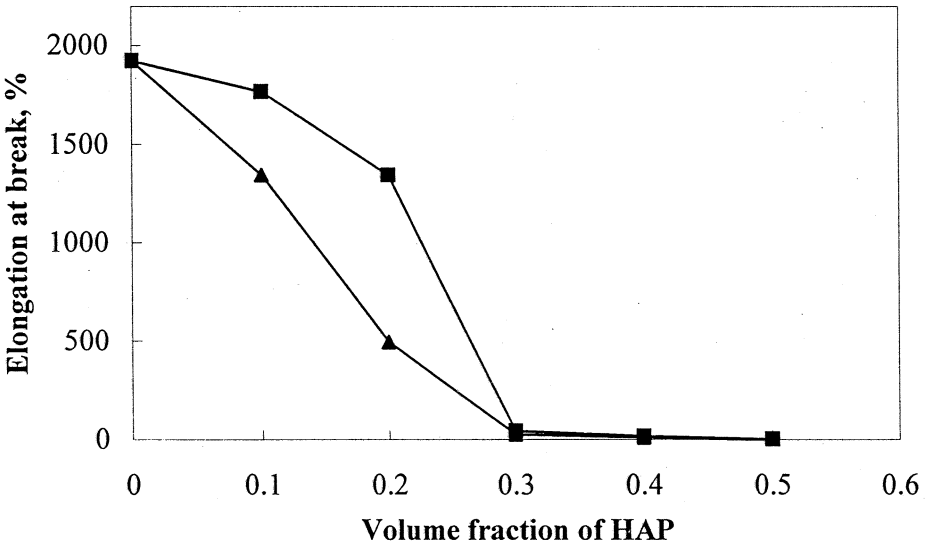

Figure 5.4. Variation of elongation at break of HAP-EVA composites fabricated from E28 as a function of HAP volume fraction for the composites fabricated from (■) spray dried and (▲) freeze dried hydroxyapatite.

It could be noted that the composites fabricated from H_s exhibited considerably higher value of strain to fracture than those fabricated from H_f at concentrations ≤ 30vol.% of HAP. This trend in the strain to fracture can be explained based on the cavitation mechanism of reinforcement (Cai and Salovey, 1999; Goodier, 1988; Eirich, 1973; Oberth, 1967). According to this theory, it is suggested that the probability of finding a large flaw leading to material fracture under a given stress concentration increases with increase in particle size. Particles with small size may induce micro flaws or cavitations without the formation of cracks. This process can convert large amounts of elastic energy into heat and surface energy. Then, it would take higher stress and more energy for the composite containing smaller particles to deform and eventually fracture. Thus, for the same loading of filler, the elongation at break increase as the particle size is decreased. The strain to failure of $E28H_s40$ was almost comparable to $E28H_f40$.

In this study, at a HAP concentration of 40vol.%, the highest tensile strength, moderate values of Young' modulus and elongation at break were obtained. It has been reported that 40vol.% of HAP loading in a HAP filled polymer system exhibits sufficient

bioactivity (Bonfield *et al.,* 1981). Hence an indepth evaluation of the mechanical properties was carried out using composites containing 40 vol.% of HAP.

5.2.2. Effect of nature of polymer matrix

Figure 5.5 gives the stress-strain of unfilled E18, E18H_s40, and E18H_f40. The stress-strain curve of E18 is similar to that of E28, except that the fracture occurs at a higher stress and lower strain to fracture than E28. The addition of 40vol.% of HAP affects the ductility of the composite catastrophically.

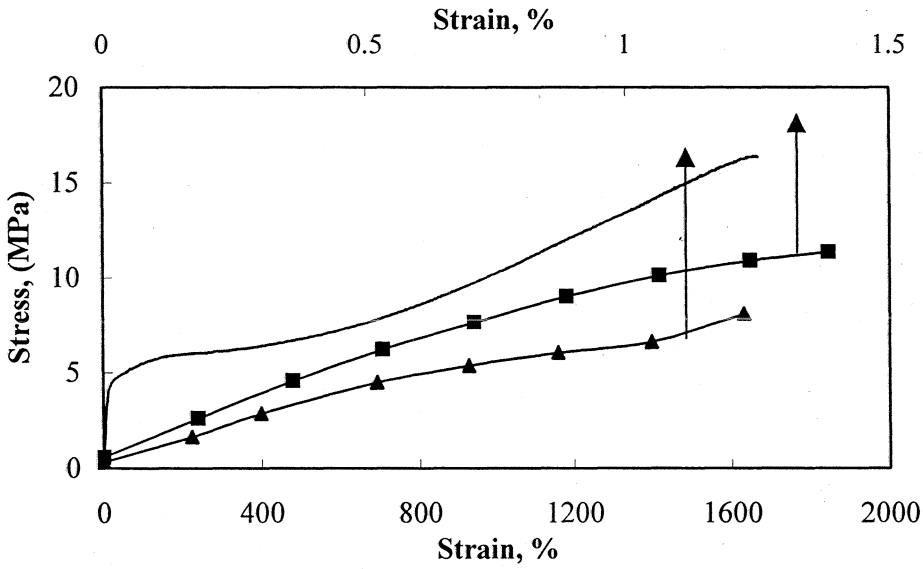

Figure 5.5. Stress-strain curves of HAP-EVA composites. (—) E18; (■) E18H_s40; (▲) E18H_f40.

The values of tensile strength, Young's modulus, and strain to fracture of E28H_s40, E28H_f40, E18H_s40, E18H_f40 and the unfilled polymers (E28, and E18) are given in Table 5.1. For the composites fabricated from both E28 and E18, addition of HAP led to increase in the values of Young's modulus with corresponding decrease in fracture strain. The values of tensile strength, however, showed a different trend. While an increment in the tensile strength value was found in the case of E28, the value decreased for the composites fabricated from E18. The values of tensile strength, and Young's modulus of E18H_s40 were, however, found to be higher than that of E28H_s40. The strain to fracture of E18H_s40, on the other hand, was lower than that of E28H_s40.

Similar variation in tensile strength, Young's modulus, and strain to fracture was noted for E18H_f40 and E28H_f40.

Table 5.1. Tensile properties of HAP-EVA composites

Material code	Tensile strength, (MPa)	Young's modulus, (GPa)	Strain at break, %
E28	9.40 ± 0.19	12.00 ± 3.86	1923 ± 40
E28H_s40	10.34 ± 0.07	581.92 ± 3.82	17.58 ± 0.37
E28H_f40	7.26 ± 0.09	477.21 ± 2.56	10.66 ± 0.07
E18	16.34 ± 3.07	80.36 ± 2.43	1668 ± 68
E18H_s40	11.35 ± 0.12	820.50 ± 4.42	1.38 ± 0.02
E18H_f40	8.07 ± 0.05	732.20 ± 4.13	1.22 ± 0.03

Tensile fracture of filled polymer system such as HAP-EVA usually proceeds by a stage of cavitation where the matrix and the filler de-bond. The composite thus acts as a foam in this stage and the ultimate strength of the system depends on the strength of this foam and the extent of any strain hardening capability that may occur in drawn polymer chains. The polymer matrices employed in the present study differed from each other in terms of vinyl acetate content and melt flow index. The E28 polymer matrix has a higher content of vinyl acetate and a higher value of MFI when compared to the E18 matrix polymer. A higher MFI value is associated with a lower value of molecular weight of the polymer. It has been reported that a high molecular weight polymer could be expected to have a greater strain hardening capability than the lower molecular grade and would consequently be capable of sustaining a higher load after cavitations have occurred (Hogg *et. al.,* 1985). This explains the higher values of tensile strength and Young's modulus of the composites fabricated from E18 when compared to those fabricated from E28.

5.3. FLEXURAL PROPERTIES

5.3.1. Effect of HAP loading and particle size

The flexural strength, and flexural modulus of E28H_s40, E28H_f40, E18H_s40, E18H_f40 and the unfilled polymers (E28 and E18) are given in Table 5.2.

Table 5.2. Flexural properties of HAP-EVA composites

Material code	Flexural strength, (MPa)	Flexural modulus, (GPa)	Flexural strain at break, %
E28	3.01 ± 0.991	0.014 ± 0.01	11.12 ± 0.53
E28H_s40	17.62 ± 0.77	1.79 ± 0.09	4.52 ± 0.22
E28H_f40	14.62 ± 0.8	1.2 ± 0.04	4.76 ± 0.28
E18	3.12 ± 1.07	0.042 ± 0.03	6.15 ± 1.07
E18H_s40	20.65 ± 2.49	1.94 ± 0.08	2.45 ± 0.58
E18H_f40	19.92 ± 1.6	1.39 ± 0.12	4.6 ± 0.53

The flexural modulus also showed considerable increase with corresponding decrease of strain at break. As expected, and similar to that found in tensile testing, the values of the flexural strength, and flexural modulus were higher for composites containing smaller particle size HAP. However, the values of flexural strength and flexural modulus of the composites were higher than the corresponding values of tensile strength and tensile modulus. The tensile properties of materials are largely determined by the flaws and the submicroscopic cracks (Nielsen, 1974). The cracks do not play such an important role in compression because the stresses tend to close the cracks rather than to open them. It is predicted that the compressive strengths of a material are nearly two to four times its tensile strength. In flexural tests, a part of the specimen is under tension and a part under compression. The compressive strengths being greater than the tensile strength, flexural strength tends to be greater than the tensile strengths.

5.3.2. Effect of nature of polymer matrix

The values of flexural strength, flexural modulus, and fracture strain of E28H_s40, E28H_f40, E18H_s40, E18H_f40 and the unfilled polymers (E28, and E18) are given in Table 5.2. Similar to that seen for the tensile properties, the composites fabricated from E18 recorded higher values for the flexural strength and flexural modulus, with a corresponding decrease in the values of strain to fracture.

5.4. IMPACT STRENGTH

5.4.1. Effect of filler particle size and nature

Figure 5.6 shows the un-notched Charpy impact test results of HAP-EVA composites fabricated from the two grades of HAP powders and two grades of polymers.

It can be seen that both, the nature of HAP and the polymer matrix affected the impact strength of the composites. Comparing the results for the two HAP powders, it shows that the composites fabricated from H_s have higher impact strength than those made from H_f, demonstrating better impact resistance of $E28H_s40$. Addition of HAP resulted in a decrease in the value of impact strength from 70.3 kJ/sq.m to 64 kJ/sq.m and 54.8 kJ/sq.m for $E28H_s40$ and $E28H_f40$, respectively. Similar trend was noted for the composites fabricated from E18. The impact strength was decreased from 75 kJ/sq.m to 40.2 kJ/sq.m and 36 kJ/sq.m, respectively for $E18H_s40$ and $E18H_f40$.

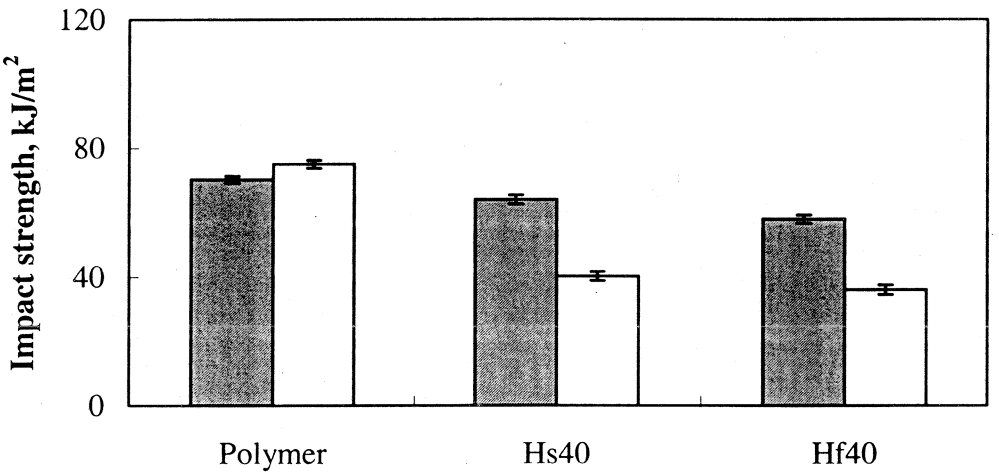

Figure 5.6. Impact strength of HAP-EVA composites fabricated from ▨ E28 and ☐ E18 polymer matrices.

The different results caused by HAP types are due to their difference in particle size and surface morphology. Generally, the addition of mineral fillers will have an embrittling effect on polymers and decrease the impact energy (Bartczak *et al.*, 1999). However, mineral fillers can also act as toughners provided they meet certain requirements in terms of their particle size and morphology (Zuiderduin *et al.*, 2003; Kim and Michler, 1998; Wang *et al.*, 1997; Hoffmann *et al.*, 1986; Liu *et al.*, 2002). It has been reported that rigid spherical particles with smooth surface and particle size less than 5μm, if dispersed homogeneously in the matrix polymer could improve the impact properties of composites (Zuiderduin *et al.*, 2003). In the case of rigid particles with irregular morphology and rough surfaces the matrix cannot fill the rough surfaces as easily as the smooth ones, especially at some deep indents (Zhang and Tanner, 2003). Therefore, more weak points exist in the composites with rough surfaced filler, resulting in poorer adhesion and a weaker interface between the filler and the matrix, which leads

to easier de-bonding during impact test. This would explain the observed trend of increased impact strength of E28H$_s$40 compared to E28H$_f$40.

5.4.2. Effect of nature of polymer matrix

The effect of polymer matrix on the impact strength of the composites also showed some differences. In general, higher the molecular weight of the polymer, higher is the impact strength. This is evident from the values of impact strength of E18 and E28. However, contrary to that expected, the impact strength values obtained for E18H$_s$40 and E18H$_f$40 were far lower than E28H$_s$40 and E28H$_f$40. This is also clear from the tensile stress-strain curves recorded for these composites (see section 5.2.2), which shows that both E18H$_s$40 and E18H$_f$40 undergoes typical brittle mode of fracture. It has been reported that a large drop in the impact strength of higher molecular weight polymers occur when the filler particles restrict the flow and orientation of the polymer chains (Hogg *et al.*, 1985). The restriction in orientation of the polymer chains disrupt the strain hardening capabilities of high molecular weight polymers resulting in lower impact properties. This could be the possible reason for the lower impact values of E18H$_s$40 and E18H$_f$40 when compared to E28H$_s$40 and E28H$_f$40.

5.5. DYNAMIC MECHANICAL ANALYSIS

The dynamic mechanical properties of the composites and the unfilled EVA are given in Figures 5.7 – 5.9. Figure 5.7 gives the variation of storage modulus values (E′) of the composites and unfilled EVA with temperature. The behaviour of all the three samples tested was found to be analogous. It could be seen that the storage modulus E′ decreases systematically with increase in the temperature; the diminution being pronounced at around –20°C. The pronounced relaxation of the virgin polymer and the composites around –20°C could be attributed to the glass transition temperature of the polymer. Below –20°C, the E′ is considerably high as the polymer is in glassy state. The stiffness (higher E′) of the polymer in this state is related to the change in the elastic energy stored on the deformation, which is associated with small displacements of the molecules from their equilibrium position (Bleach *et al.*, 2002). Around –20°C the polymer passes from the glassy state to the rubbery state (T_g), the molecular chains have considerable flexibility and they tend to adapt to conformations that lead to maximum entropy, resulting in decrease in the stiffness.

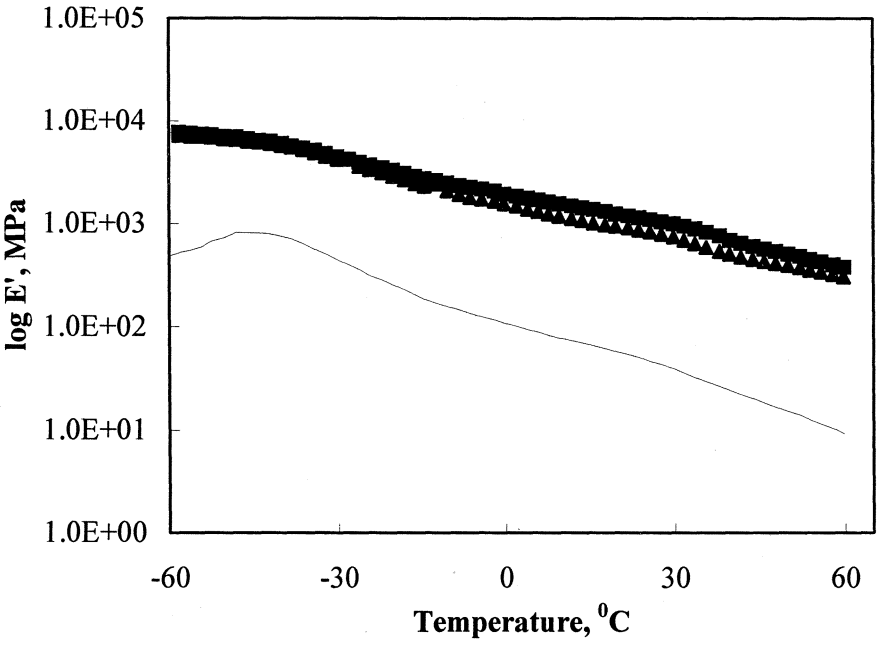

Figure 5.7. Variation of storage modulus of (—) E28, (■) E28H_s40 and (▲) E28H_f40 as a function of temperature.

Addition of HAP to the polymer increased the E′ over ten-folds within the whole range of testing temperature. In terms of E′, the effect of particle size was not profoundly seen below the T_g of the polymer matrix. However, above the T_g, E28H_f40 showed a slightly higher E′ than that of E28H_s40. Below the T_g, the dynamic modulus ratio between the components (HAP and EVA) is negligible. Hence, for the same loading of HAP, the moduli of the composites E28H_f40 and E28H_s40 become comparable. Above the T_g, the difference in dynamic modulus becomes more pronounced because of the larger modulus ratio of the components when the polymer is in the rubbery state compared to the glassy state. This observation is better explained by considering the variation of relative modulus with the temperature (Figure 5.8). The relative storage modulus values were calculated according to the equation (5.1)

$$E'_r = \frac{E'_c}{E'_m} \quad \text{.....5.1}$$

where E'_r, E'_c and E'_m are the relative modulus, storage modulus of the composite and storage modulus of virgin polymer, respectively. The increase in relative modulus with temperature suggests that the HAP controls the values of E′. Similar observations on dynamic mechanical properties of HAP reinforced polymer composites were reported by

various authors (Wang *et al.*, 1998b; Nazhat *et al.*, 2000). Nielsen and Lewis (1969) hypothesized that the changes in relative modulus with temperature for particulate reinforced composites are a consequence of thermally induced stresses in the polymer. The thermal stresses result from differences in the thermal coefficients as the composites cools from the molding temperature. Thus the stressed polymer surrounding the filler particles will have a lower modulus than the bulk polymer. Therefore the increase in relative modulus at higher temperatures is due to the reduction in thermal stresses, combined with the modulus of the filler. It was interesting to note that at the physiological temperature the composites possessed sufficient modulus, which qualifies them to be used for the intended application.

Above the T_g, E28H$_f$40 registered a slightly higher E′ value than E28H$_s$40 (Figure 5.8).

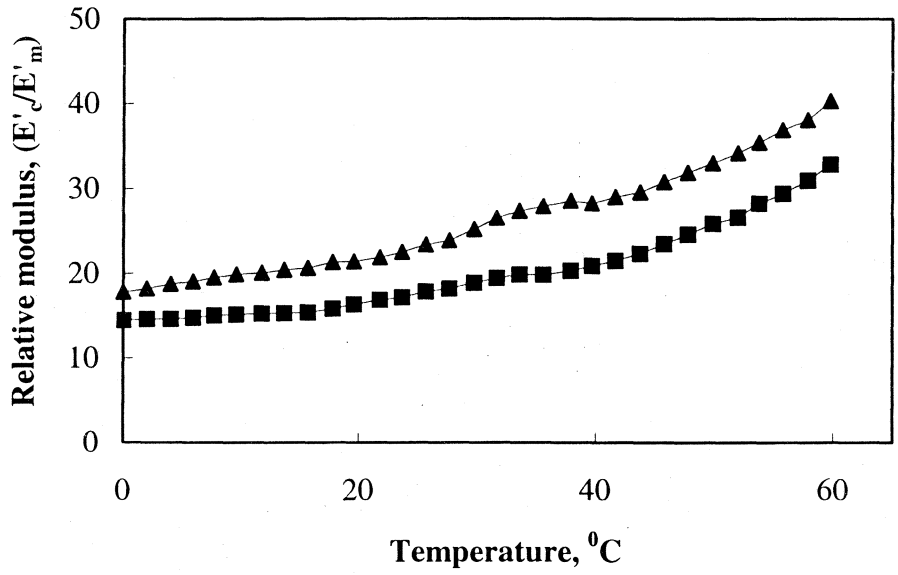

Figure 5.8. Variation of relative modulus of the composites (■) E28H$_s$40 and (▲) E28H$_f$40 as a function of temperature.

This is a consequence of the different morphological structures of the two filler particles. Liang *et al.* (2000) in their studies on the effects of glass bead size and content on the viscoelasticity of filled polypropylene (PP) composites found that the dynamic moduli of PP filled with the biggest glass bead were higher than that for smaller bead filled systems at the same test conditions. The authors hypothized that for a rigid inorganic particle filled thermoplastic composite, the morphological structure of the

interface influences the viscoelastic properties of the composites, besides depending on interfacial adhesion strength, filler size and filler concentration.

The damping factor (tan δ) gives the fractional energy lost in a system due to deformation and is often proportional to the imperfections in the elasticity of a polymer (Nielsen and Landrel, 1994). Damping is a sensitive indicator of all kinds of molecular motions and phase transitions. The temperature dependence of tan δ of neat polymer E28, and E28H_s40 and E28H_f40 are given in Figure 5.9.

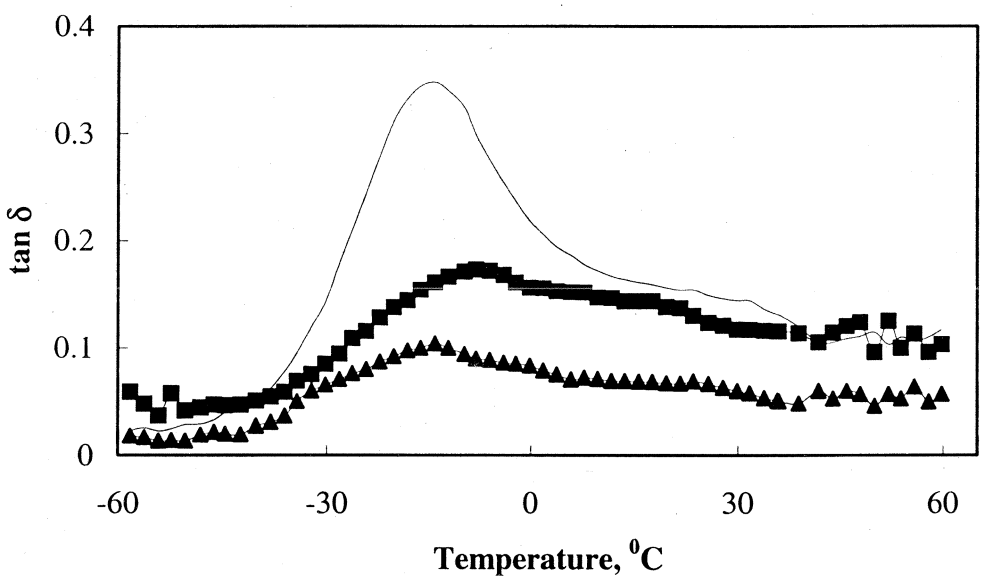

Figure 5.9. Variation of loss tangent (tan δ) of (—) E28, (■) E28H_s40 and (▲) E28H_f40 as a function of temperature.

For the neat polymer E28, the tan δ peaks at –14.2°C, which corresponds to the T_g of the polymer. At temperatures well below –14.2°C, the damping is low as nearly all the energy stored in deforming the material is quickly recovered when the stress is removed since molecular slipping and other motions are frozen in. At the glass transition region (–14.2°C) some molecular chain segments are frozen in while some are free to move. When the stress is initially applied to a frozen in chain segment which later becomes free to move while it is still under stress, the segment will move in such a manner as to reduce the stress on it (Gradin *et al.*, 1989). After moving, the segments have less stored energy because of the reduction in the stress, so excess energy is dissipated as heat (at the damping peak). At temperatures above –14.2°C, the majority of the polymer chains

become mobile (the viscosity of the polymer becomes low) and the dissipation of energy is much reduced.

Inclusion of HAP changes the damping behaviour of the polymer; the most pronounced effect being the broadening of the transition peak. Widening of glass transition region is due to the adsorption of the polymer on to the filler. Adsorption of polymer onto a surface restricts molecular motion, changes the density of packing of polymer chains, and modifies the conformation and orientation of chain segments in the neighbourhood of the surface (Xiong *et al.*, 2002). The value of tan δ decreases with the inclusion of HAP. It appears that the addition of HAP actually limited the mobility of the polymeric chains, and hence reduces the damping of the composite. This can be expected because an increase in filler content will also decrease the polymer volume and thus, the overall damping of the composite. The decrease in the tan δ value, however, varies with the type of filler used. A higher value of tan δ was noted for E28H_s40 when compared to E28H_f40 (Figure 5.9). The damping factor, tan δ, is defined as

$$\tan \delta = \frac{E''}{E'} \quad \text{.....(5.2)}$$

The loss modulus E″ corresponds to the energy lost as heat. A higher value of tan δ thus implies excessive heat generation within the polymeric composite system. Several aspects contribute to this anticipated heat generation. For example, Nielsen observed an increase in damping of mica-filled epoxy resins (Nielsen and Landrel, 1994). This increase in the damping was considered to be an upshot of liberation of heat of friction at the particle-polymer interface. Xiong *et al.* (2002) reported increased damping of filled composites in comparison with pure polymer in their studies on acrylic latex/nano-SiO_2 composites. It has been postulated by Nielsen that particle-particle interaction can evolve frictional heat (Nielsen and Landrel, 1994). The particle-particle contact can ensue from agglomeration of fillers. Particle-particle interaction is also observed when the particle size of the fillers decreases because with decreased particle size, we get an increased surface area and total number of particles (Cai and Salovey, 1999). For the same volume fraction of HAP, E28H_s40 has increased total surface area and total number of particles in comparison to E28H_f40. Hence the possibility of heat generation from particle-particle friction is fairly high in E28H_s40, which gives rise to a higher value of E″ and a higher tan δ.

Another notable difference to the damping response of $E28H_f40$ and $E28H_s40$ is with regard to the shift in the damping peak. The inclusion of H_s resulted in the shift of the maxima in the damping curve from –14.2°C to –8.2°C. Strong interactions of fillers with polymers have found to increase the T_g of the polymeric composites (Xiong *et al.*, 2002; Tjong *et al.*, 2002). In general, the interactions between two substances are ascribed mainly to the chemical bond or mechanical lock. Kikuchi and Tanaka reported the existence of chemical interactions in β-tricalcium phosphate/co-polymerized poly-l-(lactide) composites (Kikuchi and Tanaka, 2000). The authors, however, did not report any change in the T_g of the polymer matrix, indicating the weak nature of the chemical interaction. On the other hand, Nazhat *et al.*, (2001) and Bleach *et al.*, (2002) reported an increase in the matrix T_g in their studies using biphasic calcium phosphate-polylactide and HAP-polylactide composites, respectively. The increase in the matrix T_g was attributed to the partial immobilization of the polymer and the physical blocking of a number of molecular configurations as a result of adsorption on to the filler. It can hence be inferred that the upper shift caused by H_s could be due to strong mechanical lock that occurred between $E28H_s40$ and polymer matrix. The incorporation of H_f, however, did not cause any significant shifting of the damping peak indicating that the interaction of the H_f with EVA is not strong enough to alter the molecular mechanisms of the polymer chains.

A comparison of the mechanical properties of the HAP-EVA composites, at 40vol.% of HAP, is made with the human cortical bone and the clinically used bone substitutes of similar material chemistry (Table 5.3).

Table 5.3. Mechanical properties of cortical bone and various bone substitutes at the physiological temperature (37.5 °C).

Material	Young's modulus, GPa	Tensile strength, MPa	Strain to failure (%)	Damping factor, tan δ
Cortical bone*	7-20	50-150	1-3	0.01-0.4
Cancellous bone*	0.05-05	10-20	5-7	
HAP-PCL$^{\Psi}$	0.07	2.4	-	-
HAP-EVA	0.5-0.8	10-12	10-17	0.04-0.11

* (Abu Baker *et al.*, 2003c); $^{\Psi}$ (Zanetti and Nassif, 2003)

It could be seen from Table 5.3 that the values of Young's modulus and tensile strength of HAP-EVA composites are quite low when compared to the human cortical bone. This discrepancy is due to the lower strength of the matrix polymer material used

for the fabrication of these composites. Nevertheless, these values are quite higher when compared to the cranioplastic substitute of similar material chemistry and lie within the bounds of the human cancellous bone. The values of strain to failure of HAP-EVA are higher than corticle bone, which clearly indicates the toughness of these composites. The values of tan δ also lie within the limits of that of the cortical bone. A lower tan δ implies high dimensional stability, a property of immense importance for a biomaterial.

5.6. FRACTOGRAPHY

The mechanical properties of the composites are influenced by the nature of the reinforcement used. This is evident from the tensile fractographs of the composites.

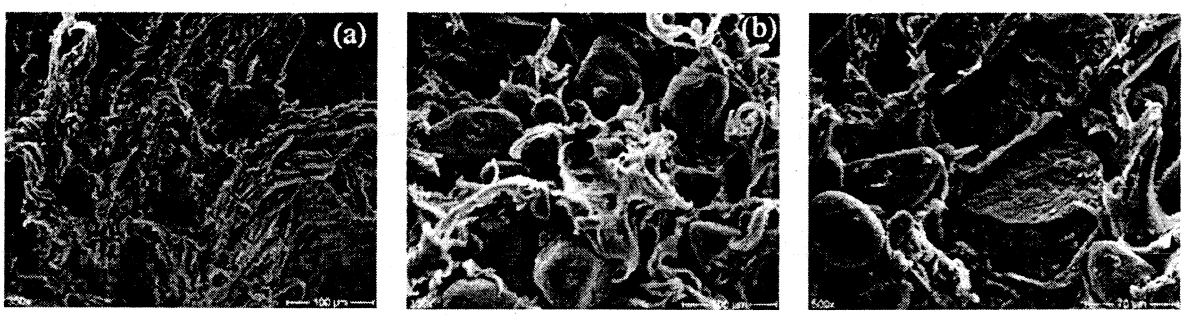

Figure 5.10. Tensile fracture morphology of HAP-EVA composites (a) E28H_f20 (x350); (b) E28H_f40 (x350) and (c) E28H_f40 (x600).

Figure 5.10 (a, b, & c) show the SEM of tensile fracture surfaces of the HAP-EVA composites fabricated from the freeze dried HAP particles at various volume percentage of HAP loading. The weak interaction of freeze dried HAP-polymer is clear from this micrograph. The 'relatively clean' surface of the particulate HAP reinforces this further. The fracture occurred mainly by the de-bonding of HAP particles from the matrix. The polymer matrix, however, underwent considerable deformation before fracture. Interestingly, in some areas, failure occurred by fracturing through the HAP particulate (Figure 5.10c). The composites were fabricated using un-sintered HAP particles. This makes the particles inherently weak and possibility of particle failure becomes higher, as the particle size is increased.

A different kind of fracture surface was noted in the case of composites fabricated from spray dried HAP particles. The composites mainly fractured by debonding (Figure 5.11a). However, unlike the composites fabricated from freeze-dried HAP particles, the spray dried particulate HAP was found entangled and embedded in the polymer matrix (Figure 5.11b). Closer examination of the composites revealed the presence of traces of

EVA polymer adhering to the surface of HAP particles at many areas (Figure 5.11c&d), which explains the improved properties of the composites fabricated from the spray dried HAP particulates.

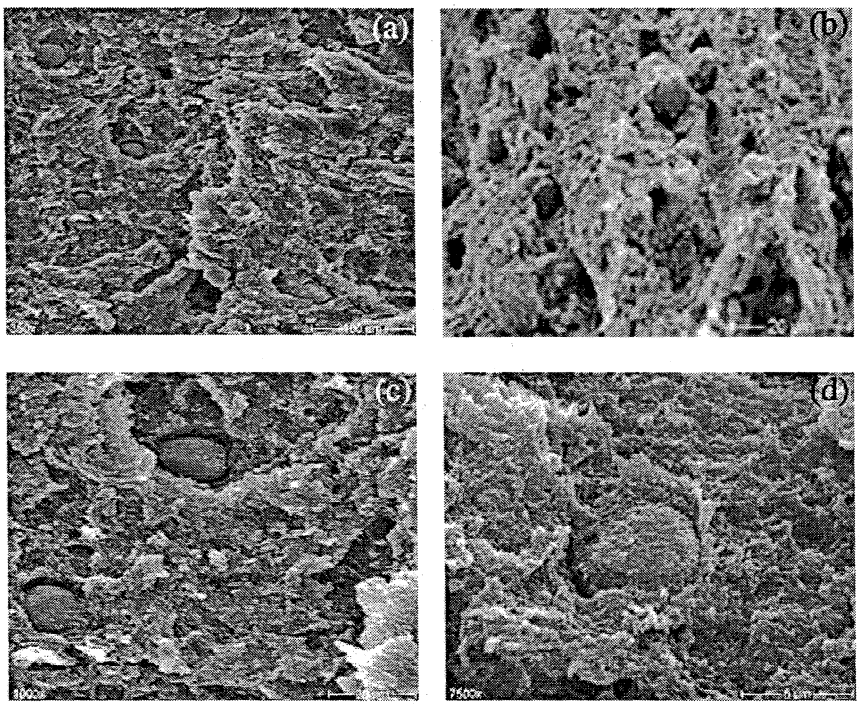

Figure 5.11. Tensile fracture morphology of HAP-EVA composites (a) E28H_s20 (x350); (b) E28H_s40 (x1500); (c) E28H_s40 (x1000) and (d) E28H_s40 (x7500).

5.7. CONCLUSIONS

The mechanical properties of HAP-EVA composites were evaluated. The mechanical testing carried out namely; tensile, flexural, impact and dynamic mechanical analysis provided useful insights on the composite properties. Generally, the composites fabricated from smaller particle size hydroxyapatite (H_s) showed improved properties compared to the higher particle size (H_f) counterpart. The fractographs of the composites showed that the polymer matrix underwent considerable deformation prior to the fracture. The composites fabricated from smaller particle size hydroxyapatite (H_s) seemed to be interacting better with the polymer matrix when compared to the freeze-dried particles.

The values of Young's modulus, tensile strength and strain at break of HAP-EVA composites with 40vol.% of HAP were found to be superior to PLLA/HAP or PCL/HAP composites for cranioplasty. The low modulus and high strain at break of HAP-EVA composites make them excellent 'surgeon friendly' cranial substitute.

CHAPTER 6

BIOLOGICAL EVALUATION

6.1. BACKGROUND

Biocompatibility has evolved over several years as a descriptive term concerned with the biological acceptability and biological performance of materials used in medicine and dentistry. Conventionally, biocompatibility has been equated with the lack of a significant interaction between materials and tissues. This has implied a combination of inertness and non-toxicity, and typical descriptions on an ideal 'biocompatible' material would be a list of negatives, such as non-degradable, non-irritant, non-toxic, non-carcinogenic and non-allergenic. In view of the fact that so few materials even approach inertness in the body, and probably no material has zero influence on tissues, this concept of biocompatibility has been questioned. Biocompatibility is, therefore, now considered in a more positive light; the definition used is that "biocompatibility refers to the ability of a material to perform with an appropriate host response, in a specific application" (Williams, 1990).

Critical biocompatibility evaluation is an essential step in the development of any material intended for biomedical applications. The performance and the biological response of biomaterials must be evaluated to determine whether their compatibility and functionality are suitable for application in physiological systems. This implies the utilization of standard practices, which recommend generic biological test methods for materials and devices according to end-use applications. These test protocols are intended to be applied to materials and medical devices for human use and recommend sufficient biological testing to establish a reasonable level of confidence concerning the response to

a given material or device to a living organism, as well as guidance in selecting the proper procedures to be carried out for the screening of new or modified materials.

Biocompatibility evaluation of medical devices involves testing either the material itself or an extract from it, or both, depending on the nature of the end-use application. For the convenience of assessment, the tests are categorized into (1) *in vitro* screening tests, followed by (2) *in vivo* toxicological/biocompatibility tests. The screening tests check the preliminary safety with respect to cells/blood and are performed regardless of the final use of the materials. *In vitro* cell culture cytotoxicity evaluation on established cell lines is the common screening test employed to assess the acute toxicity effects of material under study. A material passes this test only if the acute toxicity effects are not recorded; further tests are then done on the material to assess the toxicological/biological response by making use of suitable animal models.

The International Organization for Standardization (ISO) recommends a battery of biocompatibility studies to be carried out on all medical devices in accordance with their end-use applications. For example, for a material intended for bone substitute applications, the following battery of tests such as (1) Cell culture cytotoxicity, (2) Intracutaneous irritation, (3) Systemic toxicity, (4) Sensitization, and (5) Implantation have to be done based on the guidelines/protocols prepared by ISO-10993. This chapter discusses the biological performance of the HAP-EVA composites with potential future use as bone substitute by following standard practices for generic biological test methods for materials and devices.

6.1.1. Selection of compositions for biological evaluation

Mechanical property evaluation (chapter 5) of the HAP-EVA composites showed that the composites, fabricated from E28 polymer matrix and smaller particle size HAP (H_s), were superior to the other compositions with regard to pliability. Two compositions, namely E28H_s40 and E28H_s50, containing higher volume fraction of HAP, were selected for biological evaluation. Biological evaluation studies such as cell culture cytotoxicity, intracutaneous irritation and implantation in rabbit muscle as well as in rabbit cranium, were carried out to gauge the biological performance of these composites. Two additional evaluation studies, namely systemic toxicity and sensitization, were carried out on E28H_s40, considering its superior mechanical performance to E28H_s50.

6.2. *IN VITRO* CELL CULTURE CYTOTOXICITY

Cytotoxicity is the ability of a material or substance to produce a toxic or cellular effect with a deviation from normal morphology and functionality (Wise *et al.*, 1995). The cytotoxicity tests essentially consist of the assessment of cell morphology and viability when the cells come in contact with either the material or the extract of the material. The cells lysed or injured by the material or the extract of the material are examined. Generally, established mammalian cell line is used for the study. The L929 (mouse fibroblasts) have become the most commonly used cell line because they are easily cultured and scored. They also represent a cell line capable of being perpetually subcultured and have been shown to be among the preferred cell types for use in biocompatibility test procedures *in vitro* (Johnson *et al.*, 1983).

The response of E28H$_s$40 and E28H$_s$50 to a culture of L929 cells is shown in Figure 6.1 (a & b).

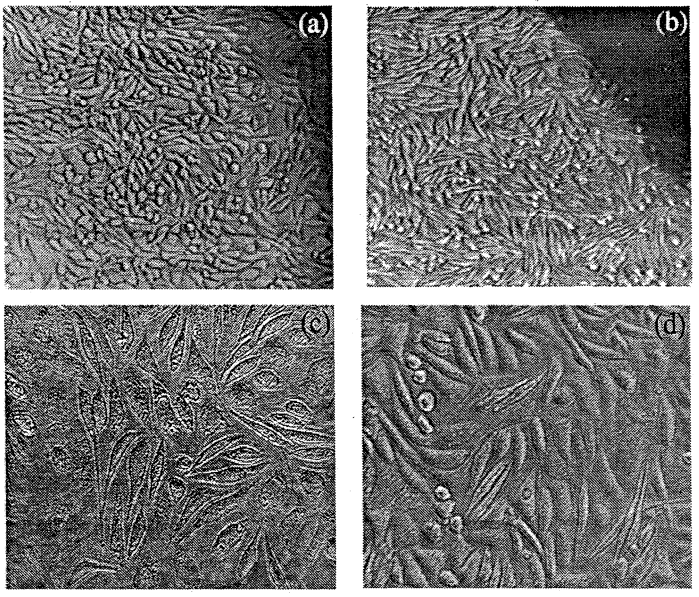

Figure 6.1. L929 cells incubated with (a) E28H$_s$40, (b) E28H$_s$50, (c) extract from E28H$_s$40 and (d) extract from E28H$_s$50 over 24 h.

It is clear from the figures that the typical spindle morphology of L929 was retained even after 24 h of contact with E28H$_s$40 and E28H$_s$50. Similar results were obtained for the test performed on the extract of the composite materials (Figure 6.1c&d). The results from the *in vitro* cell culture cytotoxicity showed that both E28H$_s$40 and E28H$_s$50 were non-cytotoxic to L929 cell line.

6.3. INTRACUTANEOUS IRRITATION

Irritation studies assess the short-term and generally localized hazards of medical devices in the immediate region of their applications. Intracutaneous irritation test is a sensitive acute toxicity-screening test and is generally accepted for detecting potential local irritation by extracts from medical devices (Timbrell, 1990). In this test, the dermal irritation caused by the substance is investigated by observing changes from erythema (redness of the skin at the site of injection) and oedema (swelling at the site of injection) following intradermal injection of the extracts from the material. The skin reactions are produced by diverse physiological mechanisms and they are easily observed visually and by palpitation.

The results of responses of intracutaneous injection for erythema and oedema of the test samples and control extracts are presented in Table 6.1 & Table 6.2 for $E28H_s40$ & $E28H_s50$, respectively. The injected test sites did not reveal gross signs of tissue reaction such as erythema and oedema in comparison to the control extract for all the time periods investigated. This biological behaviour demonstrates that no acute toxicological effect was observed by these composite materials as to their biocompatibility characteristics.

Table 6.1. Intracutaneous irritation score for the $E28H_s40$

Material code	Skin reaction	Scoring at	Irritation score	
			Saline	CSO
$E28H_s40$	Erythema	Immediate	0	0
		24 h	0	0
		48 h	0	0
		72 h	0	0
$E28H_s40$	Oedema	Immediate	0	0
		24 h	0	0
		48 h	0	0
		72 h	0	0

0-no erythema & oedema; 1-mild erythema & oedema; 2- moderate erythema & oedema; 4-severe erythema & oedema

Table 6.2. Intracutaneous irritation score for the $E28H_s50$

Material code	Skin reaction	Scoring at	Irritation score	
			Saline	CSO
$E28H_s50$	Erythema	Immediate	0	0
		24 h	0	0
		48 h	0	0
		72 h	0	0
$E28H_s50$	Oedema	Immediate	0	0
		24 h	0	0
		48 h	0	0
		72 h	0	0

0-no erythema & oedema; 1-mild erythema & oedema; 2- moderate erythema & oedema; 4-severe erythema & oedema

6.4. SYSTEMIC TOXICITY

Systemic toxicity measures the toxicity involving entire organism and is designed to determine the systemic biological responses of animals to the test material. Systemic toxicity estimates the harmful effects of either single or multiple exposures to test materials and/or extracts, in an animal model (Gad, 1997). In this study, observations are made for the whole body effects such as lethargy, hyperactivity, convulsions, loss of weight, and death. The effects observed in animals are usually directly related to the amount of the toxic substance administered orally, dermally, or via., inhalation (Ecobichon, 1992).

Table 6.3 gives the number of deaths recorded for the test and the control extracts for the intravenous and intraperitoneal injections of the $E28H_s40$. For all the observation time periods, none of the test animals treated with the sample extracts revealed any different biological reaction from those observed for the control extract. It means that no toxicity symptom in terms of release of offending, allergic, or lethal chemical components were observed for any animal exposed to the doses recommended by the guideline specified.

Table 6.3. Death rate and mortality ratio recorded for animals exposed to intravenous and intraperitoneal injections of the control and E28H$_s$40 extracts

Injection method	Animal	Death rate after injection				Mortality ratio
		4 h	24 h	48 h	72 h	
Intravenous	Test	0	0	0	0	0/5
		0	0	0	0	0/5
		0	0	0	0	0/5
		0	0	0	0	0/5
		0	0	0	0	0/5
	Control	0	0	0	0	0/5
		0	0	0	0	0/5
		0	0	0	0	0/5
		0	0	0	0	0/5
		0	0	0	0	0/5
Intraperitoneal	Test	0	0	0	0	0/5
		0	0	0	0	0/5
		0	0	0	0	0/5
		0	0	0	0	0/5
		0	0	0	0	0/5
	Control	0	0	0	0	0/5
		0	0	0	0	0/5
		0	0	0	0	0/5
		0	0	0	0	0/5
		0	0	0	0	0/5

0-no erythema & oedema; 1-mild erythema & oedema; 2- moderate erythema & oedema; 4-severe erythema & oedema

6.5. CLOSED PATCH SENSITIZATION

A dermal reaction exists whereby exposure to chemical extractables from materials elicit little reaction, but following a second dermal exposure, an effect is seen that occurs earlier in time, is more severe, and persists for a longer duration (Ecobichon, 1992). Subsequent exposures, even though weeks or years apart, result in full-blown, allergy-like, delayed reaction to the chemical. Frequently, the reaction can be elicited by much lower concentrations of agent and on areas of the skin other than those involved in the initial contact. This kind of delayed reaction to the chemical extractables from materials is mediated by the immune system and is not detectable by irritation tests, which consider only the initial responses but not delayed effects.

Various investigators have described a number of test procedures for detecting this delayed response, but all are similar in that an attempt is made to build up the

immune response by repeated application (Marzulli and Mailbach, 1987). The most widely used *in vivo* sensitization tests are the Magnusson-Kligman (1969) maximization test and the closed patch tests (Buehler, 1965). Historically, the preferred animal species for sensitization testing has been the guinea pig. It is important to keep in mind that irritation and sensitization are two different reactions. Irritation may occur upon first exposure to a chemical. Sensitization requires repeated encounters, in order to induce the immune system and then a subsequent exposure to manifest the response. Irritation is a local response while an allergic or sensitization reaction is a systemic phenomenon.

The result of the skin response to closed patch sensitization studies for $E28H_s40$ as compared to the control is given in the Table 6.4. It could be seen that for all the time periods of observation no visible skin reactions, such as erythema and oedema, were observed, which indicate that the material does not elicit any skin sensitization potential as per closed patch test.

Table 6.4. Responses to closed patch sensitization test recorded for $E28H_s40$ for test and control animals (challenge application).

Animal	Skin reaction			
	Erythema		Oedema	
	24 h	48 h	24 h	48 h
Test	0	0	0	0
	0	0	0	0
	0	0	0	0
	0	0	0	0
	0	0	0	0
	0	0	0	0
	0	0	0	0
	0	0	0	0
	0	0	0	0
	0	0	0	0
Control	0	0	0	0
	0	0	0	0
	0	0	0	0
	0	0	0	0
	0	0	0	0

0-no erythema & oedema; 1-mild erythema & oedema; 2- moderate erythema & oedema; 4-severe erythema & oedema

6.6. IMPLANTATION STUDIES

6.6.1. Intramuscular implantation in rabbit

A material replacing bone would be in contact with surrounding soft tissues (periosteum, connective tissue, and muscle). These tissues are generally considered to show a more severe inflammatory response than the bone. Hence the biocompatibility of the bone substitute material has to be evaluated in the soft tissue environment as well. Biocompatibility studies following intramuscular implantation provide a comprehensive understanding of the relationship of biologic response at cellular level to the composition and structure of the biomaterial. Many investigators have exploited this asset of *in vivo* biocompatibility testing and have reported their findings on biocompatibility of various biomaterials (Laing *et al.*, 1967; Tanaka *et al.*, 2002; Vande Vord *et al.*, 2002). Generally, the biocompatibility of candidate implant materials is based on features of "fibrous capsule" that envelops the implant (Cynthia and Myron, 1986). However, this capsule represents the end stage of a healing process (repair phase), which follows the initial inflammatory phase.

Intramuscular implantation studies on paravertebral muscles of the rabbits showed that all animals tolerated the surgery well. The post implantation period was also found to be uneventful. There were no cases of infection, paralysis, or mortality during the observation periods. The site of implantation healed without any complications. The skeletal muscle around both the control and the test samples was grossly normal at all time periods. The histological findings, however, showed some changes. Generally, the muscle tissues in the vicinity of $E28H_s50$ and $E28H_s40$ showed good healing response at 4 weeks post implantation. There was evidence of repair in the tissue around both the types of implants as early as 4 weeks following the implantation. Fibrous connective tissues were observed as a capsule around the site. Few fibroblasts, and fibrocytes were also present in the capsule. Nevertheless, in some muscle sections from $E28H_s50$, inflammatory cell infiltration was found in the vicinity of the implant (Figure 6.2a, b & c). Similar tissue response was noted around some tissue sections from $E28H_s40$ also (Figure 6.2 d, e & f). A disadvantage of *in vivo* biocompatibility testing is that it is often influenced by multiple factors. The surgical procedure itself initiates an inflammatory response. Additionally, the presence of implant also provides a continuous inflammatory stimulus. The inflammatory response is a sequential, localized tissue reaction to the

oreign material and involves an initial infiltration of neutrophils followed by macrophages Nagase *et al.*, 1988).

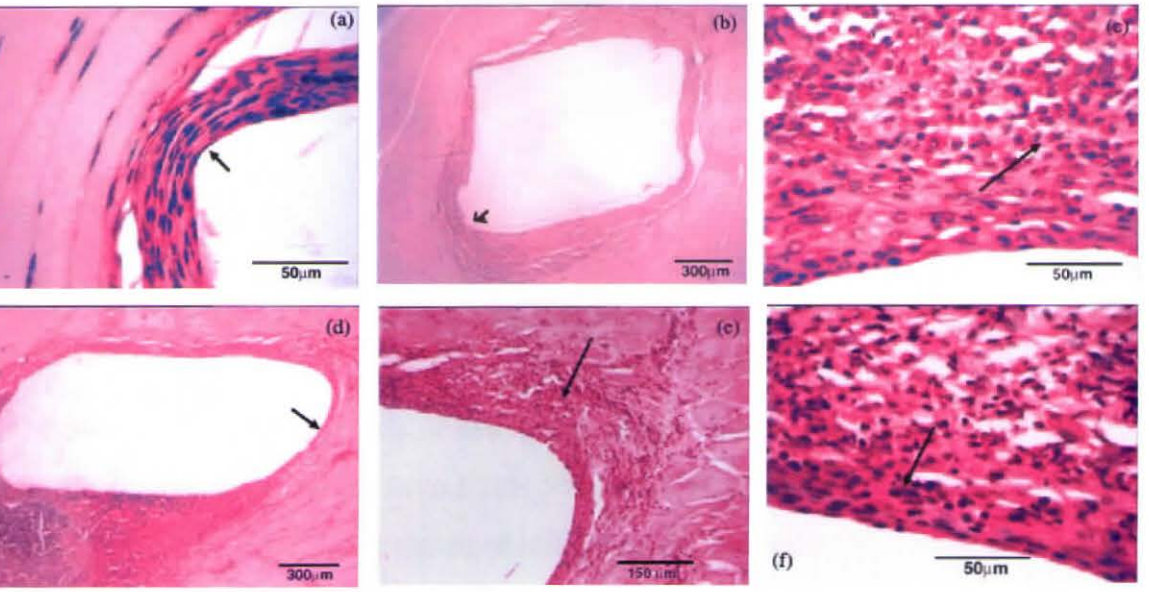

igure 6.2. Light microscopic images of E28H$_s$50 (a, b, & c) and E28H$_s$40 (d, e, & f) at weeks post implantation. The arrows shown in Figure 6.2 (a & d) shows the fibrous apsule present around the implant. The arrows in Figure 6.2 (b, c, d, e & f) show the nflammatory cells in the vicinity of the implanted composite material.

In the initial stages of inflammation, the predominant cell types present are the eutrophils. These are short living cells with short life span and which disappear after 24-48 . However, there exist examples that demand continuous recruitment of neutrophils even uring the chronic phase of inflammation. Vande Vord *et al.*, (2002) evaluated the iocompatibility of chitosan scaffold in mice and found marked neutrophil accumulation ithin the implant that resolved with increasing implantation time. Several other investigators lso reported similar observation with chitosan and concluded that the neutrophil ccumulation was due to the chemotactic nature of chitosan on neutrophils (Okamoto *et al.*, 993; Usami *et al.*, 1994; Kosaka *et al.*, 1996). Poshusta *et al* (2003) also reported the resence of neutrophils along with other inflammatory cells around the PLA/HAP implants n mice. According to them, the active inflammatory response around the implant was a esult of the degradation of the polymer. In such cases, the degradation products could also e observed both intracellular and extracellular to the phagocytic cells that are present around he implants. Besides these, geometrical properties like shape, size and surface topography f the implant and micromotions of the implant also affect the tissue reaction (Nagase *et al.*, 991; Noguchi *et al.*, 1991; Miyamoto *et al.*, 1999).

Histological observations at 12 weeks post implantation revealed that the flammatory reaction had subsided around the samples (Figure 6.3a&b).

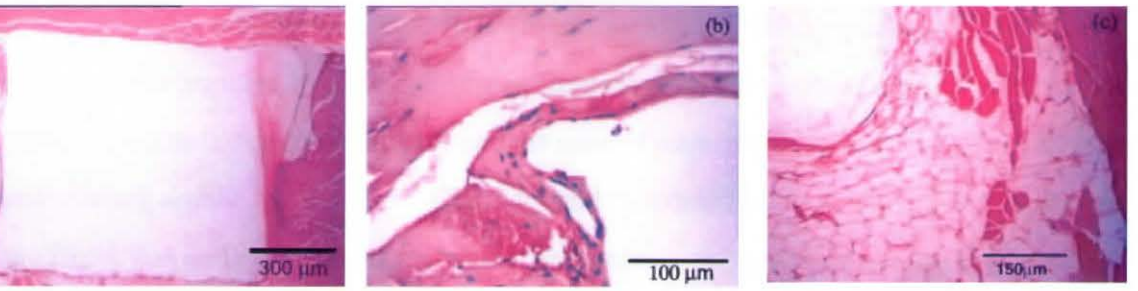

gure 6.3. Light microscopic images of E28H$_s$50 (a & b) and E28H$_s$40 (c) at 12 weeks post nplantation.

Except for the presence of few macrophages and lymphocytes, noted as focal llections around the tissues from E28H$_s$50 and E28H$_s$40, the sections from both these mples displayed marked regression of inflammation. Interestingly, significant numbers fibroblasts and fibrocytes were found in the vicinity of E28H$_s$50 at this time of study dicating encouraging signs of healing response (Table 6.5).

ble 6.5. Summary of light microscopy observations around the test materials

Parameters	Four weeks		Twelve weeks		Twenty four weeks	
	E28H$_s$50	E28H$_s$40	E28H$_s$50	E28H$_s$40	E28H$_s$50	E28H$_s$40
Necrosis	0	0	0	0	0	0
Neutrophils	+	++	±	±	0	0
Macrophages	++	++	±	±	±	±
Lymphocytes	++	++	±	±	±	±
Plasma cells	+	++	0	0	±	±
Giant cells	0	0	0	0	0	0
Eosinophils	++	++	0	±	0	0
Foreign body	++	0	+	0	0	0
Fibroblast	++	++	++	+	+++	++
Fibrocytes	0	++	+	±	++	+
Fatty infiltration	0	0	+	+	+++	+++
Calcification	0	0	0	0	0	0
Haemorrhage	0	0	0	0	0	0
Oedema	0	0	0	0	0	0

- item not present; ± - item occasionally present; + - item present in mild degree; ++ - item present in moderate degree; +++ - item present in appreciable degree.

The implanted samples also retained their structural integrity throughout the period f implantation, confirming the non-degradable nature of the samples. Regarding the muscle ections from the control samples, mild inflammation and moderate fibrosis were seen rrounding the implant. In addition, fatty infiltration (Figure 6.3c) was noticed surrounding oth the implanted composite samples and the control materials. There were signs of fibrous ssue scarring around the E28H$_s$50, E28H$_s$40, and the control sample with a few fibroblasts, any fibrocytes and excess collagen. It has been postulated that in short term implantation, high fibrocyte density and presence of few macrophages might be an indicator of ocompatibility (Therin *et al.,* 1994). A few neutophils that were occasionally present in e vicinity of the implants in the absence of the cardinal signs of inflammation would have sulted from the procedure employed for implantation. A similar inflammatory response as seen in the vicinity of the control specimen, which further confirms this observation.

At the end of 24 weeks of implantation, the inflammation around the test and the ntrol samples subsided completely (Figure 6.4). Fibrocytes and few macrophages were en surrounding the implants. A thin layer of collagen was also found encapsulating the plant in all tissue sections with no evidence of acute inflammatory reaction or cellular crosis. The fatty infiltrations were, however found to persist.

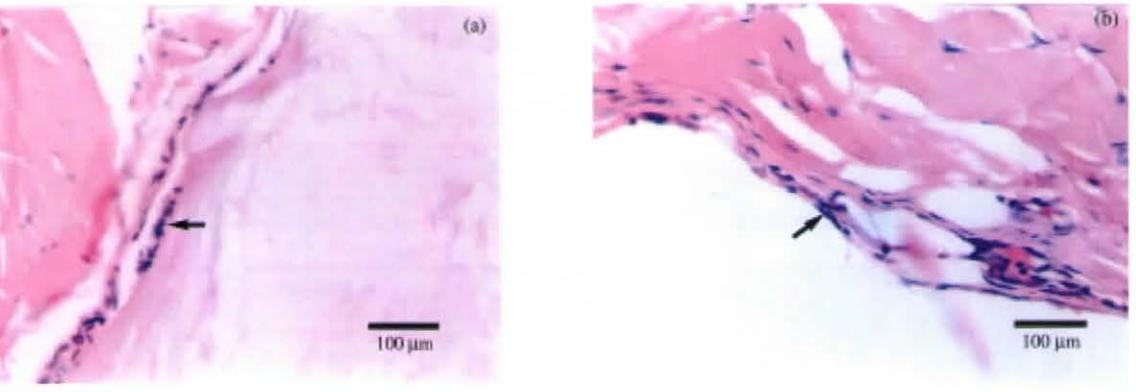

gure 6.4. Light microscopic images of (a) E28H$_s$50 and (b) E28H$_s$40 at 24 weeks post plantation. The arrow shows the fibrous capsule surrounding the implant.

Except for the slightly higher number of fibrocytes and fibroblasts seen around 28H$_s$50, the semi-quantitative soft-tissue response to E28H$_s$50, E28H$_s$40 and UHMWPE dicated no significant difference between the three-implant materials. The response is nsistent with "biocompatibility" despite of the different nature of the three materials. mi-quantitatively similar response suggests that factors, which govern the type of cell

een at the implant tissue interface, are same regardless of the difference in chemistry and omposition of the three materials.

.6.2. Implantation in rabbit cranium

.6.2.1. Results

All implantation procedures and the post-implantation period were uneventful. mplant related adverse neurological symptoms of significance were not noticed during this eriod. There were no signs of clinical inflammation around the implants in any animal at ny time period of implantation.

In the E28H$_s$40 group, histological sections at 12 weeks post-implantation exhibit oven and lamellar bone present all around the implant (Figure 6.5a). The woven bone resented was in continuation with the host bone at both the edges. Mature lamellar bone as also present in the close proximity to the implant. The new bone, however, was separated om the implant by a thin layer of fibrous tissue.

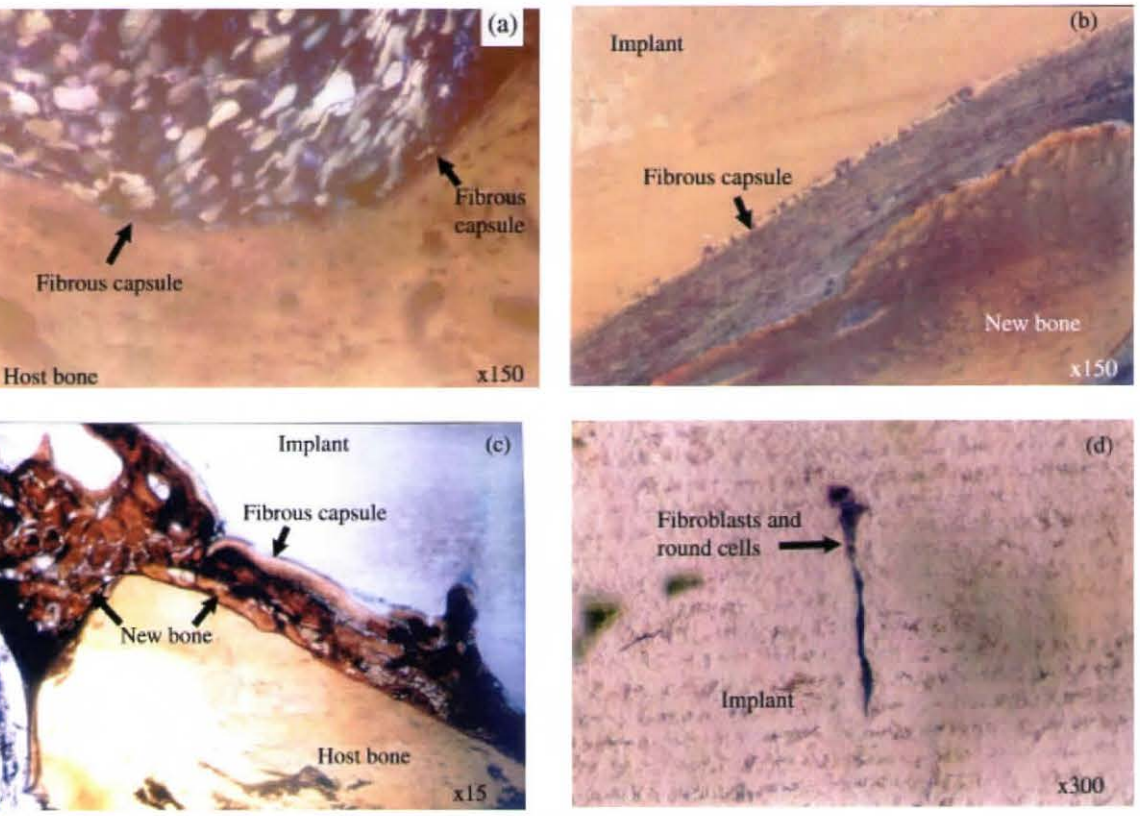

igure 6.5. Light microscopic pictures of E28H$_s$40 at (a) 12 weeks, (b) 24 weeks, and c) & (d) 48 weeks post-implantation.

At 24 weeks post-implantation (Figure 6.5b), an increased amount of newly formed, oven bone was seen juxtaposed to the implant. At this time point of implantation too, the ew bone formed was seen separated from the implant by a layer of interposing fibrous ssue. At 48 weeks post-implantation, the implant is surrounded by mature woven bone igure 6.5c). In most part, the implant is surrounded by a layer of round cells and fibroblasts, hich extend at numerous foci into the material (Figure 6.5d). In some areas woven bone ith occasional lamellae was seen in direct apposition to the implant, while in the other eas an interposing fibrous tissue layer separated the implant from the surrounding woven one. At all time periods of implantation, there was no evidence of chronic inflammation.

In the E28H$_s$50 group, at 12 weeks post-implantation fragments of the implant aterial were present with the trabecular host bone at both the ends (Figure 6.6a).

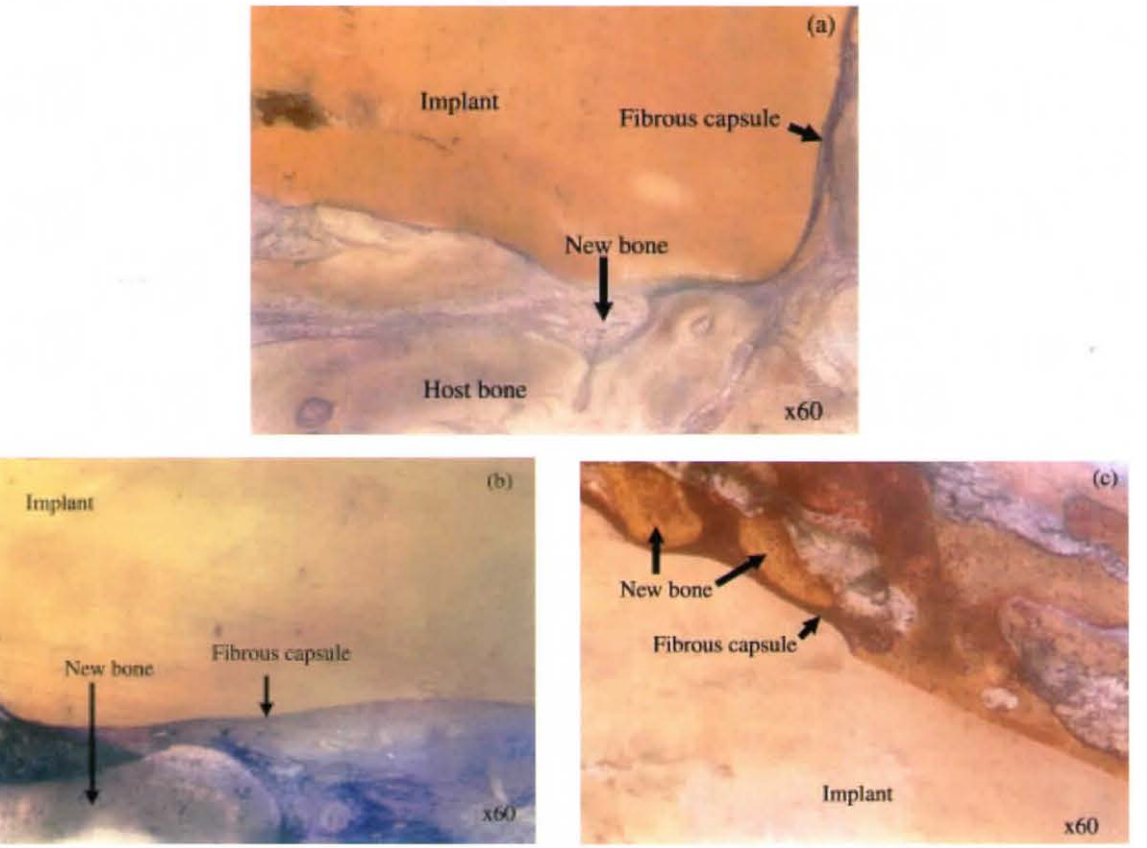

igure 6.6. Light microscopic pictures of E28H$_s$50 at (a) 12 weeks, (b) 24 weeks, and) 48 weeks post-implantation.

The trabeculae of the woven bone were seen along one edge in the defect and were continuation with the host bone at both the ends. Woven bone was seen along one lge of the implant. However, this new bone was separated from the implant by a layer of

ibrous tissue. At 24 weeks post-implantation the implant was for the most part surround by thin layer of fibrous tissue with fibrocytes and round cells, and were seen extending into ne implant (Figure 6.6b). New bone formation was seen in some areas around the implant vithout any interposition of fibrous tissue. At 48 weeks post-implantation, a thin layer of ibrous tissue was found surrounding the implant, separating it from adjacent woven bone Figure 6.6c). This bone was, however, in direct apposition with the implant material along nany areas. At all implantation periods, there was no evidence of chronic inflammation.

In the control group, at 12 weeks post-implantation woven and lamellar bone were een around the implant, along with fibroblasts, fibrocytes, macrophages, and lymphocytes Figure 6.7a). The cells appeared as an extension into the implant in occasional areas.

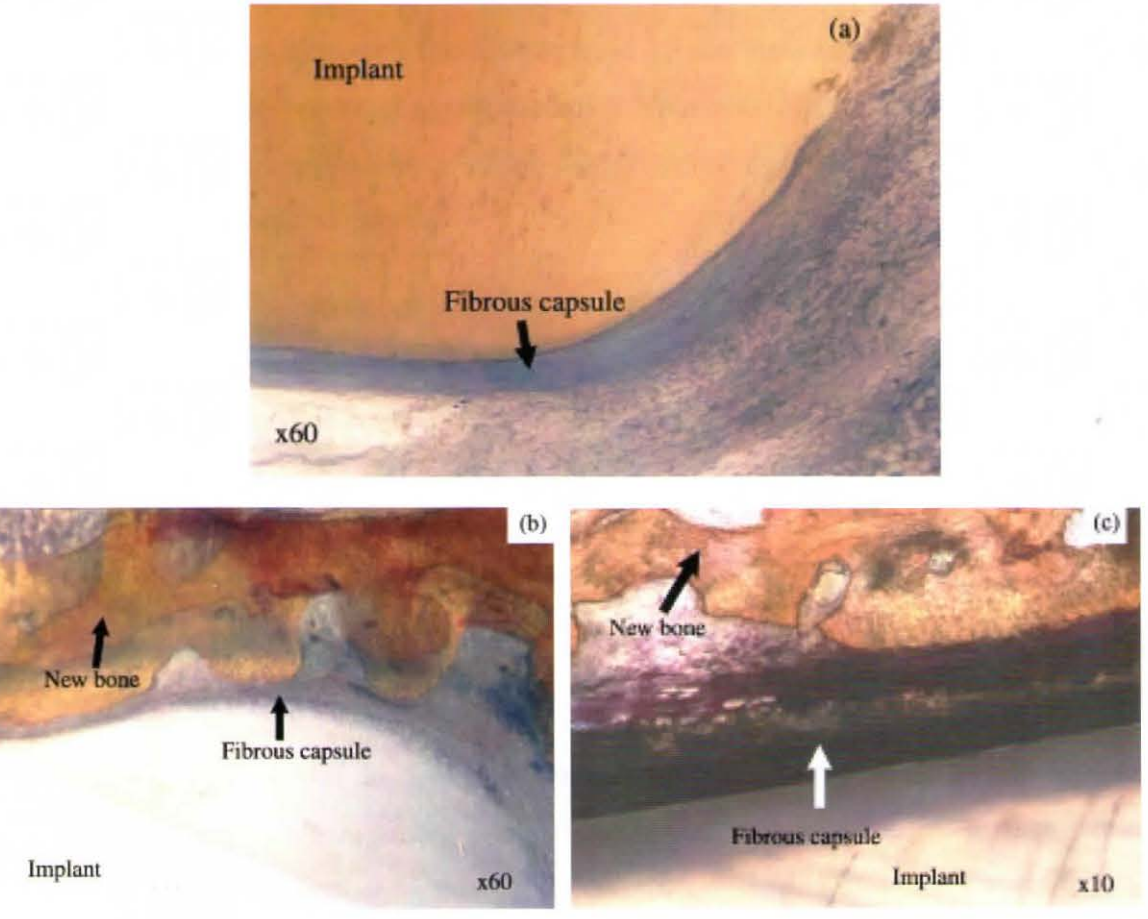

Figure 6.7. Light microscopic pictures of the control material at (a) 12 weeks, (b) 24 weeks, nd (c) 48 weeks post-implantation.

The new bone formed was separated from the implant by a layer of fibrous tissue. At 24 weeks post-implantation an increased amount of newly formed bone was found urrounding the implant, separated by a layer of fibrous tissue (Figure 6.7b). At 48 weeks

post-implantation, the implant was surrounded by the newly formed bone (Figure 6.7c). A thin layer of fibrous tissue is found interposing the implant and the surrounding bone in some areas.

6.6.2.2. Discussion

With respect to the *in vivo* biocompatibility analysis of dense implants, three areas of interest can be distinguished (Dhert *et al.*, 1993): (i) the interface, (ii) the surrounding tissue, and (iii) the implant. In the present study, gross as well as the histological appearance of the all the three types of implants showed the evidence of preservation of structural integrity and contours indicating the implant stability and integrity. During all the implantation periods there was no evidence of inflammatory response, foreign body reaction or necrosis in the surrounding bony tissues of either the composite implants or the control materials. Repair of the bone around all the three implants progressed well over a year. The morphological appearance of the tissue directly adjacent to the implant being a measure of its biocompatibility, this observation indicates the biocompatible nature of the implanted composites.

Evaluation of morphological appearance of the bone implant interface of the three implants E28H_s40, E28H_s50 and PMMA by light microscopy showed biocompatible behaviour of the materials with the surrounding tissues. At 12 weeks post-implantation, abundant new bone formation around both the composite implants and the control material could be noticed. The amounts of bone formed around the implant increased with the period of implantation. However, at all the time periods of implantation, the bone density around E28H_s40, and E28H_s50 was significantly higher in comparison with PMMA.

The implants E28H_s40, and E28H_s50 induced appositional bone growth in many areas, and irregular bone ingrowth could be observed at the composite surface, which would enhance the zones. During the early implantation periods, although the majority of the composite implants could contact with the newly formed bone directly, the composite implants were only partially integrated with the newly formed bone because of some fibrous tissues existing at the interface between the composite implants and the newborn bone. This may be due to the decrease of osteo-integration ability of the composite implant induced by the existence of bio-inert polymer phase in the composite during the beginning of the implantation period. It has been reported that the different levels of

exposure of hydroxyapatite at the implant surface causes the variation of new bone formation in the vicinity of the implant (Bonfield *et al.*, 1986). In an ultra-structural study of the interface between hydroxyapatite/polymer composite and bone, Doyle *et al.*, (1990) reported that the crystal growth of the bone apatite is often epitaxial to the nearest hydroxyapatite crystallite in the composite. It has been hypothesized that in the initial stages of bone formation, globular deposits occur on the smooth surface of the ceramic grains and in the intergrain boundaries (de Bruijn *et al.*, 1995). These deposits subsequently merge to form continuous cement like matrix to which the collagen fibers become attached (Davies *et al.*, 1991; de Bruijn *et al.*, 1992; Shen *et al.*, 1993). If a thin layer of polymer covers the hydroxyapatite crystallite, then the local mineralization presumably will not occur and the direct formation of hydroxyapatite would not occur on the material but only at some distance from the material. At 48 weeks post-implantation, however, the newborn bone was found to hug most part of the composite implants, which is in line with the observations, by several other investigators (Ignatius *et al.*, 1997; Lewandrowski *et al.*, 2000; Meijer *et al.*, 2002; Ooms *et al.*, 2003).

In all the sections, retrieved at the end of various periods of implantation, the cells responsible for bone remodeling such as osteoclasts could not be detected. However, thick cuffs of woven bone without interposition of fibrous tissue present abutting the implants shows the evidence of active remodeling. Osteoid and mineralized matrix was observed adjacent to the implants like layers, suggesting bone is deposited directly on the surface of the implant (Linder, 1985; Albrektsson and Hansson, 1986; Nanci *et al.*, 1994; Murai *et al.*, 1996). At all time periods of implantation, sections showed evidence of newborn bone in continuation with the host bone. It has been found that bone formation in the periprosthetic region occurs in two directions – (i) the healing bone approaches the biomaterial (ii) bone extends from the implant to the new bone (Puleo and Nanci, 1999). In the present study the host bone being in continuation with the woven bone, the bone formation could have resulted from approaching healing bone to the biomaterial.

The bone tissue around the PMMA implants also went through stages of active remodeling and healing. However, a fibrous capsule was found surrounding these implants at all the implantation periods and no area of direct bone apposition could be found.

6.7. CONCLUSIONS

The biological behavior of the two different compositions of HAP and EVA composites ($E28H_s40$ and $E28H_s50$) was investigated based on the guidelines/protocols prepared by ISO-10993.

Results of the cytotoxic potential evaluation revealed that no cellular degeneration or malformation occurred to the L929 cell lines when exposed to the $E28H_s40$ and $E28H_s50$ samples. The cell line L929 retained their original morphology even after being in contact with $E28H_s40$ and $E28H_s50$, either directly or by means of the extracts from these materials, suggesting that the material is non-cytotoxic to the cell-lines used for the study.

Data of the responses to erythema and oedema formation following intracutaneous injections from the extracts of $E28H_s40$ and $E28H_s50$, tested for skin irritation, showed that no type of tissue reaction was observed at any observation time investigated. It means that these composites do not cause potential local irritation by the extracts of $E28H_s40$ and $E28H_s50$.

Systemic toxicity evaluation of the sample extracts from $E28H_s40$ by intravenous and peritoneal injections revealed that no animal assayed died or showed toxic symptoms during the observation time studied. The tissue reaction ratings for erythema and oedema by intracutaneous injection of the $E28H_s40$ extracts for all the sites and observation time investigated were similar to those corresponding to the control extracts.

The results of the closed patch sensitization studies carried out on $E28H_s40$ showed that the extracts from this material does not elicit any immune response to the living system. There was no evidence of erythema and oedema formation for any observation time investigated.

The intramuscular implantation studies carried out give an understanding about the response of the soft-tissues to $E28H_s40$ and $E28H_s50$ and confirmed the biocompatible nature of these composite materials. Both $E28H_s40$ and $E28H_s50$ caused no hindrance to the healing pattern of the surrounding muscle tissue and were covered by a thin layer of fibrous tissue capsule. The healing pattern around $E28H_s50$ was, however, found to be better than $E28H_s40$ and the control.

6.7. CONCLUSIONS

The biological behavior of the two different compositions of HAP and EVA composites ($E28H_s40$ and $E28H_s50$) was investigated based on the guidelines/protocols prepared by ISO-10993.

Results of the cytotoxic potential evaluation revealed that no cellular degeneration or malformation occurred to the L929 cell lines when exposed to the $E28H_s40$ and $E28H_s50$ samples. The cell line L929 retained their original morphology even after being in contact with $E28H_s40$ and $E28H_s50$, either directly or by means of the extracts from these materials, suggesting that the material is non-cytotoxic to the cell-lines used for the study.

Data of the responses to erythema and oedema formation following intracutaneous injections from the extracts of $E28H_s40$ and $E28H_s50$, tested for skin irritation, showed that no type of tissue reaction was observed at any observation time investigated. It means that these composites do not cause potential local irritation by the extracts of $E28H_s40$ and $E28H_s50$.

Systemic toxicity evaluation of the sample extracts from $E28H_s40$ by intravenous and peritoneal injections revealed that no animal assayed died or showed toxic symptoms during the observation time studied. The tissue reaction ratings for erythema and oedema by intracutaneous injection of the $E28H_s40$ extracts for all the sites and observation time investigated were similar to those corresponding to the control extracts.

The results of the closed patch sensitization studies carried out on $E28H_s40$ showed that the extracts from this material does not elicit any immune response to the living system. There was no evidence of erythema and oedema formation for any observation time investigated.

The intramuscular implantation studies carried out give an understanding about the response of the soft-tissues to $E28H_s40$ and $E28H_s50$ and confirmed the biocompatible nature of these composite materials. Both $E28H_s40$ and $E28H_s50$ caused no hindrance to the healing pattern of the surrounding muscle tissue and were covered by a thin layer of fibrous tissue capsule. The healing pattern around $E28H_s50$ was, however, found to be better than $E28H_s40$ and the control.

The implantation of E28H$_s$40 and E28H$_s$50 in the rabbit cranium demonstrated the bone compatibility of these composite materials. The bone tissue around E28H$_s$40 and E28H$_s$50 went through stages of active remodeling and healing. The repair of the bone around the implants progressed well over a year. The newly formed bone was separated from the material by a layer fibrous tissue in certain areas. However, occasional areas of direct contact of bone with the material were also observed. Overall, these materials induced excellent tissue response when implanted in bone tissue, indicating their possible future application as bone replacement materials.

CHAPTER 7

STAMP FORMING

7.1. BACKGROUND

The development of customized and pre-fabricated implants for repairing defects in the cranium has revolutionized the neurosurgical procedures. The provision of preoperatively customised implants and the plastic replicas (biomodels) allow the surgeons to assess implant fit preoperatively, evaluate fixation sites, and obtain a valuable overview of the procedure. The patients, on the other hand, are also benefited since they get an opportunity to see the biomodel and implant before the surgery, which improve their understanding of the operation procedure (D' Urso *et al.*, 2000). In addition, customization and pre-fabrication of cranioplastic implants offer excellent cosmesis and minimizes the duration of surgery. Many techniques have been used for the pre-fabrication of customized cranioplastic implants with varying sophistication (Waite *et al.*, 1989; Joffe, *et al.*, 1992; Zonneveld, 1994).

The advent of computed tomography (CT) and magnetic resonance imaging (MRI) has revolutionized the definition and evaluation of human anatomy. Data acquired from CT and MRI can be used as a guide for the manufacture of prosthetic cranioplastic implants (Toth *et al.*, 1988). A computer numerically controlled (CNC) milling or rapid prototyping processes like stereolithography (SL) can then be used to fabricate the biomodels and the master cranioplastic implants (Rhodes *et al.*, 1987; Ashley, 1991; Fallahi *et al.*, 1999). However, these manufacturing techniques suffer from certain limitations. Computer numerically controlled milling is limited by difficulties encountered when trying to replicate complex anatomy or internal features due to

collision between the milling mould and the object which can lead to the damage of both (D' Urso *et al.*, 2000). Rapid prototyping systems such as SL require no physical moulding (Ashley, 1991; Barker *et al.*, 1993). However, the technique requires a long manufacturing time and is expensive. The other disadvantage identified is the warpage of SL parts, especially in humid conditions (Zeilhofer *et al.*, 1997). The implant that gets distorted by warping requires considerable intra-operative modifications, which adds both to the cost and duration of surgery. In this scenario, a simpler and cost effective technique for obtaining cranioplastic implants would indeed be a landmark accomplishment.

Stamp forming is a cost effective method that improves the performance/cost balance of reinforced polymeric composites via., high-speed manufacturing and shaping process (Breuer and Neitzel, 1996). Stamp forming or match-die-forming is one among the family of thermoforming processes that deal with the pressing or squeezing of pliable plastic into final shape (Throne, 1987). In its simplest concept, the process involves the deformation and shaping of a heated thermoplastic sheet over mould geometry by mechanical pressure. Stamp forming bears its name from sheet metal forming and is sometimes considered as a variation of compression moulding (Hou *et al.*, 1995; Hou and Friedrich, 1995; 1998). Stamp forming process is widely used because forming presses are readily available from very simple, hand operated small presses to fairly sophisticated computer-controlled hydraulic systems (Okine, 1989). The dies used in this forming method are generally made of metal, which can be internally heated and cooled. The process is attractive because forms of complicated contours can be easily fashioned from sheets with the aid of very simple tooling. This chapter describes the two-dimensional and three-dimensional stamp forming of HAP-EVA composites. The efficacy of the forming conditions with respect to the formed part is also discussed.

7.2. STAMP FORMING TECHNIQUE - PRINCIPLE

In a typical stamp forming process, the sheet stock, or preform, is heated in an external heating device above the melting/softening temperature of the thermoplastic matrix. When the sheet begins to soften (often referred to as the forming temperature), it is quickly transferred into a cold mould where it is stamped to conform to the mould geometry. The transfer time is of the order of a few seconds to prevent significant cooling. During the stamp forming, the laminate is cooled down under pressure by the cold mould to a temperature below the melting/softening point of the polymer. The stamp forming

procedure using a two-dimensional and a three-dimensional tool is schematically represented in the Figure 7.1 (a & b).

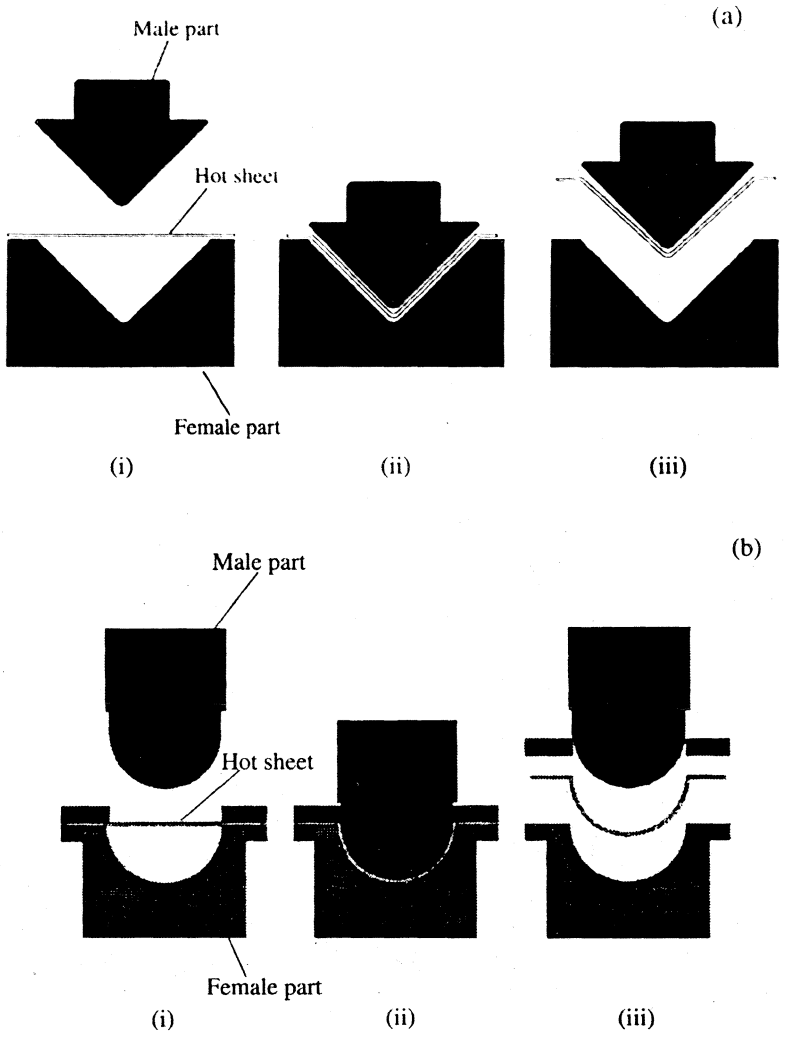

Figure 7.1. Stamp forming of the HAP-EVA sheet material into (a) V-form and (b) hemispherical form. (i) Pre-heated composite sheet placed over cold female mould, (ii) sheet formed by male part of the mould into female mould, and (iii) the male part of the mould withdrawn and material formed into the mould contours.

7.3. TWO-DIMENSIONAL FORMING USING A RIGHT ANGLE TOOL

7.3.1. Stamping temperature

One of the key parameters to obtain a good quality part is the selection of the appropriate temperature range in which the sheet can be formed. This involves heating the material to a point where it is flexible enough to be shaped while supporting its own weight during the heating process (Young *et al.*, 2000). Thus, the determination of the proper temperature range in which the sheet can be productively formed is a major predicament in stamp forming. In this investigation, three pre-heating temperatures i.e.,

80, 100, and 120°C were chosen to heat the composites. The stamping velocity of the press was varied between a maximum stamping velocity of 250 mm/s and a minimum of 80 mm/s. Figure 7.2 illustrates the typical temperature profile of HAP-EVA composites being pre-heated and stamped in the hydraulic press, as the function of processing time.

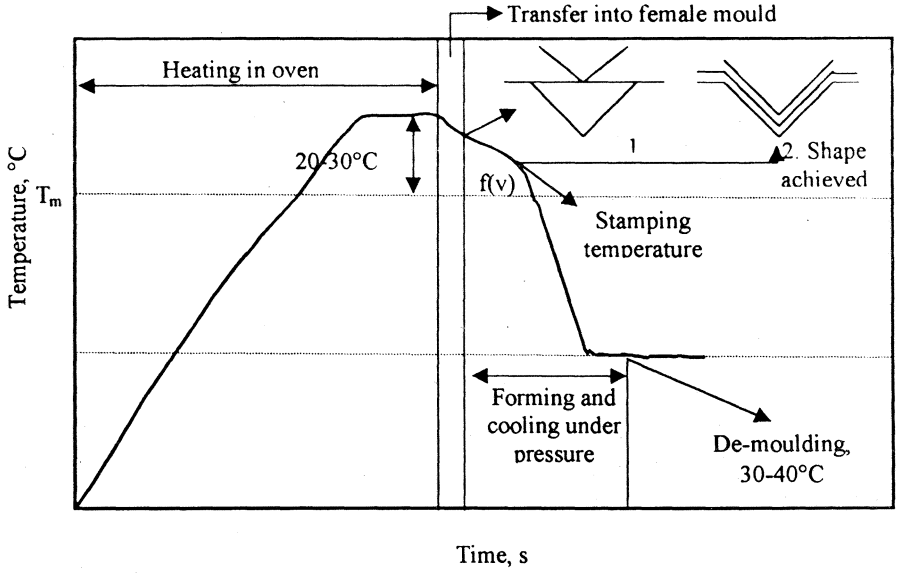

Figure 7.2. Temperature profile during stamp forming of HAP-EVA composites in the hydraulic press

When taken out of the right angle V-mould, the composite sheet had a temperature in the range 30-40°C. The temperature, at which the cooling of the laminate starts to drop more rapidly, due to contact of the tool parts with the composite, is defined as the stamping temperature. The stamping temperature of $E28H_s40$, $E28H_f40$, $E18H_s40$ and $E18H_f40$ composites as a function of stamping velocity is illustrated in Figure 7.3 (a&b) and Figure 7.4 (a&b). It is clear from the figures that a higher closing speed results in a higher stamping temperature. At a too slow stamping velocity, the actual temperature of the composite sheet falls below a temperature level necessary to allow polymer chain slipping and flowing. In this case the shear stress acting on the composite sheet does not exceed the yield stress of the polymer, which results in forms that do not replicate the mould geometry completely. A situation like this was observed at a stamping velocity of 80 mm/s. The pre-heating temperatures employed at this condition were 80°C and 100°C, for composites fabricated from E28 and E18, respectively. The deformation temperatures observed were around 70-75°C and 80-85°C, respectively, for composites fabricated from E28 and E18. Stamping of these composites resulted in V- bends with a very large forming angle (see section 8.3.2.2.). At 190 mm/s stamping velocity and pre-heating

temperatures above 100°C and 120°C, the stamping temperatures of the composites fabricated from E28 and E18, could be maintained above 90°C and 110°C, respectively. These temperatures were sufficiently above the melting point of the EVA matrices, so that sufficient chain mobility and matrix flow could occur under load. If a material flows, it can retain permanent deformation once the load is removed (Nowacki and Neitzel, 2000).

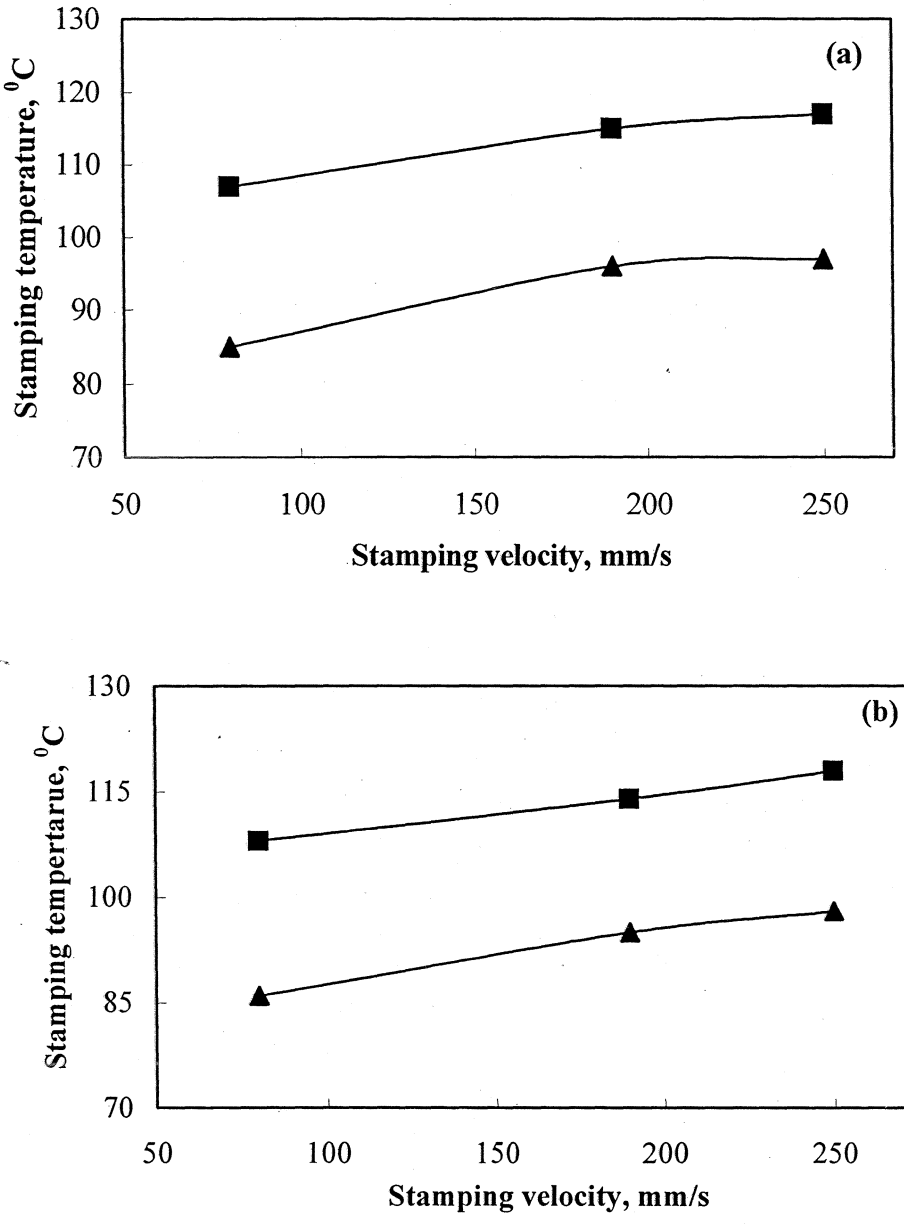

Figure 7.3. Stamping temperature of (a) E28H$_s$40 and (b) E28H$_f$40 pre-heated to (▲) 80°C and (■) 100°C as a function of stamping velocity.

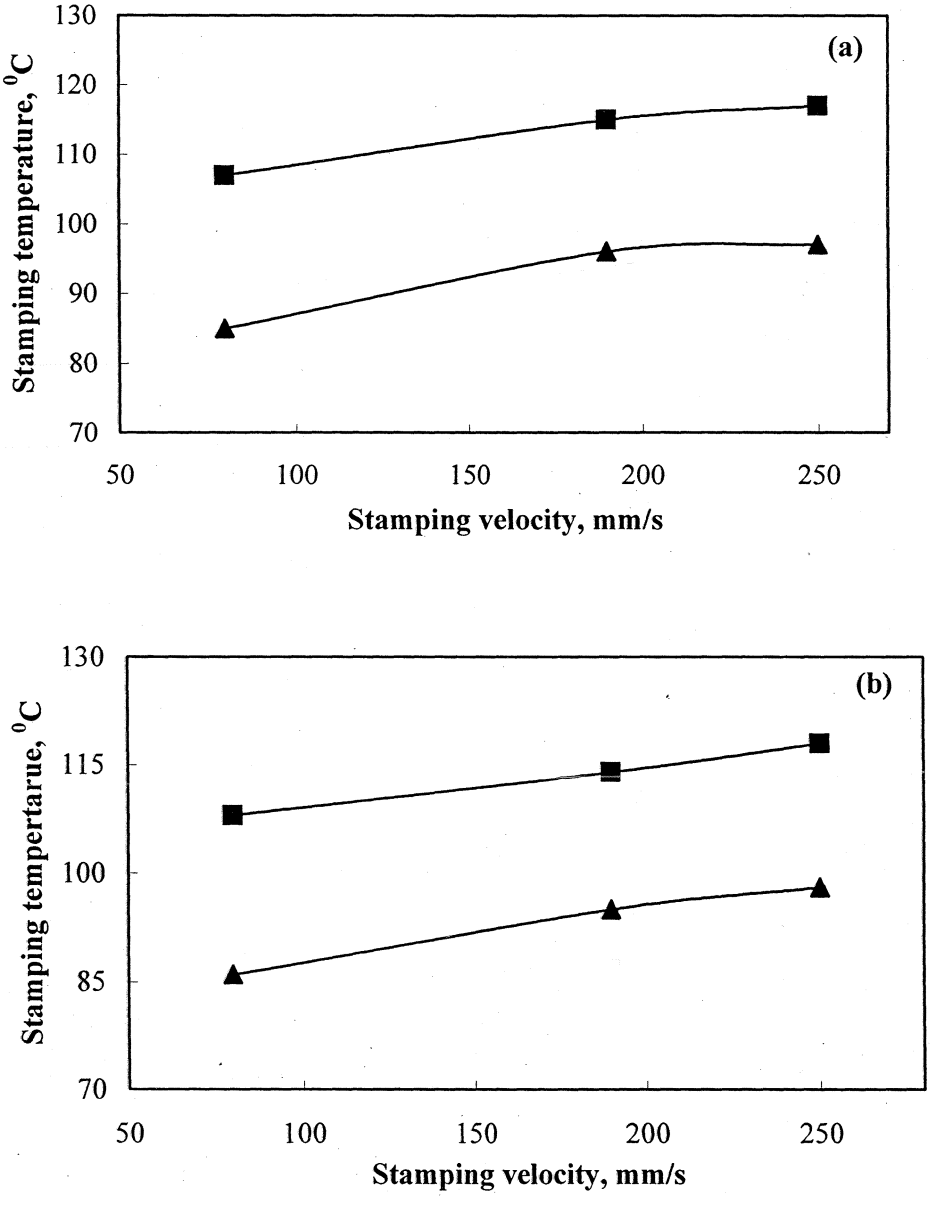

Figure 7.4. Stamping temperature of (a) E18H$_s$40 and (b) E18H$_f$40 pre-heated to (▲) 80°C and (■) 100°C as a function of stamping velocity.

At a stamping velocity of 250 mm/s, the closing time of the mould was shortened further, which in turn resulted in high stamping temperature. It was interesting to note that even though the stamping temperature of the composites formed at 250 mm/s was only slightly higher than that formed at 190 mm/s, it had tremendous impact on the quality of the bends. The composite bends formed at this condition gave rise to poor quality bends as seen from the photographs (Figure 7.5-7.7). Figure 7.5 and Figure 7.6 show the photographs of the E28H$_s$40 composite bends formed at 100°C and various stamping velocities. It could be noted that bend region of good quality was obtained when

the composite sheets were pre-heated to 100°C and stamped at 190 mm/s. Similarly in the case of E18H_s40, the composite bends formed at 120°C and 190 mm/s exhibited good quality (Figure 7.7).

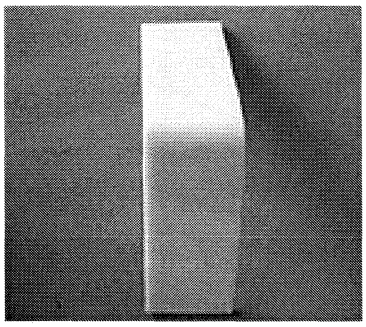

Figure 7.5. E28H_s40 bend formed at 100°C and 190mm/s stamping velocity.

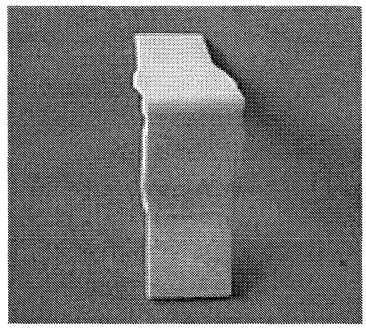

Figure 7.6. E28H_s40 bend formed at 100°C and 250mm/s stamping velocity.

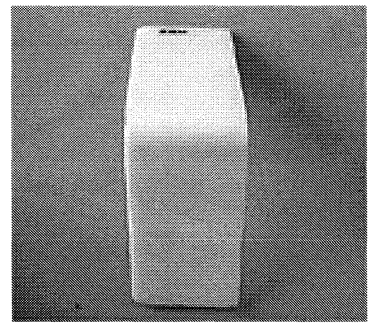

Figure 7.7. E18H4$_s$0 bend formed at 120°C and 190mm/s stamping velocity.

7.3.2. Evaluation of stamp forming performance

7.3.2.1. Part thickness

In thermoforming, one of the criteria used to distinguish a good part from a bad part is the degree of thickness uniformity in the final structure (Martin *et al.,* 2000). Hence the most important point to be considered in the stamp forming operation is the control of wall thickness distribution. In the case of uncontrolled thickness distribution the relatively thin parts tend to weaken the formed component, and it is common for the component to collapse (Collins *et al.,* 2000). The thickness variation as a function of position for stamp formed composite bends, fabricated at various pre-heating temperature and stamping velocity is shown in Figure 7.8 (a&b). As an example, the wall thickness variation with respect to position of E28H_s40 is described. It is apparent from Figure 7.8 (a&b) that the quality of the formed bend is influenced by the variation of both the stamping temperature and stamping velocity. In general, the average thickness of the bends decreased with increase in stamping velocity. The nature of the thickness distribution curve for the bends formed at 80 mm/s and 190 mm/s stamping velocity was found to be similar. The formed parts had thinner walls at the bend and thicker at the sides of the V-bend. The average thickness of the part formed at 80 mm/s was, however, slightly higher than that formed at 190 mm/s. The thickness distribution of the composite formed at 250 mm/s showed that the composites had thicker walls at the bends and thinner towards the sides.

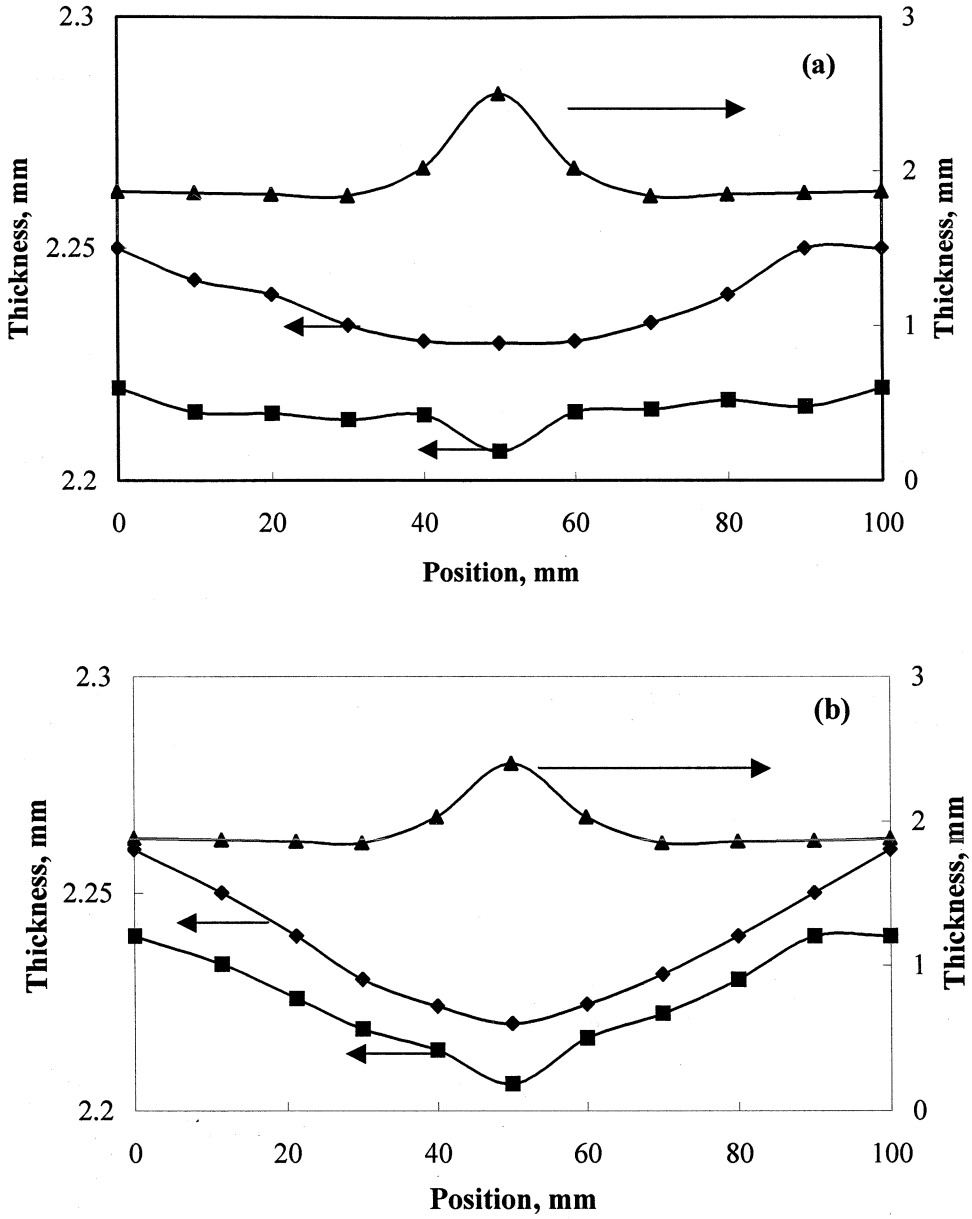

Figure 7.8. Variation of wall thickness as the function of position of (a) E28H_s40 and (b) E28H_s40 composite bends formed at 100°C and stamping velocity of (▲) 80 mm/s; (◆) 190 mm/s and (■) 250 mm/s.

Stamp forming involves a multifaceted combination of material deformation processes, and most forming processes do not yield parts having uniform wall thickness (Throne, 1987). The variations in wall thickness of the formed contours have been found to be dependent on temperature and mode of deformation (Okine, 1989). The observed variation in the wall thickness of the formed bend in the present study is the consequence of progressive down drawing of the flat composite sheet into the mould (Figure 7.9a). During the initial stages of stretching, the sheet contacts the closest flat surface of the

mould while other areas of the sheet continue to stretch. The part of the sheet that touches the cold mould in the initial stages of forming cools down, while the other areas of sheet that have yet to touch the mould are still hot. This leads to a non-uniform temperature distribution over the sheet under deformation, resulting in dissimilar material deformation histories (Lee *et al.,* 2001). At the centre of the bends the sheet contacts the mould during the remote stages of forming operation. Thus it undergoes the largest deformation resulting in the smallest wall thickness (Figure 7.9b). On the other hand, at 250 mm/s, the temperature of the sheet at the time of stamping is high. This leads to the fact that the material at the edges, first in contact with the female mould walls, is stretched out more, whereas in the centre part more material to be pulled further down into the mould. This results in the incidence of a web formation at the centre of the bends as mentioned in the previous section (Figure 7.9b).

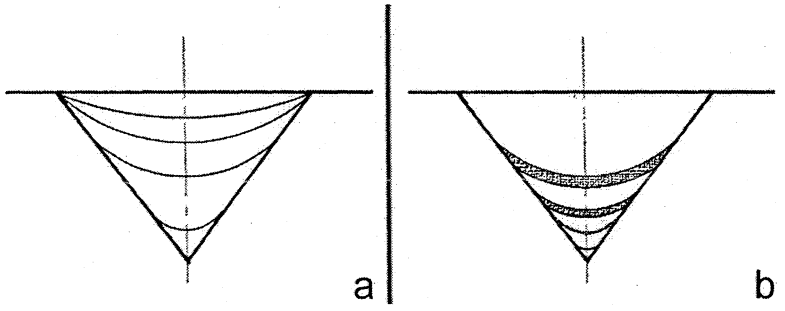

Figure 7.9. (a) Schematic of progressive draw down of the composite sheet into the V-mould, (b) reduction in sheet thickness at the bends due to the progressive down drawing.

In another series of trials, E18H_s40 and E18H_f40 composite sheets were heated to 100°C and 120°C and stamped at different velocities Figure 7.10. The nature of variation of the part thickness of the bends was found to be similar to that observed for E28H_s40 and E28H_f40. It seemed that composites stamped at 120°C and 190 mm/s stamping velocity gave rise to composite bends that faithfully replicated the V-mould geometry. The variation of the thickness of the E18H_s40 and E18H_f40 composite V-bends stamped at these conditions was also fairly uniform. The average thickness of the formed E18H_s40 and E18H_f40 V-bends was, however, found to be higher than that of the E28H_s40 and E28H_f40 V-bends. It is assumed that the different melt viscosities of the two-polymer matrix are responsible for the observed difference in thickness.

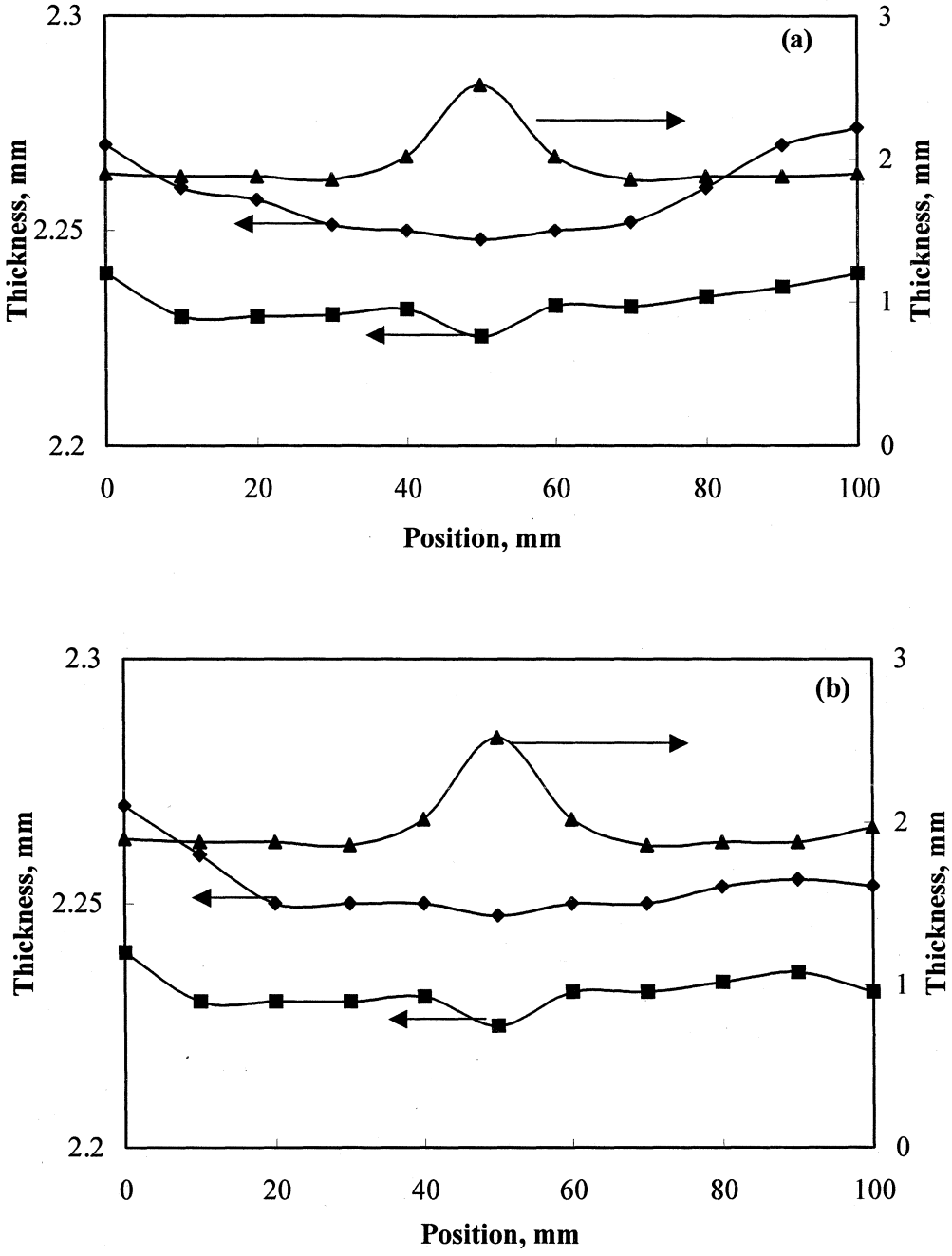

Figure 7.10. Variation of wall thickness as the function of position of (a) E18H$_s$40 and (b) E18H$_s$40 composite bends formed at 100°C and stamping velocity of (▲) 80 mm/s; (◆) 190 mm/s and (■) 250 mm/s.

7.3.2.2. Part angle

Formability is defined as the ease of forming and is often measured by the extent to which a material may be successfully formed (Bhattacharrya *et al.,* 2003). For single-curvature V-bending, formability can be assessed in terms of shape conformance ($\Delta\theta$) and

the quality of the bend region. The nature of angle of deviation depends on whether the specimen springs back or forward. If the part angle actually deformed is less than 90°, this phenomenon is called 'spring- forward' effect. If the actual angle is larger than 90°, it is called 'spring- backward' effect (Kalpakkian and Schmid, 2002). Both effects are results of the thermal expansion anisotropy of the matrix and the reinforcement (Bhattacharyya, 1997).

The variation of part angle of $E28H_s40$, $E28H_f40$, $E18H_s40$, and $E18H_f40$ bends with respect to the stamping velocity and temperature are given in the Figure 7.11 (a&b) and in Figure 7.12 (a&b).

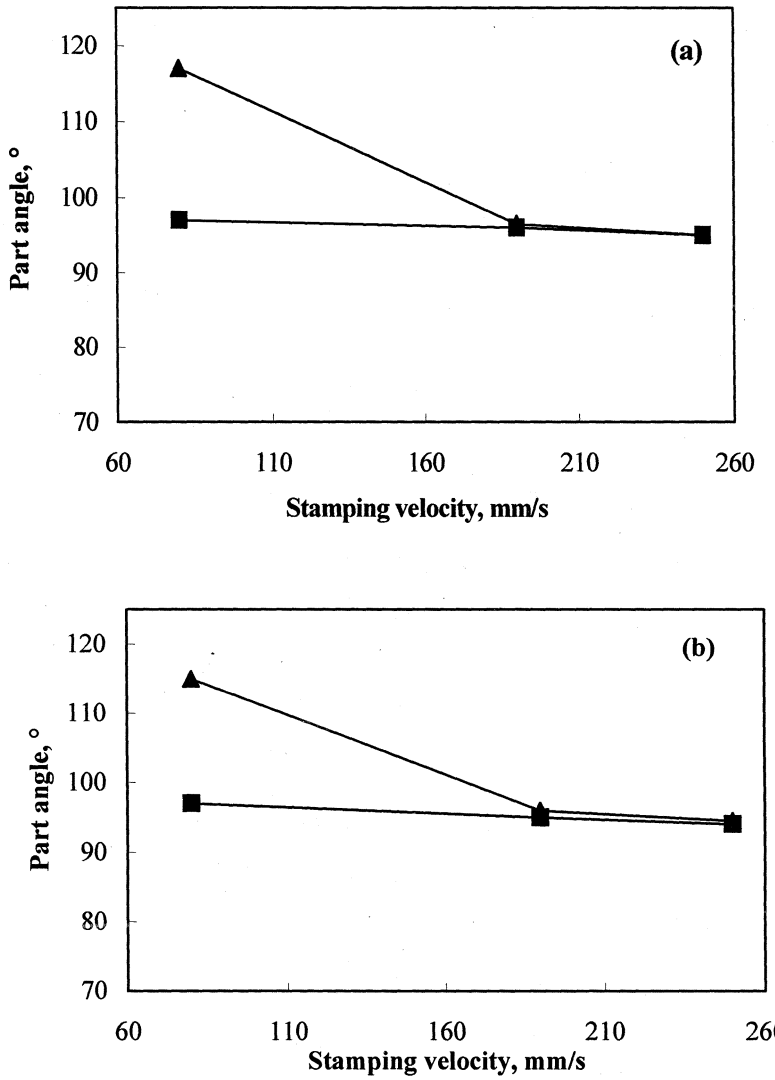

Figure 7.11. Part angle of (a) $E28H_s40$ and (b) $E28H_f40$ as a function of stamping velocity and temperature. Part formed at (▲) 80°C; and at (■) 100°C.

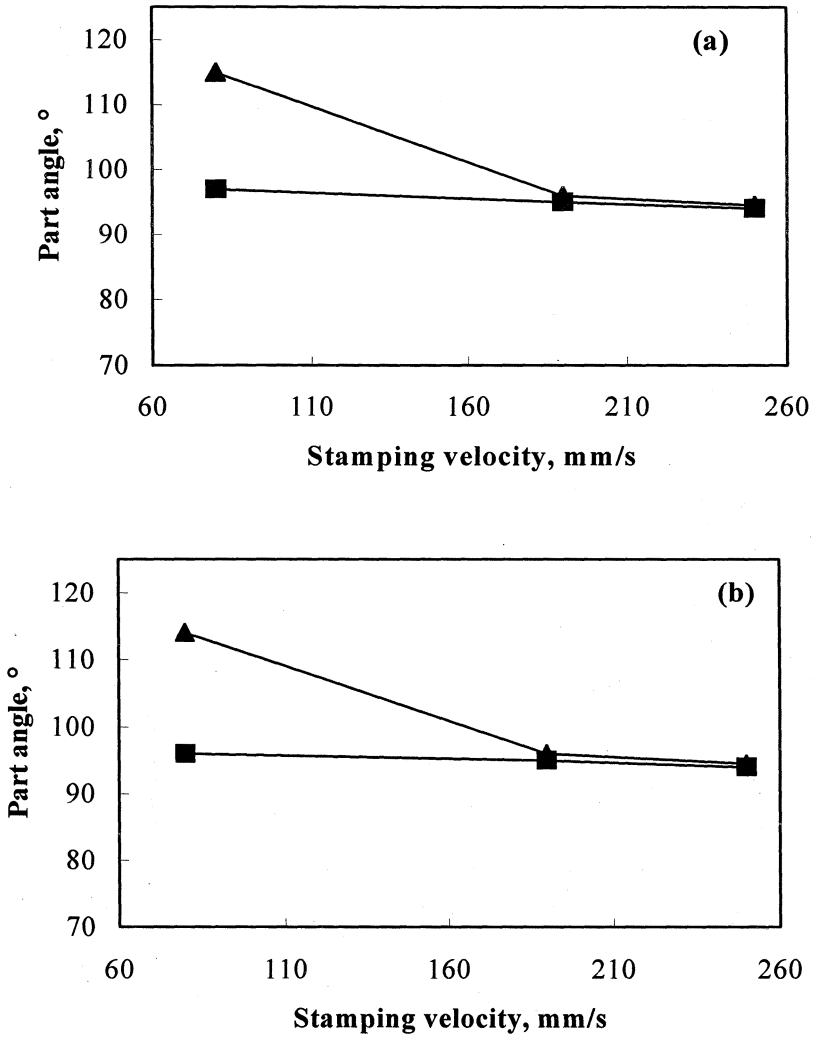

Figure 7.12. Part angle of (a) E18H_s40 and (b) E18H_f40 as a function of stamping velocity and temperature. Part formed at (▲) 80°C; and at (■) 100°C.

It is apparent from the Figures 7.11 & 7.12 that the measured angles of the formed bends are greater than 90°, i.e. the composites show a 'spring-backward' effect. Zahlan and O'Neill (Zahlan and O'Neill, 1989) devised a mathematical expression to measure the deviation in the angle ($\Delta\theta$) formed by the bending of the thermoplastic composites (equation 7.1).

$$\Delta\theta = (\alpha_r - \alpha_l)\, \theta\, \Delta T \qquad \text{.....7.1}$$

where θ = mould angle, ΔT = temperature range over which cooling takes place, α_r = radial expansion coefficient, and α_l = longitudinal expansion coefficients. When an

anisotropic composite bend cools from the processing temperature to the ambient temperature, the contraction of the curved section is non-uniform because of the mismatch in coefficients of in-plane and out-of-plane thermal expansion (Spencer *et al.,* 1991; Barnes *et al.,* 1992; Zahlan, 1988). In such cases, the radial expansion coefficient is found to be greater than the linear expansion coefficient (i.e. $\alpha_r > \alpha_l$), resulting in a reduction of the enclosed angle ($\Delta\theta$ is negative), and subsequent in a 'spring-forward' effect. (Bhattacharrya *et al.,* 2003; Hou and Friedrich, 1991). This contraction, i.e. spring forward phenomenon, has been reported mainly in long fibre reinforced composite systems.

In an isotropic material, as encountered in the present case, the contraction of the curved section is uniform ($\alpha_r = \alpha_l$) and the configuration is maintained because of the constant in-plane and out-of-plane contraction. However, when cooling from the processing temperature to ambient temperature, the EVA matrix would contract more than the reinforcement HAP (α_{EVA} = 160 - 200 x10^{-6}/°C; α_{HAP} = 13 x10^{-6}/°C, (Jiang and Shi, 1998). This leads to the development of residual thermal stresses within the composite bend. Upon removal of the load, these stresses distort elastically, thus resulting in some degree of 'spring back' (Bhattacharrya *et al.,* 2003; Hwang and Hwang, 2002).

The effects of stamping velocity and temperature on the formed angles of the different composite bends can also be seen from the Figure 7.13.

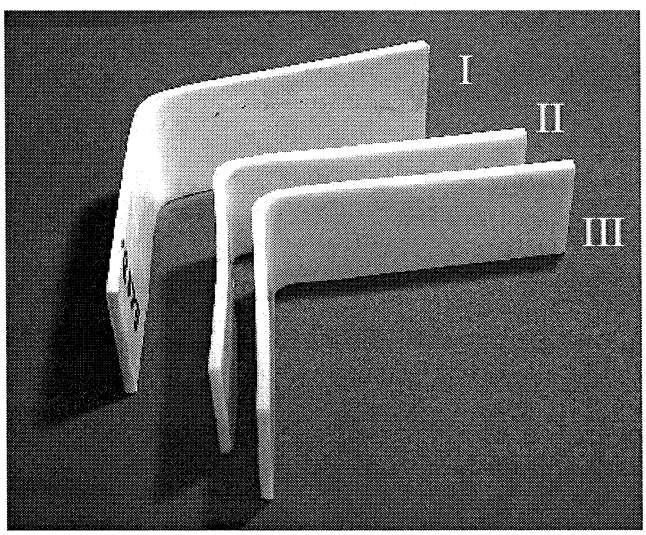

Figure 7.13. Photographs of the composite bends formed at various forming conditions. (I) E28H$_s$40 formed at 80°C & 80mm/s stamping velocity, (II) E28H$_s$40 formed at 100°C & 190 mm/s stamping, (III) E18H$_s$40 formed at 120°C & 190 mm/s.

Severe distortion of the angle was observed when E28H$_s$40 was formed at a stamping velocity of 80mm/s and a pre-heating temperature of 80°C (I in Figure 7.13). The measured angle in this case was found to be 117°. A too low starting temperature and an excessively low stamping velocity led to a fast cooling down of the composite sheet thus making it stiff. As a result, the sheet did not stretch easily and did not faithfully replicate the mould details. The formed angle decreased to 96° (II in Figure 7.13) when formed at 100°C and 190 mm/s stamping velocity. This may be attributed to a more sufficient resin flow within a wider range at which the materials are at high working temperature. The part angle of the bend formed from E18H$_s$40, formed at a pre-heating temperature of 120°C and a stamping velocity of 190 mm/s, was found to be 95° (III in Figure 7.13). It is worth mentioning at this point that, the part quality of the formed composite V-bend was not significantly affected by the nature of the HAP particles used.

Based on the experimental results a schematic diagram of the processing window for the 2-D forming of HAP-EVA composites could be evolved (Figure 7.14).

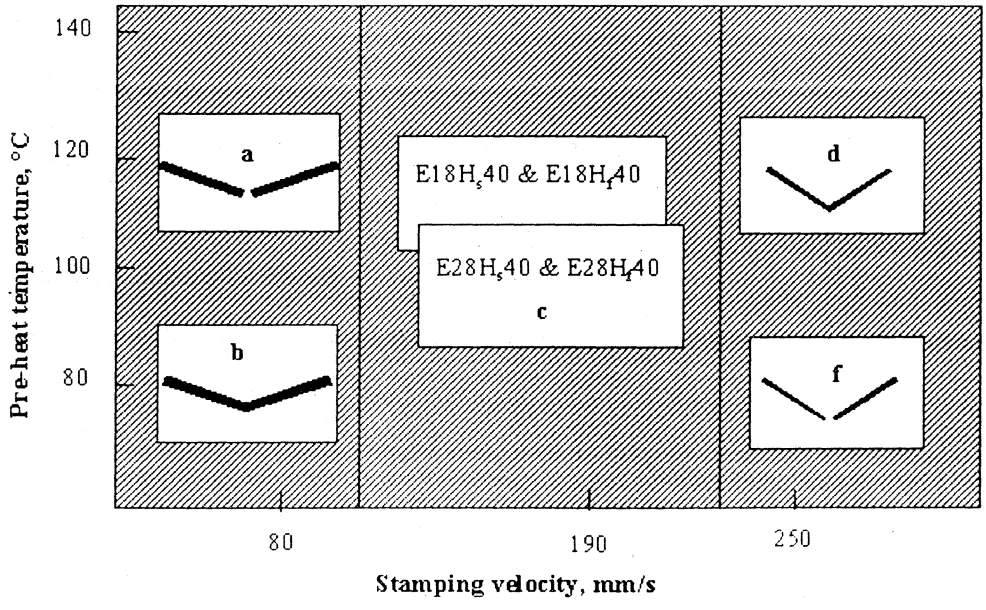

Figure 7.14. Schematic diagram showing the processing window for 2-D stamping of HAP-EVA composite. (a) Severe angle distortion and cracking at the edges of the bends (b) extensive spring back at low temperature and stamping velocity, (c) acceptable process window, (d) intense thinning, material degradation, accumulation of material at the center of the bends, (e) cracking at the center of the bends.

The experimental studies showed that for successful forming, the temperature of the sheets has to be maintained in the range 90-100°C for E28H$_s$40 and E28H$_f$40 and 110-120°C for E18H$_s$40 and E18H$_f$40. This requires the composite to be heated to at least

20°C above the melting point of the polymer matrix. The forming velocity could vary between 190-250 mm/s depending on the pre-heating temperature set. Too high pre-heating temperatures (>100°C for E28H$_s$40 and E28H$_f$40; >120°C for E18H$_s$40 and E18H$_f$40) led to severe sagging of the composite sheet, making it difficult to handle and to transport. When stamped at high velocities, this resulted in intense thinning of the walls and a web formation at the centre of the bends due to the accumulation of the material. Too low temperatures and too low stamping velocity, on the other hand, resulted in a faster cooling down of the composite, thus leading to the formation of severely distorted V-bends.

7.4. THREE-DIMENSIONAL FORMING USING HEMISPHERICAL MOULD

Based on the experimental results of 2-D stamp forming, 3-D parts, i.e., hemispherical forms were manufactured using a hemisphere mould. The following processing conditions were used in the stamp forming operation:

(a) Pre heating temperature

E28H$_s$40 & E28H$_f$40	100°C
E18H$_s$40 & E18H$_f$40	120°C

(b) Stamping velocity 190 mm/s

7.4.1. Deformation mechanism

In order to evaluate the forming performance of the hemispherical parts, it is necessary to understand the progressive stages of 3-D stamp forming operation. Figure 7.15 (a) illustrates schematically a step-by-step deformation of a flat circular laminate as it is moved into the cavity of a hemispheric mould. Segment A represents a segment of a circular laminate before forming and section 1, 2, 3, 4 and 5 lies in one plane. Segment B can be visualized as a part of a hemisphere, in which 1 and 2 consist of the wall of the hemisphere while 3, 4, and 5 are still a part of the flat laminate. Segments C and D show the progressive deformation as the flat laminate moves continuously into the hemisphere cavity.

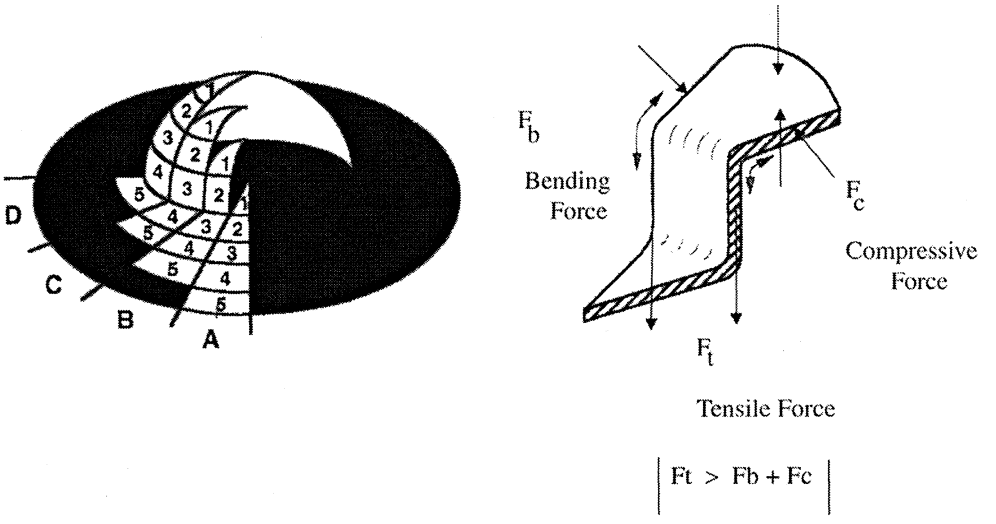

Figure 7.15. (a) Schematic of step-by-step deformation of a flat circular laminate as it is moved into the cavity of a hemispheric mould; (b) the different forces that acts on the flat laminate as it is shaped in the hemispheric mould.

The important implication of this figure is the fact that the width of the arc of sections in the flat laminate becomes progressively narrower as the section is deformed into the cavity. The 3-D forming operation leads to a decrease in laminate surface area and the principal mode of deformation is compression. This indicates, therefore, the existence of compressive forces, F_c (Figure 7.15b) perpendicular to the radius of the circular laminate. As the material moves from the flange into the cavity, each section undergoes bending deformation (bending force F_b). In case the flat laminate is clamped (held down), the hold down action can give rise to frictional force, F_r, which opposes the flow of material into the cavity. It can thus be seen that when a flat laminate is being formed into a cavity, the laminate experiences manifold force acting on it. The necessary condition for the successful transfer of the flat laminate into the cavity is that the tensile force exerted by the stamper (male mould) exceeds or equals the sum of all other forces as shown in Figure 7.15b.

$$F_t \geq F_b + F_c + F_r \quad \text{.....7.2}$$

F_t: tensile forces; F_b: bending forces; F_c: compressive forces; F_r: frictional forces

In the absence of hold-down pressure (as in the present investigation) the equation reduces to

$$F_t \geq F_b + F_c \quad \text{.....7.3}$$

7.4.2. Evaluation of stamp forming performance

7.4.2.1. Part thickness

The thickness distribution of the formed HAP-EVA hemispherical part is shown in Figure 7.16. The part thickness is plotted as a function of the part angle θ. It can be seen from the figure that the hemisphere has thinner walls at the apex of the hemispheric forms than at the outer edges.

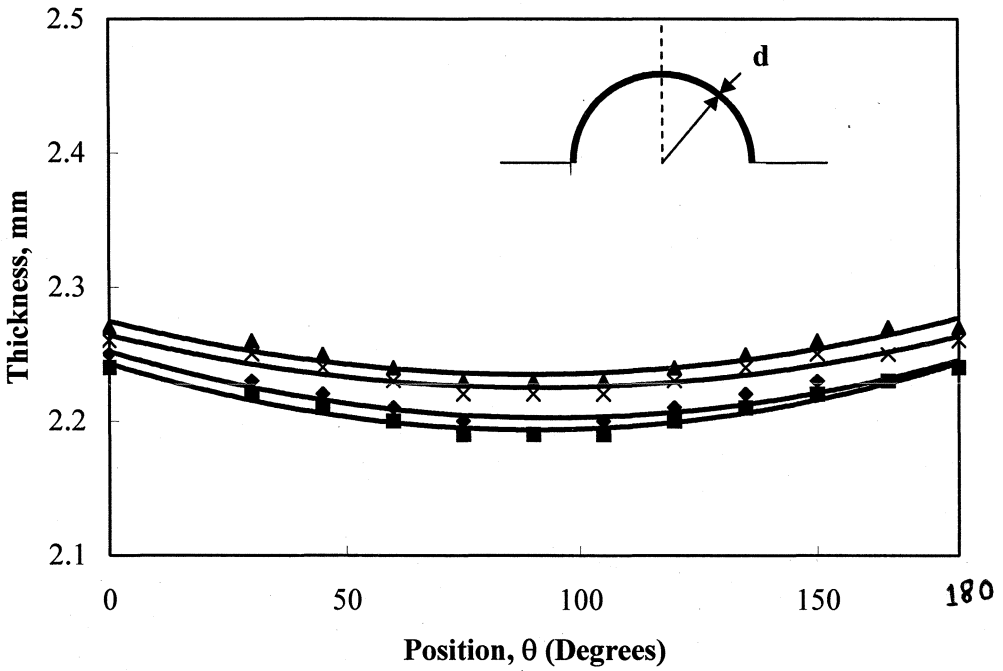

Figure 7.16. Thickness distribution of stamped spherical segment (◆) E28H_f40, (■) E28H_s40, (▲) E18H_f40, (x) E18H_s40

This non-uniform distribution of the part thickness is because of the fact that these walls are not formed at the same time but in sequence as explained in section 7.4.1. The thinnest section occurs at the apex of the hemisphere; this is due to a localized higher pressure, as the male and female mould contact first at this point. The result is that the molten matrix flows away from this region. The thickness distribution was also found to be symmetric about the apex and is due to the symmetric construction nature of 3-D mould used.

7.4.2.2. Surface characterization

Figure 7.17 (a&b) show scanning electron micrographs of the representative samples cut from E28H_s40 and E28H_f40. The difference in the surface finish is apparent from the two photomicrographs. The part fabricated from composites filled with H_s appears to be smoother than that filled with H_f at the outer surface.

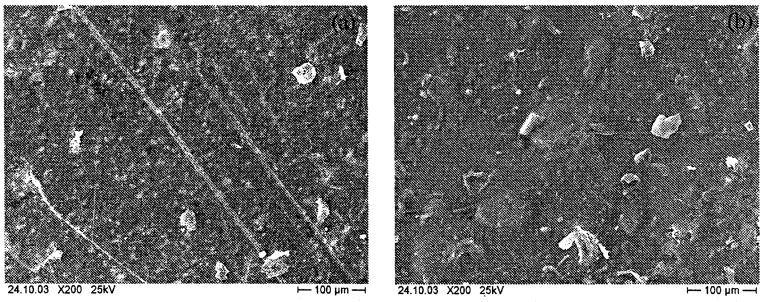

Figure 7.17. Scanning electron micrographs of the representative section of the outer surface of the sidewall from (a) E28H_s40 and (b) E28H_f40.

The laser profilometric analysis of these parts confirmed this further. Figure 7.18-7.21 give the 3-D micro-topography of the representative samples cut from the apex and sidewalls of the formed composite hemisphere, along with their representative line profiles. The various roughness parameters (R_a, R_q, R_z) were calculated through the formation of specific line profiles. The average roughness values obtained from such line profiles for all tested samples are presented in Table 7.1. It is apparent from the Figure 7.18-7.21 and the Table 7.1 that the wall at the apex was smoother than the sidewall nearer to the rim of the hemisphere.

Table 7.1. Roughness parameters of the analysed samples

Specimen	R_a (µm)	R_q (µm)	R_z (µm)
E28H_f40 (apex)	1.79	2.32	17.1
E28H_f40 (sidewall)	3.83	5.08	29.59
E28H_s40(apex)	0.37	0.53	7.83
E28H_s40 (sidewall)	0.47	0.63	7.24

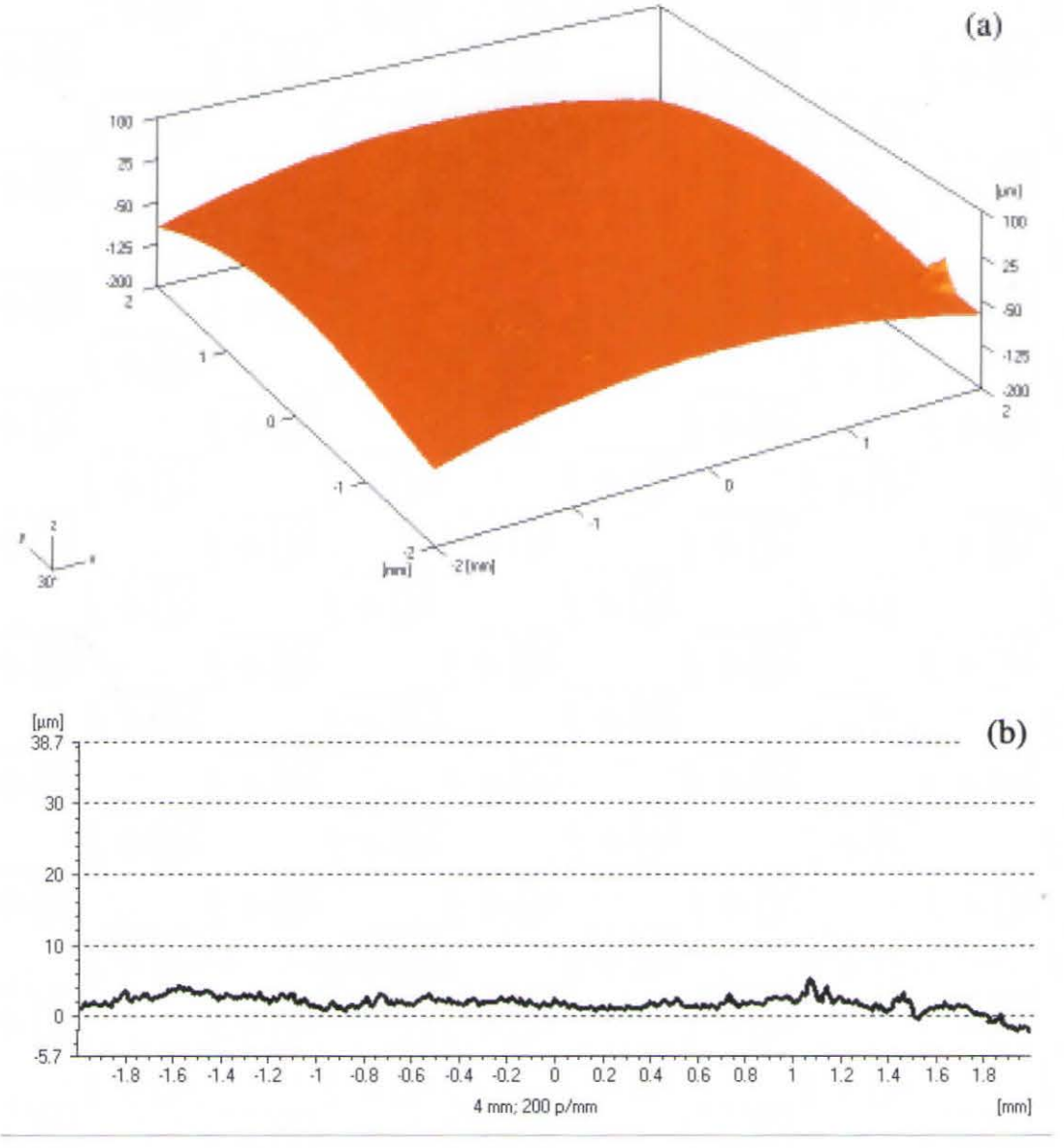

Figure 7.18. (a) Three dimensional microtopographic image of outer surface at the apex of E28H$_s$40 composite hemisphere and (b) the representative X-line profile.

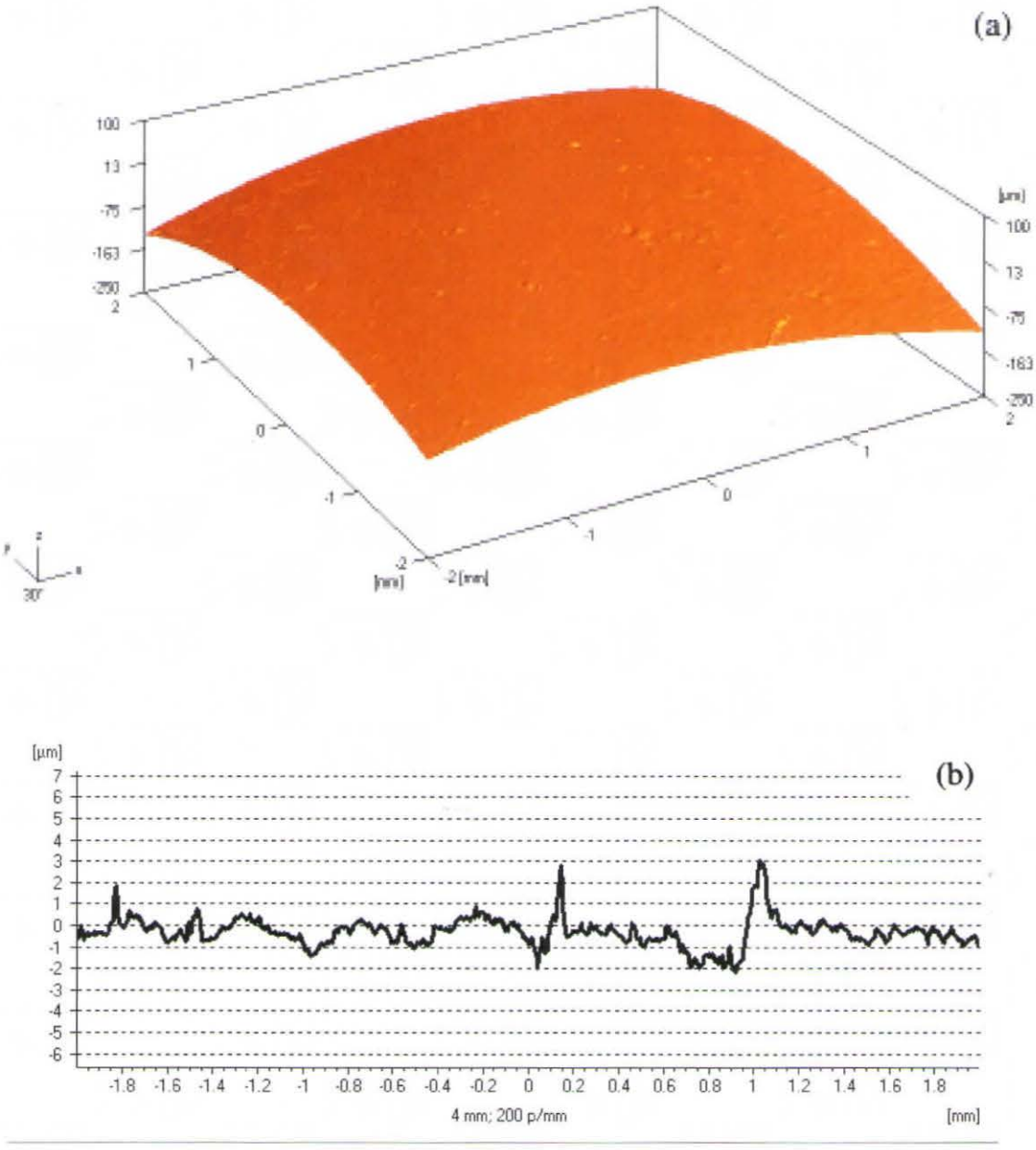

Figure 7.19. (a) Three dimensional microtopographic image of the sidewall nearer to the rim of E28H$_s$40 composite hemisphere and (b) the representative X-line profile.

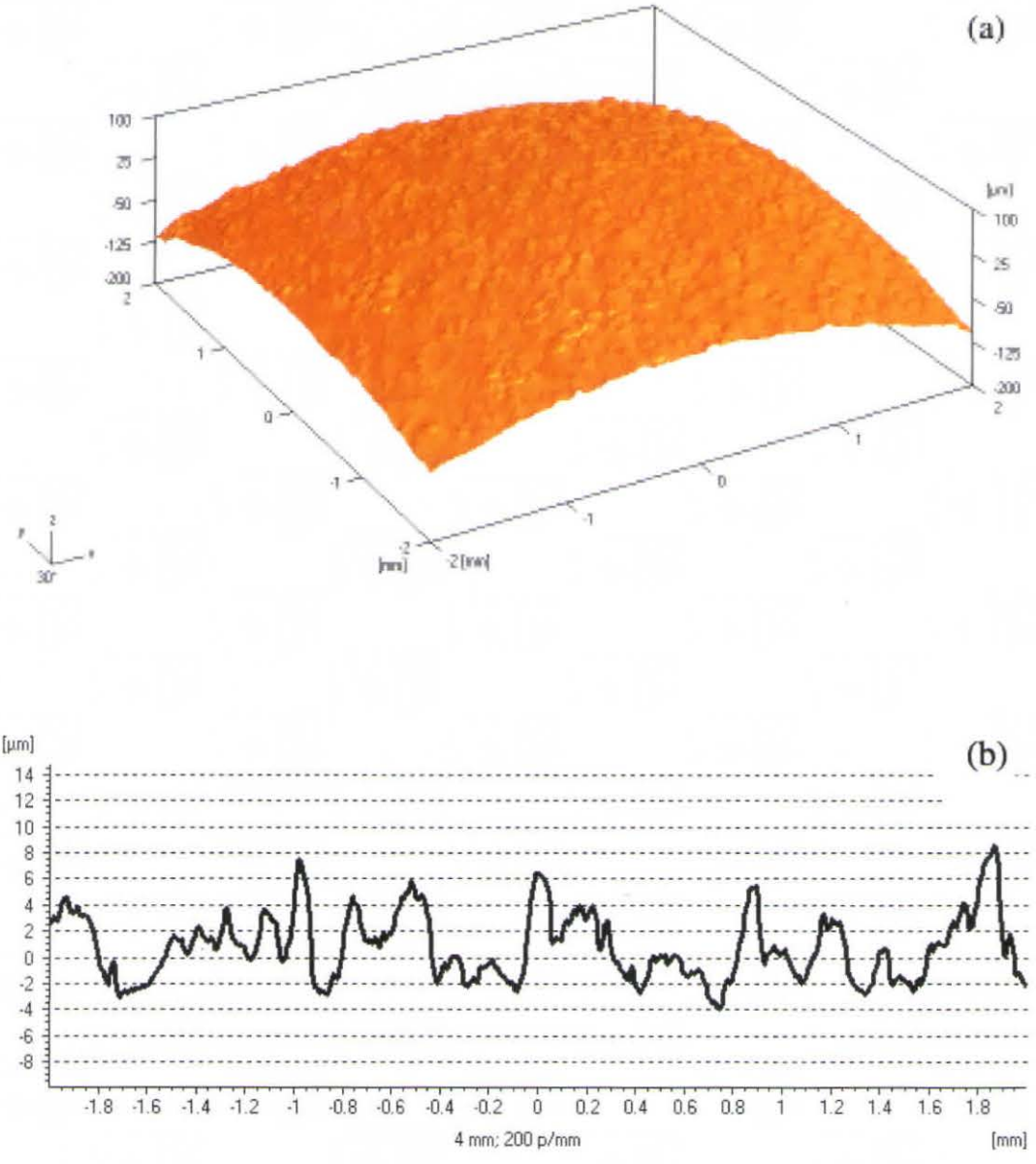

Figure 7.20. (a) Three dimensional microtopographic image of outer surface at the apex of E28H$_f$40 composite hemisphere and (b) the representative X-line profile.

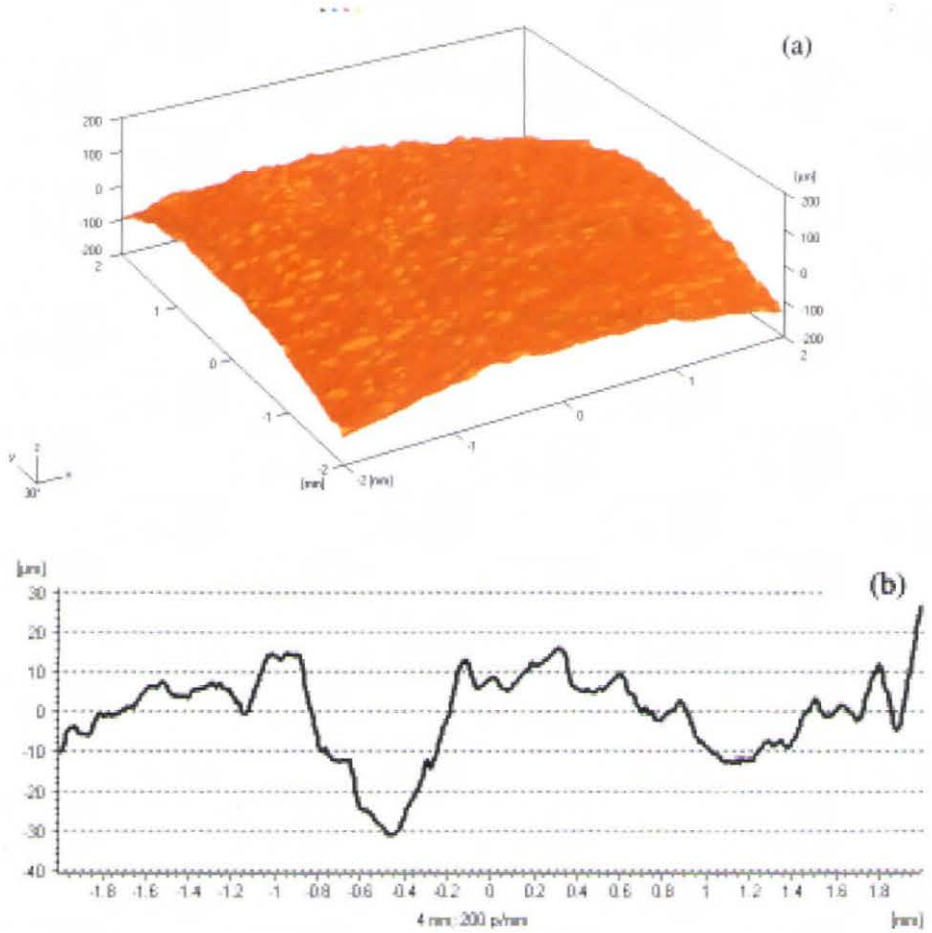

Figure 7.21. (a) Three dimensional microtopographic image of the sidewall nearer to the rim of E28H$_s$40 composite hemisphere and (b) the representative X-line profile.

It has been mentioned in section 8.4.1 that during the formation of hemisphere from a flat laminate, progressive step-by-step deformation operates and composite laminate experiences manifold force acting on it. Bhattacharyya *et al.,* (2003) performed grid strain analysis to assess the formability of the hemispherical forms. It was found that there are several strain states (Figure 7.22) observed across a thermoformed hemisphere: (1) balanced biaxial strain around the apex region, (2) plane strain in the mid-wall, (3) uniaxial strain in the lower wall, (4) plane strain near the rim. As mentioned earlier, a localized higher pressure is experienced at the apex. This results in pushing the molten matrix along with the filler towards the rim (lower pressure regions) of the hemisphere. The pressure gradient as well as the complex stretching conditions involved during the hemisphere formation thus lead to different levels of exposure of the fillers at the apex and the sidewall which accounts for the difference in the surface topography as well as the roughness of the regions at the apex and the sidewall of the hemisphere. The nature of the filler particle also contributed to the difference in surface roughness of the hemisphere.

This disparity in the surface roughness could be due to the different particle size of the HAP particles incorporated.

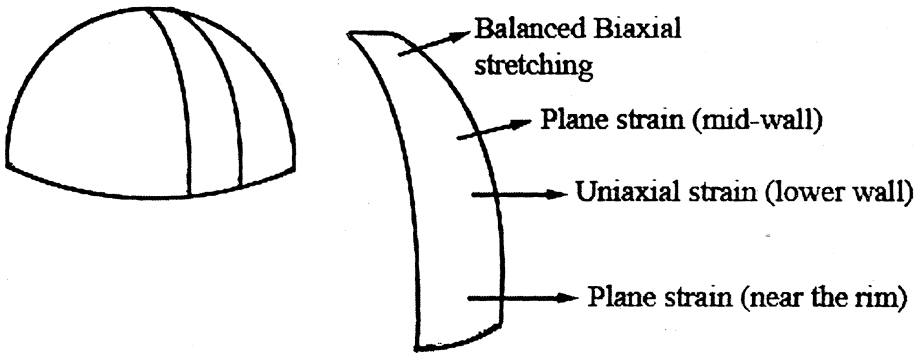

Figure 7.22. Schematic representation of the various strain states observed across a stamp formed hemisphere.

In the context of orthopaedics, exposure of HAP particles to the implant surface encourages the initial bone growth on the surface of the implant, which is to integrate into juxtaposed bone.

7.5. CONCLUSIONS

Stamp forming technique was utilized for the three-dimensional forming of HAP-EVA composite materials. Initially, two-dimensional V-bends were formed to determine the optimum processing conditions for the stamp forming of the composites. A temperature range good enough for stamp forming was above 90°C for both $E28H_s40$ and $E28H_f40$. However, both $E18H_s40$ and $E18H_f40$ composites required a temperature of above 110°C for obtaining flaw free V-bends. A stamping velocity of 190 mm/s could be used in the case of all the composites. Studies on the thickness distribution of the formed bends showed that at optimum forming conditions the bends had fairly uniform wall thickness. Irrespective of the stamping conditions employed, all the V-bends exhibited spring-backward phenomenon. The spring backward was, however, severe at low stamping temperatures and stamping velocities.

The three-dimensional forms were prepared, at the optimized condition, using a hemispherical mould. The thickness distribution in the hemispherical parts was seen to be symmetric about the central line through the apex.

Irrespective of 2-D and 3-D forming, the part quality was influenced by the nature of polymer matrix. It was noted that the wall thicknesses of the $E28H_s40$ and $E28H_f40$ forms were thinner when compared to $E18H_s40$ and $E18H_f40$, probably due to the difference in the flow properties of the E28 and E18 polymer matrices. The nature of the HAP used was also found to be affecting the part quality of the three-dimensional forms. The surface finish was found to be smoother for $E28H_s40$ and $E28H_f40$ when compared to $E18H_s40$ and $E18H_f40$ hemispheres. This disparity could be due to the difference in both particle size and morphology of the HAP used for the study.

CHAPTER 8

SUMMARY, CONCLUSIONS AND FUTURE PROSPECTS

8.1. SUMMARY AND CONCLUSIONS

The constant pursuit for an ideal analogue for sealing defective skull has given birth to a myriad of implant materials, such as biological grafts, metals, polymers, ceramics and combination of one or more of these materials. Each class of these materials is effectual in construction and augmentation of impaired cranium, but is less than ideal. While metals and polymers lack bioacitivity, biological grafts and cermics are too difficult to be shaped according to the complex contours of the skull. In this scenario, development of a material for repairing the cranial defects that meets the requirements of biocompatibility, osteoconductivity and malleability would indeed be extremely valuable in clinical practice.

This study was initiated with the aim of developing a novel 'surgeon friendly' bioactive material that could be used for renovating impaired skull contours. Hydroxyapatite was the natural choice as the filler because of its excellent biocompatibility and osteoconductivity. To combat the limitations of brittleness and snags of sculpting HAP into desired complex contours, a biocompatible thermoplastic elastomer ethylene vinyl acetate co-polymer was selected as the matrix. Two forms of hydroxyapatites, differing with respect to particle size and morphology, were chosen for the study. The spherical form of HAP (designated as H_S), was produced by spray drying technique had smaller particle size, while the freeze dried HAP (designated as H_F) had

irregular morphology and bigger particle size. Two grades of EVA, namely E28 and E18 were used as matrix materials. A torque rheometer was used to prepare the composites. Composites with HAP loading up to 50vol.% were prepared.

It was found that the flow behaviour of HAP-EVA composites dependeds on both the nature of the HAP particles and also the nature of the polymer matrix used. In general, for the same volume fraction of HAP loaded, the smaller particle sized HAP gave higher viscosity for the composite. Also the polymer with lower value of MFI gave higher viscosity for the composites. The relative viscosity of melts could be predicted using Maron-Pierce as well as Mooney equation at lower volume fractions of HAP (<30vol.%). However, at higher volume fractions of HAP, the experimental values were considerably higher than the theoretical values. Of the two grades of polymers studied, the composites fabricated from E28 gave easier processing.

The composites developed were evaluated for their tensile, flexural, impact and dynamic mechanical properties. It was found that the characteristics of HAP significantly influenced the mechanical properties of the composites. Generally, the HAP with smaller particle size gave higher values of tensile, flexural and impact strength. With respect to dynamic mechanical properties, marginally higher value of dynamic storage modulus was noted for composites fabricated from larger particle sized HAP. However, HAP with smaller particle size gave better interactions with the polymer matrix, as evident from the shift of the glass transition temperature (T_g) to the higher temperature region. This was further confirmed from the fractographs of the composite specimens, which showed the presence of mechanical interlocks between the spherical particles and the surrounding polymer matrix. The composites fabricated from bigger particle size HAP lacked such an interaction. The values of the damping factor (tan δ) decreased with the addition of either forms of HAP.

At this point, a comparison of the mechanical properties of HAP-EVA composites with that of the human cortical bone and the existing cranioplastic substitutes at the physiological conditions is worthwhile. In general, the Young's modulus and tensile strength values of the HAP-EVA composites with 40vol.% of HAP are quite low when compared to the human cortical bone (Chapter 5). Nevertheless, these values are sufficiently higher than that of the cranioplastic substitute of similar material chemistry. The strain to failure observed for HAP-EVA composites at 40vol.% of HAP is also quite

higher when compared to the cortical bone or the other polymer-ceramic composite bone substitutes. This implies the higher toughness of these composites. The lower modulus coupled with higher toughness are the bonus properties of this composite, which makes it 'surgeon friendly'. By virtue of these properties a surgeon can sculpt the composite in accordance with the defect created in the skull. This will reduce the duration of the surgery, the surgical complications and also enhance the aesthetics of the cranial constructs. It should be noted that while performing cranioplasty, manipulation of implant during surgery is obligatory, irrespective of whether the implant is prefabricated or made on the spot at the surgical table. This is important because many times the curvature and thickness of the implants are not exact, and trimming is required to eliminate differences arising from the incompatibility of shape of the edges of the implant with the incised edges of the cranial defect.

The biological performance of HAP-EVA composites was evaluated following the methods recommended as per ISO-10993 for bone substitutes. The *in vitro* cell culture cytotoxicity studies using mouse fibroblasts cell lines (L929) showed that the composites under the study were non-cytotoxic to the cell lines. Intracutaneous injections from the extracts of the composites, tested for skin irritation, showed that the composites do not cause potential local irritation. Systemic toxicity evaluation of the sample extracts from the composite by intravenous and intraperitoneal injections revealed that no animal assayed showed toxic symptoms or died during the observation period. Closed patch sensitization studies carried out on HAP-EVA composite revealed that the material had no potential to elicit the immune response in guinea pigs. Intramuscular implantation studies carried out in the rabbit paravertebral muscles, confirmed the biocompatible nature of the HAP-EVA composites. The bio-functionality of the composite material was confirmed by implantation of the material in rabbit cranium. It was encouraging to note that the bone tissue around the implanted composites went through stages of active remodeling and healing. Many areas of direct contact of bone with the material were also observed.

A cost-effective method, namely stamp forming, was attempted to obtain these composites into clinically significant forms. The idea was to obtain forms similar to the skull contour. A three dimensional hemispherical mould was thus selected. Due to the complexities involved in the three-dimensional forming, the parameters such as the

stamping temperature, stamping velocity, hold on pressure and hold up time at pressure were initially optimized with respect to a two-dimensional right angled V-mould. The quality of the formed bends depended on the stamping temperature and stamping velocity. It was also found that the two-dimensional forms (V-bends) exhibited 'spring-backward' phenomenon, irrespective of the processing conditions employed. The nature of the polymer matrix also influenced the quality of both two-dimensional and three-dimensional parts formed. The walls of the parts fabricated from the polymer with higher MFI value were thinner than those fabricated from the polymer matrix with lower MFI value. It was observed that a good quality form could be obtained when the composites were heated to a temperature about 30°C above the melting temperature of the EVA matrix. A forming velocity of 190 mm/s was found to be appropriate for obtaining good quality stamped bends.

Three-dimensional hemispherical forms were obtained at the optimized conditions. The processing cycle lasted for over 45 s. The walls of the formed hemisphere were slightly thinner at the apex and thicker towards the sides. The thickness distribution was found to be symmetric about the apex and was due to the symmetric construction nature of 3-D mould used. The nature of the HAP used also affected the part quality of the three-dimensional forms. The parts fabricated from spherical and smaller HAP particles were smoother when compared to those fabricated from irregularly shaped and bigger HAP particles. Also, for a given hemispherical form, the wall at the apex was smoother than the wall towards the rim of the hemisphere. In the context of implants intended for bone substitution, exposure of HAP to the surface of the implants is promising. This makes the implant material habitable especially for bone-forming cells (osteoblasts) such that they can colonize on the implant surface and synthesize new bone tissue. Judicious exploitation of stamp forming method could pave way to the development of customized and pre-fabricated implants for repairing defects in the cranium and revolutionize the neurosurgical procedures.

This investigation thus substantiates that a customized and prefabricated 'surgeon friendly' cranioplastic substitute, with promising mechanical and biological characteristics could be engineered.

8.2. FUTURE PROSPECTS

The present study confirmed the biocompatibility and bio-functionality of the HAP-EVA composites. The composites could also be fabricated into clinically significant shapes by making use of simple stamp forming techniques. Both these factors shed light to the possible future application of this composite as a material for replacing defective cranium. However, few more issues, as illustrated below, have to be addressed before the material goes for clinical trials.

The present study has been carried out on a small animal model. The contributions of the host bed at the implantation site to osteo-integration of bone substitute may prove critical when larger defects have to be repaired. Consequently, the results of the present study cannot be freely extrapolated to the human situation and a larger animal model seems necessary to comprehensively determine the *in vivo* material properties as well as the performance of the bone graft substitute before its clinical application. Hence, further study with a statistically significant number of animals in a larger animal model is called for. Also, prior to the clinical evaluation, systematic studies on the degradation of the material both *in vitro* and *in vivo* would ensure better biological safety of the device/implant.

REFERENCES

Abu Bakar MS, Cheang P and Khor KA. Tensile properties and microstructural analysis of spheroidized hydroxyapatite-poly(etheretherketone) biocomposites. Mat Sci Engg A, 2003a, **345**, 55-63.

Abu Bakar MS, Cheang P and Khor KA. Mechanical properties of injection moulded hydroxyapatite-polyetheretherketone biocomposites. Comp Sc Tech, 2003b, **63**, 421-425.

Abu Bakar MS, Cheng MHW, Tang SM, Yu SC, Liao K, Tan CT, Khor KA and Cheang P. Tensile properties, tension-tension fatigue and biological response of polyetheretherketone-hydroxyapatite composites for load bearing orthopaedic applications. Biomaterials, 2003c, **24**, 2245-2250.

Agarwal S and Salovey R. Model filled polymers. XV: The effects of chemical interactions and matrix molecular weight on rheology. Polym Engg Sci, 1995, **35**, 1241-1251.

Agner C, McConathy D and Dujovny M. Evaluation of autogenic, xenogeneic and alloplastic materials used for cranioplasty. Crit Rev Neurosurg, 1997, **7**, 365-372.

Agrawal CM and Athanasiou KA. Technique to control pH in vicinity of biodegrading PLA-PGA implants. J Biomed Mater Res: Appl Biomater, 1997, **38**, 105-114.

Ahmed S and Jones FR. A review of particulate reinforcement theories for polymer composites. J Mat Sci, 1990, **25**, 4933-4942.

Albrektsson T and Hansson HA. An ultrastructural characterization of the interface between bone and sputtered titanium or stainless steel surfaces. Biomaterials, 1986, **7**, 201-205.

Alesch F and Bauer R. Polyacryl prosthesis for cranioplasty – their production in silicon rubber casts. Acta Neurochir (Wien), 1985, **77**, 68-71.

Alexander H, Langrana N, Massengill JB and Weiss AB. Development of new methods for phalangeal fracture fixation. J Biomech. 1981a, **14**, 377-387.

Alexander H, Corcoran SF, Parsons JR and Weiss AB. Internal fracture fixation with partially degradable plates. 9th bioengineering conference, Elmsford, New York, 1981b.

Ashley S. Rapid prototyping systems. Mechanical Engineering, 1991, **4**, 34–43.

ASM international handbook committee. Engineering Mateirals Handbook. Vol. 1. ASM International, Metals Park, Ohio, 1987.

ASTM D790-97. Standard test method for the flexural properties of un-reinforced and reinforced plastics and electrical insulating materials. In: Annual Book of American Society of Testing Materials standards, Philadelphia, 1997.

ASTM F138-97. Standard Specification for Stainless Steel Bar and Wire for Surgical Implants. In: Annual Book of ASTM Standards, Philadelphia, 1997.

ASTM E1356-98. Standard test method for assignment of the glass transition temperatures by differential scanning calorimetry. In: Annual Book of American Society of Testing Materials standards, Philadelphia, 1998.

ASTM F75-01. Standard Specification for Cobalt-28 Chromium-6 Molybdenum Alloy Castings and Casting Alloy for Surgical Implants. In: Annual Book of ASTM Standards, Philadelphia, 2001.

ASTM F136-02. Standard Specification for Wrought Titanium-6 Aluminum-4 Vanadium ELI (Extra Low Interstitial) Alloy for Surgical Implant Applications. In: Annual Book of ASTM Standards, Philadelphia, 2002.

Athanasiou KA, Agrawal CM, Barber FA and Burkhart SS. Orthopaedic applications for PLA-PGA biodegradable polymers. Arthroscopy, 1998, **14**, 726-737.

Ayora M, Ri´os R, Quijano J and Ma´rquez A. Evaluation by torque rheometer of suspensions of semi-rigid and flexible natural fibers in a matrix of poly(vinyl chloride). Polym Composite, 1997, **18**, 549-560.

Barker TM, Earwaker WJS, Frost N and Wakely G. Integration of 3-D medical imaging and rapid prototyping to create stereo-lithographic models. Australas Phys Eng Sci Med, 1993, **16**, 79–85.

Barnes JA, Byerly G, Le Bouton MC and Zahlan N. Dimensional stability effects in thermoplastic composites – towards a predictive capability. Comp Manufact, 1992, **2**,171-178.

Bartczak Z, Argon AS, Cohen RE and Weinberg M. Toughness mechanism in semi-crystalline polymer blends: II. High-density polyethylene toughened with calcium carbonate filler particles. Polymer, 1999, **40**, 2347-2365.

Basso N and Heersche JNM. Characteristics of *in vitro* osteoblastic cell loading models. Bone 2002, **30**, 347–351.

Benzel EC, Thammavaram K and Kesterson L. The diagnosis of infections associated with acrylic cranioplasties. Neuroradiology, 1990, **32**, 151-153.

Berlin AA, Volfson SA, Enikolopian NS and Negmatov SS. Principles of polymer composites. Springer Verlag, Berlin, 1990.

Beruto DT, Mezzasalma SA, Capurro M, Botter R and Cirillo P. Use of alpha-tricalcium phosphate (TCP) as powders and as an aqueous dispersion to modify processing, microstructureand mechanical properties of polymethylmethacrylate (PMMA) bone cements and to produce bone-substitute compounds. J Biomed Mater Res, 2000, **49A**, 498-505.

Bhagawan SS, Tripathy DK, De SK, Sharma SK and Ramamurthy K. Effect of fillers on the rheological behavior of thermoplastic 1,2 polybutadiene rubber. Polym Engg Sci, 1988, **28**, 648-654.

Bhattacharyya D. Composite sheet forming, Composite materials series, vol. 11, Elsevier, Amsterdam, 1997.

Bhattacharrya D, Bowis M and Jayaraman K. Thermoforming woodfibre-polypropylene composite sheets. Comp Sci Tech, 2003, **63**, 353-365.

Bleach NC, Nazhat SN, Tanner KE, Kellomaki M and Tormala P. Effect of filler content on mechanical and dynamic mechanical properties of particulate biphasic calcium phosphate--polylactide composites. Biomaterials, 2002, **23**, 1579-1585.

Blum KS, Schneider SJ and Rosenthal AD. Methyl methacrylate cranioplasty in children: long-term results. Pediatr Neurosurg, 1997, **26**, 33-35.

Blyler LL and Daane JH. An analysis of Brabender torque rheometer data. Polym Engg Sci, 1967, **7**, 178-181.

Bomal Y and Godard P. Melt viscosity of calcium carbonate filled low-density polyethylene: Influence of matrix-filler and particle-particle Interactions. Polym Engg Sci, 1996, **36**, 237-243.

Bonfield W. Composite biomaterials, in: Kokubo T, Nakamura T, Miyaji F, eds. Bioceramics 9, Elsevier Science, Oxford, 1996, pp. 11-13.

Bonfield W. From concept to patient-engineering solutions to medical problems, in Engineers and society: the 1997 CSE international lecture, The Royal Academy of Engineering, London, 1997, pp. 5-11.

Bonfield W. 'Biomaterials: Research and Development', in European White Book on Fundamental Research in Materials Science, editor Ruehl M, MPG Press, First edition, Munich, 2003, pp 72-76.

Bonfield W, Grynpas MD, Tully AE, Bowman J and Abram J. Hydroxyapatite reinforced polyethylene - a mechanically compatible implant material for bone replacement. Biomaterials, 1981, **2**, 185-186.

Bonfield W, Doyle C and Tanner KE. *In vivo* evaluation of hydroxyapatite reinforced polyethylene composites. in: Christel P, Meunier A, Lee AJC eds. Biological and Biomechanical Performance of Biomaterials, Elsevier, Amsterdam, 1986, pp. 153-158.

Bostman O. Reaction to biodegradable implants. J Bone Joint Surg Br, 1993, **75**, 336-337.

Bostman O and Pihlajamaki HK. Adverse tissue reactions to bioabsorbable fixation devices. Clin Orthop, 2000, **371**, 216-227.

Bostman O, Vainionpaa S, Hirvensalo E, Makela A, Vihtonen K, Tormala P and Rokkanen P. Biodegradable internal fixation for malleolar fractures. A prospective randomised trial. J Bone Joint Surg, 1987, **69B**, 615-619.

Bousmina M, Ait-Kadi A and Faisant JB. Determination of shear rate and viscosity from batch mixer data. J Rheol, 1999, **43**, 415-433.

Bradley JS, Hastings JW and Johnson-Nurse C. Carbon fibre reinforced epoxy as a high strength, low modulus material for internal fixation plates. Biomaterials, 1980, **1**, 38-40.

Breuer U and Neitzel M. High speed stamp forming of thermoplastic composite sheets. Polym Polym Composite, 1996, **4**, 117-122.

Buehler EV. Delayed contact hypersensitivity in the guinea pig. Arch Dermatol, 1965, **91**, 171-175.

Cai JJ and Salovey R. Model filled rubber IV: Dependence of stress-strain relationship on filler particle morphology. J Mater Sci, 1999, **34**, 4719-4726.

Cheang P and Khor KA. Effect of particulate morphology on the tensile behaviour of polymer-hydroxyapatite composites. Mater Sci Engg, 2003, **345A**, 47-54.

Cheng AC and Wee AG. Reconstruction of cranial bone defects using alloplastic implants produced from a stereolithographically-generated cranial model. Ann Acad Med Singapore. 1999, **28**, 692-696.

Chiarini L, Figurelli S, Pollastri G, Torcia E, Ferrari F, Albanese M and Nocini PF. Cranioplasty using acrylic material: a new technical procedure. J Craniomaxillofac Surg, 2004, **32**, 5-9.

Chicarilli ZN and Ariyan S. Cranioplasty with a silicone prosthesis and split rib grafts. Head and Neck Surgery, 1986, **8**, 355-362.

Collins P, Lappin JF, Harkines-Jones EMA and Martin PJ. Investigation of heat transfer in the plug assisted thermoforming process. ANTEC Tech Papers, 2000, 788-790.

Constantino PD, Chaplin JM, Wolpoe ME, Catalano PJ, Sen C, Bederson JB and Govindaraj S. Applications of fast-setting hydroxyapatite cement: cranioplasty. Otolaryng Head Neck, 2000, **123**, 409-412.

Constantino PD, Friedman CD and Lane A. Synthetic biomaterials in facial plastic and reconstructive surgery. Fac Plast Surg, 1993, **9**, 1-15.

Cook M and Harper JF. The influence of magnesium hydroxide morphology on the crystallinity and properties of filled polypropylene. Adv Polym Tech, 1998, **17**, 53-62.

Couldwell WT, Chen TC, Weiss MH, Fukushima T and Dougherty WJ. Cranioplasty with the Medpor porous polyethylene flexblock implant. Technical note. Neurosurg, 1994, **81**, 483-486.

Countemanche AD and Thompson GB. Silastic cranioplasty following craniofacial injuries. Plast Recon Surg, 1968, **41**, 165-171.

Currey JD. The design of mineralised hard tissues for their mechanical functions. J Exp Biol, 1999, **202**, 3285-3294.

Currey JD. What should bones be designed to do? Calcif Tissue Int, 1984, **36**, S7-S10.

Cynthia AB and Myron S. Quantitative characterization of cells at the interface of long-term implants of selected polymers. J Biomed Mater Res, 1986, **20**, 653-666.

D'Urso PS, Earwaker WJ, Barker TM, Redmond MJ, Thompson RG, Effeney DJ and Tomlinson FH. Custom cranioplasty using stereolithography and acrylic. Br J Plast Surg, 2000, **53**, 200–204.

Dalby MJ, di Silvio L, Harper EJ and Bonfield W. Increasing hydroxyapatite incorporation into poly(methylmethacrylate) cement increases osteoblast adhesion and response. Biomaterials, 2002, **23**, 569-576.

Davies JE, Chernecky R, Lowenberg B and Shiga A. Deposition and resorption of calcified matrix in vitro by rat bone marrow cells. Cells Mater 1991, **1**, 13-15.

de Bruijn JD, Davies JE, Klein CPAT, de Groot K and van Blitterswijk CA. Biological responses to calcium phosphate ceramics. in: Duchyene P, Kokubo T, van Blitterswijk CA, eds. Bone-Bonding Biomaterials, Reed Health Care Communications, Leiderdorp, 1992, pp. 57-65.

de Bruijn JD, van Blitterswijk CA and Davies JE. Initial bone matrix formation at the hydroxyapatite interface *in vivo*. J Biomed Mater Res 1995, **29**, 89-99.

Dealy JM and Wissburn KF. Melt rheology and its role in plastics processing: Theory and applications, Van Nostrand Reinhold, New York, 1990.

Dean D, Min KJ and Bond A. Computer aided design of large-format prefabricated cranial plates. J Craniofac Surg. 2003, **14**, 819-832.

Dhert WJA, Klein CPAT, Jansen JA, Velde EA van der, Vriesde RC, Rizing PM and Groot K de. A histological and histomorphometrical investigation of fluorapatite, magnesiumwhitlockite and hydroxylapatite plasma-sprayed coatings in goats. J Biomed Mater Res 1993, **27**, 127-138.

di Silvio L, Dalby MJ and Bonfield W. Osteoblast behaviour on HA/PE composite surfaces with different HA volumes. Biomaterials, 2002, **23**, 101-107.

Doyle C, Luklinska ZB, Tanner KE and Bonfield W. An ultra-structural study of the interface between hydroxyapatite/polymer composite and bone. in: Heimke G, Soltesz U, Lee AJC eds. Advances in Biomaterials: Clinical Implant Materials, Elsevier, Amsterdam, 1990.

Ducic Y. Midface reconstruction with titanium mesh and hydroxyapatite cement: Report of a case. J Craniomaxillofac Trauma, 1997, **3**, 35-39.

Ducic Y. Titanium mesh and hydroxyapatite cement cranioplasty. A report of 20 cases. J Oral Maxillofac Surg, 2002, **60**, 272-276.

Dujovny M, Aviles A, Agner C, Fernandez P and Charbel FT. Cranioplasty: Cosmetic or Therapeutic. Surg Neurol, 1997, **47**, 238-241.

Durham SR, Mc Comb JG and Levy ML. Correction of large (> 25 cm^2) cranial defects with reinforced hydroxyapatite cement: Technique and complications. Neurosurgery, 2003, **52**, 842-845.

Durucan C and Brown PW. Calcium deficient hydroxyapatite–PLGA composites: mechanical and microstructural investigation. J Biomed Mater Res, 2000, **51A**, 726-734.

Ebel H, Schillinger G, Walter C, Brockhagen HG and Klug N. Titanium clamps for refixation of bone fragments in the repair of depressed skull fractures: technical note. Min Invasive Neurosurg, 2000, **43**, 212-214.

Ecobichon DJ. The basis of toxicity testing. CRC Press, Boca Raton, 1992.

Eglin D, Ali SAM and Perry CC. Comparative study of the in vitro apatite-forming ability of poly(ε-caprolactone)-silica sol-gels using three osteoconductivity tests (static, dynamicand alternate soaking process). J Biomed Mat Res, 2004, **69**A, 718-727.

Eirich FR. Failure modes of elastomers. Engineering Fracture Mechanics, 1973, **5**, 555-562.

Eppley BL, Sadove AM and Havlik RJ. Resorbable plate fixation in pediatric craniofacial surgery. Plastic and Reconstruc Surg, 1997, **100**, 1-7.

Estin D, Troffkin N and Heilman CB. Bone flap fixation with titanium clamps: a new technique. Surg Neurol, 2000, **53**, 391-394.

Fallahi B, Foroutan M, Motavalli S, Dujovny M and Limaye S. Computer-aided manufacturing of implants for the repair of large cranial defects: an improvement of the stereolithography technique. Neurol Res, 1999, **21**, 281-286.

Fearon JA, Munro IR and Bruce DA. Observations on the use of rigid fixation for craniofacial deformities in infants and young children. Plast Reconstr Surg, 1995, **95**, 634-637.

Fuente del Campo A, Pohjonen T, Tormala P and Waris T. Fixation of horizontal maxillary osteotomies with biodegradable self-reinforced absorbable poly (lactide) plates: preliminary results. Eur J Plast Surg, 1996, **19**, 7-9.

Furukawa J and Yamada E. Effect of chemical and physical crosslinks on strength of rubber and plastics - a theoretical approach. J Appl Polym Sci, 1994, **52**, 1587-1593.

Furukawa T, Matsusue Y, Yasunaga T, Shikinami Y, Okuno M and Nakamura T. Biodegradation behaviour of ultra-high-strength hydroxyapatite/poly(l-lactide) composite rods for internal fixation of bone fractures. Biomaterials, 2000a, **21**, 889 –898.

Furukawa T, Matsusue Y, Yasunaga T, Nakagawa Y, Okada Y, Shikinami Y, Okuno M and Nakamura T. Histomorphometric study on high-strength

hydroxyapatite/poly(l-lactide) composite rods for internal fixation of bone fractures. J Biomed Mater Res, 2000b, **50A**, 410 –419.

Gad CG. Safety evaluation of medical devices. Marcel Dekker, New York, 1997.

Galicich JH and Hovind KH. Stainless steel mesh-acrylic cranioplasty: Technical note. J Neurosurg, 1967, **27**, 376-378.

Gan D, Lu S, Song C and Wang Z. Physical properties of poly(etherketoneketone)/ mica composites: effect of filler content. Mater Lett, 2001, **48**, 299-302.

Gent AN. Science and Technology of Rubber, Academic Press, New York, 1978.

Ghosh T, Grmela M and Carreau PJ. Rheology of short fiber filled thermoplastics. Polym Composite, 1995, **16**, 144-153.

Goldberg DS, Bartlett S, Yu JC, Hunter JV and Whitaker LA. Critical review of microfixation in pediatric craniofacial surgery. J Craniofac Surg, 1995, **6**, 301-307.

Gomes ME, Ribeiro AS, Malafaya PB, Reis RL and Cunha AM. A new approach based on injection moulding to produce biodegradable starch-based polymeric scaffolds: morphology, mechanical and degradation behaviour. Biomaterials, 2001a, **22**, 883-889.

Gomes ME, Reis RL, Cunha AM, Blitterswijk CA and de Bruijn JD. Cytocompatibility and response of osteoblastic-like cells to starch-based polymers: effect of several additives and processing conditions. Biomaterials, 2001b, **22,** 1911-1917.

Goodier JN. J Appl Mech Tran AME, 1988, **A3**, 55-58.

Goodrich JE and Porter RS. A rheological interpretation of torque-rheometer data. Polym Engg Sci, 1967, **7**, 45-51.

Gosain AK. Biomaterials in facial reconstructions. Operative Tech Plas Recon Surg, 2002, **9**, 23-30.

Gosain AK, Song L, Corrao MA and Pintar FA. Biomechanical evaluation of titanium, biodegradable plate and screwand cyanoacrylate glue fixation systems in craniofacial surgery. Plast Reconstr Surg, 1998, **101**, 582-591.

Gosain AK and Persing JA. Biomaterials in the face: benefits and risks. J Craniofac Surg, 1999, **10**, 404-414.

Gough JE and Downes S. Osteoblast cell death on methacrylate polymers involves apoptosis. J Biomed Mater Res, 2001, **57A**, 497-505.

Gradin P, Howgate P and Selden R. Dynamic mechanical properties, in Allen G and Bevington JC (eds.) Comprehensive polymer science, Vol. 2. Polymer properties, Pergamon, Oxford, 1989.

Griffet J, Chevallier A, Hayek TE, Odin G, Pebeyre B and Accorsi E. Diaphyseal fractures treated by polylactide and hydroxyapatite pins. Experimental study in rat. J Mater Sci: Mater Med, 1999, **10**, 411-418.

Grondahl L, Cardona F, Chiem K, Wentrup-Byrne E and Bostrom T. Calcium phosphate nucleation on surface-modified PTFE membranes. J Mat Sci: Mat Med, 2003, **14**, 503-510.

Gupta SK, Reddy NM, Khosla VK, Mathuriya SN, Shama BS, Pathak A, Tewari MK and Kak VK. Growing skull fractures: a clinical study of 41 patients. Acta Neurochir (Wien), 1997, **139**, 928-932.

Haers PE and Sailer HF. Biodegradable self-reinforced poly-l/dl-lactide plates and screws in bimaxillary orthognathic surgery: short-term skeletal stability and material related failures. J Cranio Maxillofac Surg, 1998, **26**, 363-372.

Haers PE, Suuronen R, Lindqvist C and Sailer H. Biodegradable polylactide plates and screws in orthognathic surgery: technical note. J Craniomaxillofac Surg, 1998, **26**, 87-91.

Han CD, Sandford C and Yoo HJ. Effects of titanate coupling agents on the rheological and mechanical properties of filled polyolefins. Polym Engg Sci, 1978, **18**, 849-854.

Helsen JA and Breme HJ. Metals as biomaterials. John Wiley and Sons, New York, 1998.

Hench LL. Ceramics, glasses and composites in medicine. Med Instrum 1973, **7**, 136-144.

Henning W, Blencke BA, Bromer H, Deutscher KK, Gross A and Ege W. Investigations with bioactivated polymethylmethacrylates. J Biomed Mater Res, 1979, **13**, 89-99.

Hieu LC, Bohez E, Vander Sloten J, Oris P, Phien HN, Vatcharaporn E and Binh PH. Design and manufacturing of cranioplasty implants by 3-axis CNC milling. Technol Health Care, 2002, **10**, 413-423.

Higashi S, Yamamuro T, Nakamura T, Ikada Y, Hyon SH and Jamshidi K. Polymer hydroxyapatite composites for biodegradable bone fillers. Biomaterials, 1986, **7**, 183 – 187.

Hoffmann H, Grellmann W and Zilvar V. Polymer composites, Walter de Gruyter, New York, 1986.

Hogg PJ, Behiri J, Brandwood A, Bowman J and Bonfiled W. Impact testing of hydroxyapatite high density polyethylene composites. Proc Comp in Biomed Engg (Plastic and Rubber Institute, London, 1985) pp. 29/1 – 29/9.

Hou M and Freidrich K. Stamp forming of continuous carbon fibre/polypropylene composites. Comp Manufac, 1991, **2**, 3-9.

Hou M, Ye L and Mai YW. Advances in processing of continuous fibre reinforced composites with thermoplastic matrix. Rub Comp Proc Appl, 1995, **23**, 279-293.

Hou M and Friedrich K. Adjustable forming of thermoplastic composites for orthopaedic applications. J Mater Sci: Mater Med, 1998, **9**, 83-88.

Huang J, Wang M, Rehman I, Knowles J and Bonfield W. Analysis of surface structures on Bioglass /polyethylene composites *in vitro*, in: Wilson J, Hench LL, Greenspan D, eds. Bioceramics 8, Pergamon, Oxford, 1995, pp. 389 –395.

Huang J, Wang M, Rehman I and Bonfield W. Effect of particle size on the properties of Bioglass reinforced polyethylene composites, in: Kokubo T, Nakamura T, Miyaji F, eds. Bioceramics 9, Elsevier Science, Oxford, 1996, pp. 431–434.

Huang J, di Silvio L, Wang M, Tanner KE and Bonfield W. *In vitro* mechanical and biological assessment of hydroxyapatite-reinforced polyethylene composite. J Mater Sci Mater Med, 1997, **8**, 775 –779.

Hull D and Clyne TW. An introduction to composite materials. 2nd ed., Cambridge University Press, Cambridge, 1996.

Hwang SF and Hwang KJ. Stamp forming of locally heated thermoplastic composites. Composites: Part A, 2002, **33**, 669-676.

Ignatius AA, Unterricker K, Wengner K, Richter M and Claes L. A new composite made of polyurethane and glass ceramic in a loaded implant model: a biomechanical and histological analysis. J Mater Sci: Mater Med, 1997, **8**, 753-756.

Imola MJ, Hamlar DD, Shao W, Chowdhury K and Tatum S. Resorbable plate fixation in pediatric craniofacial surgery: long-term outcome. Arch Fac Plast Surg, 2001, **3**, 79-90.

Ishaug SL, Crane GM, Miller MJ, Yasko A, Yaszemski MJ and Mikos AG. Bone formation by three-dimensional stromal osteoblast culture in biodegradable polymer scaffolds. J Biomed Mater Res, 1997, **36A**, 17-28.

Ishikawa K, Miyamoto Y, Kon M, Nagayama M and Asaoka K. Non-decay type fast-setting calcium phosphate cement: composite with sodium alginate. Biomaterials, 1995, **16**, 527-532.

ISO 527-2: 1993. Plastics -- Determination of tensile properties -- Part 1: General principles. International Organization for Standardization, Geneva, Switzerland, 1993.

ISO 10993-11: 1993. Biological evaluation of medical devices -- Part 11: Tests for systemic toxicity. International Organization for Standardization, Geneva, Switzerland, 1993.

ISO 10993-10: 1995. Biological evaluation of medical devices -- Part 10: Tests for irritation and sensitization. International Organization for Standardization, Geneva, Switzerland, 1995.

ISO 10993-5: 1999. Biological evaluation of medical devices -- Part 5: Tests for *in vitro* cytotoxicity. International Organization for Standardization, Geneva, Switzerland, 1999.

Jackson IT and Adham MN. Metallic plate stabilization of bone grafts in craniofacial surgery. Br J Plas Surg, 1986, **39**, 341-344.

Jarcho M. Calcium phosphate ceramics as hard tissue prosthetics. Clin Orthop Rel Res, 1981, **157**, 259-278.

Jiang G and Shi D. Coating of hydroxyapatite on highly porous Al_2O_3 substrate for bone substitutes. J Biomed Mater Res: Appl Biomater, 1998, **43**, 77-81.

Joffe JM, McDermott PJC, Linney AD, Mosse CA and Harris M. Computer-generated titanium cranioplasty: report of a new technique for repairing skull defects. Br J Neurosurg, 1992, **6**, 343–350.

Joffe J, Harris M, Kahugu F, Nicoll S, Linney A and Richards R. A prospective study of computer-aided design and manufacture of titanium plate for cranioplasty and its clinical outcome. Br J Neurosurg, 1999, **13**, 576-580.

Johnson HJ, Northup SJ, Seagraves PA, Garvin PJ and Wallin RF. Biocompatibility tests procedures for materials evaluation *in vitro* I. Comparative test system sensitivity. J Biomed Mater Res, 1983, **17**, 571-586.

Johnson PJ, Robbins DL, Lydiatt WM and Moore GF. Salvage of an infected hydroxyapatite cement cranioplasty with preservation of the implant material. Otolaryngol Head Neck Surg, 2000, **123**, 515-517.

Kallela I, Laine P, Suuronen R, Iizuka T, Pirinen S and Lindqvist C. Skeletal stability following mandibular advancement and rigid fixation with polylactide biodegradable screws. Int J Oral Maxillo-fac Surg, 1998, **27**, 3-8.

Kalpakkian S and Schmid SR. Manufacturing Engineering and Technology, Pearson Education, Singapore, 2002.

Kamyszek T, Weihe S, Scholz M, Wehmoller M and Eufinger H. Management of craniofacial bone defects with individually prefabricated titanium implants. Follow-up and evaluation of 78 patients with 78 titanium implants 1994-1998. Mund Kiefer Gesichtschir, 2001, **5**, 233-238.

Kataoka T, Kitano T, Sasahara M and Nishijima N. Viscosity of particle filled polymer melts. Rheol Acta, 1978, **17**, 149-155.

Kataoka T, Kitano T, Oyanagi Y and Sasahara M. Viscous properties of calcium carbonate filled polymer melsts. Rheol Acta, 1979, **18**, 635-639.

Kauly T, Keren B and Siegmann A. Highly filled thermoplastic composites. II: Effects of particle size distribution on some properties. Polym Composite, 1996, **17**, 806-815.

Kawai T, Ohtsuki C, Kamitakahara M, Miyazaki T, Tanihara M, Sakaguchi Y and Konagaya S. Coating of an apatite layer on polyamide films containing sulfonic groups by a biomimetic process. Biomaterials, 2004, **25**, 4529-4534.

Kikuchi M and Tanaka J. Chemical interaction in β-tricalcium phosphate/ copolymerized poly-l-lactide composites. J Cer Soc J, 2000, **108**, 642-645.

Kim GM and Michler GH. Micromechanical deformation processes in toughened and particle-filled semicrystalline polymers: Part 1. Characterization of deformation processes in dependence on phase morphology. Polymer, 1998, **39**, 5689–5697.

Kiyokawa K, Hayakawa K, Tanabe HY, Inoue Y, Tai Y, Shigemori M and Tokutomi T. Cranioplasty with split lateral skull plate segments for reconstruction of skull defects. J Craniomaxillofac Surg, 1998, **26**, 379-385.

Kokubo T, Kim HM and Kawashita M. Novel bioactive materials with different mechanical properties. Biomaterials, 2003, **24**, 2161-2175.

Koppel DA, Moos KF and Walker FS. Skull reconstruction with a two-part interlocking custom-made titanium plate. Br J Oral Maxillofac Surg, 1999, **37**, 70-72.

Kosaka T, Koneko Y, Nakada Y, Matsura M and Tanaka S. Effect of chitosan implantation on activation of canine macrophages and polymorphonuclear cells after surgical stress. J Vet Med Sci, 1996, **58**, 963-967.

Kosinski LE and Caruthers JM. The effect of particle concentration on the rheology of polydimethylsiloxane filled with fumed silica. J Appl Poly Sci, 1986, **32**, 3393-3406.

Kulah A and Kayaalp S. Single-table autogenous calvarial grafting for cranioplasty. J Craniomaxillofac Surg, 1991, **19**, 208-211.

Kurashina K, Kurita H, Kotani A, Kobayashi S, Kyoshima K and Hirano M. Experimental cranioplasty and skeletal augmentation using an alpha-tricalcium phosphate/dicalcium phosphate dibasic/tetracalcium phosphate monoxide cement: a preliminary short-term experiment in rabbits. Biomaterials, 1998, **19**, 701-706.

Kuttenberger JJ and Hardt N. Long-term results following reconstruction of craniofacial defects with titanium micro-mesh systems. J Craniomaxillofac Surg, 2001, **29**, 75-81.

Ladizesky NH, Ward IM and Bonfield W. Hydrostatic extrusion of polyethylene filled with hydroxyapatite. Polym Adv Tech, 1997a, **8**, 496 –504.

Ladizesky NH, Ward IM and Bonfield W. Hydroxyapatite / high performance polyethylene fiber composites for high load bearing bone replacement materials. J Appl Polym Sci, 1997b, **65**, 1865 –1882.

Ladizesky NH, Pirhonen EM, Appleyard DB, Ward IM and Bonfield W. Fibre reinforcement of ceramic/polymer composites for a major load bearing bone substitute materials. Comp Sci Tech, 1998, **58**, 419 –434.

Laing PG, Ferguson AB and Hodge ES. Tissue reaction in rabbit muscle exposed to metallic implants. J Biomed Mater Res, 1967, **1**, 135-149.

Lakdawala K and Salovey R. Viscosity of copolymers containing carbon black. Polym Engg Sci, 1985, **25**, 797-803.

Lakdawala K and Salovey R. Rheology of copolymers containing carbon black. Polym Engg Sci, 1987, **27**, 1043-1049.

Langer R and Vacanti J. Tissue Engineering. Science, 1993, **260**, 920 –926.

Lara WC, Schweitzer J, Lewis RP, Odum BC, Edlich RF and Gampper TJ. Technical considerations in the use of polymethylmethacrylate in cranioplasty. J Long-Term Effects of Medical Implants, 1998, **8**, 43-53.

Laurencin CT, Ambrosio MA, Borden MD and Cooper JA. Tissue engineering: orthopaedic applications. Ann Rev Biomed Engg, 1999, **1**, 19-46.

Lee DI. The viscosity of concentrated suspensions. Trans Soc Rheo, 1969, **13**, 273-288.

Lee GCN and Purdon JR. Brabender viscometry: I. Conversion of Brabender curves to Instron flow curves. Polym Engg Sci, 1969, **9**, 360-364.

Lee JK, Virkler TL and Scott CE. Influence of initial sheet temperature on ABS thermoforming. Polym Engg Sci, 2001, **41**, 1830-1844.

Leonor IB, Sousa RA, Cunha AM, Zhong Z, Greenspan D and Reis RL. Novel starch thermoplastic/bioglass composites: mechanical properties, degradation behaviour and *in vitro* bioactivity. J Mater Sci Mater Med, 2000, **13**, 1-7.

Lewandrowski K, Gresser JD, Wise DL and Trantolo DJ. Bio-resorbable bone graft substitutes of different osteo-conductivities: a histologic evaluation of osteo-integration of poly(propylene glycol-co-fumaric acid)-based cement implant in rats. Biomaterials, 2000, **21**, 757-764.

Lewis D. Tran. 7th Ann. Meet Soc. Biomaterials, Troy, New York, 1981, 61-63.

Lewis TB and Nielsen LE. Viscosity of dispersed and aggregated suspensions of spheres. J Rheol, 1968, **12**, 421-443.

Li JS and Salovey R. Model filled polymers: the effects of particle size on the rheology of filled poly (methyl methacrylate) composites. Polym Engg Sci, 2004, **44**, 452-462.

Liang JZ, Li RKY and Tjong SC. Effects of glass bead size and content on the viscoelasticity of filled polypropylene composites. Polym Test, 2000, **19**, 213-220.

Lin KY, Bartlett SP, Yaremchuk, MJ, Grossman RF, Udupa JK and Whitaker LA. An experimental study on the effect of rigid fixation on the developing craniofacial skeleton. Plast Reconstr Surg, 1991, **87**, 229-235.

Lin TW, Cornelli AA, Frondoza CG, Roberts JC and Hungerford DS. Glass-PEEK composite promotes proliferation and osteocalcin production of human osteoblastic cells. J Biomed Mater Res 1997, **36A**, 137-144.

Lin FH, Chen TM, Wang HJ, Chou GH, Lee TW and Yao CH. Evaluation of a novel malleable, biodegradable osteoconductive composite in a rabbit cranial defect model. Mat Chem Phy, 1998, **55**, 44-50.

Linder L. High resolution microscopy of the implant-tissue interface. Acta Orthop Scand 1985, **56**, 269-272.

Liu ZH, Kwok KW, Li RKY and Choy CL. Effects of coupling agent and morphology on the impact strength of high-density polyethylene/$CaCO_3$ composites. Polymer, 2002, **43**, 2501-2506.

Losee JE, Karmacharya J, Gannon FH, Slemp AE, Ong G, Hunenko O, Gorden AD, Bartlett SP and Kirschner RE. Reconstruction of the immature craniofacial skeleton with carbonated calcium phosphate bone cement: interaction with bioresorbable mesh. J Cranifac Surg, 2003, **14**, 117-124.

Luparello D, Bruschi S, Verna G, Bogetti P, Datta G, Fraccalvieri M and Luparello V. Cranioplasty with polymethylmethacrylate. The clinico-statistical considerations. Minerva Chirurgica, 1998, **53**, 575-579.

Ma PX, Zhang R, Xiao G and Franceschi R. Engineering new bone tissue in vitro on highly porous poly(α-hydroxyl acids)/hydroxyapatite composite scaffolds. J Biomed Mater Res, 2001, **54A**, 284 –293.

Magee WP Jr, Ajkay N, Freda N and Rosenblum RS. Use of fast-setting hydroxyapatite cement for secondary craniofacial contouring. Plast Reconstr Surg, 2004, **114**, 289-297.

Magnusson B and Kligman AM. The identification of contact allergens by animal assay - the guinea pig maximization test. J Invest Derm, 1969, **52**, 268-276.

Malik TM, Farooqi MI and Vachet C. Mechanical and rheological properties of reinforced polyethylene. Polym Composite, 1992, **13**, 174-178.

Malis LI. Titanium mesh and acrylic cranioplasty. Neurosurgery, 1989, **25**, 351-355.

Manson JA and Sperling LH. Polymer blends and composites. Plenum Press, London, 1976.

Manson PN, Crawley WA and Hoopes JE. Frontal cranioplasty: risk factors and choice of cranial vault reconstructive material. Plast Reconstr Surg, 1986, **77**, 888-904.

Marcolongo M, Ducheyne P and La Course WC. Surface reaction layer formation *in vitro* on a bioactive glass fiber/polymeric composite. J Biomed Mater Res, 1997, **37A**, 440-448.

Marcolongo M, Ducheyne P, Garino J and Schepers E. Bioactive glass fiber/polymeric composites bond to bone tissue. J Biomed Mater Res, 1998, **39A**, 161-170.

Maron SH and Pierce PE. Application of Ree-Erying generalized flow theory to suspensions of spherical particles. J Coll Sc, 1956, 11, 80-95.

Marques AP, Reis RL and Hunt JA. The biocompatibility of novel starch-based polymers and composites: *in vitro* studies. Biomaterials, 2002, **23**, 1471-1478.

Marquez A, Quijano J and Gaulin M. A calibration technique to evaluate the power-law parameters of polymer melts using a torque-rheometer. Polym Engg Sci, 1996, **36**, 2556-2563.

Marra KG, Szem JW, Kumta PN, DiMilla PA and Weiss LE. *In vitro* analysis of biodegradable polymer blend/hydroxyapatite composites for bone tissue engineering. J Biomed Mater Res, 1999, **47A**, 324 –355.

Martin NJ, Lappin JF, Harkines-Jones EMA and Martin PJ. The use of hot impact testing in the simulation of the plug-assisted thermoforming process. ANTEC Tech Papers, 2000, 783-787.

Marzuli FN and Maliback HI. Dermatotoxicology, 2nd edition, Hemisphere Publishing Co., New York, 1987.

McCann KJ, Irish JC, Gullane PJ, Holmes H, Brown DH and Rotstein L. Complications associated with rigid fixation of mandibulotomies. J Otolaryngol, 1994, **23**, 210-215.

Meaney DF. Mechanical properties of implantable biomaterials. Clin Podiatr Med Surg, 1995, **12**, 363-384.

Meel BL. Fatal systemic allergic reaction following acrylic cranioplasty: a case report. J Clin Forensic Med, 2004, **11**, 205-207.

Meijer AGW, Segenhout HM, Albers FWJ and van de Want HJL. Histopathology of biocompatible hydroxyapatite-polyethylene composite in ossiculoplasty. Orl, 2002, **64**, 173-179.

Mendes SC, Reis RL, Bovell YP, Cunha AM, van Blitterswijk CA and de Bruijn JD. Biocompatibility testing of novel starch-based materials with potential application in orthopaedic surgery: a preliminary study. Biomaterials, 2001, **22**, 2057-2064.

Mendham J, Denny RC, Barnes JD and Thomas A. Vogel's text of quantitative chemical analysis, edition 6, Pearson Education, Singapore, 2002.

Miyake H, Ohta T and Tanaka H. A new technique for cranioplasty with L-shaped titanium plates and ceramic implants composed of hydroxyapatite and tricalcium phosphate (Ceratite). Neurosurgery, 2000, **46**, 414-418.

Miyamoto Y, Ishikawa K, Takechi M, Toh T, Yuasa T, Nagayama M and Suzuki K. Histological and compositional evaluations of three types of calcium phosphate cements when implanted in subcutaneous tissue immediately after mixing. J Biomed Mater Res: Appl Biomater, 1999, **48**, 36-42.

Miyamoto Y, Ishikawa K, Takechi M, Yuasa M, Kon M, Nagayama M and Asaoka K. Non-decay type fast-setting calcium phosphate cement: setting behaviour in calf serum and its tissue response. Biomaterials, 1996, **17**, 1429 –1435.

Mooney M. The viscosity of a concentrated suspension of spherical particles. J Colloid Sc, 1951, **6**, 162-170.

Moreira-Gonzalez A, Jackson IT, Miyawaki T, Barakat K and DiNick V. Clinical outcome in cranioplasty: critical review in long-term follow-up. J Craniofac Surg, 2003, **14**, 144-153.

Muehlbauer W, Anderl H, Ramatschi P, Heeckt P, Zenker J, Deubzer M, Hopner F, Vertesy E. Radical treatment of craniofacial anomalies in infancy and the use of miniplates in craniofacial surgery. Clin Plast Surg, 1987, **14**, 101-111.

Murai K, Takeshita F, Ayukawa Y, Kiyoshima T, Suetsugu T and Tanaka T. Light and electron microscopic studies of bone-titanium interface in the tibia of young and mature rats. J Biomed Mater Res, 1996, **30**, 523-533.

Nagase M, Baker DG and Schumacher HRS Jr. Prolonged inflammatory reactions induced by artificial ceramics in the rat air pouch model. J Rheumatol, 1988, **15**, 1334-1338.

Nagase M, Chen RB, Araya Y and Nakajima T. Evaluation of a bone substitute prepared from alpha-tricalcium phosphate and an acid polysaccharide solution. J Oral Maxillofac Surg, 1991, **49**, 1305-1309.

Nagata K, Shiobara Y, Kobayashi H, Shiba T, Yanagisawa A and Maruyama S. Mesh and glue technique as a new sealing technique for the use of expanded polytetrafluoroethylene dura substitute: the experimental studies of its tolerance for pressure and long-term histological changes. Neurol Surg, 1999, **27**, 1097-1103.

Nanci A, McCarthy GF, Zalzal S, Clokie CML, Warshawsky H and McKee MD. Tissue response to titanium implants in the rat tibia: ultrastructural, immunocytochemical

and lectin-cytochemical characterization of the bone-titanium interface. Cell Mater, 1994, **41**, 1-30.

Nazhat SN, Joseph R, Wang M, Smith R, Tanner KE and Bonfield W. Dynamic mechanical characterization of hydroxyapatite reinforced polyethylene: effect of particle size. J Mater Sci: Mater Med, 2000, **11**, 621-628.

Nazhat SN, Kellomaki M, Tanner KE, Tormala P and Bonfield W. Dynamic mechanical characterization of biodegradable composites of hydroxyapatites and polylactides. J Biomed Mater Res: Appl Biomater, 2001, **58**, 335-343.

Nickell WB, Jurkiewiez MJ and Salyer KE. Repair of skull defects with autogenous bone. Arch Aurg, 1972, **105**, 431-433.

Nielsen LE and Lewis TB. Temperature dependence of relative modulus in filled polymer systems. J Polym Sci, 1969, **7**, 1705-1719.

Nielsen LE. Mechanical properties of polymers and composites. Vol. 2, Marcel Dekker, New York, 1974.

Nielsen LE. Polymer Rheology. Marcel Dekker, New York, 1977.

Nielsen LE and Landrel RF. Mechanical properties of polymers and composites, Vol. 2. Marcel Dekker, New York, 1994.

Noguchi T, Yamamuro T, Oka M, Kumar P, Kotoura Y, Hyon S and Ikada Y. Polyvinyl(alcohol) hydrogel as an artificial articular cartilage: evaluation of biocompatibility. J Appl Biomater, 1991, **2**, 101-107.

Nowacki J and Neitzel M. Thermoforming of reinforced thermoplastic stiffened structures. Polym Composite, 2000, **21**, 531-538.

Oberth AE. Principle of strength reinforcement in filled rubbers. Rubber Chem Technol, 1967, **40**, 1337-1363.

O'Broin ES, Morrin M, Breathnach E, Allcutt D and Earley MJ. Titanium mesh and bone dust calvarial patch during cranioplasty. Cleft Palate Craniofac J, 1997, **34**, 354-356.

Odum BC, Bussard GM, Lewis RP, Lara WC, Edlich RF and Gampper TJ. High-density porous polyethylene for facial bone augmentation. J Long Term Effects of Medical Implants, 1998, **8**, 3-17.

Ogunniyi DS. Filler reinforcement in rubber. Elastomerics, 1988, **120**, 24-27.

Ohmori S, Sugiyama Y and Morimoto Y. A protective effect against undesirable increase of dihydroetorphine permeation through damaged skin by using pressure-sensitive adhesive tape with an ethylene-vinyl acetate co-polymer membrane. Biol Pharm Bull, 2001, **24**, 78-83.

Okamoto Y, Minami S, Matsuhashi A, Sashiwa H, Saimoto H, Shigemasa Y, Tanigawa T, Tanaka Y and Tokura S. Polymeric N-acetyl-D-glucosamine (chitin) induces histionic activation in dogs. J Vet Med Sci, 1993, **55**, 937-940.

Okine RK. Analysis of forming parts from advanced thermoplastic composite sheet materials. J Thermoplast Comp Mater, 1989, **2**, 50-76.

Onishi K, Maruyama Y, Sawaizumi M, Yataka M, Seiki Y and Shibata I. The use of HAKEN ^{TM} plate in craniofacial surgery. Neurol Surg, 1995, **23**, 595-598.

Ooms EM, Wolke JGC, van de Heuvel MT, Jeschke B and Jansen JA. Histological evaluation of the bone response to calcium phosphate cement implanted in cortical bone. Biomaterials, 2003, **24**, 989-1000.

Orringer JS, Barcelona V and Buchman SR. Reasons for removal of rigid internal fixation devices in craniofacial surgery. J Craniofac Surg, 1998, **9**, 40-44.

Papay FA, Hardy S, Morales L Jr., Walker M and Enlow D. "False" migration of rigid fixation appliances in pediatric craniofacial surgery. J Craniofac Surg, 1995, **6**, 309-313.

Park JB and Lakes RS. Biomaterials, An Introduction, 2nd ed. Plenum press, New York, 1992.

Park M, Gandhi K, Sun L, Salovey R and Aklonis JJ. Model filled polymers III: Rheological behavior of polystyrene containing cross-linked polystyrene beads. Polym Engg Sci, 1990, **30**, 1158-1164.

Peltoniemi HH, Ahovuo J, Tulamo RM, Tormala P and Waris T. Biodegradable and titanium plating in experimental craniotomies: a radiographic follow-up study. J Craniofac Surg, 1997, **8**, 446-451.

Peltoniemi HH. Biocompatibility and fixation properties of absorbable miniplates and screws in growing calvarium. An experimental study in sheep. Academic dissertation, Helsinki University Central Hospital, Helsinki, Kasarmikatu, 2000.

Persing JA, Posnick J, Magge S, Spinelli HM, Wolfe SA, Munro I and Mulliken JB. Cranial plate and screw fixation in infancy: an assessment of risk. J Craniofac Surg, 1996, **7**, 267-270.

Pinchuk L, Nott S, Schwarz M, and Kamath K. Drug delivery compositions and medical devices containing block copolymer. United States Patent 6545097, 2000.

Pochon JP and Kloti J. Cranioplasty for acquired skull defects in children – a comparison between autologous material and methylmethacrylate 1974-1990. Eur J Pediatr Surg, 1991, **1**, 199-201.

Polley JW, Figueroa A, Hung KF, Cohen Mand Lakars T. Effect of rigid microfixation on the craniomaxillofacial skeleton. J Craniofac Surg, 1995, **6**, 132-138.

Polley JW, Hung KF, Figueroa A, Lakars T and Heiberger H. Alternative techniques in rigid fixation of the craniomaxillofacial skeleton. J Craniofac Surg, 1998, **9**, 249-253.

Pompili A, Caroli F, Carpanese L, Caterino M, Raus L, Sestili G and Occhipinti E. Cranioplasty performed with a new osteoconductive osteoinducing hydroxyapatite-derived material. J Neurosurg, 1998, **89**, 236-242.

Poshusta AK, Burdick JA, Mortisen DJ, Padera RF, Ruehlman D, Yaszemski MJ and Anseth KS. Histocompatibility of photocrosslinked polyanhydrides: a novel in situ forming orthopaedic biomaterial. J Biomed Mater Res, 2003, **64A**, 62-69.

Posner AS. The chemistry of bone mineral. Bulletin (Hospital for Joint Diseases), 1978, **39**, 126-144.

Posnick JC and Yaremchuk MJ. The effects of nonresorbable internal fixation devices placed on and within a child's cranial vault: brain function, morbidity and growth restriction. Plast Reconstr Surg, 1995, **96**, 966-968.

Prolo DJ, Burres KP and Mclaughlin WT. Autogenous skull cranioplasty: fresh and preserved (frozen) with consideration of the cellular response, Neurosurgery. 1979, **4**, 18-29.

Puleo DA and Nanci A. Understanding and controlling the bone-implant interface. Biomaterials 1999, **20**, 2311-2321.

Ravaglioli A and Krajewski A. Bioceramics. Chapman and Hall, London, 1992.

Reis RL, Cunha AM, Allan PS and Bevis MJ. Mechanical behaviour of injection moulded starch based polymers. J Polym Adv Tech 1996, **7**, 784 –790.

Reis RL, Mendes SC, Cunha AM and Bevis MJ. Processing and *in vitro* degradation of starch/EVOH thermoplastic blends. Polym Int, 1997a, **43**, 347 –353.

Reis RL, Cunha AM, Allan PS and Bevis MJ. Structure development and control of injection moulded hydroxylapatite reinforced starch/EVOH composites. Adv Polym Tech 1997b, **16**, 263 –277.

Reis RL, Cunha AM, Fernandes MH and Correia RN. Treatments to induce the nucleation and growth of apatite-like layers on polymeric surfaces and foams. J Mater Sci Mater Med, 1997c, **8**, 897 –905.

Reis RL, Cunha AM and Bevis MJ. Using nonconventional processing routes to develop anisotropic and biodegradable composites of starch-based thermoplastics reinforced with bone-like ceramics. J Appl Med Polym 1998, **2**, 49 –53.

Reis RL and Cunha AM. New degradable load-bearing biomaterials composed of reinforced starch based blends. J Appl Med Polym, 2000, **4**, 1 –5.

Reis RL, Cunha AM, Oliveira MJ, Campos AR and Bevis MJ. Relationships between processing and mechanical properties of injection moulded high molecular weight polyethylene/hydroxylapatite composites. Mat Res Innovat, 2001, **4**, 263 –267.

Rhodes ML, Kuo Y, Rothman SLG and Woznick C. An application of computer graphics and networks to anatomic model and prosthesis manufacturing. IEEE CG&A, 1987, **2**, 12–25.

Ross MH, Romwell LJ and Kaye GI. Histology: a text and atlas. 3rd ed., Williams & Wilkins, Baltimore, 1995.

Rotem A. Effect of implant material properties on the performance of a hip joint replacement. J Med Engg Tech 1994, **18**, 208-217.

Sadove AM and Eppley BL. Microfixation techniques in pediatric craniomaxillofacial. Ann Plast Surg, 1991, **27**, 36-43.

Saini DR, Shenoy AV and Nadkarni VM. Melt rheology of highly loaded ferrite-filled polymer composites. Polym Composite, 1985, **7**, 193-200.

Schliephake H and Kage T. Enhancement of bone regeneration using resorbable ceramics and a polymer-ceramic composite material. J Biomed Mater Res, 2001, **56A**, 128-136.

Sclippa E and Piekarski K. Carbon fiber reinforced polyethylene for possible orthopaedic uses. J Biomed Mater Res 1973, **7**, 59-70.

Serlo W, Kaarela OI, Peltoniemi HH, Merikanto J, Ashammakhi NA, Lassila K, Pohjonen T, Tormala P and Waris TH. Use of self-reinforced polylactide osteosynthesis devices in craniofacial surgery: a long-term follow-up study. Scand Plastic Reconst Surg Hand Surg, 2001, **35**, 285-292.

Shen X, Roberts E, Peel SAF and Davies JE. Organic extracellular matrix components at the bone cell/substratum interface. Cells Mater, 1993, **3**, 257-272.

Sherburn EW and Silbergeld DL. A new method of acrylic cranioplasty: technical note. Surg Neurol, 1996, **46**, 292-296.

Sherburn EW and Silbergeld DL. Acrylic cranioplasty using miniplate struts. Neurosurgery, 1997, **40**, 885-886.

Shikinami Y and Okuno M. Bioresorbable devices made of forged composites of hydroxyapatite (HA) particles and poly-l-lactide (PLLA): Part I. Basic characteristics. Biomaterials, 1999, **20**, 859 –877.

Shvarts S, Besinque K, Atkinson R and Gill MA. New advances in contraception. 2002, Journal ce, 11-22.

Sidess A, Holdengraber Y and Buchman A. A fundamental model for prediction of optimal particulate composite properties. Composites, 1993, **24**, 355-360.

Siegel RA and Langer R. Controlled release of polypeptides and other macromolecules. Pharm Res, 1984, **1**, 2-10.

Sousa RA, Kalay G, Reis RL, Cunha AM and Bevis MJ. Injection molding of a starch/EVOH blend aimed as an alternative biomaterial for temporary applications. J Appl Polym Sci, 2000, **77**, 1303 –1315.

Sousa RA, Reis RL, Cunha AM and Bevis MJ. Structure development and interfacial interactions in HDPE/HA composites moulded with preferred orientation. J Appl Polym Sci, 2002a , **86**, 2866–2872.

Sousa RA, Mano JF, Reis RL, Cunha AM and Bevis MJ. Mechanical performance of starch based bioactive composite biomaterials molded with preferred orientation for potential medical applications. Polym Engg Sci, 2002b, **42**, 1032 –1045.

Spencer AJM, Watson P and Rogers TG. Manufacturing analysis of the spring back effect in laminated thermoplastic channel sections. Comp Manufact, 1991, **2**, 253-258.

Suuronen R, Laine P, Pohjonen T and Lindqvist C. Sagittal ramus osteotomies fixed with biodegradable screws: a preliminary report. J Oral Maxillofac Surg, 1994, **52**, 715-720.

Takechi M, Miyamoto Y, Ishikawa K, Yuasa M, Nagayama M, Kon M and Asaoka K. Non-decay type fast-setting calcium phosphate cement using chitosan. J Mater Sci Mater Med, 1996, **7**, 317–322.

Takeuchi A, Ohtsuki C, Miyazaki T, Tanaka H, Yamazaki M and Tanihara M. Deposition of bone-like apatite on silk fiber in a solution that mimics extracellular fluid. J Biomed Mater Res, 2003, **65A**, 283-289.

Tampieri A, Celotti G, Landi E, Sandri M, Roveri N and Falini G. Biologically inspired synthesis of bone-like composite: self-assembled collagen fibers/hydroxyapatite nanocrystals. J Biomed Mater Res, 2003, **67A**, 618-625.

Tams J, Joziasse CA, Bos RR, Rozema FR, Grijpma DW and Pennings AJ. High-impact poly(l/d-lactide) for fracture fixation: *in vitro* degradation and animal pilot study. Biomaterials, 1995, **16**, 1409-1415.

Tanaka K, Tamura J, Kawanabe K, Nawa M, Oka M, Uchida M, Kokubo T and Nakamura T. Ce-TZP/Al_2O_3 nanocomposite as a bearing material in total joint replacement. J Biomed Mater Res: Appl Biomater, 2002, **63**, 262-270.

Tanner KE. 'Biomaterials for orthopaedic applications'. in Sciences: Basics to Orthopaedics, Hughes SPF and Mc Carthy ID, eds, WB Saunders Company Limited, London, 1998.

TenHuisen KS and Brown PW. The formation of hydroxyapatite–gelatin composites at 38 °C. J Biomed Mater Res, 1994, **28**, 27 –33.

Therin M, Christel P and Munier A. Analysis of general features of the soft tissue repsonse to some metals and ceramics using quantitative histomorphometry. J Biomed Mater Res, 1994, **28**, 1267-1276.

Thomson RC, Yaszemski MJ, Powers JM and Mikos AG. Hydroxyapatite fiber reinforced poly (α-hydroxy ester) foams for bone regeneration. Biomaterials, 1998, **19**, 1935-1943.

Throne JL. Thermoforming. Hanser Publishers, Münich, 1987.

Timbrell JA. Introduction to Toxicology. Taylor and Francis, New York, 1990.

Tjong SC, Meng YZ and Xu Y. Structure and properties of polyamide-6/vermiculite nanocomposites prepared by direct melt compounding. J Polym Sci Part B: Polym Phys, 2002, **40**, 2860- 2870.

Tormala P, Vainionpaa S, Kilpikari J and Rokkanen P. The effects of fibre reinforcement and gold plating on the flexural and tensile strength of PGA/PLA copolymer materials *in vitro*. Biomaterials, 1987, **8**, 42-45.

Tormala P and Pohjonen, T. Ultra high strength bioabsorbable polymeric composites for surgical applications, in: Self-reinforced Bioabsorbable Polymeric Composites in Surgery, Rokkanen P and Tormala P, eds, Offsetpaino, Tampere, 1995.

Tormala P, Pohjonen T and Rokkanen P. Bioabsorbable polymers: materials technology and surgical applications. Proceedings of the Institution of Mechanical Engineers. Part H - J Engg Med, 1998, **212**, 101-111.

Toth BA, Ellis DS and Stewart WB. Computer-designed prostheses for orbitocranial reconstruction. Plast Reconstr Surg, 1988, **81**, 315–324.

Turk JB and **Parhiscar A**. Bonesource for craniomaxillofacial reconstruction. Facial Plast Surg, 2000, **16**, 7-14.

USP (XXIII)-95. The United States Pharmacopeia. United States Pharmacopeial Convention, Mack Printing Co., Easton, PA, 1995.

Ural E, Kesenci K, Fambri L, Migliaresi C and Piskin E. Poly (dl-lactide/ε caprolactone)/hydroxyapatite composites. Biomaterials, 2000, **21**, 2147 –2154.

Usami Y, Okamoto Y, Minami S, Matsuhashi A, Kumazawa NH, Tanioka S and Shigemasa Y. Migration of canine neutrophils to chitin and chitosan. J Vet Med Sci, 1994, **56**, 1215-1216.

Utracki LA and Fisa B. Rheology of fiber or flake filled plastics. Polym Composite, 1982, **3**, 193-211.

Vainionpaa S, Kilpikari J, Laiho J, Helevirta P, Rokkanen P and Tormala P. Strength and strength retention in vitro, of absorbable, self-reinforced polyglycolide (PGA) rods for fracture fixation. Biomaterials, 1987, **8**, 46-49.

Vande Vord PJ, Matthew HWT, DeSilva SP, Mayton L, Wu B and Wooley PH. Evaluation of the biocompatibility of a chitosan scaffold in mice. J Biomed Mater Res, 2002, **59A**, 585-590.

Varma HK and Sivakumar R. Preparation and characterization of free flowing hydroxyapatite powders. Phos Res Bull, 1996, **6**, 35-38.

Varma HK, Yokogawa Y, Espinosa FF, Kawamoto Y, Nishizawa K, Nagata F and Kameyama T. Porous calcium phosphate coating over phosphorylated chitosan film by a biomimetic method. Biomaterials, 1999a, **20**, 879-884.

Varma HK, Yokogawa Y, Espinosa FF, Kawamoto Y, Nishizawa K, Nagata F, Kameyama T. *In vitro* calcium phosphate growth over functionalized cotton fibers. J Mater Sci: Mater Med, 1999b, **10**, 395-400.

Varma HK, Sreenivasan K, Yokogawa Y and Hosumi A. In vitro calcium phosphate growth over surface modified PMMA film. Biomaterials, 2003, **24**, 297-303.

Vaughan J. The Physiology of Bone, 3rd edition, Clarendon Press, Oxford, 1981.

Vaz CM, Reis RL and Cunha AM. Use of coupling agents to enhance the interfacial interactions in starch-EVOH/hydroxylapatite composites. Biomaterials, 2002, **23**, 629-635.

Verbeek CJR. Highly filled polyethylene/phlogopite composites. Mater Lett, 2002a, **52**, 453-457.

Verbeek CJR. Effect of formulation variables on the mechanical properties of compression moulded phlogopite/LLDPE composites. Composites: Part A, 2002b, **33**, 589-593.

Viterbo F, Palhares A and Modenese E. Cranioplasty: The autograft option. J Craniofac Surg, 1995, **6**, 80-83.

Waite PD, Morawetz RB, Zeiger HE and Pincock JL. Reconstruction of cranial defects with porous hydroxyl-apatite blocks. Neurosurgery, 1989, **25**, 214–217.

Wan ACA, Khor E and Hastings GW. Hydroxyapatite modified chitin as potential hard tissue substitute material. J Biomed Mater Res: Appl Biomater, 1997, **38**, 235 –241.

Wang M, Bonfield W and Hench LL. Bioglass/high density polyethylene composite as a new soft tissue bonding material. in: Wilson J, Hench LL, Greenspan D, eds Bioceramics 8, Pergamon, Oxford 1995, pp. 383 –388.

Wang M, Kokubo T and Bonfield W. A-W glass-ceramic reinforced polyethylene for medical applications. in: Kokubo T, Nakamura T, Miyaji F, eds, Bioceramics 9, Elsevier, Oxford, 1996, pp. 387 –390.

Wang Y, Lu J and Wang GJ. Toughening and reinforcement of HDPE/$CaCO_3$ blends by interfacial modification - interfacial interaction. J Appl Polym Sci, 1997, **64**, 1275-1281.

Wang M, Hench LL and Bonfield W. Bioglass/high density polyethylene composite for soft tissue applications: preparation and evaluation. J Biomed Mater Res, 1998a, **42A**, 577-586.

Wang M, Joseph R and Bonfield W. Hydroxyapatite-high density polyethylene composites: effect of ceramic particle size and morphology. Biomaterials, 1998b, **19**, 2357-2366.

Wang M, Ladizesky NH, Tanner KE, Ward IM and Bonfield W. Hydrostatically extruded HAPEX. J Mater Sci, 2000, **35**, 1023-1030.

Wang M, Chen LJ, Ni J, Weng J and Yue CY. Manufacture and evaluation of bioactive and biodegradable materials and scaffolds for tissue engineering. J Mater Sci: Mater Med, 2001, **12**, 855 –860.

Wang J, Chen H and Li MH. Complication and its treatment of post-cranioplasty with silastic. Hunan Yi Ke Da Xue Xue Bao, 2002, **28**, 187-189.

Wang M. Developing bioactive composite materials for tissue replacement. Biomaterials, 2003, **24**, 2133-2151.

Ward IM, Bonfield W and Ladizesky NH. The development of load-bearing bone substitute materials. Polym Int, 1997, **43**, 333 –337.

Wellisz T, Dougherty W and Gross J. Craniofacial applications for the Medpor porous polyethylene flexblock implant. J Craniofac Surg, 1992, **3**, 101-107.

Wellisz T. Clinical experience with the Medpor porous polyethylene implant. Aesth Plas Surg, 1993, **17**, 339-44.

Williams DF. Concise encyclopedia of medical and dental materials; Pergamon press, New York, 1990.

Wiltfang J, Merten HA, Becker HJ and Luhr HG. The resorbable miniplate system Lactosorb in a growing cranio-osteoplasty animal model. J Craniomaxillofac Surg, 1999, **27**, 207-210.

Wise DL, Trantolo DJ, Altobelli DE, Yaszemski MJ, Greeser JD and Schwartz ER. Encyclopedic Handbook of Biomaterials and Bioengineering, Part A; Vol.1, Marcel Dekker Inc., New York, 1995.

Wolfe SA. Autogenous bone grafts versus alloplastic material in maxillofacial surgery. Clin Plast Surg, 1982, **9**, 539-540.

Wong L, Dufresne CR, Richtsmeier JT and Manson PN. The effect of rigid fixation on growth of the neurocranium. Plast Reconstr Surg, 1991, **88**, 395-403.

Wong L, Richtsmeier JT and Manson PN. Craniofacial growth following rigid fixation: suture excision, miniplatingand microplating. J Craniofac Surg, 1993, **4**, 234-244.

Wong L and Manson PN. Rigid mesh fixation for alloplastic cranioplasty. J Craniofac Surg, 1994, **5**, 265-269.

Wong WC, Yu Y, Wallace AL, Gianoutsos MP, H Sonnabend D and Walsh WR. Use of a polymeric device to deliver growth factors to a healing fracture. A NZ J Surg, 2003, **73**, 1022-1027.

Wright CS and Wilgis EF. Erosive silicone synovitis. Can J Surg, 1986, **29**, 45-47.

www.medcompare.com

Xavier SF, Schultz JM and Friedrich K. Fracture propagation in particulate filled polypropylene composites: Part 1. Influence of filler nature. J Mater Sci, 1990, **25,** 2411-2420.

Xiong M, Wu L, Zhou S and You B. Preparation and characterization of acrylic latex/nano-SiO_2 composites. Polym Int, 2002, **51**, 693-698.

Yamaguchi I, Tokuchi K, Fukuzaki H, Koyama Y, Takakuda K, Monma H and Tanaka J. Preparation and microstructure analysis of chitosan/hydroxyapatite nanocomposites. J Biomed Mater Res, 2001, **55A**, 20 –27.

Yamamuro T, Matsusue T, Uchida A, Shimada K, Shimozaki E and Kitaoka K. Bioabsorbable osteosynthetic implants of ultra high strength poly-l-lactide. Int Orthop (SICOT), 1994, **18**, 332-340.

Yamashima T. Modern cranioplasty with hydroxylapatite ceramic granules, buttons and plates. Neurosurgery, 1993, **33**, 939-940.

Yaremchuk MJ and Posnick JC. Resolving controversies related to plate and screw fixation in the growing craniofacial skeleton. J Craniofac Surg, 1995, **6**, 525-538.

Yaremchuk MJ. Experimental studies addressing rigid fixation in craniofacial surgery. Clin Plast Surg, 1994, **21**, 517-524.

Yasunaga T, Matsusue Y, Furukawa T, Shikinami Y, Okuno M and Nakamura T. Bonding behaviour of ultrahigh strength unsintered hydroxyapatite particles/poly(l-lactide)composites to surface of tibial cortex in rabbits. J Biomed Mater Res, 1999, **47A**, 412 –419.

Young RT, McLeod MA and Baird DG. Extensional processing behaviour of thermoplastics reinforced with a melt processable glass. Polym Composite, 2000, **21**, 900-917.

Zaborski G and Szot W. Evaluation of the usefulness of polytetrafluoroethylene (PTFE) prosthesis in cranioplasty: Experimental studies. Polim Med, 1987, **17**, 117-122.

Zahlan N. Design with thermoplastic-based composites: thermal effects considerations. Comp Manufact, 1988, **3**, 70-74.

Zahlan N and O'Neill JM. Design and fabrication of composite components; the spring forward phenomenon. Composites, 1989, **20**, 77-81.

Zanetti D and Nassif N. Transmatoid repair of minor skull base defects with flexible hydroxyapatite sheets. Skull base-Interd Ap, 2003, **13**, 1-11.

Zeilhofer HF, Sader R and Hogg M. Critical remarks on quality control in clinically used anatomical models. Computer Aided Surgery, Abstracts from CIS, September 1–5, 1997, Linz, Austria, S08–S043.

Zhang Y and Tanner KE. Impact properties of hydroxyapatite-polyethylene composites: Effect of filler volume fraction and morphology. Proceedings of 18th European Conference on Biomaterials, October 1-4, 2003, Stuttgart, Germany, p 122.

Zhang RY and Ma PX. Biomimetic polymer/apatite composite scaffolds for mineralized tissue engineering. Macromolecular Bioscience, 2004, **4**, 100-111.

Zhao J, Liao W, Wang Y, Pan J and Liu F. Preparation and degradation characteristic study of bone repair composite of DL-polylactic acid/hydroxyapatite/decalcifying bone matrix. Chin J Traumatol, 2002, **5**, 369-373.

Zhou G, Willett JL and Carriere CJ. Effect of starch content on viscosity of starch filled poly(hydroxy ester ether) composites. Polym Engg Sci, 2001, **41**, 1365-1372.

Zide MF, Kent JN and Machado L. Hydroxylapatite cranioplasty directly over dura. J Oral Maxillo Surg, 1987, **45**, 481-486.

Zonneveld FW. A decade of clinical three-dimensional imaging: a review. Part III. Image analysis and interaction, display options and physical models. Invest Radiol, 1994, **29**, 716–725.

Zuiderduin WCJ, Westzaan C, Huetink J and Gaymans RJ. Toughening of polypropylene with calcium carbonate particles. Polymer, 2003, **44**, 261-275.

ADDENDUM

9.1. SPECIFICATION OF POLYMETHYLMETHACRYLATE

Table 9.1. Properties of polymethylmethacrylate (PMMA)[#]

Parameter	
Density, g/cc	1.2
Tensile strength at break, (MPa)	50-80
Elongation at break, (%)	< 10
Young's Modulus, (GPa)	1-2

(www.tangram.co.uk)

9.2. DENSITY

The density of the composites was determined by Archimedics Principle, based upon ASTM D792-00, with a Sartorius precision balance (LA 230S, Sartorius, Germany) and Density detection kit. The specimens were weighed in air, followed by weighing in distilled water at 25°C.

Table 9.2. shows the theoretical and pre-testing measured densities for composites fabricated from H_s and H_f. The theoretical densities were calculated using values of density of 0.95 g/cc for EVA and 3.16 g/cc for HAP with their respective volume fractions.

Table 9.2. Calculated and experimentally measured densities of HAP/EVA composites.

Volume fraction of HAP	Calculated density, g/cc	Measured density (n=5), g/cc	
		$E28H_s$	$E28H_f$
0	0.95	0.94± 0.01	0.94 ± 0.01
0.1	1.22	1.15 ± 0.02	1.16 ± 0.01
0.2	1.39	1.34 ± 0.01	1.36 ± 0.01
0.3	1.61	1.54 ± 0.01	1.55 ± 0.03
0.4	1.83	1.73 ± 0.01	1.75 ± 0.01
0.5	2.06	1.96 ± 0.02	1.99 ± 0.01

The measured densities were below the theoretical values, indicating that some amount of HAP was lost in the whole process of mixing and moulding.

The dependence of Young's modulus on the density of the composites was also monitored (Figure 9.1.). An exponential increase in the values of Young's modulus with the increase in density is apparent for both types of composites. The modulus values associated with composites fabricated from H_s were found to be higher than the H_f counterpart for the same volume fraction of HAP loaded.

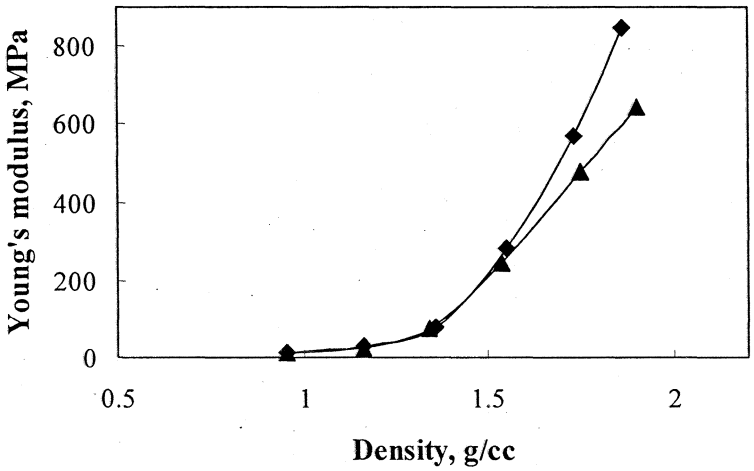

Figure 9.1. Variation in Young's modulus of HAP-EVA composites, fabricated from E28 as a function densities of the composites fabricated from (■) spray dried and (▲) freeze dried hydroxyapatite.

This observation is in accordance with the modulus (E) –density (ρ) relationship put forth by Gibson and Ashby (1988) given by the following equation.

$$E = C\rho^n$$

The constants C and n depend on the microstructure of the material. The value of n generally lies in the range $1 \leq n < 4$, a wide range of properties at a given density.

References:

ASTM D792-00. Standard test methods for density and specific gravity (relative density) of plastics by displacement. In: Annual Book of American Society of Testing Materials standards, Philadelphia, 2000.

Gibson LJ and Ashby MF. Cellular solids: Structure and properties; Pergamon Press, Oxford, 1988.

www.tangram.co.uk

LIST OF PUBLICATIONS

A. PEER REVIEWED JOURNALS

1. **Shiny Velayudhan**, P. Ramesh, M. C. Sunny and H. K.Varma.'Extrusion of hydroxyapatite into clinically significant shapes.' Materials Letters, 2000, **46**, 142-146.

2. **Shiny Velayudhan**, P.Ramesh and H.K.Varma. 'Hydroxyapatite filled ethylene vinyl acetate co-polymer composites for bone substitute applications.' Trends in Biomaterials and Artificial Organs, 2001, **14**, 21-23.

3. **Shiny Velayudhan**, P.Ramesh and H.K.Varma, 'Effect of vinyl acetate content on the sintering properties of hydroxyapatite-ethylene vinyl acetate co-polymer composites'. J. Mater Sci: Mater Med, 2002, **13**, 517-522.

4. **Shiny Velayudhan**, P. Ramesh, H. K. Varma, and K. Friedrich. 'Dynamic mechanical analysis of hydroxyapatite filled ethylene vinyl acetate copolymer'. Mat Chem Phy, 2004, **89**, 454-460.

5. **Shiny Velayudhan**, T. V. Anilkumar, T. V. Kumari, P. V. Mohanan, A. C. Fernandez, H. K. Varma and P. Ramesh. 'Biological evaluation of pliable, osteoconductive ethylene vinyl acetate copolymer-hydroxyapatite composites intended for cranioplasty'. Acta Biomaterialia, 2005, **1**, 201-209.

6. **Shiny Velayudhan**, P. Ramesh, H. K. Varma, S. Schmitt and K. Friedrich. 'Stamp forming of hydroxyapatite-polymer composites for cranioplasty: Process Optimization using a right angled V-tool'. Comp Part A: Appl Manufac (accepted).

7. **Shiny Velayudhan**, Mira Mohanty, R. Girish Menon, R. N. Bhattacharya, A. V. Lal, P. R. Umasankar, H. K. Varma and P. Ramesh. 'Bioactive, pliable, hydroxyapatite filled ethylene vinyl acetate co-polymer for cranioplasty: Implantation studies in rabbit cranium'. (submitted).

LIST OF PUBLICATIONS (CONTD...)

B. CONFERENCE ABSTRACTS

1. **Shiny Velayudhan**, P. Ramesh and H .K. Varma. 'A new binder material for the fabrication of hydroxyapatite ceramic implants', Twelfth Kerala Science Congress, Kumily, Kerala, INDIA, January 27-29, (2000).

2. **Shiny Velayudhan**, P. Ramesh and H. K. Varma. 'Hydroxyapatite filled ethylene vinyl acetate copolymer composites for bone substitute applications'. Eleventh National conference of Society of Biomaterials and Artificial Organs and Annual Conference India Chapter of Bio/Environmentally Degradable polymer Society, Material Science Centre, Indian Institute of Technology, Kharagpur, INDIA, December 6-8, 2000.

3. **Shiny Velayudhan**, P. Ramesh, H. K. Varma, S. Schmitt and K. Friedrich. 'Stamp forming of hydroxyapatite filled polymer Composites'. Proceedings of the European Society for Biomaterials Conference (ESB-2003), Stuttgart, GERMANY, October 4-7, 2003.

4. **Shiny Velayudhan**, P. Ramesh, H. K. Varma, and K. Friedrich. 'Dynamic mechanical analysis of hydroxyapatite filled polymer composites'. APT '04, Cochin University of Science and Technology, Cochin, Kerala, INDIA, January 16-17, 2004.

5. **Shiny Velayudhan**, P. Ramesh, H. K. Varma, S. Schmitt, and K. Friedrich. 'Influence of stamp forming parameters on final part properties of hydroxyapatite filled ethylene vinyl acetate co-polymer composites'. Seventh International Conference on "Flow Processes in Composite Materials", University of Delaware, Newark, USA, July 7-9, 2004.

6. **Shiny Velayudhan**, P. Ramesh, H. K. Varma, S. Schmitt, and K. Friedrich. 'Three-dimensional forming of hydroxyapatite filled ethylene vinyl acetate copolymer'. MACRO-2004, Trivandrum, INDIA, December 14-16, 2004.

BIODATA

Name	:	**Ms. Shiny Velayudhan**
Permanent address	:	Methal Valappil, P.O. Chevayoor, Cailcut-673 017, Kerala.
Date & place of birth	:	8th May, 1973; INDIA

Educational qualifications

1997-1999	:	M. Tech, Polymer Technology, Cochin University of Science and Technology, Cochin, Kerala, INDIA.
1994-1996	:	Master of Science (M. Sc.) in Chemistry, University of Calicut, Kerala, INDIA.

Awards and honors

2004	:	**Travel award** from Council of Industrial and Scientific Research (CSIR) India, for presenting research paper in the 7th International Conference on "Flow Processes in Composite Materials", Delaware, USA, July 7-9, 2004.
2003	:	**Travel award** from European Society of Biomaterials (ESB), for presenting research paper in the European Society for Biomaterials Conference (ESB-2003), Stuttgart, GERMANY, October 1-3, 2003.
2001-2003	:	**Deustcher Akademischer Austausch Dienst** (DAAD) fellowship for doctoral studies in GERMANY.
2001	:	**Best seminar award** in the Golden Jubilee Essay and Seminar Competition, organized by Rubber Technology Center, Indian Institute of Technology, Kharagpur, INDIA, September 2001.
2000	:	**Bajpai-Saha award** for the best paper in XIth National conference of Society of Biomaterials & Artificial Organs and Annual by Material Science Centre, Indian Institute of Technology, Kharagpur, INDIA, 6-8 December 2000.
1997-1999	:	**GATE' 97** (Graduate Aptitude Test in Engineering) fellowship for Masters Studies in engineering.